POLITECNICO DI MILANO

DEPARTMENT OF CIVIL AND ENVIRONMENTAL ENGINEERING

DOCTORAL PROGRAM IN ENVIRONMENTAL AND INFRASTRUCTURE ENGINEERING

ENVIRONMENTAL TECHNOLOGIES AREA

OPTIMIZATION OF ACTIVATED CARBON ADSORPTION FOR MICROPOLLUTANT REMOVAL FROM DRINKING WATER

Doctoral dissertation of:
Andrea Piazzoli

Supervisor:
Prof. Manuela Antonelli
Tutor:
Prof. Roberto Canziani
The chair of the doctoral program:
Prof. Alberto Guadagnini

30th cycle
Academic year 2017

ABSTRACT

Granular activated carbon (GAC) adsorption is known to effectively remove many classes of micropollutants affecting drinking waters. However, GAC life-time in the fixed-bed process can strongly depend on the considered target contaminants and the water composition. In presence of a mixture of micropollutants, an optimization of the GAC adsorption phase is often required to improve the treatment process efficiency. The optimization process can be figured out as the completion of three consecutive steps: 1) evaluation of GAC adsorption efficiency towards the target contaminants; 2) process simulation under full-scale conditions; 3) definition of the optimal design and operating criteria. These three different engineering tasks were studied focusing on specific classes of micropollutants considered as target contaminants, namely: heavy metals (namely, Cr(VI)), disinfection by-products (DBPs, specifically *N*-nitrosamines) and synthetic organic compounds (namely, chlorinated solvents).

Regarding heavy metals, the efficiency of GAC adsorption in the removal of Cr(VI) from a real groundwater was investigated and compared with the strong base anion (SBA) exchange process (step 1). Various commercial GACs and SBA resins were tested by equilibrium and kinetic laboratory scale experiments, for the removal of Cr(VI) and other organic and inorganic contaminants. Kinetic and isotherm models were calibrated for the studied materials, estimating their specific throughputs under full-scale conditions. Cr(VI) removal was found to depend on GAC textural properties; however, SBA exchange resulted to be the best solution, providing sorbent usage rates much lower than GAC adsorption.

The possibility to control the formation of *N*-nitrosamines, a group of emerging DBPs, from nitrogenous micropollutants by GAC adsorption was investigated (step 1). Laboratory-scale experiments on model water solutions were carried out. Firstly, the formation of specific and total *N*-nitrosamines (TONO) from various micropollutants associated to pharmaceuticals and personal care products was studied, observing relevant TONO formation yields, mainly associated to unknown *N*-nitrosamine species and dependent on the precursor molecular structure. Secondly, the effectiveness of GAC adsorption in reducing the *N*-nitrosamine formation potential of the precursors was evaluated, testing two possible treatment solutions: adsorption phase before oxidation treatment, to reduce *N*-nitrosamine precursor concentration, and adsorption phase after oxidation treatment, to remove the formed *N*-nitrosamines. Pre-adsorption of *N*-nitrosamine precursors resulted to be an effective option, while post-adsorption efficiency was found to depend on TONO pool composition.

Among synthetic organic compounds, the problem of breakthrough prediction (step 2) for chlorinated solvents in a full-scale GAC adsorption system was firstly investigated. Practical criteria for the application of the Homogeneous Surface Diffusion Model (HSDM) to predict tetrachloroethylene and chloroform breakthrough in two full-scale GAC filters were proposed, focusing on the main aspects of the simulation process: i) experimental determination of model parameters for a multi-component groundwater, ii) model adaptation to case-specific conditions and sensitivity analysis, iii) validation with full-scale data. The accurate estimation of model parameters was found to depend on the contaminant characteristics. The importance of introducing time-varying parameters (such as flow rate and contaminant influent concentrations) was also highlighted to best simulate the full-scale process.

Secondly, the optimal design parameters and operating strategies for a full-scale GAC system treating groundwater contaminated by chlorinated solvents were investigated (step 3). Five full-scale operating GAC filters, containing different GAC types, were monitored to observe contaminant breakthrough profiles. The observed data were used to calibrate a predictive model, which was then used to simulate a large-scale GAC system under different scenarios, covering GAC configurations, main design and operating parameters, target contaminant and treatment objective. For each

simulated scenario, GAC costs (derived from the specific throughput) and management complexity (in terms of GAC replacement strategy and frequency) were evaluated as process performance indicators during a long-term time frame. Results showed that the best configuration is a compromise between conflicting performance indicators.

Contents

<div align="right">CHAPTER 1</div>

State of the art

1. Micropollutants in drinking water

Micropollutants or trace contaminants are generally referred to anthropogenic chemical substances (as well as their transformation by-products) present in aquatic environment at sub-ng L^{-1}-μg L^{-1} concentration level ([1,2]). Micropollutants may include both organic and inorganic substances used for domestic, industrial or agricultural purposes, which can enter the aquatic environment and reach natural drinking water sources through the water cycle (Figure 1) ([3]).

Many micropollutants are known to be hazardous for human health and their concentration in drinking waters has been already regulated for several years. Various drinking-water regulations have been promulgated for controlling: 1) synthetic organic contaminants, both volatile and non-volatile; 2) inorganic contaminants, including corrosion products; 3) microbiological contaminants; 4) radio-nuclides; and 5) disinfection by-products (DBPs) ([4]). The European Drinking Water Directive (98/83/EC) set standards for 48 parameters, among which 26 chemicals selected for their potential impact on human health. Chemicals include trace elements like heavy metals (As, Ni, Pb, Cr) and organic substances, like cyanide, polycyclic aromatic hydrocarbons, pesticides, chlorinated solvents (tetra- and tri-chloroethylene, 1,2-dichloroethane) and DBPs (trihalomethanes).

Legislation about drinking water quality, however, is in continue evolution, due to the new evidences about occurrence and harmful effects of new substances in water sources. In fact, around 300 million tons of synthetic compounds used in industrial and consumer products are found in fresh waters ([5]). Several classes of compounds, such as fertilizers, pesticides, pharmaceuticals and personal care products (PPCPs), steroid hormones, surfactants and industrial chemicals have been identified in environmental samples, including drinking waters ([5–7]). The emission of so-called emerging unregulated contaminants has recently become an environmental issue, and there is widespread consensus that this kind of contamination requires legislative intervention ([7]). Emerging contaminants can be defined as pollutants that are currently not included in routine monitoring programmes and which may be candidates for future regulation, depending on research on their (eco)toxicity, potential health effects and public perception and on monitoring data regarding their occurrence in the various environmental compartments ([1,2]).
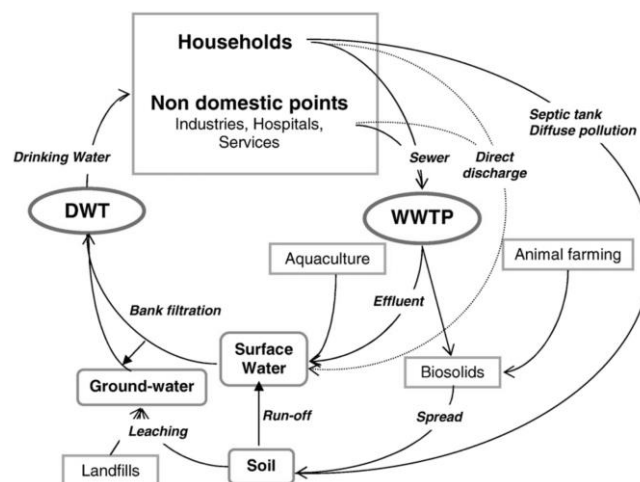
Figure 1 Urban water cycle showing possible origins and routes of micropollutants ([3]).

The European Union Water Framework Directive (2000/60/EC) of November 2001 identified 33 priority substances to be monitored in water, representing a significant risk to or via the aquatic environment; Directive 2008/105/EC adopted environmental quality standards for these 33 substances and the Directive 2013/39/EU increased the number of priority substances up to 45 ([8,9]). Recently, the Commission Decision 2015/495/EU creates the first watch list of substances to be monitored in the field of water policy.

The United States Environmental Protection Agency (US EPA) had listed 3 pharmaceuticals, 8 synthetic hormones and several DBPs and pesticides in the Contaminant Candidate List-3 (CCL-3), while 17 organic micropollutants were included in the Unregulated Contaminants Monitoring Rule-3 (UCMR-3) of 2011, to monitor their occurrence for future regulatory consideration ([10]). In February 2015, US EPA published the draft CCL-4, containing 100 chemicals (including compounds used in commerce, pesticides, biological toxins, DBPs, pharmaceuticals) that were proven to occur or are anticipated to occur in drinking water systems and will be considered for potential regulation. The UCMR-4 has been proposed in November 2015 and the monitoring of the included contaminants will occur during the period 2016-2018 ([1,6,10]).

The presence of emerging micropollutants affects different sectors of water cycle, with potential harmful effects on different receptors (Figure 1); despite being the farthest compartment from pollution sources (Figure 1), drinking water can also be affected by the presence of micropollutants ([3]). Several studies can be found in literature showing the occurrence of emerging contaminants in surface water (lake and river), and groundwater and drinking water treatment plant influent (*inter alia* [2,3,11–13]). One of the latest reviews about the occurrence of emerging contaminants in the aquatic environment was published by Luo et al. (2014) ([2]); the study summarizes worldwide data about the detection of micropollutants in different water matrices, showing levels from ng L^{-1} to µg L^{-1} in surface water and groundwater. For instance, Figure 2 reports the concentrations of the most abundant micropollutants found in drinking water, compared to their *predicted no effect concentration* (PNEC).

Considering the evolution of drinking water quality legislation, the removal of micropollutants during drinking water production is a current key issue. According to precautionary principles, proper techniques must be adopted and possible upgrades of the plants must be considered to maximize the removal of micropollutants and to face the future drinking water directives and standards.
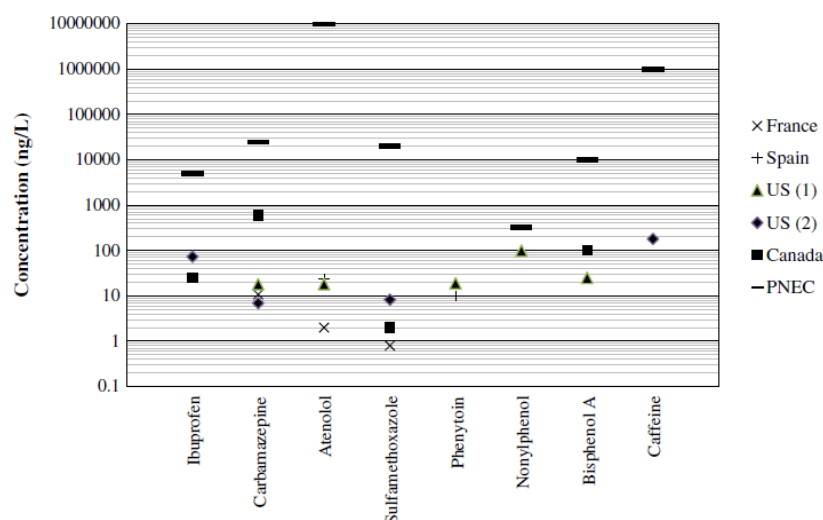
Figure 2 Maximum occurrence concentrations of the most abundant emerging micropollutants in drinking water, compared with their *predicted no effect concentration* (PNEC) ([2]).

2. Activated carbon adsorption

2.1 Process description and fundamentals

Adsorption is a spontaneous mass transfer process during which dissolved species (adsorbates) are transported by diffusion into the grains of a porous adsorbent solid and are then adsorbed onto their extensive inner surface [14]. It is a spontaneous process that takes place if the free energy of adsorption (ΔG_{ads}) is negative [15]. The uptake of an adsorbate onto the solid surface can occur by physical attraction (physical adsorption) or chemical reaction (chemisorption) [14,15]. Physical adsorption is an exothermic process with a heat of adsorption in the range 4-40 kJ mol^{-1} governed by non-specific binding mechanisms like van der Waals forces; it is relatively rapid, reversible and it is the most common mechanism in water treatment applications. Chemisorption involves a chemical reaction through which the adsorbate is chemically bounded (heat of adsorption >200 kJ mol^{-1}) to the adsorbent surface; chemisorption is typically highly selective and irreversible.

Thanks to its high porosity and large internal surface area, activated carbon (AC) is one of the most effective adsorbents in drinking water treatment applications [16]. AC is a heterogeneous adsorbent that, thanks to its wide range of pore sizes, varying from micropores (<2 nm) to macropores (>50 nm), facilitates the adsorbate diffusion from the bulk solution to the adsorption sites [14]. Activated carbons are produced by pyrolytic carbonization of organic raw materials (i.e. mineral coal, wood, coconut shell), conducted at high temperature (850-1000°C) in absence of air, during which volatile components are released and graphite is formed [14]. Afterwards, the porous structure is developed by the activation step, that can be obtained by chemical (using acid solutions, basic solutions or complexing agents) or, more often, by physical treatment (using water vapor, N_2 or CO_2 high temperature gas flow) [14].

2.2 Main factors affecting the adsorption process

The main factors influencing the adsorption process are the characteristics of the adsorbent, of the adsorbate and of the solution. These three factors are discussed in the following sections.

2.2.1   *Adsorbent characteristics*

The main adsorbent characteristics affecting the adsorption process are the pore texture and the surface chemistry; all these properties strictly depend on the preparation methods and the precursor materials [15]. The adsorption capacity and kinetics depend on the accessibility of the adsorbate to the inner surface of the adsorbent, which is strongly related to the pore size [15]. According to IUPAC, pores are classified depending on their size (D_P): micropore (D_P<20 nm), mesopores (20 nm< D_P<500 nm) and macropores (D_P>500 nm). For optimum adsorption, the molecular size of the adsorbate needs to correspond as much as possible to the pore size of the AC [17]. In fact, the enthalpies of adsorption are higher when molecules are adsorbed in pores close to the molecular dimension, increasing adsorption rate and capacity [17]. Pore size distribution of AC usually fall into the small- and medium-size range [17].

High microporosity is usually related to larger surface area, which also determines higher adsorption capacities [18,19]. Surface area of sorbent materials is usually quantified by BET (Brunauer, Emmett, and Teller) method based on gas (usually nitrogen) adsorption, and, for ACs, it can vary from 400 to 1500 m^2 g^{-1} [14,20].

Iodine number (ASTM4604) is a parameter often provided by AC manufacturers and it represents the amount of iodine adsorbed (in milligrams) by 1 g of carbon under standard test conditions. High iodine number corresponds to high surface area and high porosity, and it can be considered a quite good indicator of adsorption capacity towards small size molecules [21].

The surface chemistry of AC determines the surface charge, the hydrophobicity and the electronic density of the graphene layer and affects the interactions with the adsorbates [15]. Surface chemistry depends on the heteroatom content, mainly on the presence and the nature of oxygen complexes [22]. Surface oxygen complexes of acid character (such as carboxyl and phenolic groups) result in a negative charge, while a positive surface charge is given by basic oxygen complexes as well as electron-rich regions in the graphene layer [23]. At first, surface charge influences the interactions and the adsorption of ionic compounds; secondly, the relative abundance of acid and basic functional groups affects the surface hydrophobicity, which determines the hydrophobic interactions [19]. A lower surface acidity gives to AC a higher hydrophobicity, that is favourable of the adsorption of relatively hydrophobic compounds, as in the case of many organic micropollutants [24]. The surface functionalities are usually determined by titration methods [25].

A parameter well correlated with surface chemistry is the pH of point of zero charge (pH_{PZC}), that is the pH at which the total surface charge of carbon particles is null [26]. A lower content of acid functional groups corresponds to higher pH_{PZC}. Carbon pH_{PZC} and the pH of the solution affect the adsorption of charged molecules: the lower is the pH of the solution with respect to the pH_{PZC}, the more protonated is the carbon surface; on the contrary, negative charges increases when the pH of the solution is above the pH_{PZC} [26].

2.2.2   Adsorbate characteristics

The interactions between adsorbent and adsorbate also depend on the physical-chemical properties of the adsorbate; the most important are [14,15]:

− *Molecular size.* Adsorbate molecular size controls the accessibility to the carbon pores: in general, attractive forces like van der Waals forces increases with adsorbate molecular size, enhancing the strength of adsorption bounds.

− *Solubility.* Adsorbate solubility in water determines the hydrophobic interactions with AC and it is a direct indication of adsorption strength: the lower is the solubility, the higher is the adsorption strength.

− *Polarity.* Since water is a polar solvent and AC is a nonpolar adsorbent, more nonpolar compounds are adsorbed more strongly onto AC.

− *Polarizability.* For neutral adsorbates (such as many organic compounds), the interaction forces with the adsorbent increase with adsorbate polarizability.

− *pk_a.* The dissociation of polar compounds and adsorbates with ionic functional groups influences the attraction forces with the adsorbent and it is closely related to the solution pH. The adsorption is generally weaker for more acid and more basic forms, since water-adsorbate forces become stronger and water molecules compete with adsorbate for polar functional groups on AC surface.

2.2.3   Water matrix characteristics

Various physical-chemical characteristics of the water solution as well as its composition control the interactions between adsorbate and adsorbent [14,15,24,27,28]:

− *pH.* As already discussed in the previous sections, the solution pH influences both the carbon surface charge (depending on pH_{PZC}) and the dissociation of the adsorbate (depending on pk_a).

− *Ionic strength.* The attractive or repulsive forces between adsorbent and polar adsorbates are affected by the ionic species present in solution, due to the partial neutralization of the carbon surface charge by means of the dissolved ions (screening effect).

− *Temperature.* Being an exothermic process, adsorption is favoured by lower temperature.

- *Adsorbate initial concentration.* Diffusion mechanisms are enhanced by higher adsorbate concentration, increasing the gradient at the external liquid film and at the inner surface of the adsorbent pores.
- *Presence of competitors.* Adsorbate-adsorbent interactions in multicomponent systems are strongly influenced by competition for adsorption sites. The adsorption of components with weaker affinity to the AC can be reduced by components with stronger affinity, which are preferentially adsorbed. Less-adsorbable compounds can also be replaced by components with stronger affinity. One of the most important and studied competition phenomena is that between organic micropollutants, present at ng L^{-1}-μg L^{-1} levels, and natural organic matter (NOM), generally present at mg L^{-1} levels. Many studies demonstrated that the presence of NOM significantly reduces the AC adsorption capacity towards micropollutants, directly depending on NOM initial concentration and nature (molecular size distribution and chemical composition).

2.3 Adsorption isotherms

Adsorption isotherm is one of the most used assay to quantify the affinity between an adsorbent and an adsorbate. Adsorption isotherm is a curve describing the phenomenon governing the uptake of a substance from the liquid- (bulk solution) to the solid-phase (adsorbent) at a constant temperature and pH under equilibrium conditions [29]. Adsorption equilibrium is established when adsorbate concentration in the bulk solution is in a dynamic balance with the concentration at the adsorbent interface, hence, when all the uptake/release mechanisms have approached an equilibrium [30]. Isotherms are experimentally performed by exposing known quantities of adsorbent and adsorbate in a fixed volume of liquid for a enough long contact time [31]. The mathematical correlation describing adsorption isotherms are typically derived by graphically expressing the residual solute concentration of the adsorbate (C_e, μg L^{-1}) with the adsorbate concentration retained on solid particles (q_e, μg mg^{-1}), whixh is calculated as:

e.1)
$$q_e = (C_0 - C_e)\frac{V}{M}$$

where C_0 (μg L^{-1}) is the initial liquid-phase concentration of the adsorbate, V (L) is the volume of the solution and M (mg) is the mass of the adsorbent [30].

Over the years, a wide variety of equilibrium isotherm models (*inter alia*: Langmuir, Freundlich, Brunauer–Emmett–Teller, Redlich–Peterson, Dubinin–Radushkevich, Temkin, Toth, Koble–Corrigan, Sips, Khan, Hill, Flory–Huggins and Radke–Prausnitz isotherm) have been formulated in terms of three fundamental approaches: kinetic considerations about sorption and desorption rates (i.e. Langmuir), process thermodynamics (i.e. Freundlich) and potential theory (i.e. Dubinin–Radushkevich) [29]. Apart from the mechanistic assumptions behind the mathematical formulations, Giles et al. (1974) [32] proposed a classification of isotherm models based on the shape of the C_e vs. q_e plot; four particular cases can be observed (Figure 3):

- 'C' isotherms, in which the ratio between q_e and C_e remains constant at any concentration;
- 'L' isotherms, in which the ratio between C_e and q_e decreases when increasing the solute concentration, resulting in a concave curve. This kind of isotherm describes a progressive saturation of the adsorbent;
- 'H' isotherms, a particular case of 'L' isotherms, in which the initial slope is very high (approaching to infinite for the lowest C_e values), representing a very high affinity between adsorbate and adsorbent;
- 'S' isotherms, figuring as sigmoidal curves with an inflection point and describing the phenomenon of cooperative adsorption [33].
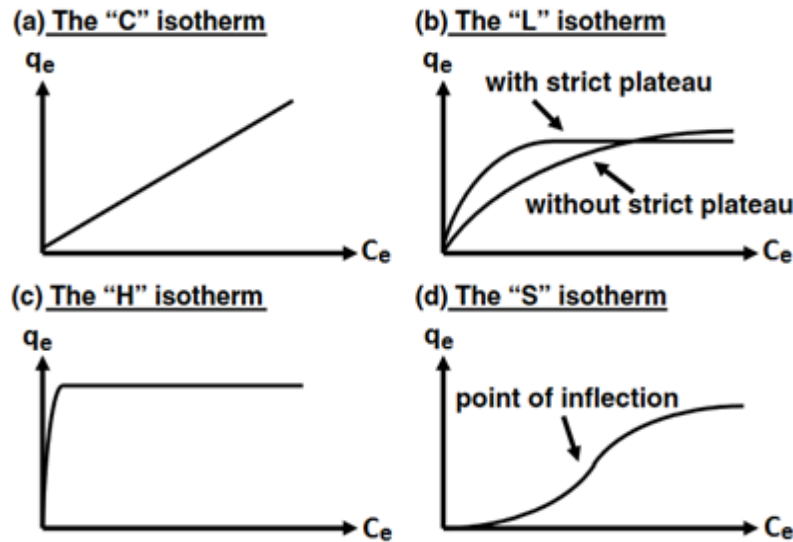
Figure 3 The four main types of isotherms according to Giles et al. (1974) ([32]).

The most widely used isotherm models are Freundlich and Langmuir isotherms, belonging to 'L' or 'H' types ([30]).

Freundlich isotherm ([34]) is an empirical model based on a thermodynamic approach, describing non-ideal and reversible adsorption. It assumes multilayer adsorption, with non-uniform distribution of adsorption heat and affinities over the heterogeneous surface. It is based on the following relation:

e.2)
$$q_e = K_F C_e^{\frac{1}{n}}$$

where K_F (($\mu g\ mg^{-1}$)($L\ \mu g^{-1}$)$^{1/n}$) and $1/n$ (-) are the Freundlich constant and the exponent, respectively. K_F is related to the adsorption capacity; $1/n$ is a function of the strength of the adsorption bond and can vary from 0 (q_e independent on C_e, representing irreversible adsorption) to 1 (q_e strongly dependent on C_e, representing weak adsorption bond).

Langmuir isotherm ([35]), based on kinetic considerations, assumes monolayer adsorption, with adsorbent having a limited adsorption capacity (q_L); all the adsorption sites are assumed to be identical, energetically and sterically independent on the adsorbed quantity. Langmuir equation is expressed as:

e.3)
$$q_e = \frac{q_L K_L C_e}{1 + K_L C_e}$$

where q_L ($\mu g\ mg^{-1}$) is the maximum adsorption capacity and K_L ($L\ \mu g^{-1}$) is the equilibrium constant, related to the strength of the adsorption bond.

The above-mentioned isotherm models describe a mono-component adsorption, in which the uptake of a single adsorbate is not interfered by the presence of other competitors. However, real adsorption systems are commonly characterized by the simultaneous presence of several compounds; in these multicomponent systems, the equilibrium distribution of one adsorbate between solid and liquid phases can be altered by the presence of other solutes ([36]). Various multicomponent isotherm models have been proposed, such as the modified Freundlich model, the modified Langmuir model, the Ideal Adsorbed Solution Theory (IAST) ([30,37,38]). Despite various studies demonstrated the effectiveness of these models in describing binary or tri-components adsorption, they also showed some important limitations: at first, since both mono- and multi-component model parameters must be determined, experimental studies are usually expensive and time-consuming, and they can be not feasible when increasing the number of adsorbates or working with real water matrices ([39]). Moreover, an accurate

and reliable description of the experimental data is not always achieved, probably due to an incomplete description of the all involved competitive mechanisms ([36,38]). For these reasons, further research is still needed to better understand multicomponent adsorption and to develop simple, effective and reliable models to be applied in complex real-water matrices.

2.4 Activated carbon adsorption in water treatment

Activated carbon can be used as powder (Powdered Activated Carbon – PAC) or in the granular form (Granular Activated Carbon – GAC).

PAC, with particle size <74 μm (200 sieve), is usually added to water at various locations in the water treatment train and it is then removed by sedimentation and/or filtration ([14,40]). PAC is usually added to water as a suspension at doses between 5 and 25 mg L^{-1} for contact times between 0.5 and 2 h, even though the best doses and contact times to get satisfactory removal efficiencies should be evaluated by preliminary jar tests ([14]).

The main advantages of using PAC in drinking water treatment are ([41]): 1) it can be applied periodically (only when needed), for instance, during pollution episodes, spring runoff or chemical spill in the water source; 2) it can be used with a relatively small capital cost (specific reactor for adsorption phase is often not required).

For continuous removal of synthetic organic contaminants in the ng L^{-1}-μg L^{-1} concentration range, GAC is usually the preferred solution ([14]). GAC, with particle size >100 mm (140 sieve), is used into fixed-bed contactors (gravity or pressure columns) continuously fed with water.

During the fixed-bed process, a single adsorbate is adsorbed onto the GAC bed cross-sections, which are progressively saturated ([15]). The dynamics of GAC column saturation and the resulting effluent concentration profile of the adsorbate (breakthrough curve) are represented in Figure 4. At a generic time, moving from the top down to the bottom, three parts within the GAC columns could be distinguished ([14]): 1) a first part with completely saturated GAC, with no residual adsorption capacity (in black in Figure 4); 2) a second part, called Mass Transfer Zone (MTZ), in which GAC is not completely saturated and the adsorption takes place (in grey in Figure 4) ; 3) a third part with fresh GAC not containing adsorbate and still having its initial adsorption capacity (in white in Figure 4). As time proceeds, MTZ of the adsorbate slowly moves through the bed, progressively saturating GAC. At the last stages of the process, MTZ moves close enough to the outlet of the column such that measurable adsorbate concentration is observed in the effluent and breakthrough occurs. As the MTZ leaves the GAC column, adsorbate concentration in the effluent start to increase, displaying the breakthrough curve.

Once the breakthrough concentration of the adsorbate (target contaminant) reaches a predetermined level (treatment objective), the GAC in the adsorber is replaced. GAC can be easily removed, reactivated and reused in consecutive treatment cycles.
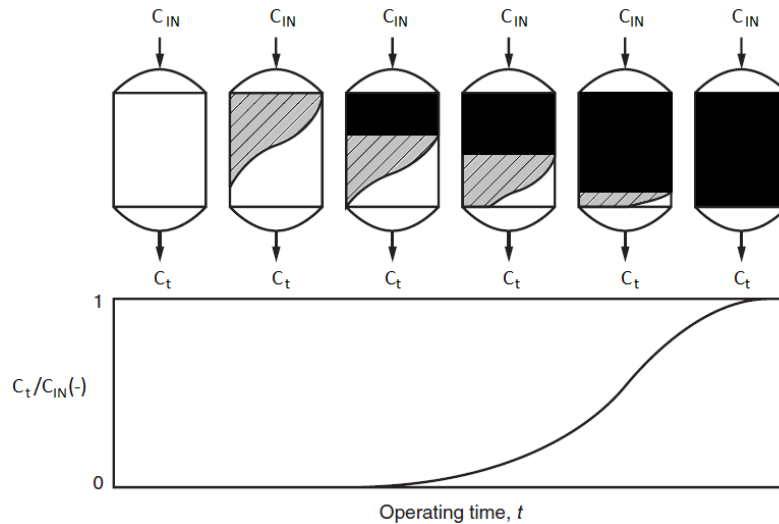
Figure 4 Dynamics of GAC column saturation and the resulting breakthrough curve (C_t: effluent adsorbate concentration at time t; C_{IN}: influent adsorbate concentration) (taken from [14] and modified).

Below, a list of definitions regarding some important parameters for the design and the evaluation of GAC treatment is given ([14]):

- *Bed porosity* (ε_b) is the void volume in the column with respect to the total volume occupied by the adsorbent particles (dimensionless). It corresponds on the fraction of the bed occupied by the solution and its knowledge is particularly important for process modelling (see section 2.5). It can be calculated by the following relationship:

$$e.5) \; \varepsilon_b = 1 - \frac{\rho_b}{\rho_P}$$

  where ρ_P (g_{GAC} L_{GAC}^{-1}) is the adsorbent particle density (typically assumed equal to that of graphite, corresponding to 2000-2200 g L^{-1}) and ρ_b (g_{GAC} L_{BED}^{-1}) is the bed apparent density, corresponding to the density of GAC per volume of GAC bed and experimentally determined according to a standard method (ASTM 2854).

- *Empty Bed Contact Time* (EBCT) is the ratio between the bed volume (V) and the water flow rate (Q). Typically, EBCT values range between 5 and 30 minutes, while water velocity (v) ranges between 5 and 15 m h^{-1}. For fixed EBCT and v values, water flow rate depends on the column cross-sectional area (A).

$$e.4) \qquad EBCT = \frac{V}{Q} = \frac{A\,L}{A\,v}$$

- The *Bed Volumes* (BV) represent the volume of treated water (V_W) at a generic time (t) divided by the GAC volume in the fixed-bed (V):

$$e.8) \qquad BV = \frac{V_W}{V} = \frac{t\,Q}{V}$$

  The breakthrough of a target contaminant from a GAC adsorber is often expressed as a function of the treated BV, instead of the operation time, to consider the effect of water flow rate.

- The *specific throughput* (V_{SP}) is used to quantify GAC adsorber performances and corresponds to V_W divided by the mass of GAC (M):

$$e.6) \qquad V_{SP} = \frac{V_W}{M} = \frac{t_{BT}\,Q}{M} = \frac{t_{BT}\,V}{M\,EBCT}$$

  where t_{BT} is the time to breakthrough at the treatment objective.

− Adsorbent Usage Rate (AUR) is often used alternatively to V_{SP}:

$$\text{e.7)} \qquad AUR = \frac{1}{V_{SP}} = \frac{M}{V_W} = \frac{M}{t_{BT} \, Q} = \frac{M \, EBCT}{t_{BT} \, V}$$

GAC phase can be operated under different configurations ([42–45]). The simplest configuration is a single column, whose operations have been previously described. An option to increase bed lifetime is to operate two single columns in series in a lead-lag configuration ([14]): the influent is first fed into the lead column and then flows through the lag column. MTZ is let move through both the columns until the lag column effluent reaches the treatment objective. Respect to a single column configuration, GAC in lead column is more exploited, and, if the MTZ is shorter than bed length, it can be fully saturated. A further improvement of AUR can be obtained by staggering the replacement of GAC in the two columns ([45]): when breakthrough is reached, only the GAC in the lead column is replaced and it is moved to the lag position. The lead-lag rotation can be repeated, with columns switching places as the effluent concentration from each lag column reaches the treatment objective.

Single column or single lead-lag pair configuration is feasible only when the water flow rate to be treated does not result in too high axial velocities. In large-scale plants, however, the total flow rate must be often split into different parallel columns to comply with hydraulic constrains ([43–45]). A parallel configuration consists of two or more identical single columns that are fed with the same influent in equal proportions, with effluent blending before discharge ([44]). Adsorbent usage rate in parallel configuration can be improved by staggering the column operations, by replacing with fresh GAC only a sub-group of filters when the treatment objective is reached ([45]). In this way, effluent concentration from single filters is let increase above the target limit, but never surpassing the treatment objective in the blended effluent. GAC is so exploited for a longer time, improving the AUR ([45]).

Finally, the advantages of parallel and lead-lag configurations can be combined by adopting a configuration consisting in various pairs of lead-lag filters operating in parallel with effluent blending ([44]).

Previous studies ([42–47]) compared the performances of different filter configurations by simulating the operations of ideal GAC treatment systems under given sets of conditions; most of these studies based the comparisons on two parameters: the shape of the breakthrough profile of the target contaminant, expressed as mass transfer zone (MTZ) length, and the treatment objective, expressed as the ratio of the effluent to the influent concentration (C/C_{IN}). Despite general indications can be derived from the literature, GAC system simulation is always required to properly select the best adsorption configuration in specific real-scale situations ([44]). In fact, for a given configuration, AUR can strongly depend on the size of the plant, involving the total flow rate to be treated and the hydraulic limitations on filter number and size.

2.5 Modelling GAC fixed-bed process

The prediction of contaminant breakthrough in fixed-bed filters is a fundamental step for the design and the management of a GAC system ([48,49]). Different alternative methods to model breakthrough profile were proposed in literature (*inter alia*,[50–52]), but a general procedure has not yet been established. The methods mostly referred to in the literature are based on the use of mathematical models, that are calibrated by means of experimental data ([53]). However, these methods can be extremely different depending on their mathematical formulation and the kind of experiments required to determine case-specific parameters ([50,53]). Overall, the choice of the best model to be adopted is not an easy task, since a compromise between different aspects must be found, such as model accuracy, general validity and complexity in obtaining experimental data ([50,53]).

Looking at the literature, three main groups of breakthrough models could be identified, which are described in the following sections:
 – Homogeneous Surface Diffusion Model (HSDM);
 – Rapid Small Scale Column Tests (RSSCT);
 – Single-equation kinetic models based on pilot-scale data.

2.5.1 Homogeneous Surface Diffusion Model

Various mathematical models have been proposed in the literature based on a physical description of the adsorption process onto GAC in fixed-bed filters, by considering two main steps [54]: 1) the transport within the adsorbent particles; 2) the hydrodynamic transport through the fixed-bed filter.

Regarding the first step, the uptake of an adsorbate onto the adsorbent particle is assumed to be driven by sequential diffusion mechanisms, as represented in Figure 5 [55]: diffusion from the bulk solution to the external adsorbent surface (film diffusion); diffusion in the liquid in the pores (pore diffusion) or along the surface (surface diffusion). When pore diffusion is neglected, the model is called Homogeneous Surface Diffusion Model [55] and it is the mostly referred to [28,55–60].

Assuming isotropic surface diffusion coefficient and particle porosity throughout the spherical adsorbent particle, the equation describing surface diffusion is derived by the mass balance in radial coordinates (r), according to Fick's second law [54]:

e.9)
$$\frac{\partial q}{\partial t} = \frac{1}{r^2}\frac{\partial}{\partial r}\left[D_S r^2 \frac{\partial q}{\partial r}\right]$$

where q ($\mu g\ mg^{-1}$) is the solid-phase concentration and D_S ($m^2\ s^{-1}$) is the surface diffusion coefficient. Initially, solid phase concentration is considered null [54]:

e.10)
$$q\ (t=0, z, r) = 0$$

Boundary conditions at the center (r=0) and at the external surface of the adsorbent grain (r=R_P) are respectively [54]:

e.11)
$$\frac{\partial q}{\partial r} = 0, r=0$$

e.12)
$$\rho_b D_S \frac{\partial q}{\partial r} = k_f (C_b - C_S), r=R_P$$

where ρ_b ($mg\ m^{-3}$) is the bulk density of the adsorbent in the fixed-bed, C_b and C_S ($\mu g\ L^{-1}$) are, respectively, the adsorbate liquid concentration in the bulk solution and at the particle external surface, R_p (m) is the particle radius and k_f ($m\ s^{-1}$) is the external film mass transfer coefficient. In equation e.8, the relationship between q(r=R_P) and C_S is assumed to be governed by isotherm equilibrium and it is commonly expressed by isotherm models like Freundlich or Langmuir equations (e.2 and e.3, respectively) [54].

The transport of the adsorbate through the fixed-bed is modelled assuming plug-flow conditions, constant hydraulic loading rate and liquid axial flux only governed by advection (Figure 6) [54]. The equation is derived by the mass balance over an infinitesimal element of the filter in linear coordinates (z) [54]:

e.13)
$$\varepsilon_b \frac{\partial C_b}{\partial t} + v\frac{\partial C_b}{\partial z} + \frac{3(1-\varepsilon_b)}{R_P}k_f(C_b - C_S) = 0$$

where t (s) is time, ε_b (dimensionless) is the bed porosity and v ($m\ s^{-1}$) is the axial velocity. Initial (e.14) and boundary conditions (e.15) relative to equation e.8 are expressed as follows [54]:

e.14)
$$C_b\ (t=0, z) = 0$$

e.15)
$$C_b\ (t>0, z=0) = C_{IN}$$

where C_{IN} ($\mu g\ L^{-1}$) is the influent concentration.
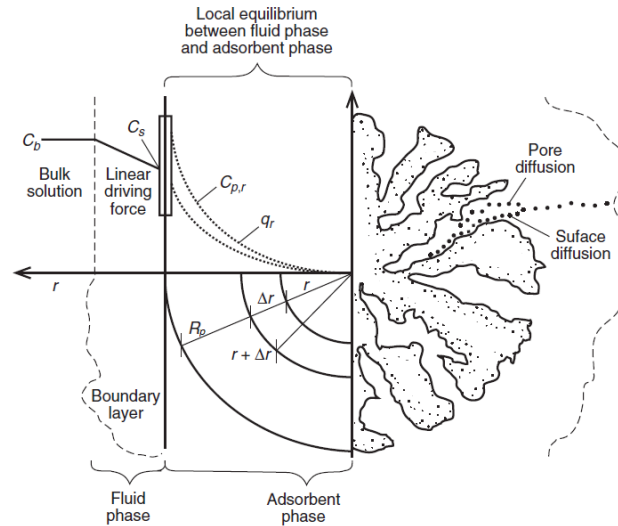
Figure 5 Mechanisms and assumptions incorporated in HSDM ([60]).
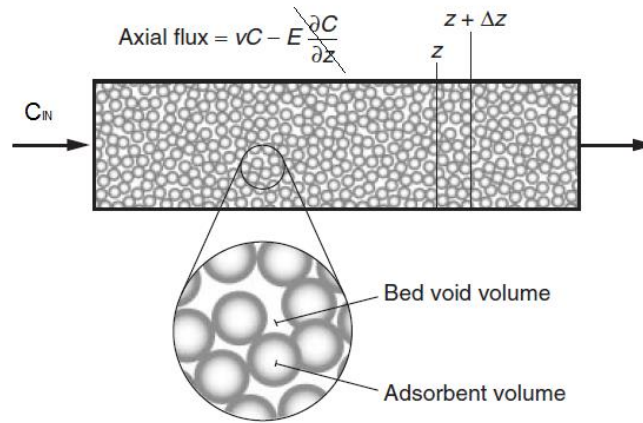
Figure 6 Axial transport through adsorbent fixed-bed according to HSDM ([14]).

Equations e.9-e.15 can be written in dimensionless form by introducing dimensionless variables X, Y, T, R, Z, Dg, St and Bi ([54]):

e.16) $\quad X = \dfrac{C_b}{C_{IN}}$ e.17) $\quad Y = \dfrac{q}{q_{max}}$

e.18) $\quad T = \dfrac{tv}{z\varepsilon_b Dg}$ e.19) $\quad R = \dfrac{r}{R_P}$

e.20) $\quad Z = \dfrac{z}{L}$ e.21) $\quad Dg = \dfrac{\rho_b q_{max}}{\varepsilon_b C_{IN}}$

e.22) $\quad St = \dfrac{k_f M_{GAC}}{\rho_P R_P Q}$ e.23) $\quad Bi = \dfrac{k_f C_{IN} R_P}{\rho_P D_S q_{max}}$

where q_{max} is the q_S value calculated in correspondence of C_{IN} by isotherm equation, L (m) is the bed length, M_{GAC} (mg) is the mass of adsorbent, ρ_P (mg m^{-3}) is the particle density and Q (L s^{-1}) is the water flow rate. HSDM equations e.9 and e.13 written in dimensionless form are as follows ([54]):

e.24) $$\frac{\partial Y}{\partial T} = \frac{St}{Bi}\left(\frac{\partial^2 Y}{\partial R^2} + \frac{2}{R}\frac{\partial Y}{\partial R}\right)$$

e.25)
$$\frac{1}{Dg}\frac{\partial X}{\partial T} + \frac{\partial X}{\partial Z} + 3St(X - X_S) = 0$$

The solute distribution parameter (Dg), the Stanton number (St) and the Biot number (Bi) are parameters of particular interest in describing the adsorption process [14]:

- Dg represents the ratio between the adsorbate mass in the solid-phase and in the liquid-phase at equilibrium, and it is directly related to the adsorption capacity.
- St is the ratio between the transport velocity in the liquid film and the axial velocity (by advection flow) in the fixed-bed; St is related to the length of the MTZ with respect to the filter length: in particular, a higher St corresponds to a lower MTZ-bed length ratio.
- Bi is the ratio between the transport velocity in the liquid film and through the particle surface (surface diffusion). For Bi>30, surface diffusion becomes the rate-limiting step, while for Bi<0.5 the process is limited by liquid film diffusion.

A particular case of HSDM often used in the literature is the Linear Driving Force (LDF) model [54,61]. The intraparticle diffusion rate (e.8) is approximated with a linear relation [54]:

e.26)
$$\frac{\partial q}{\partial t} = \frac{15D_S}{R_P^2}(q(r = R_P) - \bar{q})$$

where $\bar{q}$ is the average solid-phase concentration in the adsorbent particle. This approximation allows to significantly reduce the computation efforts and to increase the calculation speed; on the other hand, LDF results coincide with those of HSDM only in a limited range of values of Bi and St numbers, so the two models cannot be always considered equivalents [54].

HSDM has effectively been used in many papers to predict fixed-bed adsorber dynamics for many contaminants commonly found in drinking water and wastewaters (*inter alia* [28,56–60]). The key-point in using HSDM is the correct determination of case-specific parameters, including equilibrium and kinetic parameters [50]. Equilibrium parameters are commonly estimated by the determination of adsorption isotherms [15], while kinetic parameters, being external (k_f) and intraparticle (D_S) mass-transfer coefficients, can be estimated in different ways. As for external mass-transfer coefficient, many semi-empirical correlations were proposed with some dimensionless parameters, such as Reynolds (Re), Schmidt (Sc), and Sherwood (Sh) numbers (*inter alia* [62–64]). However, these correlations are rarely accurate, strongly depending on the characteristics of the adsorbent grain and the case-specific hydrodynamic conditions [55]. As for intraparticle mass transfer coefficient, different experimental procedures were proposed based on batch kinetic studies, such as Crank, Vermeulen and Reichenberg methods [61,65]. However, the application of coefficients obtained in this way remains limited to the study of adsorbent surface properties and there are only few works in literature in which they were used to simulate breakthrough of a fixed-bed adsorbent [61]. Despite their relative higher complexity, Short Bed Adsorber tests (SBA) [66] are the most widely referred method for experimentally determining both mass transfer coefficients in GAC systems. SBA tests consist in conducting continuous fixed-bed adsorption process into a GAC column enough short to get immediate effluent concentration >0 [66]. The test is carried out until an almost complete (at least 75-80%) breakthrough profile of the adsorbate is observed [66]. An example of SBA test results, obtained by Knappe et al. (1999) [28] for the adsorption of atrazine onto GAC in river water, is reported in Figure 7. Since in SBA tests the column length is much shorter than MTZ, it is possible to separately observe the effects of the two intraparticle diffusion mechanisms: through the liquid film, in the first part of the breakthrough curve, and through the particle surface, in the second part. k_f is so estimated by fitting the initial intercept of the breakthrough curve (typically, the first 30-60 minutes data), while D_S is determined

via a regression along the breakthrough curve, keeping k_f constant ([55,66]). Fitting SBA data usually guarantees an accurate estimation of kinetic coefficients since, as shown in Figure 7, HSDM is much more sensitive to k_f in the first part of the breakthrough curve, while the sensitivity to D_S increases with time ([28]).

Many studies showed the effectiveness of SBA tests in estimating model parameters and simulating breakthrough profiles for several contaminants (*inter alia*, [28,55,57,58]). The main advantage of SBA tests is that kinetic parameters are estimated in a fixed-bed with characteristics (such as particle size, packing conditions, water matrix and axial velocity) very similar to those of the large-scale filter to be modelled ([55]). However, practical applicability of SBA tests for full-scale adsorbers or real water media is not fully established, since most of the works deal only with single-component adsorption and report experimental results obtained under controlled conditions (synthetic solutions, stable experimental parameters). A disadvantage of the breakthrough predictions by the HSDM is that the simulated results may not reflect long-term adsorption capacity variation due, for instance, to organic matter fouling, seasonal trends or biological removal of the contaminants.
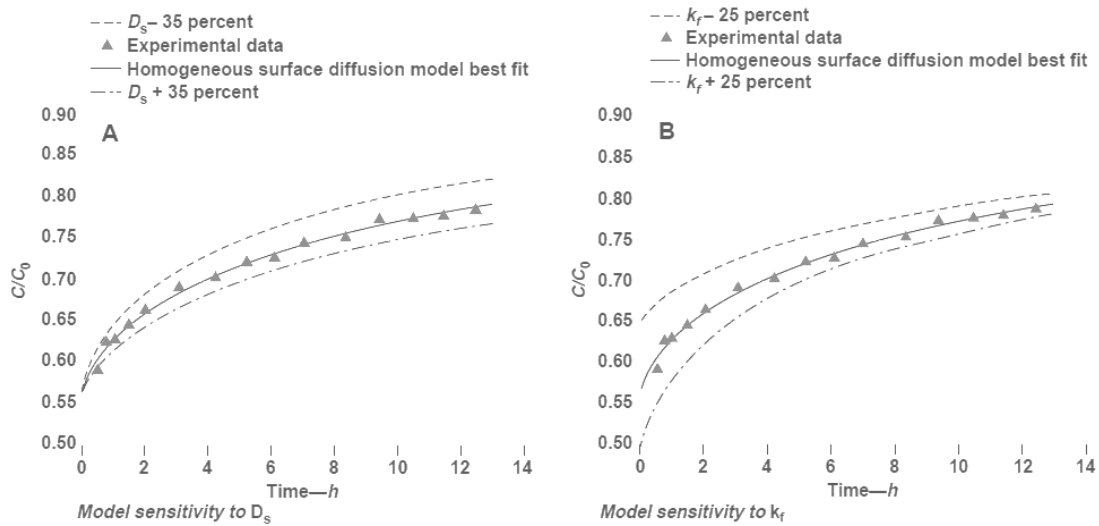
Figure 7 Results of SBA test for the study of atrazine adsorption onto GAC in river water: experimental data, HSDM data fit and model sensitivity to D_S and k_f ([28]).

2.5.2 Rapid Small Scale Column Tests

Rapid Small Scale Column Tests ([51]) are based on the use of mathematical methods to scale-down the full-scale adsorber to a small-scale column, maintaining performance similarity which results in identical breakthrough profiles ([67]). Scaling equations are based on mass transfer models (Pore Surface Diffusion Model) and upon similitude between transport mechanisms at full- and large-scale ([67]). RSSCT equations, developed keeping the dimensionless parameters (pore solute distribution parameter, pore diffusion modulus, surface diffusion modulus, Peclet number and the Stanton number) constant, allows to relate the design of the large column to that of the small column. RSSCT design equations are summarized in Table 1 ([51,68]). There are two common RSSCT design approaches ([68]): the constant diffusivity (CD) and the proportional diffusivity (PD). The CD approach assumes that the effective surface diffusivity is not dependent on particle size, and hence identical for full-scale and small-scale ([51,69,70]). In the CD design the diffusivity factor X (e.27) is equal to zero, so the ratio between $d_{P,SC}$ and $d_{P,LC}$, also called scaling factor, is elevated to the second power. The CD approach is used when target compounds are present at higher concentration and background natural organic matter is present at low concentration (e.g. low TOC groundwater) ([51,69,70]). The PD approach assumes that the effective surface diffusivity is linearly proportional to the particle size (X=1) and surface diffusion is

the controlling mechanism ([51,69,70]). The PD design equations may result in long columns and, thus, large head loss and large water requirement ([51,69,70]). An additional equation (e.31) is so used to reduce the column length and hydraulic loading rate, introducing the minimum Reynolds number ($Re_{SC,min}$). $Re_{SC,min}$ is calculated based on the Schmidt number (e.33), which, in turn, is calculated considering the liquid diffusivity of the smallest (in terms of molecular weight) adsorbate to be monitored during RSSCT run (e.34). The PD design is usually adopted to simulate NOM adsorption and may also offer advantages for simulating micropollutant removal in the presence of NOM ([69]).

An example of RSSCT results is reported in Figure 8 ([69]): TCE breakthrough data observed in small column (RSSCT) designed according to CD and PD approaches were scaled up and compared to large column (pilot-scale) data. None of the two scaling models well fit pilot-scale data, with PD-RSSCT data showing the worst performance. The authors explained these results by the presence of NOM, reducing GAC adsorption capacity by blocking GAC pores and competing for adsorption sites. A fouling factor Y, multiplying the diffusivity factor X, was so introduced to scale the bed volumes from the RSSCT to those expected at the pilot-scale.

Table 1 RSSCT scaling equations (LC: large column, SC: small column, X: diffusivity factor, defined by e.29, t: run duration, v: fluid velocity, Re: Reynolds number, Sc: Schmidt number, D_L: liquid diffusivity of the smallest adsorbate) ([51,68]).

Scaling assumption	Scaling equations	General equations
Constant diffusivity (CD): X=0	e.27) $\dfrac{EBCT_{SC}}{EBCT_{LC}} = \left[\dfrac{d_{P,SC}}{d_{P,LC}}\right]^{2-X} = \dfrac{t_{SC}}{t_{LC}}$ e.28) $\dfrac{v_{SC}}{v_{LC}} = \dfrac{d_{P,LC}}{d_{P,SC}}$	e.31) $\dfrac{v_{SC}}{v_{LC}} = \left[\dfrac{d_{P,LC}}{d_{P,SC}}\right]\dfrac{Re_{SC,min}}{Re_{LC}}$ e.32) $Re = \dfrac{v\,\rho_L\,d_P}{\mu}$
Proportional diffusivity (PD): X=1	e.29) $\dfrac{D_{SC}}{D_{LC}} = \left[\dfrac{d_{P,SC}}{d_{P,LC}}\right]^{X}$ e.30) $\dfrac{EBCT_{SC}}{EBCT_{LC}} = \left[\dfrac{d_{P,SC}}{d_{P,LC}}\right] = \dfrac{t_{SC}}{t_{LC}}$	e.33) $Re_{SC,min} = \dfrac{500}{Sc}$ e.34) $Sc = \dfrac{v}{D_L}$
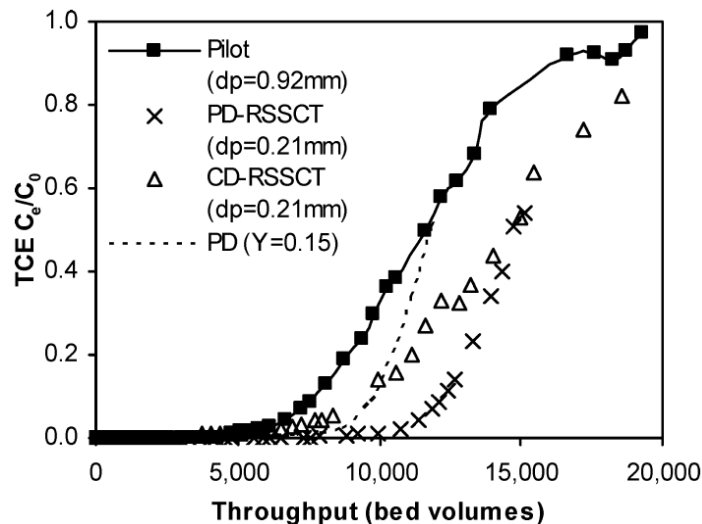
Figure 8 Comparison of pilot-scale TCE breakthrough curves with CD-RSSCT and PD-RSSCT predictions. The dashed line shows the PD-RSSCT data normalized for particle size using a fouling factor Y=0.15 ([69]).

Several works can be found in the literature using RSSCT to predict full-scale GAC performances, simulating the breakthrough of many classes of contaminants (*inter alia*: [52,70–74]). RSSCT are particularly useful when studying the removal of a mixture of contaminants, since the breakthrough curves for each compound can be observed by a single experimental trial, directly displaying the effects of competitive phenomena ([49,52]). Compared to pilot-scale studies, RSSCT are less time consuming and require a much smaller volume of water. Compared to predictive methods based on mathematical models (i.e. HSDM), RSSCT do not require extensive isotherm or kinetic studies to obtain a full-scale performance prediction ([52]). It is pointed out that, when used to scale down full-scale columns characterized by large size, high flow rate and long run duration, scaling equations may result in not feasible RSSCT design parameters, typically corresponding to too long run duration. RSSCT can also have some disadvantages related to their predictive performances ([53,71,73]): at first, as discussed for HSDM, they may not reflect long-term adsorption capacity variations. Secondly, the improper choice of the design approach (CD or PD) may result in very different breakthrough predictions. The design approach can be selected according to literature data which, however, are strictly specific for each combination of adsorbent, adsorbate and water matrix. The dependence of surface diffusivity on particle size should be evaluated by means of adsorption batch experiments that, however, can be time-consuming and expensive.

2.5.3   *Single-equation kinetic models based on pilot-scale data*

Another group of semi-empirical mathematical models widely used in the literature is composed by a single equation describing the concentration-time profile in a continuous flowing system. Breakthrough data over time are expressed as a function of few and easily known operating parameters (i.e. water flow rate, GAC mass, influent concentration) and some model-specific parameters describing adsorption kinetics and capacity ([75–77]). The most often used models belonging to this group are Adams-Bohart, Bed Depth Service Time (BDST), Thomas, Clark and Yoon-Nelson models, whose equations are summarized in Table 2 ([76,77]).

Table 2 Kinetic breakthrough models based on pilot-scale data (C_t: effluent concentration (μg L^{-1}) at time t (s), C_{IN}: influent concentration, L: bed length (m), v: water velocity (m s^{-1}), Q: water flow rate (L s^{-1}), M: GAC mass (mg)).

Model	Equation	Model-specific parameters
Adams-Bohart	e.35) $\frac{C_t}{C_{IN}} = exp\left(k_{AB}C_{IN}t - k_{AB}N_0\frac{L}{v}\right)$	k_{AB}: mass transfer coefficient (L μg^{-1} s^{-1}) N_0: saturation concentration (μg L^{-1})
BDST	e.36) $C_{IN}t = \frac{q_e L}{v} - \frac{1}{k_{BDST}}ln\left(\frac{C_{IN}}{C_t} - 1\right)$	k_{BDST}: rate constant (μg s^{-1}) q_e: maximum adsorption capacity (μg mg^{-1})
Thomas	e.37) $\frac{C_t}{C_{IN}} = [1 + exp(k_{Th}q_e MQ^{-1} - k_{Th}C_{IN}t)]^{-1}$	k_{Th}: rate constant (L μg^{1} s^{-1}) q_e: maximum adsorption capacity (μg mg^{-1})
Clark	e.38) $\frac{C_t}{C_{IN}} = \left(\frac{1}{1+Ae^{-rt}}\right)^{\frac{1}{n-1}}$	A, r: empirical parameters (-) n: Freundlich exponent (-)
Yoon-Nelson	e.39) $\frac{C_t}{C_{IN}-C_t} = exp(k_{YN}t - k_{YN}\tau)$	k_{YN}: rate constant (s^{-1}) τ: time required to 50% breakthrough (s)

Model-specific parameters are typically determined by fitting pilot- or full-scale data, hence requiring relatively time- and cost-consuming experimental trials. Although these models provide a simple and comprehensive approach to run and to evaluate fixed-bed tests, their validity is limited to the range of conditions used ([75–77]). For this reason, this class of models is commonly used to interpret column data and to evaluate the role of operating parameters (i.e. water flow rate, influent concentration, GAC mass), but it has been rarely used to predict breakthrough profile for real-scale GAC filters ([75–77]). In this sense, they cannot be considered predictive models, as HSDM or RSSCT. On the other hand, thanks to their simplicity, they can be useful to simulate GAC systems under different operating conditions and to look for the best design and operating parameters for real-scale applications.

2.6 Micropollutant removal by activated carbon adsorption

Activated carbon adsorption has been proven as an effective technique for the removal of several trace organic and inorganic contaminants in drinking water treatment, including taste- and odour-causing compounds, synthetic organic chemicals, colour-forming organics, DBP precursors and inorganic constituents, such as perchlorate, arsenic, and some heavy metals ([14]). Thanks to its broad-spectrum efficiency, adsorption onto AC is considered as one of the best available environmental control technologies and it is often adopted along the drinking water treatment train ([15]). In fact, the US EPA has designed granular activated carbon (GAC) adsorption as the best available technique for the treatment of many regulated organic pollutants ([74,78]).

Scientific literature provides a wide number of studies in which many combinations of activated carbons and micropollutants have been experimentally tested, for determining AC performances, by means of lab-scale batch tests and continuous fixed-bed tests (at lab-, pilot- or full-scale).

Lab-scale batch tests typically consist in equilibrium isotherm determination or batch experiments to test the effect of PAC dose and contact time on removal efficiencies ([57,79–81]). Independently from the scope, batch tests usually constitute the first experimental information to quantify the adsorbent capacity and to verify the process applicability. A summary of some results available in the literature regarding the adsorption by batch experiments of different kinds of micropollutants is reported in Table 3. Equilibrium isotherms (parameters reported in Table 3) for different volatile organic compounds, such as chlorinated solvents (i.e. PCE, TEC, chloroform) and MTBE, have been determined in various studies ([57,82,83]), showing good adsorption capacities for commercial activated carbons at initial concentrations in the order of 10^2 $\mu g\ L^{-1}$. Commercial ACs were found to be effective towards metals, such as Cr(VI) or As, and perfluorinated acids (PFOS, PFOA), as indicated by isotherms determined in various studies (Table 3). Ormad et al. (2008) ([79]) investigated the adsorption of 43 pesticides in surface water, obtaining removal efficiencies varying from 40% (Desethylatrazine) to 100% (Aldrin), for 10 mg L^{-1} PAC dose and 5 min contact time (using a commercial PAC). Various works can be found studying the simultaneous removal of pesticides, PPCPs and hormones (at initial concentrations in the range 0.01-0.9 $\mu g\ L^{-1}$) from surface waters: removal efficiencies varying in a wide range of values (from 10-15% to >99.5%) testing 1 mg L^{-1} PAC dose for long equilibrium time ([81,84]), or applying 5 mg L^{-1} PAC and 4 h contact time ([74,80]).

Overall, the available studies show that activated carbon is effective in removing a wide range of compounds, having very different physical-chemical properties; however, the adsorption capacities determined in different studies cannot be easily compared due to two main aspects:

– differences in experimental conditions, such as adsorbent type, initial adsorbate concentration, water matrix, carbon dose and contact time;

– differences in reporting experimental results, being expressed in terms of percentage removal efficiency for a given dose and contact time or in terms of isotherm parameters.

Various publications can be found in the literature studying the breakthrough of micropollutants during fixed-bed GAC adsorption (Table 4). Compared to batch studies, dynamic column studies can

provide useful indications for the implementation of GAC process, such as the determination of system size requirement, contact time and sorbent usage rates ([15]). A bibliographic review was carried out to collect breakthrough data for a wide number of compounds, covering the main classes of micropollutants that can affect drinking water sources. Besides micropollutants, some surrogates of DBP precursors were considered, such as DOC, TOC, UVA254, THM and NDMA formation potentials (FP). The main experimental conditions regarding the reviewed publications are summarised in Table 4. It can be noticed that each study differs for some fundamental aspects, such as: the scale of the experiments (lab-scale – RSSCT, pilot- or full-scale), the fixed-bed operating conditions (EBCT, depending on filter size and water flow rate), the water matrix (model solutions, groundwater, surface water or wastewater), the micropollutant influent concentration (from ng L^{-1} to µg L^{-1}), the used GAC. Since all these factors strongly affect the adsorption process, it is not easy to compare the results of different studies. However, literature data may allow to preliminary compare the adsorbability of different compounds and to roughly estimate the behaviour of fixed-bed adsorbers in presence of a mixture of micropollutants.

The results of the reviewed studies are summarized in Figure 9 (a, b and c), showing the ranges of bed volumes to 10% breakthrough ($BV_{10\% \ BT}$) observed for various micropollutants, grouped in different classes. Some studies provided the $BV_{10\% \ BT}$ values observed for different water matrices or GACs; in this case, ranges showed in Figure 9 correspond to the minimum and maximum values reported in the study. When $BV_{10\% \ BT}$ values were not directly provided in the papers, they were visually estimated from the reported breakthrough profiles; in this case, the uncertainty in $BV_{10\% \ BT}$ determination was taken into account and the estimated value was reported in Figure 9 as an interval.

In all the reviewed studies, high-weight organic molecules like pesticides, PPCPs and hormones showed longer breakthroughs, with $BV_{10\% \ BT}$ values almost always $>10 \cdot 10^3$. For these compounds, lower $BV_{10\% \ BT}$ values have been observed for wastewaters (brown bars in Figure 9) with respect to surface waters (blue bars in Figure 9), suggesting a role of water matrix in GAC adsorption capacity. Earlier breakthroughs were observed for more volatile compounds, such as chlorinated solvents and MTBE, perfluorinated acids and hexavalent chromium. Surrogates of DBP precursors, typically associated to the NOM content, were found to have a very early (even immediate) breakthrough, also due to the relatively high influent concentrations, being in the range of mg L^{-1}.

As already pointed out, it is not possible to derive general conclusions comparing results obtained from different works. However, literature data reported in Figure 9 suggest that micropollutants can have very different breakthrough profiles, whit $BV_{10\% \ BT}$ covering a very wide range of values, from $<1 \cdot 10^3$ BV up to $>100 \cdot 10^3$ BV. It can be concluded that, although all these compounds can be effectively removed by GAC, they can appear in the effluent at very different time stages. Hence, in presence of a mixture of micropollutants, the GAC life-time can be extremely different depending on the considered target contaminants and the treatment objectives, with a strong influence on process efficiency.

Table 3 Results of batch-scale experiments for the adsorption of various micropollutants derived from the literature (η: removal efficiency F: Freundlich isotherm; L: Langmuir isotherm). Water matrix (MS: model solution, SW: surface water, GW: groundwater, WW: wastewater), GAC type, initial adsorbate concentration (C_0) and studied compounds are reported.

Ref	Water matrix	GAC type	C_0 ($\mu g\ L^{-1}$)	Compound	Provided results
a	MS	commercial AC (not-specified)	100	chloroform	equilibrium solid-phase conc. $=0.1$-$0.9\ \mu g\ mg^{-1}$ for a liquid-phase conc. of $30\ \mu g\ L^{-1}$
b	MS	Aquacarb 207EA™, Sutcliffe Carbon (UK)	500	PCE	isotherm parameters (T=20°C): F: $K_F=0.78$ ($\mu g\ mg^{-1}$)(L ug^{-1})$^{1/n}$, $1/n=0.68$ L: $q_L=567.4\ \mu g\ mg^{-1}$, $K_L=0.26$ L mg^{-1}
b	MS	Aquacarb 207EA™, Sutcliffe Carbon (UK)	500	TCE	isotherm parameters (T=20°C): F: $K_F=0.44$ ($\mu g\ mg^{-1}$)(L ug^{-1})$^{1/n}$, $1/n=0.68$ L: $q_L=238.7\ \mu g\ mg^{-1}$, $K_L=0.17$ L mg^{-1}
c	SW	CC-602 (US)	100	MTBE	isotherm parameters (T=25°C): F: $K_F=0.07$ ($\mu g\ mg^{-1}$)(L μg^{-1})$^{1/n}$, $1/n=0.66$
d	GW	F400, CAZ and CAP (US)	25-1500	As	isotherm parameters (T=25-35°C): L: $q_L=0.2$-$1.0\ \mu g\ mg^{-1}$, $K_L=(3.2$-$9.0)\cdot10^{-3}$ L μg^{-1}
e	MS	F400, Calgon, and LB830, North Western Acrbon (US)	20-2000	Cr(VI)	isotherm parameters (not-specified T): F: $K_F=0.01$-0.02 ($\mu g\ mg^{-1}$)(L ug^{-1})$^{1/n}$, $1/n=0.4$-0.5
f	WW	PAC, Sigma–Aldrich (SGP)	10-300	PFOA	isotherm parameters (T=25°C): F: $K_F=0.5$-10.0 ($\mu g\ mg^{-1}$)(L ug^{-1})$^{1/n}$, $1/n=0.51$-0.74
f	WW	PAC, Sigma–Aldrich (SGP)	10-300	PFOS	isotherm parameters (T=25°C): F: $K_F=1.1$-17.4 ($\mu g\ mg^{-1}$)(L ug^{-1})$^{1/n}$, $1/n=0.48$-0.66
g	SW	Chiemivall Plus (E)	0.5-0.6	43 pesticides	η (10 mg L^{-1} PAC, 5 min t_C): from 40% (Desethylatrazine) to 100% (Aldrin)
h, i	SW	CC-602, Ambersorb 563 (US)	0.2-0.9	4 pesticides	equilibrium η (1 mg L^{-1} PAC): from 36% (DEET) to 65% (Acetaminophen)
h, i	SW	CC-602, Ambersorb 563 (US)	0.2-0.9	17 PPCP	equilibrium η (1 mg L^{-1} PAC): from 10-15% (Iopromide) to >99.8% (Oxybenzone and Triclosan)
h, i	SW	CC-602, Ambersorb 563 (US)	0.2-0.9	4 hormones	equilibrium η (1 mg L^{-1} PAC): from 20% (Estriol) to 85-90% (Estrone)

(continues in the next page)

26

(continues from the previous page)

j	SW	WPM, Calgon (US)	0.01-0.25	4 pesticides	η (5 mg L^{-1} PAC, 4 h t_C): from 45-50% (DEET) to 70-75% (Acetaminophen)
				17 PPCP	η (5 mg L^{-1} PAC, 4 h t_C): from 15% (Ibuprofen) to 90-95% (Oxybenzone)
				4 hormones	η (5 mg L^{-1} PAC, 4 h t_C): from 60% (Estriol) to 80-85% (Estradiol)
l	SW	WPM, Calgon (US)	0.1	15 pesticides	η (5 mg L^{-1} PAC, 4 h t_C): from 50% (DEET) to 80-85% (DDD)
				25 PPCP	η (5 mg L^{-1} PAC, 4 h t_C): from 15% (Ibuprofen) to >95% (Oxybenzone)
				4 hormones	η (5 mg L^{-1} PAC, 4 h t_C): from 75-80% (Estrone) to 85-90% (Progesterone-A)

a) Abe et al., 2001 [83] b) Erto et al., 2009 [82] c) Rossner and Knappe, 2008 [57]

d) Vitela-Rodriguez and Rangel-Mendez, 2013 [85] e) Han et al., 2000 [86] f) Yu et al., 2012 [87]

g) Ormad et al., 2007 [79] h) Knappe et al., 2007 [84] i) Rossner et al., 2009 [81]

j) Westerhoff et al., 2005 [74] l) Snyder et al., 2007 [80]

Table 4 Details of the reviewed publications: reference, scale of the study, EBCT, water matrix (MS: model solution, GW: groundwater, WW: wastewater, SW: surface water), influent adsorbate concentrations (C_{IN}), GAC types.

Ref.	Scale	EBCT (min)	Water matrix	C_{IN}	GAC
a	RSSCT	1	MS	500 μg L^{-1}	DTO activated carbon (PL)
b	pilot	9.6	MS	100 μg L^{-1}	CC-602 (US)
c	RSSCT	1	GW	40-60 μg L^{-1}	UltraCarb Siemens Water Tech., S.A.I. carbon, iron impregnated SuperDarco carbon (US)
d	pilot	5	GW	100 μg L^{-1}	Calgon Carbon GAC (US)
e	RSSCT	11-14	WW	5-10 mg L^{-1} DOC, 0.10-0.16 UVA254, 0.9-3.6 μg L^{-1} diltiazem, 50-900 ng L^{-1} all the others	Norit Darco GAC, Calgon Filtrasorb F300 (US)
f	pilot	7-7.5	SW	2-4 mg L^{-1} DOC, 2.9 μg L^{-1} iopromide, 3-450 ng L^{-1} all the others	GAC 1240, Norit (US)
g	RSSCT	7.6	SW	100-200 ng L^{-1}	lignite HD400, Norit (US)
h	full	20-21	WW	116-552 ng L^{-1}	HDB, HD3000 and GAC 820 from Norit, WPH from Calgon Carbon (US)
i	RSSCT	10	SW	40-47 μg L^{-1}	Calgon F-400, Norit 1240, Calgon F-200, PicaCarb 830 (US)
j	RSSCT	7.6	SW	6-234 ng L^{-1}	HD4000 and SuperDarco, Norit (US)

a) Pelech et al., 2006 ([88])

b) Rossner and Knappe, 2008 ([57])

c) Chen et al., 2007 ([89])

d) Mc Guire et al., 2006 ([90])

e) Anumol et al., 2015 ([52])

f) Kennedy et al., 2015 ([49])

g) Redding et al., 2009 ([91])

h) Hanigan et al., 2012 ([92])

i) Rodriguez-Fuentes et al. 2005 ([93])

j) Snyder et al., 2007, ([80])

Figure 9 (a) Range of bed volumes to 10% breakthrough (logarithmic scale) for various micropollutants derived from the literature. Letters between brackets indicate the literature reference, according to Table 4. Bar colour indicate the water matrix used in the study.

Figure 9 (b) Range of bed volumes to 10% breakthrough (logarithmic scale) for various micropollutants derived from the literature. Letters between brackets indicate the literature reference, according to Table 4. Bar colour indicate the water matrix used in the study.
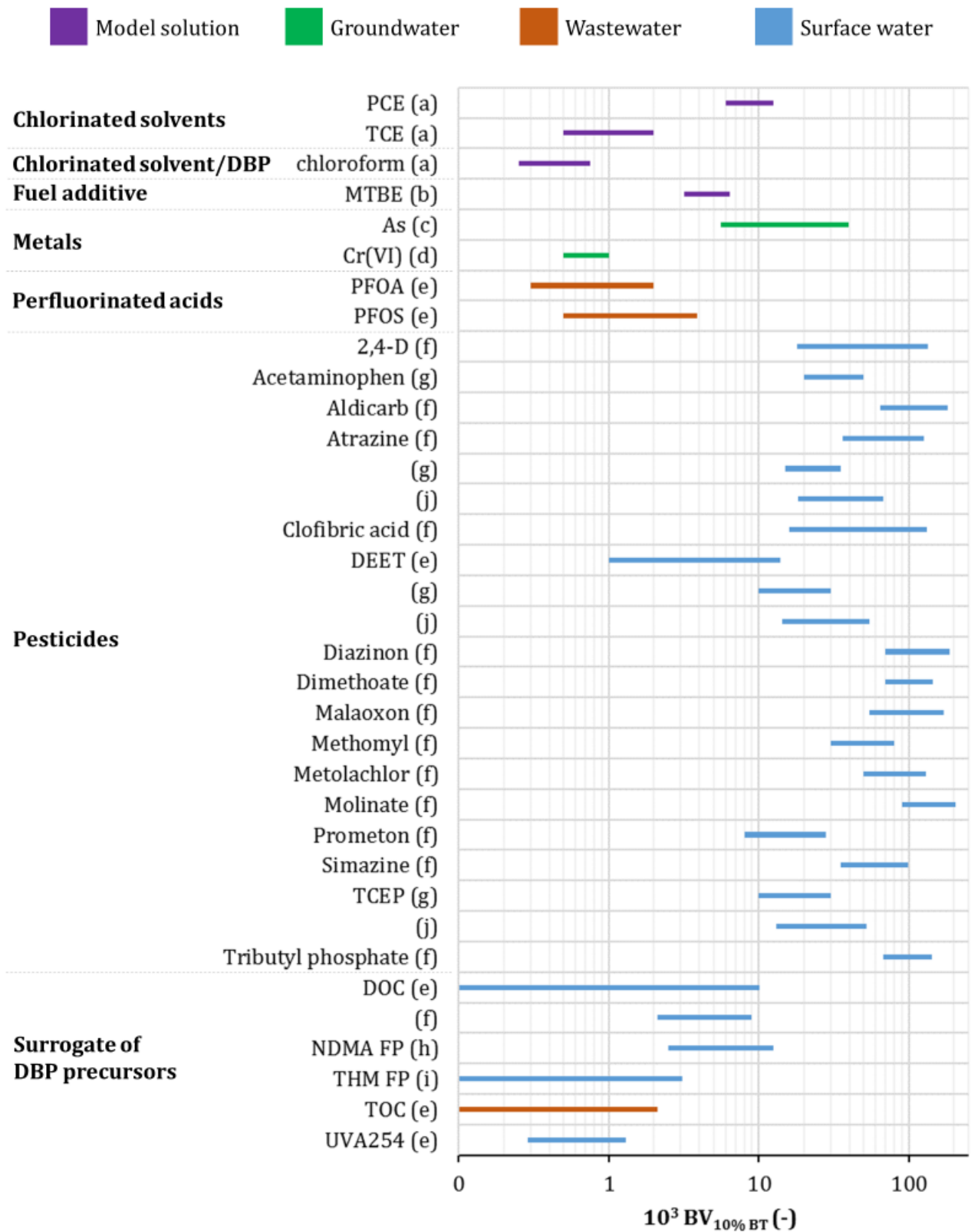
Figure 9 (c) Range of bed volumes to 10% breakthrough (logarithmic scale) for various micropollutants derived from the literature. Letters between brackets indicate the literature reference, according to Table 4. Bar colour indicate the water matrix used in the study.
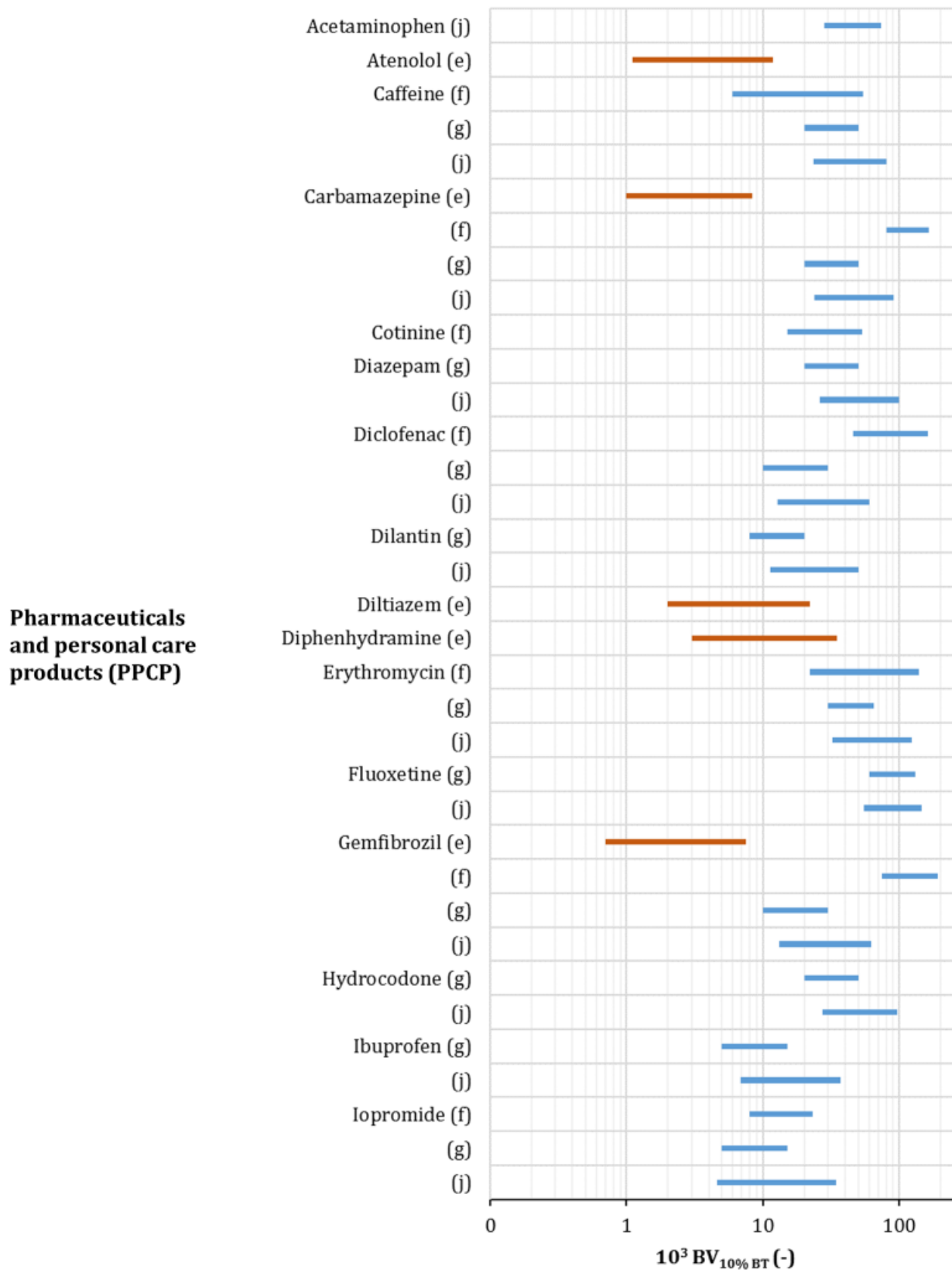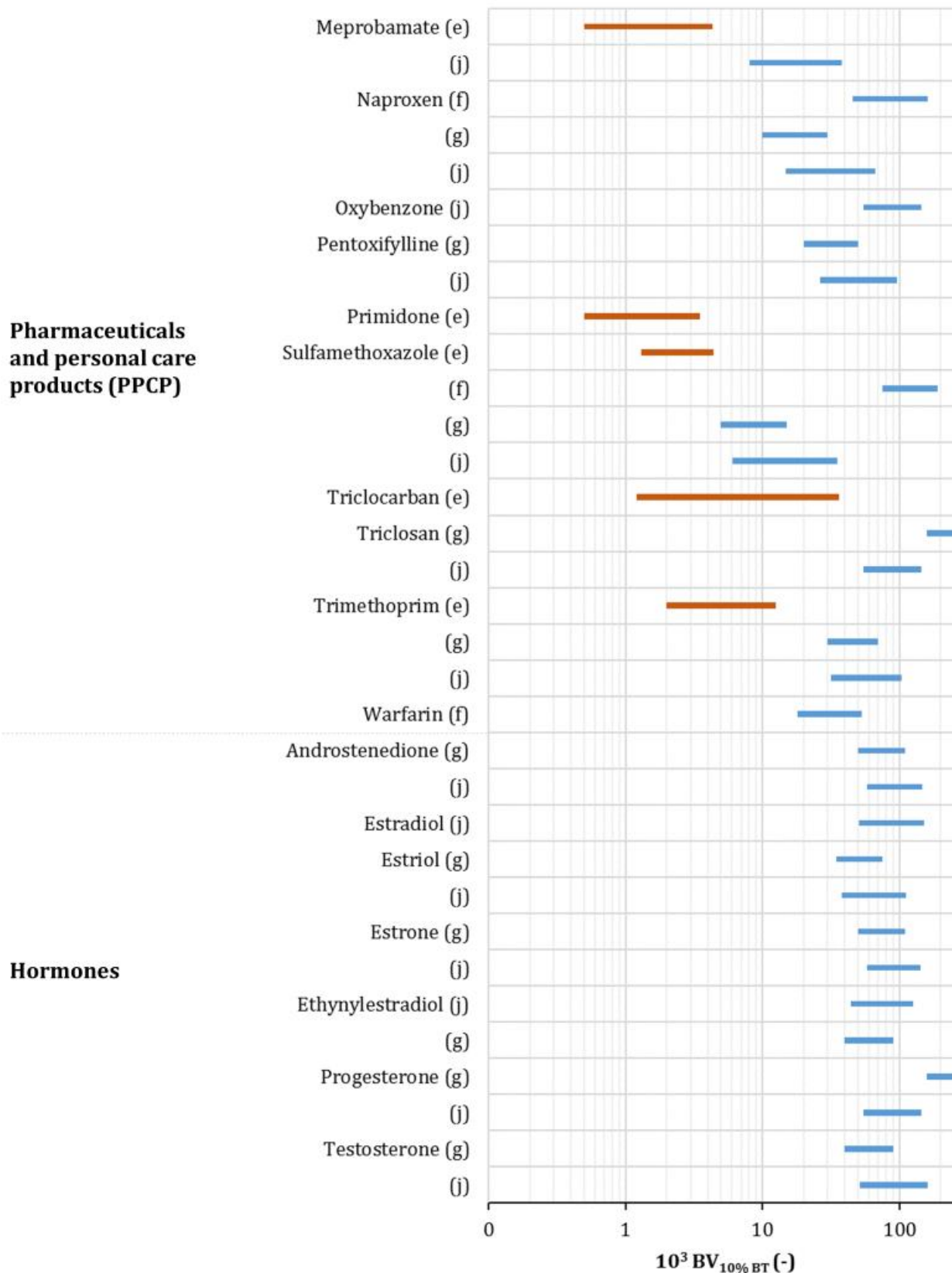
References

(1)   Richardson, S. D.; Kimura, S. Y. Water Analysis: Emerging Contaminants and Current Issues. *Anal. Chem.* **2016**, *88* (1), 546–582.

(2)   Luo, Y.; Guo, W.; Ngo, H. H.; Nghiem, L. D.; Hai, F. I.; Zhang, J.; Liang, S.; Wang, X. C. A review on the occurrence of micropollutants in the aquatic environment and their fate and removal during wastewater treatment. *Sci. Total Environ.* **2014**, *473*, 619–641.

(3)   Mompelat, S.; Le Bot, B.; Thomas, O. Occurrence and fate of pharmaceutical products and by-products, from resource to drinking water. *Environ. Int.* **2009**, *35* (5), 803–814.

(4)   Benjamin W. Lykins; Robert M. Clark. U.S. Drinking-Water Regulations: Treatment Technologies and Cost. *J. Environ. Eng.* **1994**, *120* (4), 783–802.

(5)   Schwarzenbach, R. P.; Escher, B. I.; Fenner, K.; Hofstetter, T. B.; Johnson, C. A.; Gunten, U. von; Wehrli, B. The Challenge of Micropollutants in Aquatic Systems. *Science* **2006**, *313* (5790), 1072–1077.

(6)   Richardson, S. D.; Ternes, T. A. Water analysis: emerging contaminants and current issues. *Anal. Chem.* **2014**, *86* (6), 2813–2848.

(7)   Petrović, M.; Gonzalez, S.; Barceló, D. Analysis and removal of emerging contaminants in wastewater and drinking water. *TrAC Trends Anal. Chem.* **2003**, *22* (10), 685–696.

(8)   Launay, M. A.; Dittmer, U.; Steinmetz, H. Organic micropollutants discharged by combined sewer overflows – Characterisation of pollutant sources and stormwater-related processes. *Water Res.* **2016**, *104*, 82–92.

(9)   Robles-Molina, J.; Gilbert-López, B.; García-Reyes, J. F.; Molina-Díaz, A. Monitoring of selected priority and emerging contaminants in the Guadalquivir River and other related surface waters in the province of Jaén, South East Spain. *Sci. Total Environ.* **2014**, *479*, 247–257.

(10)   Sudhakaran, S.; Lattemann, S.; Amy, G. L. Appropriate drinking water treatment processes for organic micropollutants removal based on experimental and model studies — A multi-criteria analysis study. *Sci. Total Environ.* **2013**, *442*, 478–488.

(11)   Teijon, G.; Candela, L.; Tamoh, K.; Molina-Díaz, A.; Fernández-Alba, A. R. Occurrence of emerging contaminants, priority substances (2008/105/CE) and heavy metals in treated wastewater and groundwater at Depurbaix facility (Barcelona, Spain). *Sci. Total Environ.* **2010**, *408* (17), 3584–3595.

(12)   Lapworth, D. J.; Baran, N.; Stuart, M. E.; Ward, R. S. Emerging organic contaminants in groundwater: a review of sources, fate and occurrence. *Environ. Pollut.* **2012**, *163*, 287–303.

(13)   Estévez, E.; del Carmen Cabrera, M.; Molina-Díaz, A.; Robles-Molina, J.; del Pino Palacios-Díaz, M. Screening of emerging contaminants and priority substances (2008/105/EC) in reclaimed water for irrigation and groundwater in a volcanic aquifer (Gran Canaria, Canary Islands, Spain). *Sci. Total Environ.* **2012**, *433*, 538–546.

(14)   Crittenden, J. C.; Trussell, R. R.; Hand, D. W.; Howe, K. J.; Tchobanoglous, G. *MWH's water treatment: principles and design*; John Wiley & Sons, 2012.

(15)   Moreno-Castilla, C. Adsorption of organic molecules from aqueous solutions on carbon materials. *Carbon* **2004**, *42* (1), 83–94.

(16)   Oxenford, J. L.; Lykins, B. W. Conference summary: practical aspects of the design and use of GAC. *J.-Am. Water Works Assoc.* **1991**, *83* (1), 58–64.

(17)   Almazan-Almazan, M. C.; Perez-Mendoza, M.; Domingo-Garcia, M.; Fernandez-Morales, I.; del Rey-Bueno, F.; Garcia-Rodriguez, A.; Lopez-Garzon, F. J. The role of the porosity and oxygen groups on the adsorption of n-alkanes, benzene, trichloroethylene and 1, 2-dichloroethane on active carbons at zero surface coverage. *Carbon* **2007**, *45* (9), 1777–1785.

(18)   Gao, F.; Zhao, D.-L.; Li, Y.; Li, X.-G. Preparation and hydrogen storage of activated rayon-based carbon fibers with high specific surface area. *J. Phys. Chem. Solids* **2010**, *71* (4), 444–447.

(19)   Liu, Z.; Li, L.; Tang, L.; Shi, R.; Gu, Q.; Liang, X.; Yao, X. Investigation of adsorption performance on 1, 2-dichloroethane by heat and acid modified activated carbon. *J. Environ. Chem. Eng.* **2013**, *1* (3), 131–136.

(20)   Brunauer, S.; Emmett, P. H.; Teller, E. Adsorption of gases in multimolecular layers. *J. Am. Chem. Soc.* **1938**, *60* (2), 309–319.

(21)   Chae, S.-H.; Kim, S.-S.; Jeong, W.; Park, N.-S. Evaluation of physical properties and adsorption capacity of regenerated granular activated carbons (GACs). *Korean J. Chem. Eng.* **2013**, *30* (4), 891–897.

(22)   Di Natale, F.; Lancia, A.; Molino, A.; Musmarra, D. Removal of chromium ions form aqueous solutions by adsorption on activated carbon and char. *J. Hazard. Mater.* **2007**, *145* (3), 381–390.

(23)   Park, S.-J.; Jang, Y.-S.; Shim, J.-W.; Ryu, S.-K. Studies on pore structures and surface functional groups of pitch-based activated carbon fibers. *J. Colloid Interface Sci.* **2003**, *260* (2), 259–264.

(24)   Quinlivan, P. A.; Li, L.; Knappe, D. R. Effects of activated carbon characteristics on the simultaneous adsorption of aqueous organic micropollutants and natural organic matter. *Water Res.* **2005**, *39* (8), 1663–1673.

(25)   Boehm, H. P. Surface oxides on carbon and their analysis: a critical assessment. *Carbon* **2002**, *40* (2), 145–149.

(26)   Lopez-Ramon, M. V.; Stoeckli, F.; Moreno-Castilla, C.; Carrasco-Marin, F. On the characterization of acidic and basic surface sites on carbons by various techniques. *Carbon* **1999**, *37* (8), 1215–1221.

(27)   Newcombe, G.; Morrison, J.; Hepplewhite, C.; Knappe, D. R. U. Simultaneous adsorption of MIB and NOM onto activated carbon: II. Competitive effects. *Carbon* **2002**, *40* (12), 2147–2156.

(28)   Knappe, D. R.; Snoeyink, V. L.; Roche, P.; Prados, M. J.; Bourbigot, M.-M. Atrazine removal by preloaded GAC. *Am. Water Works Assoc. J.* **1999**, *91* (10), 97.

(29)   Foo, [5 5] KY; Hameed, B. H. Insights into the modeling of adsorption isotherm systems. *Chem. Eng. J.* **2010**, *156* (1), 2–10.

(30)   Limousin, G.; Gaudet, J.-P.; Charlet, L.; Szenknect, S.; Barthes, V.; Krimissa, M. Sorption isotherms: a review on physical bases, modeling and measurement. *Appl. Geochem.* **2007**, *22* (2), 249–275.

(31)   ASTM. ASTM D5919-96 method - Standard Practice for Determination of Adsorptive Capacity of Activated Carbon by a Micro-Isotherm Technique for Adsorbates at ppb Concentrations https://www.google.it/search?q=ASTM+D5919-96+method&ie=utf-8&oe=utf-8&client=firefox-b&gfe_rd=cr&ei=S_h2WbKgJ7DCXuGmuLgO (accessed Jul 25, 2017).

(32)   Giles, C. H.; Smith, D.; Huitson, A. A general treatment and classification of the solute adsorption isotherm. I. Theoretical. *J. Colloid Interface Sci.* **1974**, *47* (3), 755–765.

(33)   Hinz, C. Description of sorption data with isotherm equations. *Geoderma* **2001**, *99* (3), 225–243.

(34)   Freundlich, H. M. F.; others. Over the adsorption in solution. *J Phys Chem* **1906**, *57* (385471), 1100–1107.

(35)   Langmuir, I. The constitution and fundamental properties of solids and liquids. Part I. Solids. *J. Am. Chem. Soc.* **1916**, *38* (11), 2221–2295.

(36)   Erto, A.; Lancia, A.; Musmarra, D. A modelling analysis of PCE/TCE mixture adsorption based on Ideal Adsorbed Solution Theory. *Sep. Purif. Technol.* **2011**, *80* (1), 140–147.

(37)   Escudero, C.; Poch, J.; Villaescusa, I. Modelling of breakthrough curves of single and binary mixtures of Cu (II), Cd (II), Ni (II) and Pb (II) sorption onto grape stalks waste. *Chem. Eng. J.* **2013**, *217*, 129–138.

(38)   Najm, I. N.; Snoeyink, V. L.; Lykins Jr, B. W.; Adams, J. Q. Using powdered activated carbon: a critical review. *J. Am. Water Works Assoc.* **1991**, 65–76.

(39)   Tefera, D. T.; Hashisho, Z.; Philips, J. H.; Anderson, J. E.; Nichols, M. Modeling competitive adsorption of mixtures of volatile organic compounds in a fixed-bed of beaded activated carbon. *Environ. Sci. Technol.* **2014**, *48* (9), 5108–5117.

(40)   Eddy, M. &; Burton, F. L.; Stensel, H. D.; Tchobanoglous, G. *Wastewater engineering: treatment and reuse*; McGraw Hill, 2003.

(41)   Knappe, D. R. U.; Matsui, Y.; Snoeyink, V. L.; Roche, P.; Prados, M. J.; Bourbigot, M.-M. Predicting the Capacity of Powdered Activated Carbon for Trace Organic Compounds in Natural Waters. *Environ. Sci. Technol.* **1998**, *32* (11), 1694–1698.

(42)   Denning, P. C.; Dvorak, B. I. Maximizing sorbent life: Comparison of columns in parallel, lead-lag series, and with bypass blending. *Water Environ. Res.* **2009**, *81* (2), 206–216.

(43)   Dvorak, B. I.; Maher, M. K. GAC contactor design for NOM removal: implications of EBCT and blending. *J. Environ. Eng.* **1999**, *125* (2), 161–165.

(44)   Stewart, B. A.; New, C. W.; Hosni, A. A.; Dvorak, B. I. Framework for Evaluating Sorbent Usage Rate of Various Sorption Column Configurations with and without Bypass Blending. *J. Environ. Eng.* **2012**, *139* (4), 554–563.

(45)   Dvorak, B. I.; Morley, M.; Denning, P. Relative Impact on GAC Usage Rates of Operating Strategies for Treatment of Contaminated Groundwater. *Pract. Period. Hazard. Toxic Radioact. Waste Manag.* **2008**, *12* (2), 60–69.

(46)   Crittenden, J. C.; Hand, D. W.; Arora, H.; Lykins Jr, B. W. Design considerations for GAC treatment of organic chemicals. *J. Am. Water Works Assoc.* **1987**, 74–82.

(47)   Hutchins, R. A. Designing granular activated carbon systems for maximum performance. In *Proceedings of the Annual WWEMA Industrial Pollution Conference*; 1977; pp 491–512.

(48)   Yu, Z.; Peldszus, S.; Huck, P. M. Adsorption of selected pharmaceuticals and an endocrine disrupting compound by granular activated carbon. 2. Model prediction. *Environ. Sci. Technol.* **2009**, *43* (5), 1474–1479.

(49)   Kennedy, A. M.; Reinert, A. M.; Knappe, D. R.; Ferrer, I.; Summers, R. S. Full-and pilot-scale GAC adsorption of organic micropollutants. *Water Res.* **2015**, *68*, 238–248.

(50)   Worch, E. Fixed-bed adsorption in drinking water treatment: a critical review on models and parameter estimation. *J. Water Supply Res. Technol.-Aqua* **2008**, *57* (3), 171–183.

(51)   Crittenden, J. C.; Reddy, P. S.; Arora, H.; Trynoski, J.; Hand, D. W.; Perram, D. L.; Summers, R. S. Predicting GAC performance with rapid small-scale column tests. *J. Am. Water Works Assoc.* **1991**, 77–87.

(52)   Anumol, T.; Sgroi, M.; Park, M.; Roccaro, P.; Snyder, S. A. Predicting trace organic compound breakthrough in granular activated carbon using fluorescence and UV absorbance as surrogates. *Water Res.* **2015**, *76*, 76–87.

(53)   Jarvie, M. E.; Hand, D. W.; Bhuvendralingam, S.; Crittenden, J. C.; Hokanson, D. R. Simulating the performance of fixed-bed granular activated carbon adsorbers: Removal of synthetic organic chemicals in the presence of background organic matter. *Water Res.* **2005**, *39* (11), 2407–2421.

(54)   Sperlich, A.; Schimmelpfennig, S.; Baumgarten, B.; Genz, A.; Amy, G.; Worch, E.; Jekel, M. Predicting anion breakthrough in granular ferric hydroxide (GFH) adsorption filters. *Water Res.* **2008**, *42* (8), 2073–2082.

(55)   Richard, D.; Núñez, M. de L. D.; Schweich, D. Adsorption of complex phenolic compounds on active charcoal: breakthrough curves. *Chem. Eng. J.* **2010**, *158* (2), 213–219.

(56)   Pérez-Foguet, A.; Casoni, E.; Huerta, A. Dimensionless analysis of HSDM and application to simulation of breakthrough curves of highly adsorbent porous media. *J. Environ. Eng.* **2012**, *139* (5), 667–676.

(57)   Rossner, A.; Knappe, D. R. MTBE adsorption on alternative adsorbents and packed bed adsorber performance. *Water Res.* **2008**, *42* (8), 2287–2299.

(58)   Ho, L.; Newcombe, G. Granular activated carbon adsorption of 2-methylisoborneol (MIB): pilot- and laboratory-scale evaluations. *J. Environ. Eng.* **2010**, *136* (9), 965–974.

(59)   Schideman, L. C.; Mariñas, B. J.; Snoeyink, V. L.; Campos, C. Three-component competitive adsorption model for fixed-bed and moving-bed granular activated carbon adsorbers. Part I. Model development. *Environ. Sci. Technol.* **2006**, *40* (21), 6805–6811.

(60)   Zhang, Q.; Crittenden, J.; Hristovski, K.; Hand, D.; Westerhoff, P. User-oriented batch reactor solutions to the homogeneous surface diffusion model for different activated carbon dosages. *Water Res.* **2009**, *43* (7), 1859–1866.

(61)   García-Mateos, F. J.; Ruiz-Rosas, R.; Marqués, M. D.; Cotoruelo, L. M.; Rodríguez-Mirasol, J.; Cordero, T. Removal of paracetamol on biomass-derived activated carbon: modeling the fixed bed breakthrough curves using batch adsorption experiments. *Chem. Eng. J.* **2015**, *279*, 18–30.

(62)   Williamson, J. E.; Bazaire, K. E.; Geankoplis, C. J. Liquid-phase mass transfer at low Reynolds numbers. *Ind. Eng. Chem. Fundam.* **1963**, *2* (2), 126–129.

(63)   Wilson, E. J.; Geankoplis, C. J. Liquid mass transfer at very low Reynolds numbers in packed beds. *Ind. Eng. Chem. Fundam.* **1966**, *5* (1), 9–14.

(64)   Yoshida, F.; Ramaswami, D.; Hougen, O. A. Temperatures and partial pressures at the surfaces of catalyst particles. *AIChE J.* **1962**, *8* (1), 5–11.

(65)   Cotoruelo, L. M.; Marqués, M. D.; Rodríguez-Mirasol, J.; Rodríguez, J. J.; Cordero, T. Lignin-based activated carbons for adsorption of sodium dodecylbenzene sulfonate: Equilibrium and kinetic studies. *J. Colloid Interface Sci.* **2009**, *332* (1), 39–45.

(66)   Weber Jr, W. J.; Liu, K. T. Determination of mass transport parameters for fixed-bed adsorbers. *Chem. Eng. Commun.* **1980**, *6* (1–3), 49–60.

(67)   Sperlich, A.; Werner, A.; Genz, A.; Amy, G.; Worch, E.; Jekel, M. Breakthrough behavior of granular ferric hydroxide (GFH) fixed-bed adsorption filters: modeling and experimental approaches. *Water Res.* **2005**, *39* (6), 1190–1198.

(68)   Westerhoff, P.; Highfield, D.; Badruzzaman, M.; Yoon, Y. Rapid small-scale column tests for arsenate removal in iron oxide packed bed columns. *J. Environ. Eng.* **2005**, *131* (2), 262–271.

(69)   Corwin, C. J.; Summers, R. S. Scaling trace organic contaminant adsorption capacity by granular activated carbon. *Environ. Sci. Technol.* **2010**, *44* (14), 5403–5408.

(70)   Morley, M. C.; Henke, J. L.; Speitel Jr, G. E. Adsorption of RDX and HMX in rapid small-scale column tests: Implications for full-scale adsorbers. *J. Environ. Eng.* **2005**, *131* (1), 29–37.

(71)   Corwin, C. J.; Summers, R. S. Adsorption and desorption of trace organic contaminants from granular activated carbon adsorbers after intermittent loading and throughout backwash cycles. *Water Res.* **2011**, *45* (2), 417–426.

(72)   Summers, R. S.; Kim, S. M.; Shimabuku, K.; Chae, S.-H.; Corwin, C. J. Granular activated carbon adsorption of MIB in the presence of dissolved organic matter. *Water Res.* **2013**, *47* (10), 3507–3513.

(73)   Knappe, D. R.; Snoeyink, V. L.; Roche, P.; Prados, M. J.; Bourbigot, M.-M. The effect of preloading on rapid small-scale column test predictions of atrazine removal by GAC adsorbers. *Water Res.* **1997**, *31* (11), 2899–2909.

(74)   Westerhoff, P.; Yoon, Y.; Snyder, S.; Wert, E. Fate of endocrine-disruptor, pharmaceutical, and personal care product chemicals during simulated drinking water treatment processes. *Environ. Sci. Technol.* **2005**, *39* (17), 6649–6663.

(75)   Aksu, Z.; Gönen, F. Biosorption of phenol by immobilized activated sludge in a continuous packed bed: prediction of breakthrough curves. *Process Biochem.* **2004**, *39* (5), 599–613.

(76)   Baral, S. S.; Das, N.; Ramulu, T. S.; Sahoo, S. K.; Das, S. N.; Chaudhury, G. R. Removal of Cr (VI) by thermally activated weed Salvinia cucullata in a fixed-bed column. *J. Hazard. Mater.* **2009**, *161* (2), 1427–1435.

(77)   Han, R.; Wang, Y.; Zhao, X.; Wang, Y.; Xie, F.; Cheng, J.; Tang, M. Adsorption of methylene blue by phoenix tree leaf powder in a fixed-bed column: experiments and prediction of breakthrough curves. *Desalination* **2009**, *245* (1–3), 284–297.

(78)   Sotelo, J. L.; Rodríguez, A.; Álvarez, S.; García, J. Removal of caffeine and diclofenac on activated carbon in fixed bed column. *Chem. Eng. Res. Des.* **2012**, *90* (7), 967–974.

(79)   Ormad, M. P.; Miguel, N.; Claver, A.; Matesanz, J. M.; Ovelleiro, J. L. Pesticides removal in the process of drinking water production. *Chemosphere* **2008**, *71* (1), 97–106.

(80)   Snyder, S. A.; Adham, S.; Redding, A. M.; Cannon, F. S.; DeCarolis, J.; Oppenheimer, J.; Wert, E. C.; Yoon, Y. Role of membranes and activated carbon in the removal of endocrine disruptors and pharmaceuticals. *Desalination* **2007**, *202* (1), 156–181.

(81)   Rossner, A.; Snyder, S. A.; Knappe, D. R. Removal of emerging contaminants of concern by alternative adsorbents. *Water Res.* **2009**, *43* (15), 3787–3796.

(82)   Erto, A.; Andreozzi, R.; Di Natale, F.; Lancia, A.; Musmarra, D. Experimental and isotherm-models analysis on TCE and PCE adsorption onto activated carbon. **2009**.

(83)   Abe, I.; Fukuhara, T.; Maruyama, J.; Tatsumoto, H.; Iwasaki, S. Preparation of carbonaceous adsorbents for removal of chloroform from drinking water. *Carbon* **2001**, *39* (7), 1069–1073.

(84)   Knappe, D. R.; Rossner, A.; Snyder, S. A.; Strickland, C. *Alternative adsorbents for the removal of polar organic contaminants*; American Water Works Association, 2007.

(85)   Vitela-Rodriguez, A. V.; Rangel-Mendez, J. R. Arsenic removal by modified activated carbons with iron hydro(oxide) nanoparticles. *J. Environ. Manage.* **2013**, *114*, 225–231.

(86)   Han, I.; Schlautman, M. A.; Batchelor, B. Removal of hexavalent chromium from groundwater by granular activated carbon. *Water Environ. Res.* **2000**, *72* (1), 29–39.

(87)   Yu, J.; Lv, L.; Lan, P.; Zhang, S.; Pan, B.; Zhang, W. Effect of effluent organic matter on the adsorption of perfluorinated compounds onto activated carbon. *J. Hazard. Mater.* **2012**, *225*, 99–106.

(88)   Pelech, R.; Milchert, E.; Bartkowiak, M. Fixed-bed adsorption of chlorinated hydrocarbons from multicomponent aqueous solution onto activated carbon: Equilibrium column model. *J. Colloid Interface Sci.* **2006**, *296* (2), 458–464.

(89)   Chen, W.; Parette, R.; Zou, J.; Cannon, F. S.; Dempsey, B. A. Arsenic removal by iron-modified activated carbon. *Water Res.* **2007**, *41* (9), 1851–1858.

(90)   McGuire, M. J.; Blute, N. K.; Seidel, C.; Qin, G.; Fong, L. Pilot-scale studies of hexavalent chromium removal from drinking water. *J. Am. Water Works Assoc.* **2006**, *98* (2), 134–143.

(91)   Redding, A. M.; Cannon, F. S.; Snyder, S. A.; Vanderford, B. J. A QSAR-like analysis of the adsorption of endocrine disrupting compounds, pharmaceuticals, and personal care products on modified activated carbons. *Water Res.* **2009**, *43* (15), 3849–3861.

(92)   Hanigan, D.; Zhang, J.; Herckes, P.; Krasner, S. W.; Chen, C.; Westerhoff, P. Adsorption of N-nitrosodimethylamine precursors by powdered and granular activated carbon. *Environ. Sci. Technol.* **2012**, *46* (22), 12630–12639.

(93)   Rodriguez-Fuentes, R.; Hilts, B. A.; Dvorak, B. I. Disinfection by-product precursor adsorption as function of GAC properties: Case study. *J. Environ. Eng.* **2005**, *131* (10), 1462–1465.

<div align="right">CHAPTER 2</div>

Design of the research

Water sources in industrialized areas are often contaminated by a wide variety of anthropogenic micropollutants. Despite they are present at low concentrations (sub-ng L^{-1} - μg L^{-1}), these contaminants may represent a health hazard, because of their extremely high toxicity or carcinogenicity. Various micropollutants have already been regulated and many countries specified limits for their concentration in drinking water. On the other hand, a relevant number of compounds is still unregulated or just candidate for future regulation, depending on the research on their potential health effects and occurrence in water sources. Proper control strategies must be so adopted in drinking water facilities to comply with quality standards and to face possible regulation changes.

Adsorption onto granular activated carbon (GAC) is considered as one of the best available drinking water treatment technologies. GAC effectiveness was demonstrated for several classes of micropollutants; however, GAC adsorption capacity can be extremely different towards the variety of contaminants affecting drinking water sources. Depending on water composition and quality standards, two questions must be answered for the design of an efficient water treatment train including a GAC adsorption phase:

– for which contaminants activated carbon adsorption is the most efficient technique?
– how to optimize adsorption phase performances (in terms of removal efficiency and economical costs)?

Scientific literature is not always enough exhaustive to answer these questions and proper experimental and simulation tools must be adopted. For a given target contaminant, there could be three main engineering tasks to be faced to optimize the adsorption phase and, consequently, the whole water treatment process:

1) evaluation of GAC adsorption efficiency and comparison with the removal extent of other available techniques;
2) process simulation under full-scale conditions;
3) definition of the optimal design and operating criteria.

In the present PhD thesis, the problem of optimizing GAC treatment process was faced considering three of the main classes of micropollutants that can affect drinking water treatment plants:

– synthetic organic compounds;
– heavy metals;
– disinfection by-products.

For each class, specific contaminants were selected and, depending on the state of the art, one or more of the above-mentioned engineering tasks regarding GAC treatment optimization were investigated.

The whole PhD thesis is divided in five thematic chapters, each one presenting a research work structured as a scientific paper: an introduction presenting the state of the art and the goals of the study, the definition of materials and methods, the presentation and the discussion of the results and the conclusions.

A schematic view of the research work, showing the engineering tasks investigated per each class of contaminants, and a summary of the PhD thesis structure are reported in Figure 1 and Table 1.

Chapter 3 deals with the removal of heavy metals. Specifically, the study is focused on hexavalent chromium, Cr(VI), for which more restrictive regulation limits are currently being introduced in various parts of the world (i.e. Italy and California). Several processes, including activated carbon adsorption, are considered effective in chromium removal, but their performances strongly depend on the specific conditions. Due to the inconsistency of literature data, obtained in a wide variety of

experimental conditions, comparison of different techniques is not easy. The aim of this chapter was to preliminary assess the effectiveness of GAC adsorption for the treatment of a real groundwater matrix contaminated by Cr(VI) and other inorganic and organic contaminants. Ion exchange was also studied and considered as benchmark to evaluate GAC performances. The two treatments were experimentally tested at laboratory scale determining equilibrium isotherms and sorption kinetics. The obtained data allowed, at first, to preliminary assess the effectiveness of the two techniques towards chromium and their full-scale feasibility; secondly, their global efficiency was evaluated looking at the removal of the other contaminants present in the tested water, namely ionic species (nitrate, sulphate) and organic micropollutants (chlorinated solvents, pesticides).

Chapters 4 and 5 deals with disinfection by-products. *N*-nitrosamines are a group of by-products of emerging healthy and regulatory concern, characterized by extremely high carcinogenicity at drinking water concentrations in the low ng L^{-1} level. Previous studies demonstrated that many chemical constituents of pesticides, pharmaceuticals, personal care and household products are potential *N*-nitrosamine precursors. Since these compounds can easily enter the aquatic system, their occurrence in drinking water sources must be carefully taken into consideration, because of the possibility to form *N*-nitrosamines during water disinfection.

The aim of the study presented in Chapter 4 was to investigate *N*-nitrosamine formation in presence of various precursors deriving from PPCPs. Lab-scale experiments on model solutions were carried out to quantify the potential hazardousness of the studied precursors, to identify the formed by-products and to study the reaction mechanisms. In Chapter 5, activated carbon adsorption was tested as possible solution for reducing the *N*-nitrosamine formation potential associated to the studied precursors. Lab-scale tests were conducted to preliminary assess the performances of activated carbon in two possible treatment solutions: adsorption phase before disinfection, to reduce precursor concentration; and adsorption phase after disinfection, to remove the formed *N*-nitrosamines.

Chapter 6 and 7 deals with synthetic organic compounds, in particular organic chlorinated solvents such as perchloroethylene, trichloroethylene and chloroform. Fixed-bed adsorption process is considered the best available technique for this class of contaminants. However, in presence of a mixture of these micropollutants, the optimal design and management criteria must be defined to minimize adsorbent usage rate and the related treatment costs. A fundamental step for process optimization is the breakthrough prediction for fixed-bed filters, that, however, is one of the main current engineering issues. Various predictive models have been proposed in the literature, but there is still not a well-established procedure for real-scale applications. High model accuracy usually requires more complex mathematical formulations and experiments to determine case-specific parameters. Moreover, the practical applicability of the models proposed in the literature is not fully established with real water media. An experimental activity consisting in lab-scale tests and monitoring campaigns of various full-scale operating GAC filters was carried out; obtained data allowed to test different modelling approaches and to address two engineering tasks: process simulation, namely the prediction of GAC filter breakthrough (Chapter 6), and optimization of process design and management (Chapter 7).

The study presented in Chapter 6 faces the problem of breakthrough prediction for a full-scale adsorption system, treating groundwater contaminated by different organic chlorinated solvents. The Homogeneous Surface Diffusion Model (HSDM), requiring relatively complex experimental and computational issues, but theoretically providing a higher accuracy, was selected. Practical criteria for the application of HSDM to real multi-component water solution were proposed, considering two main aspects: 1) the experimental determination of case-specific model parameters, considering competition effects between the adsorbed contaminants; 2) the simulation of large-scale filters, accounting for time-varying operating parameters.

The aim of the work presented in Chapter 7 was to determine the optimal design parameters and operating strategy for a large-scale GAC system treating groundwater contaminated by several organic micropollutants (chlorinated solvents and pesticides). Firstly, the breakthrough profiles of the studied contaminants were monitored from different full-scale operating GAC filters. Breakthrough data were used to calibrate a single-equation model and to find a correlation with GAC properties. Different scenarios were then simulated to evaluate the performances of different GAC phase configurations, as a function of the considered target contaminant and the treatment objective, varying the main design parameters and management strategies.

The carried-out research works deepened various aspects of the application of GAC adsorption process for the removal of micropollutants from drinking water. Independently form the specific contaminant, the following general conclusion could be derived:

- lab-scale experiments, as equilibrium adsorption tests, are the first experimental tool to evaluate the GAC effectiveness towards a contaminant. The use of real-water matrices in the experiments is fundamental to really test the process performances and to evaluate the most affecting factors;

- various modelling approaches are available to simulate the fixed-bed adsorption process, each one having pros and cons; the choice of the most proper one is a trade-off between various factors: model accuracy, easiness in parameter estimation, adaptation and sensitivity to real-scale conditions, applicability to different operating conditions;

- the simulation of the full-scale process is fundamental to determine the optimal design and management parameters. However, a life-cycle thinking approach is required for a comprehensive evaluation of the economic and environmental costs of the process and for the comparison with other available techniques, considering all the aspects involved in the process implementation.
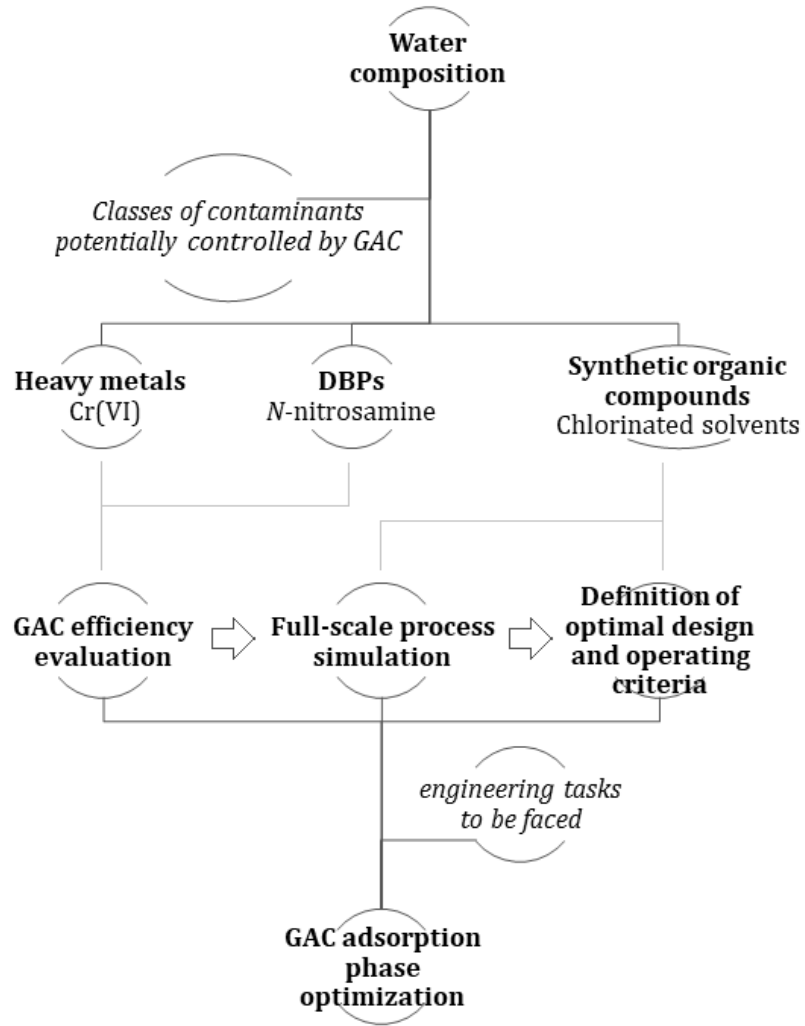
Figure 1 Schematic view of the research work.

Table 1 Structure of the PhD thesis.

Investigated engineering tasks	Contaminants	Chapter
1) GAC efficiency evaluation	**Heavy metals** Cr(VI)	3
	DBPs *N*-nitrosamines	4, 5
2) Full-scale process simulation	**Synthetic organic compounds**	6
3) Definition of optimal design and operating criteria	Chlorinated solvents	7

CHAPTER 3

Feasibility assessment of chromium removal from groundwater for drinking purposes by sorption on granular activated carbon and strong base anion exchange

Abstract

The goal of this study was to compare the performances of strong base anion (SBA) exchange and activated carbon adsorption in the removal of hexavalent chromium, Cr(VI), from a real groundwater matrix exploited for drinking purposes. Two SBA resins and three granular activated carbons (GAC) were tested by batch experiments for kinetics and equilibrium isotherm determination. SBA resins showed higher affinity towards Cr(VI) (present in raw water at about 20 μg L^{-1}) with respect to the GACs, with faster kinetics and higher equilibrium adsorption capacities. Among GACs, vegetal-based carbons showed higher Cr(VI) removal efficiencies than the mineral-based carbon, which can be related to the more developed textural properties. SBA resins also displayed relevant removal capacities towards nitrate and sulfate (present at mg L^{-1} concentration levels), while boron (present at about 60 μg L^{-1}) was effectively removed by GACs. Batch experiment results were used to estimate the chromium throughputs for the studied materials, to preliminary compare their performances in a real-scale application. The monitoring of a real-scale GAC adsorption phase permitted to validate throughputs estimation and confirmed that, despite being effective towards synthetic organics, GAC adsorption is a not feasible solution for Cr(VI) removal, with extremely early breakthrough. SBA exchange process resulted to be the most preferable solution, providing the best sorbent usage rates. However, SBA resin usage rates can strongly increase when considering the removal of nitrate and sulfate ions, requiring much shorter cycle times.

Keywords: chromium; activated carbon adsorption; anion exchange; groundwater; drinking water.

1. Introduction

Heavy metals are important sources of environmental pollution in industrialized areas, because of their toxicity even at low concentrations [1]. A big concern is related to the contamination of water sources by chromium, deriving from the release in the environment of various kinds of industrial effluents [2,3]. Chromium is essentially present in fresh water as trivalent, Cr(III), and hexavalent, Cr(VI), and the latter one is recognized to be highly toxic, carcinogenic and mutagenic [4]. Cr(VI) may exist in aqueous solution as neutral or anionic species, such as H_2CrO_4, $HCrO_4^-$, CrO_4^{2-} and $Cr_2O_7^{2-}$, mainly depending on pH and total chromium concentration [5]. At pH>6.5, typical of surface water and groundwater, chromate anion (CrO_4^{2-}) is the prevalent Cr(VI) form [6].

Many countries specified standards for chromium concentration in drinking water, being, for example, 50 and 100 $\mu g\,L^{-1}$ of total chromium in Europe and USA, respectively (*European drinking water directive, 1998; US-EPA, 2012*). In some parts of the world, maximum levels of Cr(VI) have been set for drinking water: for instance, Italy and California have recently regulated Cr(VI) concentration at 10 $\mu g\,L^{-1}$. Since total and hexavalent chromium concentration in surface and groundwater sources can exceed these levels [7–10], proper treatment techniques can be required in drinking water treatment plants. Several processes are considered effective for the removal of chromium, including coagulation/filtration, ion exchange, reverse osmosis, adsorption, membrane filtration, lime softening and electrochemical reduction [3,10]. However, the performance and the actual applicability of these processes in drinking water treatment strongly depend on water chemistry (i.e. pH, chromium concentration) and the specific application [2,3,11]. Despite the large number of papers published on the removal of chromium from fresh water and wastewater, only few studies can be found in literature comparing various processes and it can be hard to derive general information that can be used to select the best alternative [2,3,7,10].

Among the available processes, strong base anion exchange by means of synthetic organic resins is a widely used method for the removal of heavy metals and recent studies have shown the performances of many ion exchangers towards Cr(VI) ions [4,12–15]. Adsorption is another attractive choice for chromium removal and several works showed the effectiveness of many carbon-based adsorbents, such as commercial and synthetic activated carbons or low cost adsorbents derived from waste materials [5]. On the other hand, both the processes can be strongly sensitive to the characteristics of the solution, such as pH, ionic composition, organic and solid content [6,16,17].

Despite strong base anion exchange and activated carbon adsorption are reported to be effective engineered solutions for chromium removal, few studies can be found regarding their application in the treatment of groundwater for drinking purposes, in particular testing real groundwater matrices [10,12,18,19]. Most of the works, in fact, deal with synthetic water, often reproducing industrial wastewater characterized by relatively high chromium concentrations (order of mg L^{-1} and more) and acid pH (1-6) [2,4,5,5,13–15,19,20]. Fresh waters are usually characterized by lower Cr concentrations (order of $\mu g\,L^{-1}$), higher pH and buffer capacity [21], and, in these conditions, the performance of both the processes can significantly get worse [6,16,17]. However, the presence of a strong base anion exchange phase or an activated carbon adsorption phase can be already required in drinking water treatment plants for the removal of other regulated contaminants, such as nitrate [19] or organic micropollutants [22,23], respectively. Hence, it is worth to evaluate the possibility to concurrently abate chromium concentrations, in order to reduce the costs and the complexity of the treatment trains. To the best authors' knowledge, only few studies have been performed so far to evaluate the applicability of these two processes for the treatment of real groundwater matrices aimed at potable use [12,18,19].

The main goal of this work was to assess the effectiveness of strong base anion exchange and activated carbon adsorption in the removal of chromium from groundwater, exploited for drinking purposes and contaminated by a mixture of various inorganic and organic pollutants. Different materials were tested, evaluating sorption kinetics and equilibrium isotherms. Studied materials were two commercial strong base anion (SBA) exchange resins, specifically designed for water demineralization, and three commercial granular activated carbons (GAC), two of vegetal (coconut shell) and one of

mineral (coal) origin. Lab-scale results were elaborated to compare the removal efficiencies of the materials towards chromium and to derive preliminary indications for their full-scale application, both considering the removal of the other contaminants in solution (i.e. nitrate and sulfate ions, chlorinated solvents, pesticides) and estimating the breakthrough profiles. Finally, a full-scale operating GAC adsorption phase was monitored to observe the breakthrough of chromium and the other contaminants, in order to validate lab-scale experimental results.

2. Experimental

2.1 Materials

Groundwater used in batch experiments was sampled from a well located in Milan urban area (Italy), capturing groundwater for drinking purposes. A total of 10 groundwater samples was collected for the experimental trials and characterized as follows (see section 2.7): pH and the concentrations of 22 metals and transition metals were measured in all the 10 samples; the main physical-chemical parameters (temperature, electrical conductivity - CES, total dissolved solids - TDS, alkalinity and total hardness) and the concentrations of 14 ionic species, 24 volatile organic compounds (VOCs), and 27 pesticides were evaluated on 4 samples.

Sorbents tested in this study were two strong base anion-exchange resins: Jacobi Resinex™ A-4 (R-A4) and Purolite® A600 (P-A600); and three granular activated carbons: Chemviron Acticarbone NCL 1240 (GAC-V-A), Jacobi Aquasorb® CY (GAC-V-B) and Chemviron GAC-1240 (GAC-M). The main physical properties and specifications of SBA resins and GACs, as provided by the suppliers, are reported in Tables 1 and 2, respectively. GACs were further characterized as described in section 2.2. Both SBA resins and GACs were used in their original particle size and preliminarily rinsed for 15 min into a magnetically stirred beaker with deionized water at 1:1 volume ratio.

All the reagents for analyses were purchased from Sigma-Aldrich.

Table 1 Main characteristics of SBA resins as provided by the manufacturers.

SBA Resin	Purolite® A600 (P-A600)	Resinex™ A-4 (R-A4)
Polymer structure	Crosslinked polystyrene divinylbenzene	
Functional group	Quaternary Ammonium, Type 1	
Ionic form	Cl⁻	
Total capacity (eq L⁻¹)	>1.4	1.3
Particle size range (μm)	300-1200	420-1250
Bulk density (g L⁻¹)	685-720 (average 702)	670
Moisture retention (%)	43-48	50-56
Virgin material cost (€ L⁻¹)	7.0	3.5

Table 2 Main characteristics of GACs as provided by the manufacturers.

GAC	Chemviron Acticarbone NCL 1240 (GAC-V-A)	Jacobi Aquasorb® CY (GAC-V-B)	Chemviron GAC-1240 (GAC-M)
Particle size	12x40 mesh (0.425-1.700 mm)		
Apparent density (kg m³)	500	460	510
Backwashed and drained density (kg m³)	450	390	470
Total ash content (%)	<5	<4	-
Moisture content (%)	<5	<5	<2
Virgin material cost (€ kg⁻¹)	1.5	1.5	2.0

2.2 GAC characterization

Surface characteristics of the carbons were determined by N_2 adsorption and desorption at T=77 K (Tristar II 3020 V1.03, Micrometrics Instruments Corporation), after pre-treatment of the samples for 4 h at T=150°C under nitrogen atmosphere. Carbon surface area was determined according to the BET method ([24]), specific area and volume of micropores were determined by the t-Plot method ([25]), pore size distribution was determined by the BJH method ([26]).

The pH of point of zero charge (pH_PZC) of the carbons was determined by the pH drift method ([27]): 0.3 g of carbon were added in 100 mL of 0.01 N NaCl solution, after pH adjustment by means of 0.1 N HCl or NaOH solutions; for each GAC, 5 initial pH values were evaluated (in duplicate), measuring the final pH of the solution after 48 h of mixing on a magnetic stirrer; pH_PZC was determined plotting initial vs. final pH values.

Carbon-oxygen surface groups were determined by Boehm titration method ([28]): weighted carbon aliquots were dosed (at a concentration of about 500 mg L^{-1}) into 0.054 N NaOH, 0.051 N Na_2CO_3, 0.050 N $NaHCO_3$ and 0.072 N HCl solutions, respectively; after 24 h of agitation, solutions were filtered (0.22 μm PDVF filter) and titrated: basic solutions were retro-titrated with NaOH, while HCl solution was directly titrated. During titrations, nitrogen gas was continuously bubbled into the solutions.

Iodine number was determined according to ASTM4604.

2.3 Experimental procedures

Sorption kinetics and isotherms were investigated in batch system, varying the contact time and the sorbent dose.

1 L Pyrex bottles were filled with sampled groundwater, in which SBA resin or GAC weighted aliquots were also added; test bottles were then closed and mixed on a magnetic stirrer (550 RPM) for the desired contact time at the constant temperature of 23 °C. Experiments for kinetics determination were carried out fixing the dose of sorbent and varying contact time, while tests for equilibrium isotherms were performed at fixed contact time and varying sorbent doses. Tested contact time intervals and sorbent doses were determined by a series of preliminary tests (results not reported). For SBA resin, a dose of 1000 mg L^{-1} was tested in kinetic experiments for contact times between 15 min and 24 h, while sorption isotherms were investigated at 24 h contact time and sorbent doses between 50 and 1000 mg L^{-1}. For GACs, sorption kinetics were evaluated for contact times between 15 min and 48 h, fixing the GAC dose at 1000 mg L^{-1}, for GAC-V-A and GAC-V-B, and 2500 mg L^{-1}, for GAC-M. Equilibrium isotherms were investigated at a contact time of 48 h and varying sorbent doses from 200 to 1000 mg L^{-1}, for GAC-V-A and GAC-V-B, from 1000 to 2500 mg L^{-1} for GAC-M. At the end of each contact time, water samples were filtered through paper filter and analysed for pH and residual concentration of metals, transition metals and ionic species. The whole experimental procedure was also carried out without sorbent addition in test bottles, to verify that sample manipulation did not lead to variations of total chromium concentration and pH. All the trials were performed in duplicate. The parameters described in section 2.1 were determined in the groundwater samples used for batch experiments to evaluate their initial composition and characteristics.

The amount of a species sorbed onto the solid phase, q (μg mg^{-1}), was calculated from experimental data as follows:

e.1)
$$q = (C_0 - C_{res})\frac{V}{M}$$

where C_0 and C_{res} are initial and residual concentrations of the species (μg L^{-1}), V (L) is the volume of the liquid phase and M (mg) is the mass of dosed sorbent.

2.4 Kinetic and equilibrium models

Experimental data from kinetic studies were tested with two models, being pseudo-first order and pseudo-second order kinetics, whose equations are expressed as follows ([29,30]):

e.2) $\qquad \dfrac{dq_t}{dt} = k'(q_e - q_t)$ $\qquad$ e.3) $\qquad \dfrac{dq_t}{dt} = k''(q_e - q_t)^2$

where q_e and q_t are the amounts of sorbate (μg mg^{-1}) at equilibrium and at time t, respectively, k' (h^{-1}) and k'' (mg μg^{-1} h^{-1}) are the rate constants. Equations e.2 and e.3 were integrated for comparison with experimental data.

Two sorption isotherm models were used to describe equilibrium data, being Freundlich and Langmuir models, whose equations are ([31]):

e.4) $$q_e = K_F C_e^{1/n}$$ e.5) $$q_e = \frac{q_L K_L C_e}{1 + K_L C_e}$$

where C_e (μg L^{-1}) is the equilibrium liquid concentration, K_F ((μg mg^{-1})(L μg^{-1})$^{1/n}$) and $1/n$ (-) are the constant and the exponent of Freundlich equation; q_L (μg mg^{-1}) and K_L (L μg^{-1}) are, respectively, the maximum sorption capacity and equilibrium constant of Langmuir model.

Models were calibrated fitting experimental data, estimating the parameters by non-linear regression analysis applying least square method (Matlab, Mathworks 2014).

2.5 Calculation of theoretical sorbent usage rate and specific throughput

The theoretical sorbent usage rate, SUR (g L-1), was calculated by Equation e.6, derived by the steady state mass-balance around a hypothetical fixed-bed reactor ([32]):

e.6) $$SUR_{th} = (C_0 - C_e)\frac{1}{q_0}$$

where q_0 (μg g^{-1}) is the maximum equilibrium solid-phase concentration, calculated by isotherm equation (e.4 or e.5) setting $C_e = C_0$.

The theoretical specific throughput, $V_{SP,th}$ (L g^{-1}) was calculated as the inverse of SUR_{th}:

e.7) $$V_{SP,th} = SUR_{th}^{-1}$$

2.6 Full-scale GAC adsorption phase monitoring

A full-scale operating GAC adsorption phase was monitored for about 1 year, measuring the concentrations of metals, transition metals, anionic species, VOCs and pesticides (see Section 2.7) in the influent and effluent water (with a frequency of about 20 days). The GAC adsorption phase belongs to a drinking water treatment plant (DWTP) located in Milan urban area (Italy), fed on groundwater captured by a group of 20 wells, including the well exploited for batch experiments. The DWTP is composed by 10 fixed-bed in-parallel filters containing GAC-M. The volume of water treated by the whole adsorption phase, V_t (L), was measured over time. For each V_t value, the average water flow rate fed on each fixed-bed filter, Q (L s^{-1}), and the corresponding specific throughput, $V_{SP,OBS}$ (L g^{-1}), were calculated as:

e.8) $$Q = \frac{V_t}{n_f \cdot t}$$ e.9) $$V_{SP,OBS} = \frac{V_t}{n_f \cdot V_f \cdot \rho_b}$$

where n_f (-) is the number of GAC fixed-bed filters (10), t (s) is the time between two consecutive V_t measurements, V_f is the GAC volume of each fixed-bed filter (18 m^3) and ρ_b is the apparent density of GAC-M in the fixed-bed filter (470 g L^{-1}).

2.7 Analytical methods

Concentrations of Al, Sb, Ag, As, Ba, B, Cd, Ca, Cr_{tot}, Fe, Mg, Mn, Hg, Ni, Pb, K, Cu, Se, Na, Sr, V and Zn, were analyzed by ICP/MS spectrometry (Agilent 7500ce, EPA 200.8 method).

Concentrations of ammonium, cyanide, bromate, bromide, carbonate, chlorate, chloride, chloride, fluoride, phosphate, nitrate, nitrite, sulfate and sulfide were determined by ionic chromatography (Dionex ICS 2500, EPA 300.1 method).

The concentrations of 24 volatile organic compounds (VOCs) was determined by gas-chromatographer (Agilent Technologies GC-6890N Series gas-chromatographer) coupled with a single quadrupole mass analyzer (Agilent Technologies MS 5793 Network mass analyzer) with a dynamic headspace system (Purge&Trap O-I-Analytical Eclipse 4660 with 4551-A auto-sampler), according to methods EPA

524.3-09 and EPA 5030C-03. Volatile fraction extraction was made by stripping with ultra-pure helium and concentration on multi-phasic filter at 20 °C, followed by filter heating at 200 °C.

The concentrations of 27 pesticides concentration was determined by a gas-chromatographer (Agilent Technologies GC-7890A gas-chromatographer) coupled with a triple quadrupole mass/mass detector (Agilent Technologies MSD-7000A mass detector) after solid phase extraction according to the APAT-IRSA 5060/03 method. Organic compounds were extracted (Autotrace SPE workstation Zymark) using methanol, water and acetone/isopropanol 9:1 for cartridge activation and elution (Chromabond HR-X SPE cartridges).

Cr(VI) concentration was analyzed by colorimetric method (APAT-IRSA 3150) at a wavelength of 540 nm (optical path: 1 cm), using a UV–vis T80+ spectrophotometer (Shimadzu UV 2401 PC). pH was determined by a portable probe (pH6 XS Instrument, TECNOVETRO).

TDS, alkalinity, total hardness and CES were determined through an autotitrator (MAN-TECH) by APAT-IRSA/CNR (2003) methods.

All the analyses have been performed by the laboratory of Metropolitana Milanese S.p.A. (MM), which manages the integrated water service in Milan (I).

3. Results and discussion

3.1 Characteristics of the tested groundwater

Table 3 reports the composition of the groundwater tested in batch experiments for kinetics and isotherm determination, as average of the values measured in collected samples: only compounds found above the limit of quantification (LOQ) are reported.

Samples were characterized by an almost neutral pH and by physical-chemical parameters typical of groundwaters ([33–36]). Temperature and pH were almost constant during the experimental campaign, while the other parameters, such as alkalinity, electrical conductivity, total hardness and TDS, were characterized by a higher variability, of about 20-25%.

Nitrate was present at significant concentrations, about 85% of the WHO's guideline value of 50 mg L^{-1} (*WHO, 2011*). Among detected metals, chromium was the species present at the most relevant concentrations, being 38% of the European regulation limit (50 μg L^{-1} of Cr$_{tot}$); the other species did not affect drinking water quality, not being regulated or being present at concentrations very lower than standards (such as B, Fe, Na). Tested groundwater also contained several organic micropollutants at detectable concentrations, including various chlorinated solvents and pesticides.

3.2 Evaluation of chromium oxidation state and speciation

It has been verified by preliminary tests that sample manipulation and experimental procedure did not lead to variations of the initial total chromium concentration. It could be so assumed that the reduction of Cr$_{tot}$ concentration observed during the experiments was only due to the presence of the sorbents.

Initial concentrations of both total and hexavalent chromium were measured in groundwater samples used for the experimental trials: the ratio between Cr(VI) and Cr$_{tot}$ resulted to be 1.0±0.06 on average (4 samples). Hence, it could be assumed that almost all the chromium was initially present in the hexavalent form and that the fraction of Cr(III), given by the difference between Cr$_{tot}$ and Cr(VI), could be considered negligible. Moreover, kinetic experiments (results reported in the following sections) showed that the ratio between Cr(VI) and Cr$_{tot}$ did not vary over contact time, indicating that no significant variation in Cr oxidation state occurred during adsorption and ion exchange processes. Plotting all the 80 observed Cr(VI) vs. Cr$_{tot}$ concentration data (S.I.1, Figure S1), a good linear regression (R^2=0.93) with slope equal to 1.02±0.061 L mg^{-1} and intercept equal to 0.01±0.005 mg L^{-1} (estimate±95% confidence interval,) was obtained, indicating that Cr(VI) and Cr$_{tot}$ concentrations coincided both in blank samples and after contact with sorbents.

Cr(VI) may exist in aqueous solution under neutral (H_2CrO_4) or anionic ($HCrO_4^-$, CrO_4^{2-} and $Cr_2O_7^{2-}$) forms, mainly depending on pH and total chromium concentration ([5]). The speciation of Cr(VI) is an important aspect to be considered, since the affinity of a sorbent varies with the different chromium

species ([13,17]). At the Cr_{tot} concentration and pH values measured during the experimental trials, it could be assumed that all the Cr(VI) in liquid phase was in the form of chromate ion (CrO_4^{2-}). Chromium speciation could be considered almost constant, since no significant variation of water pH was observed during isotherm and kinetic experiments. In fact, the pH of samples treated with SBA resins or GACs was always in the range 7.0-7.8 and a maximum variation of 4% with respect to the blank sample was observed at the end of the contact time.

In the following paragraphs, all the chromium data are reported as total chromium concentrations, being determined by a more precise analytical method and since most of the standard regulation levels are expressed as Cr_{tot}; however, according to the observed results, they can be considered equivalent to that of Cr(VI) in the form of chromate ion.

Table 3 Tested groundwater characteristics (average±st.dev. values): at the sampling point for kinetic and isotherm experiments and at the influent of full-scale GAC adsorption phase. The LOQ of the analytical method and the European regulation limits for drinking water ([37]) are also reported.

Parameter	Batch tests	Full-scale monitoring	LOQ	European regulation limit
T at the sampling point (°C)	14.2±1.20	14.7±0.82	-	-
pH (-)	7.6±0.20	7.8±0.07	-	6.5-9.5
Electrical conductivity at 20°C (μS cm^{-1})	600±147.3	681±9.1	-	2500
TDS at 180°C (mg L^{-1})	390.2±95.77	442.7±5.93	-	1500
Alkalinity (mg L^{-1})	166.7±35.85	198.7±3.36	-	-
Total hardness (°F)	25.64±5.943	30.77±2.684	-	10-50
Cl$^-$ (mg L^{-1})	27.3±0.58	27.5±0.58	0.01	250
NO$_3^-$ (mg L^{-1})	42.7±1.15	43.5±0.85	0.01	50
SO$_4^{2-}$ (mg L^{-1})	40.0±1.00	41.4±0.75	0.01	250
Ba (μg L^{-1})	28±3.7	21±1.0	1	-
Ca (mg L^{-1})	94±5.6	88±6.6	1	-
K (mg L^{-1})	2±0.7	1±0.0	1	-
Mg (mg L^{-1})	19±2.0	18±1.7	1	-
Na (mg L^{-1})	11±1.0	11±1.0	1	200
B (μg L^{-1})	61±6.2	60±1.7	1	1000
Cr_{tot} (μg L^{-1})	18±1.3	17±2.0	2	50
Cr(VI) (μg L^{-1})	19±1.0	18±0.8	2	-
Fe (μg L^{-1})	9±8.1	63±85.3	5	200
Sb (μg L^{-1})	1±1.0	<DL	1	-
St (μg L^{-1})	438±35.8	<DL	1	-
chloroform (μg L^{-1})	2.8±0.50	2.0±0.47	1	100 [a]
tetrachloroethylene, PCE (μg L^{-1})	9.0±2.16	8.8±2.10	1	10 [b]
trichloroethylene, TCE (μg L^{-1})	1.5±0.58	1.1±0.32	1	10 [b]
cis-1,2-dichloroethylene (μg L^{-1})	0.8±0.50	1.0±0.00	1	-
Freon 141b (μg L^{-1})	1.1±0.28	1.1±0.32	1	-
atrazine (μg L^{-1})	0.01±0.000	0.01±0.005	0.01	0.1 [c]
terbuthylazine (μg L^{-1})	0.01±0.000	0.01±0.000	0.01	0.1 [c]
2,6-dichloro benzamide (μg L^{-1})	0.02±0.005	0.03±0.011	0.01	0.1 [c]
atrazine desethyl (μg L^{-1})	0.01±0.005	0.01±0.005	0.01	0.1 [c]
terbuthylazine desethyl (μg L^{-1})	0.01±0.000	0.02±0.005	0.01	0.1 [c]
tris(2-chloroethyl)phosphate (μg L^{-1})	0.03±0.008	0.02±0.013	0.01	0.1 [c]

[a] total trihalomethanes
[b] sum of PCE and TCE
[c] 0.1 μg L^{-1} for single pesticide, 0.5 μg L^{-1} for total pesticides

3.3 Anion-Exchange Resins

3.3.1 Kinetics

Figure 1 shows the effect of contact time on the removal of chromium by SBA resins; experimental results are reported in terms of q_t, calculated by equation e.1. For both the SBA resins, results showed a higher chromium removal rate in the first 30 min, gradually decreasing over time until the reaching of a plateau within 5-6 h. The Cr_{tot} equilibrium solid-phase concentration (q_t values observed at 24 h contact time) corresponded to about 0.019 µg mg^{-1} (0.33 µeq g^{-1} and 0.23 µeq L^{-1} of chromate ions) for both the resins. Experimental data were interpolated with pseudo-first (equation e.2) and pseudo-second order (equation e.3) kinetic models: simulated data are reported in Figure 1, while estimated parameters are reported in Table 4, together with their 95% confidence intervals and determination coefficient of non-linear regressions. For both the models, the q_e values of the two resins resulted to be almost coincident, while rate constants resulted slightly higher for P-A600 than for R-A4, even if the differences were not statistically significant. Both the models were effective in simulating observed data ($R^2 > 0.95$), but pseudo-first order model showed slightly higher R^2 values and lower uncertainty in parameter estimates (narrower 95% confidence intervals), for both the resins. Moreover, pseudo-first order model better estimated the observed q_e values, while pseudo-second order kinetic tended to overestimate equilibrium solid-phase concentrations. These results are consistent with previous works, indicating that the ion uptake from aqueous phase to ion exchange materials follows reversible first-order kinetics, with monolayer chemical sorption on particle surface ([13,38,39]). The better data fitting by pseudo-first order respect to pseudo-second order model may indicate the predominance of the mass transfer step with respect to the sorption step, probably due to the relatively large particle size ([40]). According to previous studies (*inter alia*, [39,41]), chromium exchange can be considered as a reversible process (described by equation e.10), where k' represents the overall first-order rate constant and it is given by the contribution of the forward (k_1), being the Cr(VI) uptake, and backward (k_2), being the Cr(VI) release, rate constants:

e.10)
$$A \underset{k_2}{\overset{k_1}{\rightleftarrows}} B$$
e.11)
$$k' = k_1 + k_2$$

Using experimental data and k' values previously estimated, k_1 and k_2 were calculated as proposed by Gode and Pehlivan (2003) ([41]), combining equation e.11 with equation e.12, derived from the equation describing Cr sorption rate from the liquid-phase:

e.12)
$$\frac{X_e}{C_0 - X_e} = \frac{k_1}{k_2}$$

where X_e (µg L^{-1}) is the amount of chromium transferred from liquid- to solid-phase at equilibrium (determined by experimental data). Results (reported in Table 4) showed that, for both the resins, the forward rate constant was much higher than the backward rate constant, indicating that chromium uptake was the prevalent mechanism.

SBA resins also displayed a relevant removal of nitrate and sulfate ions, while the concentrations of the other anions and metals present in the tested groundwater did not show any significant variation over time, except in case of chloride. In fact, being the mobile ion, Cl$^-$ was released by the SBA resins leading to an increase of its liquid-phase concentration over time (S.I.2, Figure S2). NO_3^- and SO_4^{2-} are present in raw groundwater at concentrations much higher than chromium (Table 3), with equivalent concentrations (corresponding to 694 and 854 µeq L^{-1}, respectively) at least three orders of magnitude higher than that of Cr (corresponding to 0.29 µeq L^{-1}). Results of NO_3^- and SO_4^{2-} sorption kinetics, reported in S.I.2 (Figure S3), showed a saturation trend over contact time; as for Cr, an equilibrium solid-phase concentration was obtained with both the SBA resins after about 5 h contact time; for P-A600, q_e were equal to 0.845 meq g^{-1} (593 meq L^{-1}) and 0.449 meq g^{-1} (315 meq L^{-1}) for sulfate and nitrate ions, respectively; R-A4 showed q_e values equal to 0.242 µeq mg^{-1} (162 meq L^{-1}) for sulfate and 0.300 µeq mg^{-1} (201 meq L^{-1}) for nitrate. According to the obtained data, P-A600 showed a higher capacity than R-A4 towards both the ions; however, the order of affinity was different for the two

resins, being SO_4^{2-}>NO_3^- for P-A600 and NO_3>SO_4^{2-} for R-A4. The preference towards competitive species is an important aspect to be considered in full-scale column application. In fact, considering the fixed-bed process, chromatographic peaking of the less-preferred species can occur when the maximum exchange capacity of the resin is exceeded, resulting in effluent concentration higher than the influent one ([12,19]). The release of nitrate could be of particular concern, since it can result in effluent concentrations higher than the regulation limits. Hence, despite having a lower capacity, R-A4 could be preferable in presence of relatively high nitrate concentrations, especially when close to the regulation limit, as in the case of the present study. It is pointed out that the maximum capacity of the resins has never been reached during the experiments and it was not possible to observe the release of one of the ions. Further studies are so needed to better investigate the affinity of the resins towards nitrate and sulfate ions and to observe the release rates of the sorbed anions.

3.3.2   Equilibrium isotherms

Results of sorption isotherms experiments with SBA resins are reported in Figure 2, showing q_e vs. C_e data obtained for the two resins. Experimental data were interpolated with Freundlich and Langmuir models (equations e.4 and e.5, respectively): simulated data are plotted in Figure 2, while non-linear regression parameters are reported in Table 5. Both the models effectively fit experimental data (R^2>0.97), but Freundlich model resulted more appropriate than Langmuir model: in fact, Freundlich constant (K_F) estimated for P-A600 and R-A4 resulted significantly different, reflecting the different removal efficiency of the materials suggested by experimental data. On the contrary, Langmuir maximum adsorption capacity values (q_L) are affected by a higher uncertainty and do not reflect the higher adsorption capacity of P-A600. According to Freundlich isotherm assumptions, the binding strength of metal ions sorption onto ion exchange resins is assumed to decrease with increasing the degree of site occupation ([4,38,39]). The relatively high values of Freundlich exponents (0.782 and 0.905 for P-A600 and R-A4, respectively) indicated a high level of binding site occupation, as well as favorable sorption conditions.

Equilibrium sorption capacities observed in this study for P-A600 and R-A4 are much lower than those reported in literature for other similar anion-exchange resins ([4,13,14,38,39,41,42]); however, most of the reviewed studies dealt with synthetic water matrices characterized by higher chromium concentrations (>5 mg L^{-1} of Cr(VI)) and lower pH (2-5). It is known that pH strongly influences Cr(VI) removal efficiency by means of SBA resins, whose sorption capacities could drastically decrease passing from acid to neutral pH ([38]). In fact, due to the chemistry of ion exchange process, the amount of chromate ions (CrO_4^{2-}) taken by one active site of resin is half of that of hydrogen chromate ($HCrO_4^-$). Since, at the pH values observed in this study (7.6±0.20) almost all the chromium was in CrO_4^{2-} form, the resin performances were at least halved respect to a more acidic pH (<6), at which $HCrO_4^-$ would be the prevalent chromium form. Isotherm parameters obtained in this study can be considered valid for applications on real groundwater matrices characterized by relatively low Cr liquid concentrations (in the order of μg L^{-1}) and neutral pH.

As for nitrate and sulfate, isotherm experiments showed significant removal of these ions, with solid-phase concentrations increasing with the resin dose. Solid- vs. liquid-phase equilibrium concentrations obtained for P-A600 and R-A4 are reported in S.I.2 (Figure S4). Isotherm data were consistent with the results of kinetic experiments, showing higher sorption capacities for P-A600 with respect to R-A4 and displaying the different order of affinity of the resins towards the two ions (SO_4^{2-}>NO_3^- for P-A600 and NO_3^->SO_4^{2-} for R-A4).
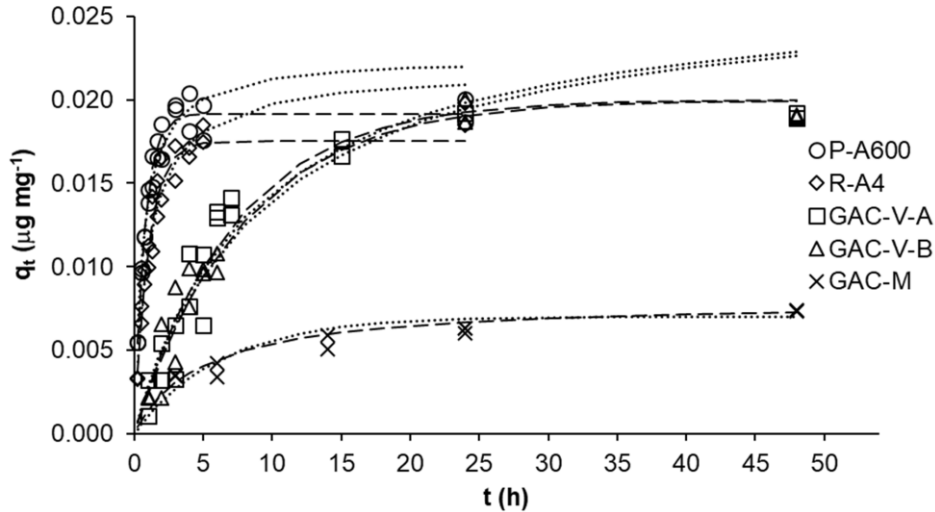
Figure 1 Kinetics of Cr_{tot} sorption onto SBA resins (1000 mg L^{-1} dose) and GACs (1000 mg L^{-1} dose for GAC-V-A and GAC-V-B, 2500 mg L^{-1} dose for GAC-M). Dotted and dashed lines are the curves simulated by pseudo-first and pseudo-second order kinetic models, respectively.
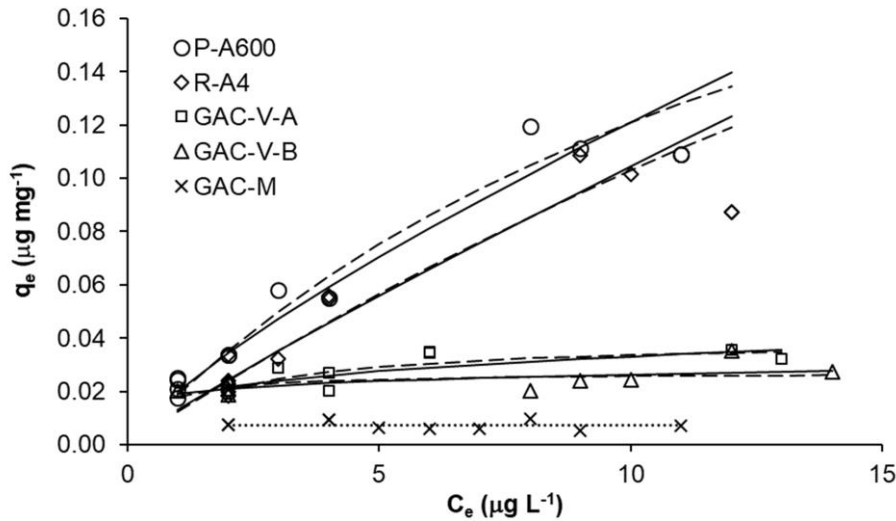
Figure 2 Solid-phase concentration vs. residual liquid-phase Cr_{tot} concentration for SBA resins and GACs. Solid and dashed lines are the curves simulated by Freundlich and Langmuir isotherm models, respectively; for GAC-M, dotted line corresponds to the average q_e value (0.0074 µg mg^{-1}).

Table 4 Parameters (estimate±95% confidence interval), number of data used for the regression and determination coefficients (R^2) of pseudo-first and pseudo-second order kinetic models for Cr_{tot} sorption.

Kinetic model	parameters	P-A600	R-A4	GAC-V-A	GAC-V-B	GAC-M
Pseudo-first order	q_e [µg mg^{-1}]	0.019 ±0.0007	0.018 ±0.0010	0.020 ±0.0029	0.020 ±0.0030	0.007 ±0.0009
	k' [h^{-1}]	1.331 ±0.1569	0.965 ±0.1553	0.138 ±0.0406	0.127 ±0.0364	0.162 ±0.0720
	n. of data	20	20	18	18	17
	R^2 [-]	0.970	0.956	0.912	0.933	0.854
	k_1 [h^{-1}]	1.312	0.861	0.052	0.044	0.017
	k_2 [h^{-1}]	0.019	0.104	0.086	0.083	0.145

(continues in the next page)

(continues from the previous page)

Kinetic model	parameters	P-A600	R-A4	GAC-V-A	GAC-V-B	GAC-M
Pseudo-second order	q_e [µg mg^{-1}]	0.023 ±0.0015	0.022 ±0.0020	0.027 ±0.0059	0.027 ±0.0057	0.008 ±0.0010
	k'' [mg µg^{-1} h^{-1}]	69.753 ±20.2237	45.254 ±15.7801	4.262 ±2.8365	3.998 ±2.4644	25.769 ±14.9761
	n. of data	20	20	18	18	17
	R^2 [-]	0.948	0.948	0.900	0.931	0.911

Table 5 Parameters (estimate±95% confidence interval), number of data used for the regression and determination coefficients (R^2) of Freundlich and Langmuir isotherm models for Cr_{tot} sorption.

Isotherm model	parameters	P-A600	R-A4	GAC-V-A	GAC-V-B	GAC-M
Freundlich	K_F [(µg mg^{-1})(L µg^{-1})$^{1/n}$]	0.020 ±0.0033	0.013 ±0.0038	0.018 ±0.0055	0.019 ±0.0058	-
	1/n [-]	0.782 ±0.0866	0.905 ±0.1471	0.2648 ±0.6325	0.142 ±0.1548	-
	n. of data	12	12	10	10	10
	R^2 [-]	0.987	0.967	0.6325	0.419	-
Langmuir	q_L [µg mg^{-1}]	0.310 ±0.1374	0.571 ±0.749	0.040 ±0.0097	0.027 ±0.0062	-
	K_L [L µg^{-1}]	0.064 ±0.0394	0.022 ±0.0340	0.534 ±0.4290	1.937 ±3.0725	-
	n. of data	12	12	10	10	10
	R^2 [-]	0.984	0.969	0.702	0.342	-

3.4 Granular Activated Carbons

3.4.1 GAC characterization

N_2 isotherms obtained for the tested activated carbons (reported in S.I.3, Figure S7) showed a type I shape, that, according to BDDT (Brunauer–Deming–Deming–Teller) classification, indicates the predominance of micropores ([43]). This was confirmed by the pore size distributions of the three GACs (S.I.3, Figure S8), showing that most of the pore volume was concentrated in pores having diameters below 5 nm. All the carbons showed relatively narrow pore size distributions, with single picks at about 3.7, 4.3 and 4.0 nm, for GAC-M, GAC-V-A and GAC-V-B, respectively. The average pore diameters (Table 6) resulted to be slightly higher than 3 nm for all the carbons. Values of BET surface area, micropore surface area and micropore volume area are reported in Table 6. Mineral-based carbon (GAC-M) showed the lowest values for all the parameters: BET surface area was 32% and 44% lower than those determined for GAC-V-A and GAC-V-B, respectively, while micropore area and volume were more than 70% lower. Iodine number values (Table 6) showed a similar trend and were well correlated to the pore structural properties such as BET surface area, micropore surface area and micropore volume (S.I.3, Figure S10).

The results of Boehm titration (Table 6) showed the prevalence of basic carbon-oxygen functionalities onto the carbon surfaces. This characteristic implies a higher carbon affinity for hydrophobic compounds (such as many organic micropollutants) and also for chromate ions, which are supposed to be adsorbed by protonated basic surface groups ([17,27,44]).

The results of pH-drift method, expressed as initial vs. final pH values, are reported in S.I.3 (Figure S9): pH_{PZC} values around 10 were obtained for all the GACs (Table 6), reflecting the relative low content of acid surface groups ([27]).

Table 6 Textural properties and surface functionalities determined on the three GACs.

Adsorbent		**GAC-V-A**	**GAC-V-B**	**GAC-M**
BET surface area (m^2 g^{-1})		1151	1409	767
t-plot micropore area (m^2 g^{-1})		933	1058	241
t-plot micropore volume (cm^3 g^{-1})		0.364	0.424	0.105
BJH adsorption average pore diameter (nm)		3.439	3.160	3.227
Iodine number (mg g^{-1})		1135	1250	864
pH$_{PZC}$ (-)		10.0	9.7	9.7
Surface functional groups (meq g^{-1})	Total basic	1.813	1.966	1.697
	Carboxylic	0.062	0.039	0.061
	Lactonic	0.009	0.003	0.017
	Phenolic	0.360	0.116	0.263
	Total acid	0.431	0.158	0.342

3.4.2 Kinetics

Figure 1 shows the kinetics of Cr$_{tot}$ removal by means of activated carbons. Chromium adsorption rates of all the carbons gradually decreased over time, achieving a plateau after about 24 h. Very similar results were obtained for GAC-V-A and GAC-V-B, while data showed a strong difference between vegetal-based carbons and the mineral-based one, in terms of adsorption rate and equilibrium capacity. Experimental data were interpolated with pseudo-first and pseudo-second order kinetic models (equation e.2 and e.3, respectively): simulated data are reported in Figure 1, while parameters of non-linear regressions are reported in Table 4. Both the kinetic models well fit experimental data (R^2>0.85); as for SBA resins, however, q$_e$ estimated by pseudo-first order model were closer to the equilibrium values observed at t=48 h (0.018, 0.019 and 0.007 µg mg^{-1} for GAC-V-A, GAC-V-B and GAC-M, respectively). The values of model parameters indicated very similar sorption kinetics for vegetal-based carbons; on the other hand, mineral-based carbon showed faster sorption rates but a very lower equilibrium adsorption capacity. Forward (k$_1$) and backward (k$_2$) rate constants of pseudo-first order model (equations e.10 and e.11) were calculated also for GAC data (Table 4): conversely to SBA resins, all the carbons showed k$_2$ values higher than k$_1$, about 2 times higher for vegetal-based carbons and up to 8 times higher for GAC-M. These findings strongly indicate not-favorable conditions for chromium uptake, since desorption process resulted to be more important than the adsorption process.

Besides chromium, a reduction of boron concentration over time was observed during kinetic experiments, while none of the other anionic and metal species present in the tested groundwater showed a relevant variation. Boron was present at initial concentrations around 60 µg L^{-1}, not representing a cause of concern for drinking water quality standards (Table 2). Boron adsorption kinetics for the studied GACs are reported in S.I.2 (Figure S5 a). Although experimental data were more dispersed than in the case of Cr, boron sorption showed an increasing saturation trend over time. As for Cr, kinetics of B removal was very similar for the two vegetal-based GACs, reaching maximum q$_t$ values (at 48 h contact time) of about 0.04 µg mg^{-1}, while GAC-M reached capacities around 0.01 µg mg^{-1}. For each carbon, boron adsorption rates and equilibrium capacities were in the same order of magnitude of those observed for Cr (S.I.2, Figure S5 b), even if the two species are probably involved in different sorption mechanisms. While chromium is in the form of CrO$_4^{2-}$ ions, boron is present in water in the form of boric acid (H$_3$BO$_3$), that is undissociated at pH around neutrality (pK_a=9.24 ([45])). According to previous studies (*inter alia* [45,46]), a possible explanation to the observed boron removal is that H$_3$BO$_3$ can be chemically adsorbed reacting with diol complexes (functional groups containing two hydroxyl groups) present on carbon surface.

3.4.3 Equilibrium isotherms

Results of equilibrium isotherm tests, reported in Figure 2, confirmed the lower removal capacity of GAC-M, showing q$_e$ values less than 50% of those observed for vegetal-based GACs.

The adsorption behavior of activated carbons can depend both on porous structure and surface functional groups: the adsorption capacity is usually related to the pore structural properties, such as specific surface area, pore volume, surface and size distribution, while the chemical interactions with the adsorbates are affected by surface functionalities [43]. It is known that the adsorption of metal ions mostly depends on carbon chemical properties, due to the functional groups on carbon surface [43,44,47]. In this study, the higher chromium adsorption capacity observed for vegetal-based carbons with respect to mineral-based carbon could be better correlated with their more developed pore structure (higher BET surface area, micropore volume and area) and higher iodine number. On the other hand, surface functionalization was similar for three GACs, having comparable content of basic groups and pH_{PZC}.

Looking at liquid- vs. solid-phase concentration data in Figure 2, it can be noted that all the carbons showed a weak (for GAC-V-A and GAC-V-B) or even null (for GAC-M) dependence of q_e on C_e. This behavior is commonly related to high heterogeneity of adsorption sites and strong adsorption bindings [18,31]. Considering isotherm and kinetic results, it can be supposed that chromium adsorption onto GACs is not a favorable process, probably limited by mass transfer step [31].

Experimental data were interpolated by Freundlich and Langmuir isotherms (equation e.4 and e.5, respectively): results of non-linear regression are reported in Table 4, while simulated data are showed in Figure 2. For GAC-V-A and GAC-V-B, the models did not well fit the observed data, as indicated by the low determination coefficients ($R^2 < 0.70$). Moreover, the estimates of $1/n$ and K_L, reflecting the dependence of q_e on C_e in Freundlich and Langmuir models, respectively, were affected by high uncertainty. Although the high data variability, isotherm results for vegetal-based carbons can be considered quite well comparable with those previously determined by Han et al. (2000) [18], reporting very similar Freundlich constants (0.01-0.02 ($\mu g\ mg^{-1}$)(L μg^{-1})$^{1/n}$) for the adsorption of Cr(VI) onto two commercial GACs in synthetic groundwater under similar conditions (pH 7.5, C_0=0.02-2 $\mu g\ L^{-1}$); on the other hand, the same authors obtained higher $1/n$ values (0.4-0.5), indicating a higher adsorption energy. For GAC-M, it was not possible to accurately estimate model parameters, since the results of non-linear regression were extremely sensitive to the set initial values. As shown in Figure 2, equilibrium solid-phase concentrations resulted almost constant over C_e, with an average value of 0.0074±0.00158 $\mu g\ mg^{-1}$.

Besides chromium, an increasing boron removal over GAC dose was observed in isotherm experiments. Boron equilibrium adsorption data are reported in S.I.2 (Figure S6). Boron isotherms were similar to those obtained for chromium, with q_e values ranging between 0.036 and 0.107 $\mu g\ mg^{-1}$ for GAC-V-A, between 0.029 and 0.125 $\mu g\ mg^{-1}$ for GAC-V-B, in C_e ranges of 10-48 $\mu g\ L^{-1}$ and 19-47 $\mu g\ L^{-1}$, respectively; for GAC-M, equilibrium solid-phase concentrations were almost constant (not dependent on C_e), on average equal to 0.010±0.0055 $\mu g\ mg^{-1}$.

3.5 Comparison of the two processes in chromium removal

Isotherm data were used to calculate the theoretical adsorbent usage rates (SUR_{th}) and specific throughputs ($V_{SP,th}$) for chromium removal. For a fixed contaminant removal (C/C_0), SUR_{th} represents the amount of sorbent required to treat a unit volume of water, while $V_{SP,th}$ is the volume of water treated per unit mass of sorbent. These quantities are widely used in engineering applications to roughly estimate the sorbent life-time and, considering a fixed-bed reactor configuration, to preliminary compare the performances of different sorbents independently from the design and the operating parameters (i.e. water flow rate, sorbent mass, fixed-bed size) [32].

SUR_{th} values were calculated by Equation e.6, setting the initial Cr_{tot} concentration (C_0) to 18 $\mu g\ L^{-1}$ and varying C_e values from 0 to C_0 (corresponding to C/C_0 values from 0 to 1); q_0 was calculated by Freundlich model (equation e.4) considering the parameters reported in Table 5; for GAC-M, q_0 was set equal to the average q_e value observed in isotherm experiments (0.0074 $\mu g\ mg^{-1}$). The corresponding values of theoretical specific throughput ($V_{SP,th}$) were calculated by equation e.7.

Cr_{tot} breakthrough data (expressed as C/C_0) as a function of $V_{SP,th}$ estimated for each material are reported in Figure 3. It can be observed that the two SBA resins showed similar results, as well as GAC-V-A and GAC-V-B, while GAC-M displayed the lowest $V_{SP,th}$ values; for a given C/C_0 value, $V_{SP,th}$ of SBA resins were about 5 and 25 times higher than those calculated for vegetal-based (GAC-V-A and GAC-V-B) and mineral-based (GAC-M) carbons, respectively. Due to the different isotherm parameters, activated carbons also showed a higher slope of the theoretical breakthrough profile, with removal efficiency more rapidly decreasing with the specific throughput. Definitely, anion exchange process resulted to be much more effective than GAC adsorption in removing chromium from the tested groundwater. In fact, independently from reactor configuration, SBA resins assure significantly higher throughputs and lower usage rates, resulting in longer sorbent life-times. A comprehensive comparison between the studied materials should include an estimation of the treatment costs. Considering the calculated specific throughputs and the cost of the virgin materials (Tables 1 and 2), the cost to treat a unit volume of water up to the 5% chromium breakthrough would be 0.5 € m^{-3} for R-A4, 0.9 € m^{-3} for P-A600 and GAC-V-B, 0.7 € m^{-3} for GAC-V-A and 4.7 € m^{-3} for GAC-M. However, further information related to the implementation of the treatment processes must be considered in the analysis, such as plant costs, water pumping, regeneration and disposal of the exhausted material.

Data reported in Figure 3 represent an estimation of Cr breakthrough profile; pilot-scale tests are needed to derive real-scale design parameters and to test the competitive sorption of other contaminants (i.e. NO_3^- and SO_4^{2-} with SBA resins). Anyway, simulated data for P-A600 were well comparable with pilot-scale data obtained by Seidel et al. (2014) ([19]), observing a 100% breakthrough of Cr(VI) at V_{SP} of about 60 L g^{-1} (14-16 µg L^{-1} influent concentration).

A full scale GAC adsorption phase (containing GAC-M) was monitored for comparison with theoretical data derived from batch experiments. During the monitoring period, the average water flow rate treated by each filter was 20.1±3.86 L s^{-1} (calculated by equation e.8), while the average total chromium influent concentration was 17.1±1.97 µg L^{-1}. All Q and Cr_{tot} C_0 values observed during GAC adsorption phase monitoring are reported in S.I.4 (Figure S11). Tested groundwater (composition reported in Table 3) also contained various organic contaminants, such as chlorinated solvents and pesticides, at detectable concentrations.

Effluent Cr_{tot} concentrations (expressed as C/C_0) are shown in Figure 3, as a function of the specific throughput ($V_{SP,OBS}$), calculated by equation e.9. It can be observed that chromium breakthrough was almost immediate, with C/C_0 passing from 0 to 1 within only a $V_{SP,OBS}$ of 5 L g^{-1}, corresponding, in a full scale fixed-bed filter, to 27 days and 1889 BV treated. GAC-M full scale data are quite well comparable with those simulated by using isotherm data, showing similar breakthrough profiles (both in terms of breakthrough time and slope). Observed results confirmed that fixed-bed adsorption using GAC-M is not an efficient solution for chromium removal, since the maximum adsorption capacity is exceeded at very low specific throughput values.

Despite being less effective than SBA resins, the studied vegetal GACs showed noteworthy chromium removal capacities, theoretically allowing to treat a certain amount of water controlling Cr effluent concentration. Hence, the possibility to concurrently remove organics and Cr in GAC adsorption phase could be an interesting solution to avoid a specific treatment phase for Cr and to reduce treatment costs. Consistently with batch experiments, the other ionic species (sulfate, nitrate) and metals were not removed in full-scale GAC adsorption phase; on the other hand, a significant removal of VOCs and pesticides was observed. Pesticide effluent concentrations were <LOQ for the whole monitoring period, while VOCs showed different breakthrough profiles, displaying variable affinity with the adsorbent. Chloroform was the first organic compound appearing in the effluent and it could be theoretically assumed as the limiting organic contaminant, determining the life-time of the GAC bed. Chloroform data (C/C_0 vs. $V_{SP,OBS}$) are shown in Figure 3, while the breakthrough data observed for the other VOCs are reported in S.I.4 (Table S2). As shown in Figure 3, chloroform breakthrough occurred much later than chromium, reaching a C/C_0 value equal to 1 within $V_{SP,OBS}$ of 17 L g^{-1}, corresponding to 90 days and about 5100 BV treated. Hence, a GAC adsorption phase designed for removing Cr_{tot} concentration would be not feasible, implying a significant reduction of bed-life and an unsuitable

increase of operating costs. According to $V_{SP,th}$ estimated for Cr removal, the life-time of GAC-V-A and GAC-V-B could be significantly longer than GAC-M, but still too much low for full scale applications.

If designed only for chromate control, anion exchange process resulted to be largely the most efficient solution, providing much longer resin life-time and, consequently, lower operating costs (lower virgin resin demand and less frequent regeneration cycles). However, it should be stressed that the resin usage rate can dramatically get worse if the phase is conceived also to remove nitrate and sulfate ions, resulting in much shorter cycle times. In fact, considering the initial concentrations observed in the studied groundwater (Table 3), the theoretical breakthrough of nitrate and sulfate would occur much earlier than that of chromium, with $C/C_0 > 0$ at specific throughputs < 2 L g^{-1} (S.I.5, Figure S12). Moreover, it is essential to take into consideration the uptake of competitive anions present at the mg L^{-1} level, such as nitrate, sulfate and bicarbonate ions (this not measured in this study but almost coincident with water alkalinity). In fact, this phenomenon may lead to exceed the maximum exchange capacity of the resin and result in a release of the less-preferred species. For instance, previous studies ([12,19]) observed the chromatographic peak of nitrate anions in pilot-scale columns after throughputs corresponding to 0.06-0.07 L g^{-1} (Amberlite PWA 410, C_0: 23 mg L^{-1} of NO_3^-, 90 mg L^{-1} of SO_4^{2-}, 0.25 mg L^{-1} of PO_4^{3-}) and 0.5-0.6 L g^{-1} (P-A600, C_0: 6 mg L^{-1} of NO_3^-, 17-21 mg L^{-1} of SO_4^{2-}), with peak at least 2-times higher than the influent water concentration.
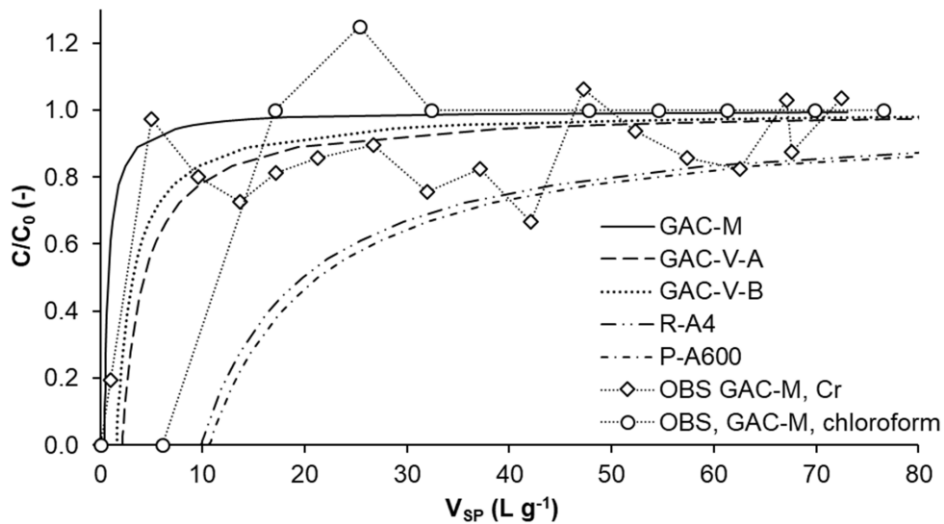
Figure 3 Theoretical Cr_{tot} breakthrough (C/C_0) as a function of the specific throughput (V_{SP}) (estimated assuming C_0=18 µg L^{-1}). Cr_{tot} and chloroform breakthrough data observed in real-scale adsorbers are also reported.

4. Conclusions

Two strong base anion exchange resins (P-A600 and R-A4) and three granular activated carbons (GAC-M, GAC-V-A and GAC-V-B) were tested in the removal of chromium, predominantly present as chromate ion (C_0=18 µg L^{-1}), from a real groundwater matrix.

P-A600 and R-A4 showed similar chromium sorption kinetics, suggesting a not-reversible sorption mechanism, and also relevant removal capacities towards nitrate and sulfate ions, with different order of affinity ($SO_4^{2-} > NO_3^-$ for P-A600 and $NO_3^- > SO_4^{2-}$ for R-A4).

Activated carbons potentially permit to remove chromium, but data suggest that chromium desorption is more important than adsorption process. GAC-V-A and GAC-V-B showed a similar performance with a weak dependence of q_e on C_e, while for GAC-M, q_e resulted to be independent on C_e. Moreover, mineral-based GAC showed a lower Cr removal capacity with respect to vegetal-based GACs, reflecting the less favorable pore structural properties. Indeed GAC adsorption allows to remove chromium from groundwater, however the specific characteristics of the material must be carefully taken into

consideration, since adsorption capacity are associated to higher iodine number and more developed pore structure (higher BET surface area, micropore volume and area).

Based on the theoretical sorbent usage rates and specific throughputs for Cr removal, anion exchange process resulted to be much more effective than GAC adsorption, with $V_{SP,th}$ values about 5 and 25 times higher than those calculated, respectively, for vegetal-based carbons and GAC-M. The monitoring of a real-scale GAC adsorption phase confirmed that GAC adsorption is a not feasible solution for chromium removal, with chromium breakthrough much faster than that of the other organic contaminants. Overall, SBA exchange process resulted to be the most preferable solution to remove chromium from the tested groundwater, providing the best sorbent usage rates. However, SBA resin performances can dramatically decrease when considering the removal of other anions (i.e. nitrate and sulfate) present at three-order higher concentrations (mg L^{-1}), due to the much shorter breakthrough times (throughput <2 L g^{-1}) and the possible release of anions after SBA resin exhaustion.

References

(1)   Hashim, M. A.; Mukhopadhyay, S.; Sahu, J. N.; Sengupta, B. Remediation technologies for heavy metal contaminated groundwater. *J. Environ. Manage.* **2011**, *92* (10), 2355–2388.

(2)   Owlad, M.; Aroua, M. K.; Daud, W. A. W.; Baroutian, S. Removal of hexavalent chromium-contaminated water and wastewater: a review. *Water. Air. Soil Pollut.* **2009**, *200* (1–4), 59–77.

(3)   Sharma, S. K.; Petrusevski, B.; Amy, G. Chromium removal from water: a review. *J. Water Supply Res. Technol.-AQUA* **2008**, *57* (8), 541–553.

(4)   Rivero, M. J.; Primo, O.; Ortiz, M. I. Modelling of Cr (VI) removal from polluted groundwaters by ion exchange. *J. Chem. Technol. Biotechnol.* **2004**, *79* (8), 822–829.

(5)   Mohan, D.; Pittman, C. U. Activated carbons and low cost adsorbents for remediation of tri-and hexavalent chromium from water. *J. Hazard. Mater.* **2006**, *137* (2), 762–811.

(6)   Mohan, D.; Singh, K. P.; Singh, V. K. Removal of hexavalent chromium from aqueous solution using low-cost activated carbons derived from agricultural waste materials and activated carbon fabric cloth. *Ind. Eng. Chem. Res.* **2005**, *44* (4), 1027–1042.

(7)   McNeill, L.; McLean, J.; Edwards, M.; Parks, J. State of the science of hexavalent chromium in drinking water. *Water Res. Found.* **2012**.

(8)   Jacobs, J. A.; Testa, S. M. *Overview of chromium (VI) in the environment: background and history*; CRC Press: Boca Raton, FL, 2005.

(9)   Sutton, R. *Chromium-6 in US tap water*; Environmental Working Group, 2010.

(10)   McNeill, L. S.; McLean, J. E.; Parks, J. L.; Edwards, M. A.; others. Hexavalent chromium review, part 2: Chemistry, occurrence, and treatment. *J.-Am. Water Works Assoc.* **2012**, *104* (7), E395–E405.

(11)   US EPA, O. Drinking Water Treatability Database (TDB) https://www.epa.gov/water-research/drinking-water-treatability-database-tdb-0 (accessed May 11, 2017).

(12)   McGuire, M. J.; Blute, N. K.; Seidel, C.; Qin, G.; Fong, L. Pilot-scale studies of hexavalent chromium removal from drinking water. *J. Am. Water Works Assoc.* **2006**, *98* (2), 134–143.

(13)   Edebali, S.; Pehlivan, E. Evaluation of Amberlite IRA96 and Dowex 1$\times$ 8 ion-exchange resins for the removal of Cr (VI) from aqueous solution. *Chem. Eng. J.* **2010**, *161* (1), 161–166.

(14)   Alguacil, F. J.; Alonso, M.; Lozano, L. J. Chromium (III) recovery from waste acid solution by ion exchange processing using Amberlite IR-120 resin: batch and continuous ion exchange modelling. *Chemosphere* **2004**, *57* (8), 789–793.

(15)   Shi, T.; Wang, Z.; Liu, Y.; Jia, S.; Changming, D. Removal of hexavalent chromium from aqueous solutions by D301, D314 and D354 anion-exchange resins. *J. Hazard. Mater.* **2009**, *161* (2), 900–906.

(16)   Kurniawan, T. A.; Chan, G. Y.; Lo, W.-H.; Babel, S. Physico–chemical treatment techniques for wastewater laden with heavy metals. *Chem. Eng. J.* **2006**, *118* (1), 83–98.

(17)   Di Natale, F.; Lancia, A.; Molino, A.; Musmarra, D. Removal of chromium ions form aqueous solutions by adsorption on activated carbon and char. *J. Hazard. Mater.* **2007**, *145* (3), 381–390.

(18)   Han, I.; Schlautman, M. A.; Batchelor, B. Removal of hexavalent chromium from groundwater by granular activated carbon. *Water Environ. Res.* **2000**, *72* (1), 29–39.

(19)   Seidel, C.; Gorman, C.; Ghosh, A.; Dufour, T.; Mead, C.; Henderson, J.; Li, X.; Darby, J.; Green, P.; McNeill, L.; et al. Hexavalent Chromium Treatment with Strong Base Anion Exchange [Project. **2014**.

(20)   Barkat, M.; Nibou, D.; Chegrouche, S.; Mellah, A. Kinetics and thermodynamics studies of chromium (VI) ions adsorption onto activated carbon from aqueous solutions. *Chem. Eng. Process. Process Intensif.* **2009**, *48* (1), 38–47.

(21)   Chromium   in   Drinking   Water: A   Technical   Information   Primer   - UpdatedChromiumInDrinkingWaterSummaryFinal.pdf

http://www.plainfieldnj.gov/docs2016/UpdatedChromiumInDrinkingWaterSummaryFinal.pdf (accessed May 11, 2017).

(22)   Crittenden, J. C.; Trussell, R. R.; Hand, D. W.; Howe, K. J.; Tchobanoglous, G. *MWH's water treatment: principles and design*; John Wiley & Sons, 2012.

(23)   Sotelo, J. L.; Rodríguez, A.; Álvarez, S.; García, J. Removal of caffeine and diclofenac on activated carbon in fixed bed column. *Chem. Eng. Res. Des.* **2012**, *90* (7), 967–974.

(24)   Brunauer, S.; Emmett, P. H.; Teller, E. Adsorption of gases in multimolecular layers. *J. Am. Chem. Soc.* **1938**, *60* (2), 309–319.

(25)   Barrett, E. P.; Joyner, L. G.; Halenda, P. P. The determination of pore volume and area distributions in porous substances. I. Computations from nitrogen isotherms. *J. Am. Chem. Soc.* **1951**, *73* (1), 373–380.

(26)   HORVÁTH, G.; Kawazoe, K. Method for the calculation of effective pore size distribution in molecular sieve carbon. *J. Chem. Eng. Jpn.* **1983**, *16* (6), 470–475.

(27)   Lopez-Ramon, M. V.; Stoeckli, F.; Moreno-Castilla, C.; Carrasco-Marin, F. On the characterization of acidic and basic surface sites on carbons by various techniques. *Carbon* **1999**, *37* (8), 1215–1221.

(28)   Boehm, H. P. Surface oxides on carbon and their analysis: a critical assessment. *Carbon* **2002**, *40* (2), 145–149.

(29)   García-Mateos, F. J.; Ruiz-Rosas, R.; Marqués, M. D.; Cotoruelo, L. M.; Rodríguez-Mirasol, J.; Cordero, T. Removal of paracetamol on biomass-derived activated carbon: modeling the fixed bed breakthrough curves using batch adsorption experiments. *Chem. Eng. J.* **2015**, *279*, 18–30.

(30)   Azizian, S. Kinetic models of sorption: a theoretical analysis. *J. Colloid Interface Sci.* **2004**, *276* (1), 47–52.

(31)   Foo, [5 5] KY; Hameed, B. H. Insights into the modeling of adsorption isotherm systems. *Chem. Eng. J.* **2010**, *156* (1), 2–10.

(32)   Jarvie, M. E.; Hand, D. W.; Bhuvendralingam, S.; Crittenden, J. C.; Hokanson, D. R. Simulating the performance of fixed-bed granular activated carbon adsorbers: Removal of synthetic organic chemicals in the presence of background organic matter. *Water Res.* **2005**, *39* (11), 2407–2421.

(33)   Lo, I. M. C.; Lam, C. S. C.; Lai, K. C. K. Hardness and carbonate effects on the reactivity of zero-valent iron for Cr(VI) removal. *Water Res.* **2006**, *40* (3), 595–605.

(34)   Wendland, F.; Blum, A.; Coetsiers, M.; Gorova, R.; Griffioen, J.; Grima, J.; Hinsby, K.; Kunkel, R.; Marandi, A.; Melo, T.; et al. European aquifer typology: a practical framework for an overview of major groundwater composition at European scale. *Environ. Geol.* **2008**, *55* (1), 77–85.

(35)   Helena, B.; Pardo, R.; Vega, M.; Barrado, E.; Fernandez, J. M.; Fernandez, L. Temporal evolution of groundwater composition in an alluvial aquifer (Pisuerga River, Spain) by principal component analysis. *Water Res.* **2000**, *34* (3), 807–816.

(36)   de Andrade, E. M.; Palácio, H. A. Q.; Souza, I. H.; de Oliveira Leão, R. A.; Guerreiro, M. J. Land use effects in groundwater composition of an alluvial aquifer (Trussu River, Brazil) by multivariate techniques. *Environ. Res.* **2008**, *106* (2), 170–177.

(37)   EC. Council Directive 98/83/EC of 3 November 1998 on the quality of water intended for human consumption http://eur-lex.europa.eu/legal-content/EN/TXT/?uri=CELEX%3A01998L0083-20151027 (accessed Aug 29, 2017).

(38)   Pehlivan, E.; Cetin, S. Sorption of Cr (VI) ions on two Lewatit-anion exchange resins and their quantitative determination using UV–visible spectrophotometer. *J. Hazard. Mater.* **2009**, *163* (1), 448–453.

(39)   Gode, F.; Pehlivan, E. Removal of Cr(VI) from aqueous solution by two Lewatit-anion exchange resins. *J. Hazard. Mater.* **2005**, *119* (1–3), 175–182.

(40)   Pirilä, M.; Cerro, G. J. F. C.; Ainassaari, K.; Gómez, M. M.; Matějová, L.; Keiski, R. L.; others. Adsorption of As (V), Cd (II) and Pb (II), in multicomponent aqueous systems using activated carbons. *Water Environ. Res.* **2017**.

(41)   Gode, F.; Pehlivan, E. A comparative study of two chelating ion-exchange resins for the removal of chromium(III) from aqueous solution. *J. Hazard. Mater.* **2003**, *100* (1–3), 231–243.

(42)   Rengaraj, S.; Yeon, K.-H.; Moon, S.-H. Removal of chromium from water and wastewater by ion exchange resins. *J. Hazard. Mater.* **2001**, *87* (1), 273–287.

(43)   Park, S.-J.; Jang, Y.-S.; Shim, J.-W.; Ryu, S.-K. Studies on pore structures and surface functional groups of pitch-based activated carbon fibers. *J. Colloid Interface Sci.* **2003**, *260* (2), 259–264.

(44)   Liu, Z.; Li, L.; Tang, L.; Shi, R.; Gu, Q.; Liang, X.; Yao, X. Investigation of adsorption performance on 1, 2-dichloroethane by heat and acid modified activated carbon. *J. Environ. Chem. Eng.* **2013**, *1* (3), 131–136.

(45)   Çelik, Z. C.; Can, B. Z.; Kocakerim, M. M. Boron removal from aqueous solutions by activated carbon impregnated with salicylic acid. *J. Hazard. Mater.* **2008**, *152* (1), 415–422.

(46)   Rajaković, L. V.; Ristić, M. D. Sorption of boric acid and borax by activated carbon impregnated with various compounds. *Carbon* **1996**, *34* (6), 769–774.

(47)   Liu, S. X.; Chen, X.; Chen, X. Y.; Liu, Z. F.; Wang, H. L. Activated carbon with excellent chromium (VI) adsorption performance prepared by acid–base surface modification. *J. Hazard. Mater.* **2007**, *141* (1), 315–319.

Supporting Information

S.I.1 Hexavalent and total chromium concentrations in tested groundwater samples

The observed Cr(VI) vs. Cr_{tot} concentration data are shown in Figure S1. The estimated linear model (parameter estimates±95% confidence intervals, determination coefficient, adjusted determination coefficient, p-value and number of data) obtained by linear regression is as follows:

e.S1)
$$Cr(VI) = (0.015 \pm 0.0051) + (1.025 \pm 0.00607) \cdot Cr_{tot}$$
(R^2=0.931, R^2_{adj}=0.930, p-value<0.001, n=80)
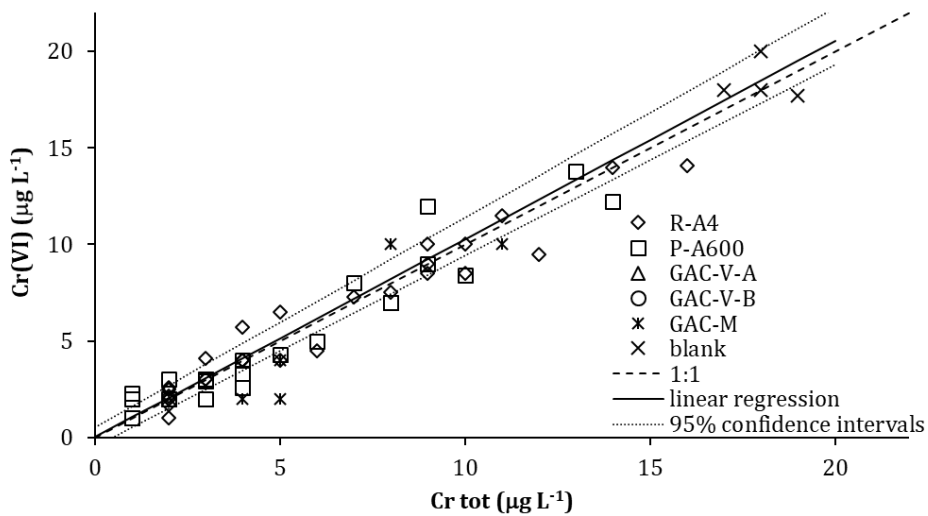
Figure S1 Cr_{TOT} vs. Cr(VI) data measured in samples from kinetic experiments with different sorbents. 1:1 line, linear regression curve and the relative 95% confidence intervals are also reported.

S.I.2 Kinetic and equilibrium isotherm experiments
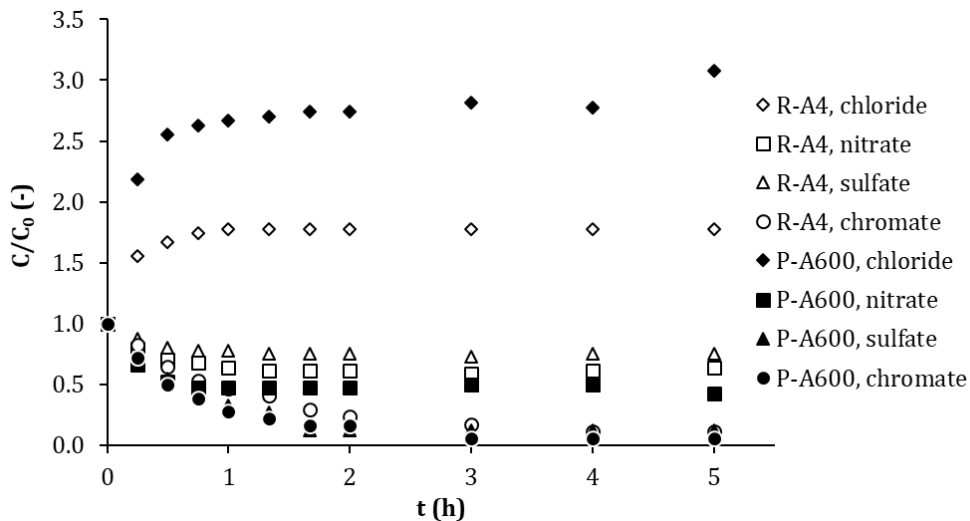
Figure S2 Liquid-phase normalized concentrations of nitrate, sulfate, Cr_{tot} (chromate) and chloride over time determined in kinetic experiments with SBA resins.
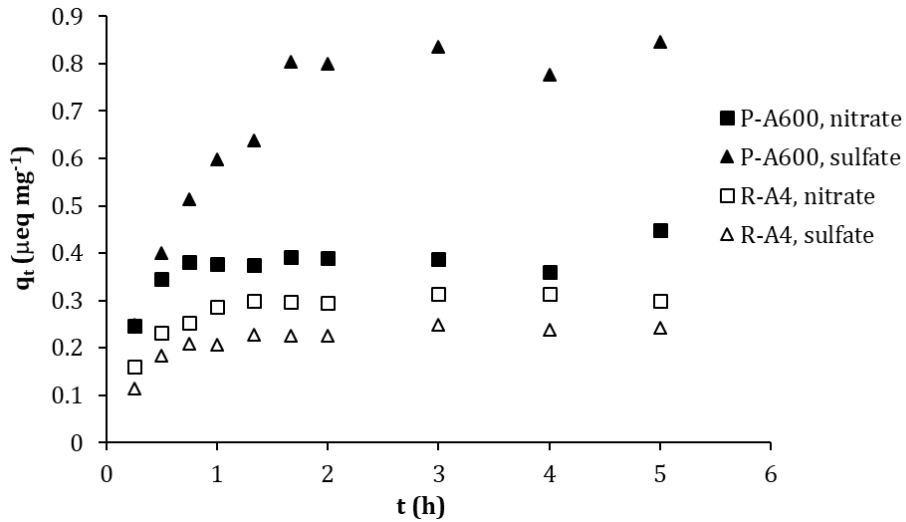
Figure S3 Solid-phase concentration of nitrate and sulfate ions over time determined in kinetic experiments with SBA resins.
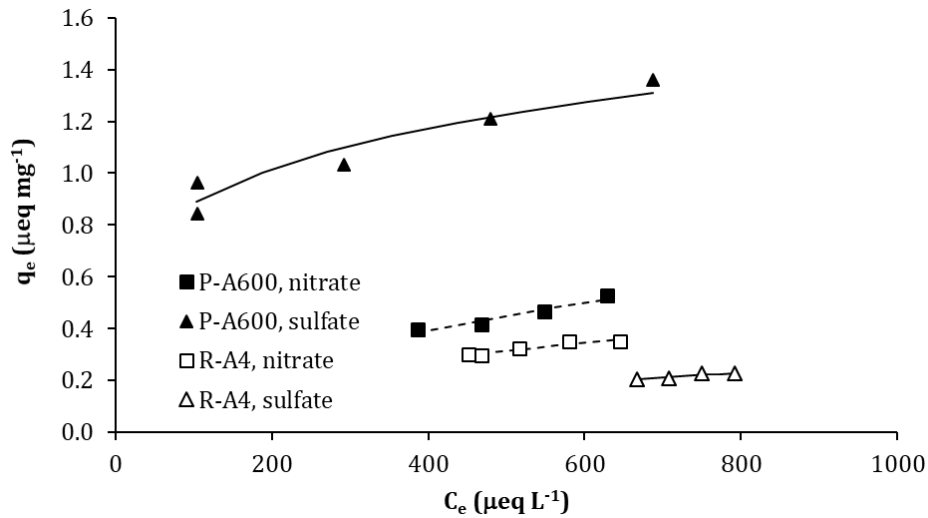
Figure S4 Solid- vs. residual liquid-phase concentrations of nitrate and sulfate ions determined in isotherm experiments with SBA resins. Lines are the curves simulated by Freundlich isotherm models.

Table S1 Parameters (estimate±95% confidence interval), number of data used for regression and determination coefficients (R^2) of Freundlich isotherms for nitrate and sulfate sorption onto SBA resins.

parameters	P-A600		R-A4	
	nitrate	sulfate	nitrate	sulfate
K_F [(μeq mg^{-1})(L μeq^{-1})$^{1/n}$]	0.009±0.0256	0.330±0.2339	0.013±0.0268	0.002±0.0097
1/n [-]	0.619±0.4283	0.212±0.1217	0.509±0.3211	0.749±0.9743
n. of data	5	5	5	5
R^2 [-]	0.953	0.916	0.893	0.846
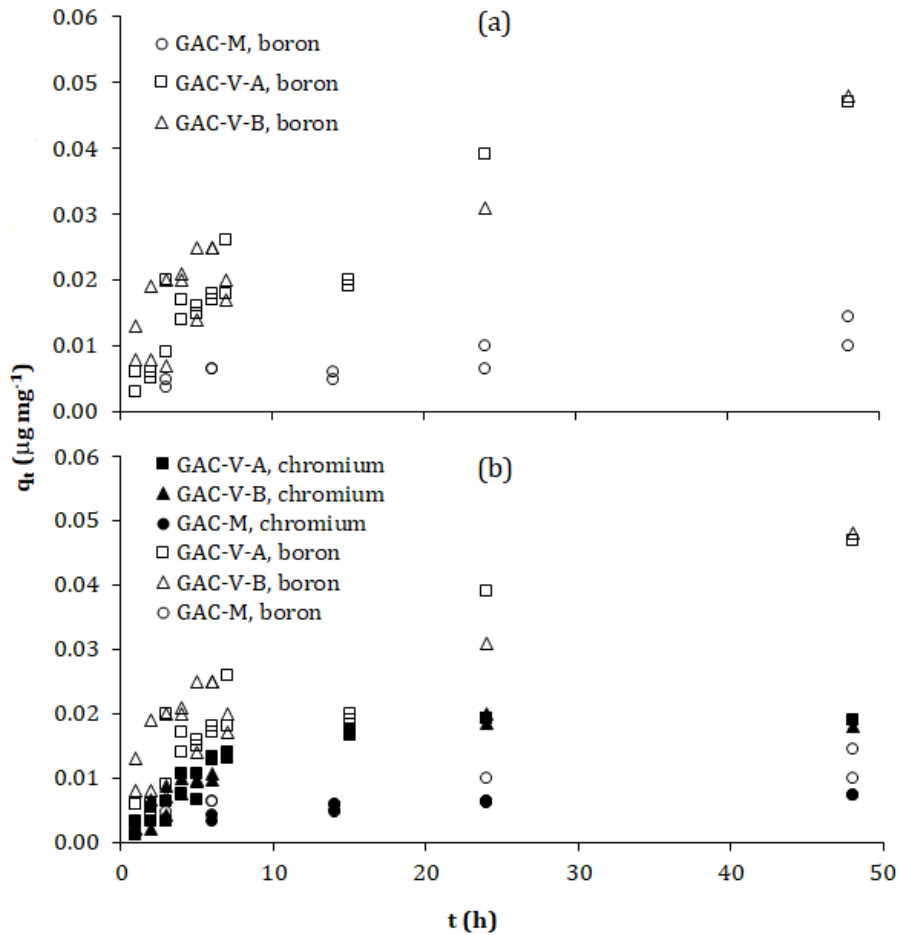
Figure S5 a) solid-phase concentration of boron over time determined in kinetic experiments with GACs; b) comparison between boron and chromium kinetics.
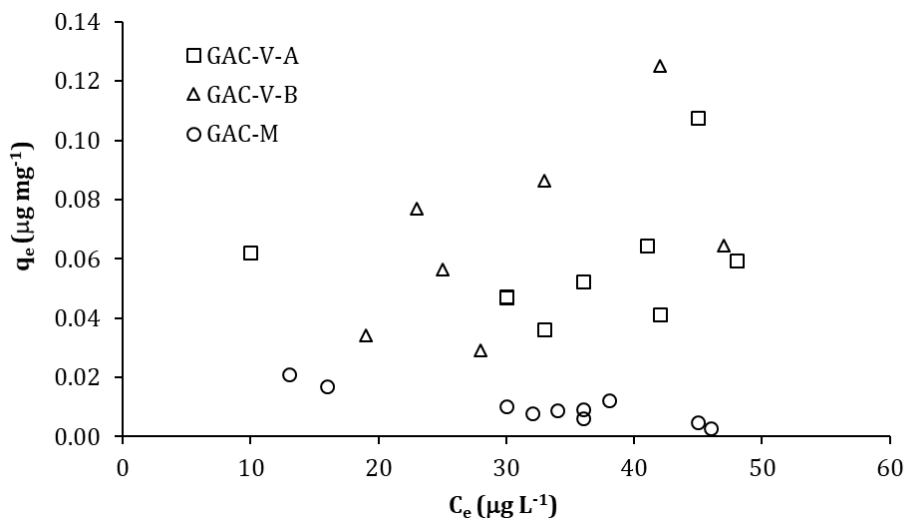
Figure S6 Solid- vs. residual liquid-phase concentrations of boron determined in isotherm experiments with carbons.

S.I.3 GAC characterization
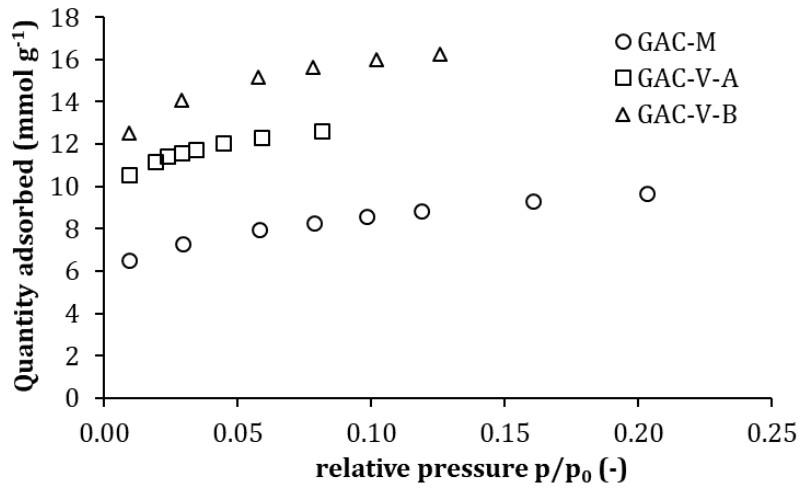
Figure S7 N_2/77 K isotherms of the carbons for BET surface area determination.
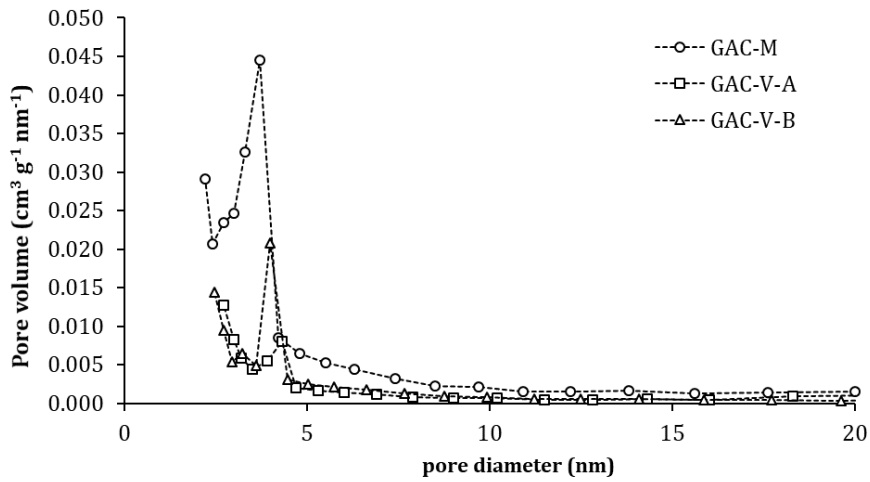
Figure S8 Pore size distribution of the carbons.
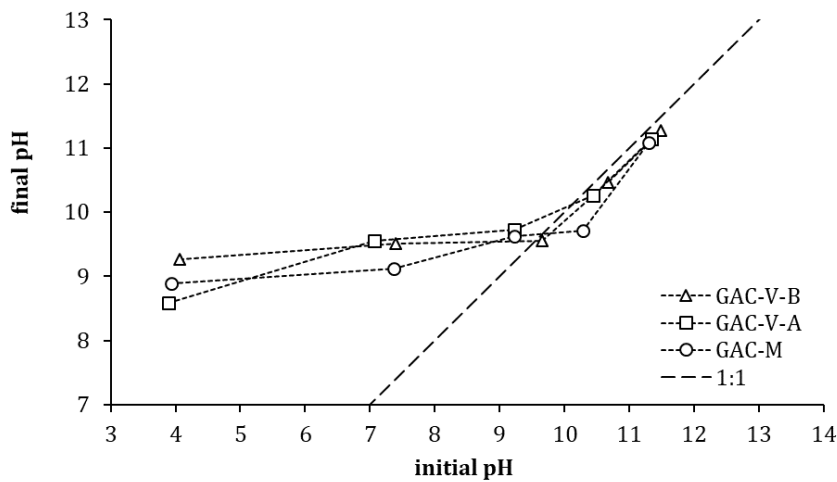
Figure S9 Initial vs. final pH measured by pH drift method for the carbons. Each point is the average value of two experimental replicates.
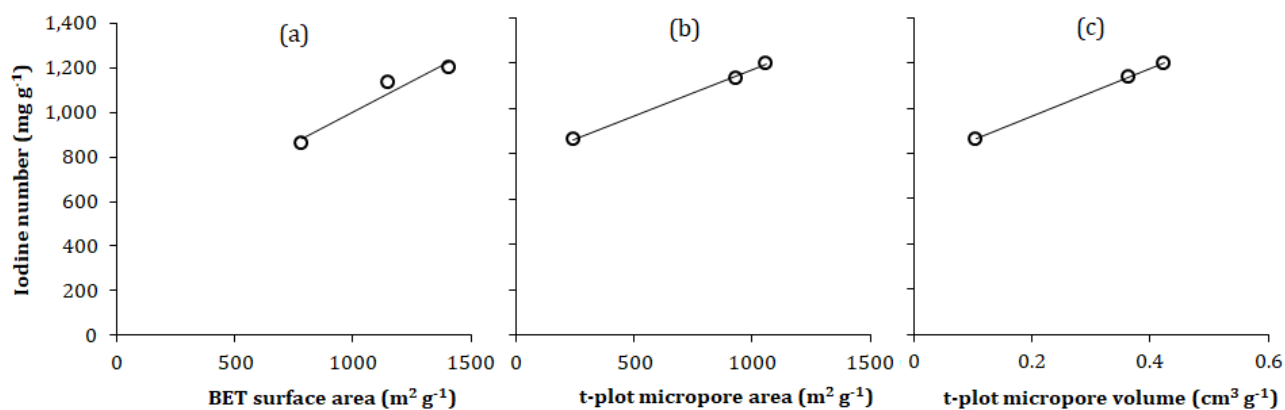
Figure S10 Linear regression between iodine number and (a) BET surface area (R^2=0.94), (b) t-plot micropore area (R^2>0.99) and (c) t-plot micropore volume (R^2>0.99) of the three GACs.

S.I.4 Real-scale adsorption phase monitoring
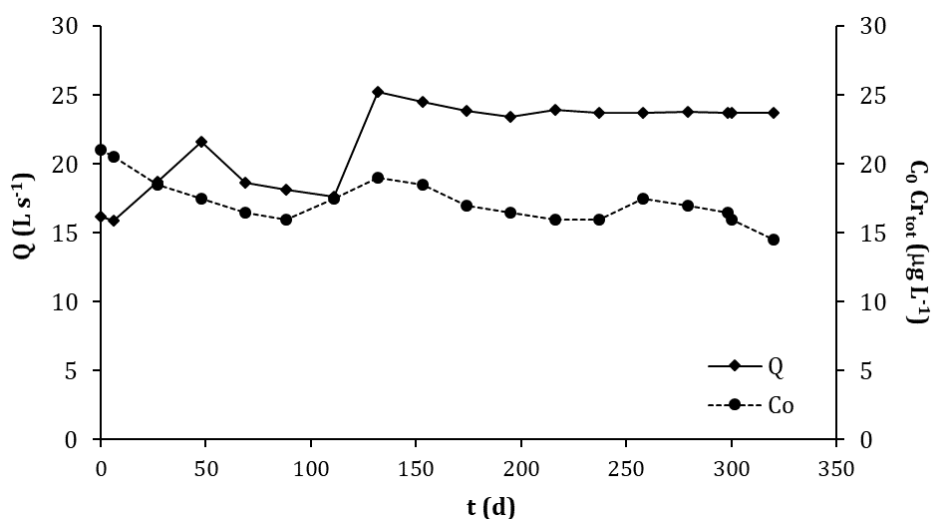
Figure S11 Water flow rate (Q) and influent Cr_{TOT} concentration (C_0) measured during real-scale adsorption phase monitoring. Q values are referred to a single filter.

Table S2 Influent (C_0, average±st.dev.) and normalized effluent (C/C_0) concentrations of VOCs observed over specific throughput in real-scale GAC adsorption phase.

contaminant	freon 141b	cis-1,2-dichloroethylene	chloroform	TCE	PCE
C_0 (µg L^{-1})	1.1±0.32	1.0±0.00	2.0±0.47	1.1±0.32	8.8±2.10
$V_{SP,OBS}$ (L g^{-1})	C/C_0 (-)				
0.0	0.00	0.00	0.00	0.00	0.00
6.1	0.00	0.00	0.00	0.00	0.00
17.1	1.00	0.00	1.00	0.00	0.00
25.3	1.00	0.00	1.25	0.00	0.00
32.3	1.00	0.00	1.00	0.00	0.00
47.7	1.00	0.00	1.00	0.00	0.00
54.5	1.00	1.00	1.00	1.00	0.00
61.3	1.00	1.00	1.00	0.00	0.00
69.8	1.00	1.00	1.00	1.00	0.00
76.6	1.00	1.00	1.00	0.00	0.00

S.I.5 Theoretical breakthrough for sulfate and nitrate ions

The breakthrough of sulfate and nitrate ions for SBA resins has been estimated with the same procedure followed for chromium, by using equations e.4 (section 2.4), e.6 and e.7 (section 2.5), considering the influent concentrations (C_0) reported in Table 3 (section 3.1) and the Freundlich parameters reported in Table S1 (S.I.2). The theoretical breakthrough curves of chromate, sulfate and nitrate for P-A600 and R-A4, expressed as C/C_0 vs. $V_{SP,th}$, are reported in Figure S12.
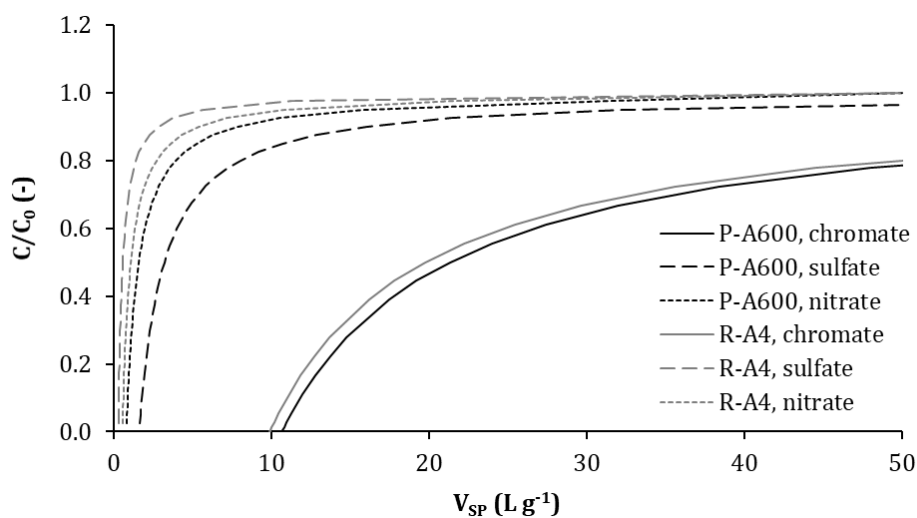
Figure S12 Theoretical breakthrough (C/C_0) of chromate, sulfate and nitrate ions as a function of the specific throughput (V_{SP}).

Specific and total *N*-nitrosamines formation potential of nitrogenous micropollutants and model amines during oxidation treatments

Abstract

N-nitrosamines are a group of potent human carcinogens that can be formed during oxidative treatment of drinking water and wastewater. Many tertiary and quaternary amines present in consumer products (e.g., pharmaceuticals, personal care and household products) are known to be *N*-nitrosodimethylamine (NDMA) precursors during chloramination, but the formation of other *N*-nitrosamines has been rarely studied. This study investigates the specific and total *N*-nitrosamine (TONO) formation potential (FP) of various precursors from nitrogen-containing micropollutants (chlorhexidine, metformin, benzalkonium chloride and cetyltrimethylammonium chloride) and tertiary and quaternary model amines (trimethyl amine, *N,N*-dimethylbutyl amine, *N,N*-dimethylbenzyl amine and tetramethyl ammonium). Various oxidative treatments (namely chloramination, chlorination and ozonation) were preliminary tested for all the studied nitrogenous micropollutants and the highest TONO FP were observed upon chloramination, with molar yields in the range 0.04-11.92%. However, the observed TONO pools constituted mostly of uncharacterized species, not included in US-EPA 8270 *N*-nitrosamines standard mix. Only the quaternary ammonium compound benzalkonium chloride showed quantifiable NDMA FP (0.56% molar yield), however, explaining only a minor fraction of the observed TONO FP. The studied model amines showed molar NDMA yields from 0.10% (trimethyl amine) to 5.05% (*N,N*-dimethylbenzyl amine), very similar to the molar TONO yields. The comparison of the FPs of micropollutants and model compounds showed that the presence of electron donating functional groups (such as a benzyl group) in tertiary and quaternary amine precursors leads to a higher formation of NDMA and uncharacterized *N*-nitrosamines, respectively. LC-qTOF screening of a list of proposed *N*-nitrosamine structures has enabled to identify a novel *N*-nitrosamine (*N*-nitroso-*N*-methyldodecylamine) from the chloramination of benzalkonium chloride. This finding supports the hypothesis that different functional groups in quaternary amines can act as leaving groups during chloramination and form differing *N*-nitrosamine structures at significant yield. Molar TONO yields determined for micropollutants were finally validated under experimental conditions closer to real water matrices, confirming their representativeness also for lower concentration ranges.

Keywords: total *N*-nitrosamines (TONO), NDMA, nitrogenous micropollutants, *N*-nitrosamines formation potential, chloramination.

1. Introduction

N-nitrosamines are a group of emerging disinfection by-products that can be formed during chloramination, chlorination and ozonation of drinking water and wastewater ([1–3]). Several *N*-nitrosamines are classified as probable human carcinogens and mutagens, with low nanogram-per-litre drinking water concentrations associated with a 10^{-6} lifetime excess cancer risk ([4]). US-EPA listed 5 *N*-nitrosamines on the Contaminant Candidate List 3 (CCL3) and is considering promulgation of regulation limits for their concentrations in drinking water ([2]).

Previous studies ([3,5–7]) showed that various consumer products, such as pharmaceuticals, personal care and household products, play an important role in the formation of *N*-nitrosamines. These classes of compounds are typically present in municipal wastewater effluents, wherefrom they are discharged into the aquatic environment and may reach water resources used for drinking water production ([8]). Zeng and Mitch (2015) ([5]) found that domestic greywater and blackwater streams are significant sources of chloramine-reactive and ozone-reactive *N*-nitrosamine precursors. Even though specific precursors have not been characterized, *N*-nitrosamine formation was associated with the presence of shampoos, handsoaps, dishsoaps and pharmaceuticals. Specific *N*-nitrosamine precursors may include tertiary or quaternary amines, being common macro-constituents of many consumer products ([9,10]).

Various tertiary amines commonly present in herbicides and in pharmaceutical and personal care products were found to be *N*-nitrosodimethylamine (NDMA) precursors during chloramination, showing molar conversion yields varying from <1% up to 60-90% for ranitidine ([3,7,10–16]). Various mechanisms have been proposed for NDMA formation during chloramination of tertiary amines ([17–20]). NDMA formation was initially attributed to the liberation of the dimethylamine (DMA) moiety via reactions of chlorine or monochloramine followed by reactions between DMA and dichloramine ([2,3,12]). Further studies suggested that tertiary amines can also form *N*-nitrosamines without proceeding through a secondary amine intermediate, but through nucleophilic attack of the amine on chloramine ([15]). Recent studies showed that the stability and the electron distribution of the moieties bound to the DMA group play a key role in NDMA formation and strongly affect NDMA conversion yields ([20]). In particular, the presence of an electron-donating group close to the DMA moiety can increase the electron density on the nitrogen atom, enhancing a nucleophilic attack on the chloramines ([7,10,15]).

Compared to tertiary amines, only few studies investigated the formation of *N*-nitrosamines from specific quaternary ammonium compounds (QACs). Kemper et al. (2010) ([6]) found that NDMA is formed during chloramination of different QACs used as surfactant and disinfection agents, such as quaternary alkylamines and benzyl trialkylamines, with relatively low molar yields (0.03-0.28%). So far, the formation mechanism of the formation of *N*-nitrosamines from QACs remains unclear. The full substitution of the nitrogen and the positive charge on the quaternary amine should hinder the reaction with chloramines ([2]). QACs can contain impurities that might constitute potential *N*-nitrosamines precursors. However, Kemper et al. (2010) ([6]) have shown that the formation of *N*-nitrosodibutylamine (NDBA) by chloramination of benzyltributylammonium chloride only slightly decreased after purification. This indicates that the QAC itself, rather than impurities, was the dominant *N*-nitrosamine precursor. Even though the reaction pathways have not been defined, the same authors suggested that the NDMA formation from QACs may involve amidogen or chloramino radicals formed from chloramines. Some quaternary amine monomers (e.g., choline, cocoamidopropyl betaine) and polymers (e.g., polyquaternium-7, polyDADMAC and polyacrylamide) were also found to form NDMA during free chlorine and chlorine dioxide disinfection, with low molar yields between 0.0003% and 0.3% ([21]).

The majority of the studies in the literature deals with the formation of NDMA, being the most often detected *N*-nitrosamine in tap and wastewater ([22,23]). However, previous studies showed that NDMA is often a minor part of the total *N*-nitrosamines (TONO) pool ([5,9,24]). Analysing 36 drinking water treatment plants and distribution systems, Dai and Mitch (2013) ([9]) found that NDMA made up only

5% of the TONO pool on a median basis. Zeng and Mitch (2015) ([5]) observed that the contribution of NDMA to TONO was 1-11% and 3-60% in domestic greywater streams treated by chloramine and ozone, respectively. The same authors suggested that the precursors of the uncharacterized *N*-nitrosamine fraction were associated to common macro-constituents of consumer products, such as QACs present in shampoos and soaps.

While many NDMA precursors were identified in the literature, the determination of the TONO formation potential (FP) of specific model compounds is not a common procedure. The investigations of *N*-nitrosamine formation are typically limited to the species detected by US-EPA method 521 ([25]), while the identity of the other components of the TONO pool remains unclear.

The goal of this study was to investigate the formation of *N*-nitrosamines during chloramination, ozonation and chlorination of various nitrogenous compounds, that can be discharged to municipal wastewater and may end up in the receiving water bodies. The investigated compounds included two quaternary ammonium compounds used as disinfectants and surfactants (benzalkonium chloride, BZK, a mixture of benzyl trialkylamines, and cetyltrimethylammonium chloride, CTMA, a quaternary alkylamine) and two biguanides (chlorhexidine, CHD, an antiseptic agent used in disinfectants, pharmaceuticals and cosmetics, and metformin, MET, a prescription drug used for treating diabetes).

Laboratory-scale experiments on model solutions were performed to determine the formation potential of total and specific *N*-nitrosamines for the studied precursors as a function of the pH. Besides analysis of TONO and *N*-nitrosamines from the US-EPA 8270 standard mix ([25]), high resolution MS analyses were carried out to identify the components of the unknown fraction of TONO. The role of the molecular structure of the precursors on *N*-nitrosamine formation was further investigated by model tertiary and quaternary amines (such as trimethyl amine, *N,N*-dimethylbutyl amine, *N,N*-dimethylbenzyl amine and tetramethyl ammonium) containing functional groups similar to the selected consumer product moieties.

2. Materials and methods
2.1 Chemicals and reagents

All the experiments were conducted in ultrapure water (Milli-Q, Millipore) buffered with a phosphate buffer (0.5 M) at different pH values (6, 7 or 8).

Chlorhexidine dihydrochloride (CHD, >98%), metformin hydrochloride (MET, 99%), benzalkonium chloride (BZK, >95%), cetyltrimethylammonium chloride (CTMA, 25%wt in H_2O), tetramethylammonium chloride (TMA, >99%), trimethylamine (TrMA, 98%), *N,N*-dimethylbenzyl amine (DMBzA, >99%) and *N,N*-dimethylbutyl amine (DMBA, 99%) were purchased from Sigma-Aldrich. The molecular structures and main properties of the selected compounds are provided in Table 1. Concentrated stock solutions of each precursor were prepared in ultrapure water. The US-EPA 8270 *N*-nitrosamine standard mix, containing *N*-nitrosodimethylamine (NDMA), *N*-nitrosodiethylamine (NDEA), *N*-nitrosomethylethylamine (NMEA), *N*-nitrosomorpholine (NMOR), *N*-nitrosodibutylamine (NDBA), *N*-nitrosopiperidine (NPIP), *N*-nitrosopyrrolidine (NPYR), *N*-nitrosodipropylamine (NDPA) and *N*-nitrosodiphenylamine (NDPhA), was purchased from Sigma-Aldrich. Monochloramine stock solutions were prepared daily as described by Le Roux et al. (2011) ([7]) using sodium hypochlorite (NaOCl, 15-20%, Sigma-Aldrich) and ammonium chloride (99.9%, VWR Chemicals). The concentrations of monochloramine (NH_2Cl) and dichloramine ($NHCl_2$) (see section 2.3) in the stock solutions were measured after preparation; the $NHCl_2$ concentration was always not quantifiable (see section 2.3). Ascorbic acid, HPLC grade acetonitrile, dichloromethane and methanol were purchased from Sigma-Aldrich. Sodium hypochlorite stock solution was daily prepared in ultrapure water. Ozone gas was produced from ultrapure oxygen gas (>99.9995%) by ozone generator (Innovatech, CMG 3-5). Ozone stock solution was prepared injecting the produced ozone gas by a tube equipped with a fritted glass into a 1 L glass bottle filled with ultrapure water maintained at low

temperature with an ice bath. Ozone concentration in the stock solution was measured before use (section 2.3).

2.2 Experimental procedures

2.2.1 Preliminary oxidation tests

Preliminary oxidation experiments (chloramination, chlorination and ozonation) with CHD, MET, BZK and CTMA were conducted in 10 mL solutions, composed of variable volumes of precursor stock solution, sodium phosphate buffer (125 mM, pH 7), pre-formed oxidant stock solution and ultrapure water. The initial concentration of the precursors was set at 0.1 mM for CHD and 0.5 mM for all the other precursors. Chloramination and chlorination tests were performed at 7 days reaction time and initial oxidant concentration (NH_2Cl or NaOCl) corresponding to 10- fold molar excess, for BZK, and 200-fold molar excess, for CHD, MET and CTMA, with respect to the initial precursor concentration (according to preliminary tests, assuring the maximum *N*-nitrosamine production). In ozonation tests, a known volume of ozone stock solution was added by a glass syringe obtaining an ozone concentration of 0.6 mM. After an initial mixing on magnetic stirrer, the solution was left for 24 h under dark and calm conditions. The monitoring of ozone residual concentration over time (section 2.3) during preliminary tests showed that 24 h contact time was enough for the complete consumption of the dosed ozone. TONO concentration (section 2.3) was measured at the end of the oxidation tests. All the experiments were performed in duplicate.

2.2.2 Chloramination tests

The self-decay of monochloramine at various initial concentrations (1, 5, 20 and 100 mM) and pH values (6, 7 and 8) was investigated by measuring the NH_2Cl concentration over time (see section 2.3) in buffered ultrapure water solutions. Chloramination experiments were conducted in amber borosilicate bottles at room temperature (23°C) under two experimental setups (ES), denoted ES1 for high concentrations of precursors and ES2 for more realistic lower concentrations of precursors.

Under ES1, reactions were conducted in 10 mL solutions, composed of variable volumes of precursor stock solution, sodium phosphate buffer (125 mM), pre-formed monochloramine stock solution and ultrapure water. The initial concentration of the precursors was set to 0.1 mM for CHD and 0.5 mM for all the other precursors. *N*-nitrosamine FP is the operationally defined maximum *N*-nitrosamine concentration that can be formed from a precursor, using a NH_2Cl concentration and a contact time much higher than applied during drinking water treatment ([2]). In this study, the experimental conditions to be adopted in the FP tests (i.e., reaction time, initial concentrations of precursors and monochloramine) under ES1 were selected according to a series of preliminary kinetic tests. The kinetics of *N*-nitrosamine formation from CHD, MET, BZK and CTMA at pH 7 were investigated by testing different initial NH_2Cl concentrations (corresponding to 10-, 20-, 40-, 100- and 200-fold molar excess) and reaction times (1, 2, 5, 7 and 10 days) and measuring TONO concentrations and the residual precursor concentrations (only for CHD and BZK) (SI, Text S3). According to the results of kinetic tests (discussed in section 3.1), FP tests at pH 6, 7 and 8 were conducted with all the precursors (micropollutants and model compounds) at a reaction time of 7 days and a 200-fold molar excess of NH_2Cl relative to the precursor compound; only in the case of BZK, FP tests were performed with a 10-fold NH_2Cl molar excess, assuring the highest *N*-nitrosamine production (according to kinetic test results discussed in section 3.1). The concentrations of TONO and *N*-nitrosamines of the US-EPA 8270 standard mix (see section 2.3) were measured at the end of the FP tests.

In ES2, 7 days FP tests were conducted in 0.5 L solutions, containing deionized water, 1 mM sodium phosphate buffer (pH 8), 100 μM and 0.5 μM initial concentrations of monochloramine and precursor, respectively (corresponding to a 200-fold NH_2Cl molar excess). The TONO concentration was measured after sample pre-concentration by solid phase extraction (see section 2.3).

The molar yield of *N*-nitrosamines formation was calculated as the ratio between the produced molar concentration of the *N*-nitrosamine and the molar concentration of the precursor.

For all the chloramination experiments, reaction solutions were quenched at the end of the pre-determined reaction time by dosing an ascorbic acid stock solution (280 mM) to get a stoichiometric excess relative to the initial NH_2Cl concentration. Quenched solutions were stored at 4°C in the dark. All the experiments were performed in duplicate.

2.3 Analytical methods

NH_2Cl and $NHCl_2$ concentrations were determined spectrophotemetrically (Shimadzu, UV-1800) using their respective molar extinction coefficients at 245 and 295 nm, respectively, and solving the equations expressing absorbance values at the two wavelengths simultaneously ([26]). The $NHCl_2$ concentration is quantifiable only when the ratio between absorbance values at 295 nm and 245 nm is ≥3%, corresponding to a $NHCl_2$:NH_2Cl molar ratio ≤0.01%.

Ozone concentration in stock solutions was determined spectrophotometrically (Shimadzu, UV-1800) by mixing 1 mL of ozone solution with 2 mL of 50 mM H_3PO_4 solution in a 1 cm quartz cuvette and assuming a molar extinction coefficient at 260 nm of 3200 M^{-1} cm^{-1}. Ozone decay in oxidation tests solutions was monitored by the Indigo method ([27]).

Total *N*-nitrosamine concentrations were measured by a method based on UV photolysis and chemiluminescence measurement of nitric oxide (see Breider and von Gunten (2017) ([28]) for more details). The chemiluminescence signal was related to the TONO concentration by a standard curve, obtained with different concentrations of the US-EPA 8270 *N*-nitrosamine standard mix (from 0.8 to 16.2 µM). The test solutions in absence of monochloramine were compared with ultrapure water, to verify the absence of a background signal. The calibration was repeated daily before each measurement trial. The limit of detection (LOD) and quantification (LOQ) at the 95% confidence level of the analytical method were calculated based on the standard error (SE) and the slope (m) of the calibration curve (LOD=3.3×SE/m, LOQ=10×SE/m). Average (±standard deviation) LOD and LOQ resulted equal to 0.3±0.15 µM and 1.0±0.45 µM, respectively. For each sample, TONO was measured in triplicate.
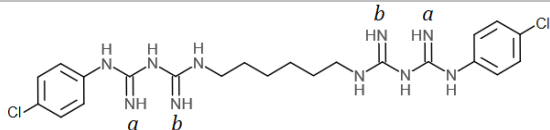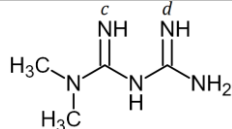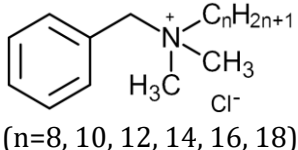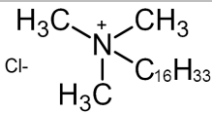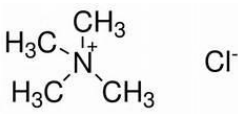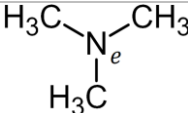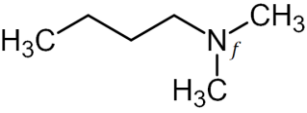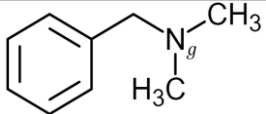
US-EPA 8270 standard mix *N*-nitrosamines were analysed by GC-MS/MS (Trace 1310 Series GC, Thermo) according to the method described by Chen et al. (2012) ([29]). LOD and LOQ for the investigated *N*-nitrosamines are reported in S.I.1 (Table S1). The measurements were done in duplicate.

Samples obtained from FP tests in ES1 were analysed by liquid chromatography quadrupole time-of-flight mass spectrometry (LC-qTOF). All the details about the analytical method and instruments are reported in S.I.2. Data obtained by LC-qTOF analysis were elaborated to verify the presence of a list of proposed compounds, according to the following procedure: the exact mass (*m/z*) of each compound was extracted from the chromatogram. If a peak with intensity at least 3 orders of magnitude higher than the background noise was observed, the mass spectrum in correspondence of the peak retention time was further analysed. A list of possible molecular formulas was generated by the ChemCalc software ([30]) from the masses observed in the MS spectrum. If the mass of a possible molecular formula corresponded to the theoretical one with an error <5 ppm, the identification was considered positive.

Samples obtained in FP tests under ES2 were pre-concentrated by solid phase extraction (SPE) following a modified US-EPA Method 521 protocol: 0.5 L samples were passed under vacuum through pre-conditioned Superclean Coconut charcoal $2g/6cm^3$ cartridges (Supelco), subsequently dried with ultrapure nitrogen gas flow for 15 min. Cartridges were eluted with 6 mL of HPLC grade acetonitrile (dichloromethane was not used as eluent it could be not injected into the nitric oxide analyser). The solvent was evaporated at ambient temperature with a nitrogen flow to a volume of about 2 mL. The

recovery of TONO by SPE (η) was specifically assessed for the TONO pools produced by CHD, BZK, CTMA and MET, according to the following procedure: firstly, a 7 days chloramination test was conducted in ES1 (as described in section 2.2) and TONO concentration (C_1) was measured; samples (V_1=10 mL) were then diluted by ultrapure water, obtaining 0.5 L (V_2) solution of a known TONO concentration (C_2), calculated considering the dilution factor ($C_2=C_1\cdot V_1/V_2$). The sample was then concentrated by SPE in about 2 mL (V_3) and the TONO concentration (C_3) was measured. The TONO recovery was finally calculated ($\eta=C_3\cdot V_3/C_2/V_2$). The recovery efficiency of SPE was also evaluated for a solution containing 0.16 µM US-EPA 8270 *N*-nitrosamine standard mix, 1 mM phosphate buffer (pH 8) and 2 mM ascorbic acid.

Table 1 Selected micropollutants and model compounds: molecular structure, molecular weight (MW) and experimentally determined pK_a values (references given in the footnotes). For CHD and MET, the pK_a values are referred to the equilibrium $C=NH_2^+ \leftrightarrows C=NH + H^+$.

Compound	Structure	MW (g mol^{-1})	pK_a
Micropollutants			
Chlorhexidine dihydrochloride (CHD)		578.4	2.20 [a] 10.30 [b]
Metformin hydrochloride (MET)		165.6	10.27 [c] 2.97 [d]
Benzalkonium chloride (BZK)	(n=8, 10, 12, 14, 16, 18)	283.4-423.4 (average 348.4)	-
Cetyl trimethyl ammonium chloride (CTMA)		319.4	-
Model compounds			
Tetramethyl ammonium chloride (TMA)		109.6	-
Trimethyl amine (TrMA)		59.1	9.80 [e]
N,N-dimethylbutyl amine (DMBA)		101.2	10.19 [f]
N,N-dimethylbenzyl amine (DMBzA)		135.2	8.91 [g]

a, b (31)

c, d (32)

e, f, g ChemIDplus-Toxnet database (https://chem.nlm.nih.gov/chemidplus/).

3. Results and discussion

3.1 Preliminary comparison of oxidation treatments

Three oxidative treatments commonly applied for water pre-oxidation and disinfection were tested. TONO concentrations formed by chloramination, ozonation and chlorination of CHD, BZK, CTMA and MET, reported as formation molar yields, are shown in Figure 1. According to previous studies ([21,33]), the highest TONO production was obtained during chloramination (molar yields between 0.09% and 4.93%), for all the micropollutants; for CHD and CTMA, ozonation led to higher TONO molar yields than chlorination, while an opposite behaviour was observed for BZK. Not quantifiable TONO concentrations were observed during ozonation and chlorination of MET.

Giving the highest *N*-nitrosamine production and assuring significant experimental results for all the precursors, only chloramination was further investigated in this study.
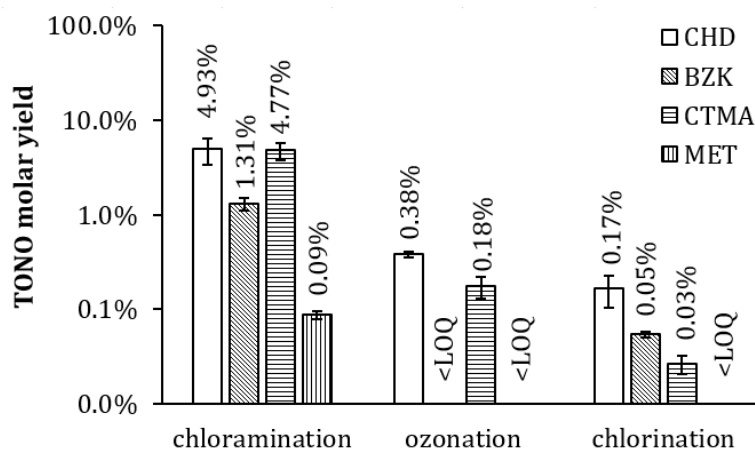
Figure 1 TONO molar yields at pH 7 for CHD, BZK, CTMA and MET during preliminary tests with different oxidants. Initial precursor concentration was 0.1 mM for CHD and 0.5 mM for the other compounds; initial NH_2Cl and NaOCl molar excess was 10-fold for BZK and 200-fold for the other compounds; initial ozone concentration was 0.6 mM; reaction time was 7 days, for chloramination and chlorination, 24 h for ozonation. Data represent the average ± standard deviation of three measurement repetitions on two experiment replicates.

3.2 Total *N*-nitrosamine formation potential (FP) during chloramination of micropollutants

The results of kinetic tests are shown in Figure 2, reporting the TONO concentrations observed for BZK, CTMA, CHD and MET at pH 7 as a function of the reaction time and the monochloramine dose. For each NH_2Cl dose, all the selected micropollutants showed a similar trend for the TONO concentrations, rapidly increasing in the first 2-5 days and reaching a saturation concentration after about 7 days. For CTMA and MET, a higher NH_2Cl dose yielded a higher TONO formation (TONO concentrations from MET detected only for 100- and 200-fold NH_2Cl molar excess); a similar trend was observed for CHD, for which TONO production was comparable at the highest NH_2Cl doses (100- and 200-fold molar excess). An opposite behaviour was observed for BZK, for which TONO concentrations obtained at 10- and 20-fold molar excess were about 2-times higher than those obtained at 100- and 200-fold molar excess. This opposing trend for BZK compared to the other precursors is unclear and further studies are needed to elucidate this phenomenon. The monitoring of residual CHD and BZK concentrations during kinetic tests (S.I.3, Figure S2) showed that the precursors were rapidly consumed, with a >85% removal after 1 day of reaction. At the same time, NH_2Cl concentration was expected to decrease over time by disproportionation, as indicated by the monitoring of NH_2Cl decay in control solutions (S.I.3, Figure S1).

Based on the results of kinetic tests, a 200-fold NH_2Cl molar excess was adopted for conducting FP tests with CHD, MET and CTMA, leading to the maximum TONO formation, while a 10-fold NH_2Cl molar excess was adopted for BZK. For all the precursors, a reaction time of 7 days was selected for FP tests, being sufficient to reach the maximum TONO concentrations.

Samples obtained from FP tests at pH 6, 7 and 8 were firstly analysed for the specific *N*-nitrosamines present in the US-EPA 8270 standard mix. Among the analysed samples, NDMA concentrations higher than the LOQ (0.09 μM) were measured only for BZK at pH 8, while in all the other samples NDMA was not detectable. None of the other *N*-nitrosamines of the US-EPA 8270 standard mix was detected after the FP tests for any of the precursors.

The average NDMA concentration formed by BZK was 2.81±0.13 μM, corresponding to a molar formation yield of 0.56±0.03% (Table 2). This value is consistent with previous observations ([6]) at pH 7 for the two main constituents of the benzalkonium chloride mixture: benzyldimethyldodecylamine (0.28% molar NDMA yield) and benzyldimethyltetradecylamine (0.26% molar NDMA yield).

No NDMA formation was observed for CTMA and MET. However, this result was not unexpected, based on previous findings. In fact, relatively low molar NDMA yields for CTMA (0.03%) and MET (<0.04%) have been observed in previous studies ([6,10]). Hence, considering these low molar yield values, NDMA concentrations close to the LOQ would have been expected in the current study and were therefore not detected.

The determined TONO FP for CHD, MET, BZK and CTMA at various pH values are reported in Table 2, expressed as molar TONO yields. Unlike the US-EPA 8270 standard mix for *N*-nitrosamines, TONO measurements displayed detectable *N*-nitrosamine concentrations in all the samples. It can be observed that, for all precursor compounds, TONO formation increased with increasing pH. The pH-dependence of the *N*-nitrosamine formation can be explained by (i) the increasing NH_2Cl stability with increasing pH and (ii) the acid-base speciation of some of the precursors. (i) The NH_2Cl self-decomposition (S.I.3, Figure S1) is slower at higher pH values, resulting in a higher NH_2Cl exposure during the FP test, which in turn may lead to a higher total *N*-nitrosamine production. For CHD and MET, the increase in TONO formation with increasing pH can also be explained by the acid-base speciation of these compounds (pK_a-values in Table 1). The deprotonated forms of CHD and MET (as well as TrMA, DMBA and DMBzA) increase with increasing pH, which enhances the nucleophilic attack on NH_2Cl, resulting in significantly higher *N*-nitrosamine yields ([15]).

Among the studied precursor compounds, CHD exhibited the highest molar TONO yields at all pH values, ranging from 2.64±1.45% at pH 6 to 11.92±0.83% at pH 8. Molar TONO yields ≤4.93±1.42% (pH 8) were obtained for CTMA, while BZK showed molar conversions of ≤2.12±0.40%, depending on pH. Among the studied micropollutants, MET showed the lowest TONO yields (≤0.21±0.03%), being at least one order of magnitude lower than for the other compounds, for a given pH value.

These results demonstrate that, despite the low NDMA yields, the studied precursors can produce significant total *N*-nitrosamine concentrations. The composition of the formed TONOs is unknown and is further discussed in section 3.3. Even though the overall mutagenicity potential of the TONO pool cannot be easily evaluated, the molar TONO yields suggest that the corresponding precursors should be taken into consideration during chloramination of wastewaters and drinking waters. Being associated to consumer products, the studied precursors can easily enter the aquatic system by wastewater discharge. For example, BZK homologues have been detected in wastewater effluents, river waters and groundwaters at concentrations ranging from 10 ng L^{-1} to 65 μg L^{-1} ([34–37]). Relevant concentrations (≤0.66 μg L^{-1}) of alkyltrimethylammonium chloride compounds, including CTMA, were found in Taiwanese rivers ([38]), while concentrations in the range 10-150 ng L^{-1} were detected in Austrian surface waters ([37]). CHD concentrations of up to 5 ng L^{-1} have been found in a drinking water reservoirs in Turkey ([39]), while concentrations between 46.1 and 78.1 ng L^{-1} were detected in a Spanish DWTP influent treating river water ([40]). Scheurer et al. (2012) ([41]) detected MET

concentrations between 18 and 105 µg L⁻¹ in 5 German WWTP influents and estimated a discharge in recipient rivers between 8 and 700 g d⁻¹, due to their incomplete elimination during wastewater treatment. The same authors found MET concentrations between 0.06 and 2.1 µg L⁻¹ in 8 German rivers. Considering the highest concentrations reported in the literature for surface waters or DWTP intakes and applying the maximum TONO molar yields determined in this study (at pH 8), TONO FP of the selected precursors could vary from 0.02 nM (1.2 ng L⁻¹ expressed as NDMA) to 3.97 nM (293.5 ng L⁻¹ expressed as NDMA), for CHD and BZK, respectively. Although intake concentrations are strongly case specific, these estimates indicate that the contribution of the studied precursors could be relevant. The determined TONO FPs are consistent with those previously observed by Dai and Mitch (2013) ([9]) in drinking water systems, with measured TONO concentrations in the same order of magnitude (1 nM median concentration). An additional important factor to be considered for evaluating the actual exposure to *N*-nitrosamine precursors is their fate in aquatic systems, leading to a natural attenuation of their concentrations at DWTP intakes. For instance, QACs are known to be easily adsorbed onto negatively charged solids, such as soils and sludge, and to have a relatively low biodegradability, especially when containing benzyl or alkyl functional groups ([42–45]). In contrast to a low *N*-nitrosamine molar yield, MET is characterized by high mobility in natural aquatic systems and can be easily distributed in the aquatic environment, due to the high persistence and low hydrophobicity (log K_{OW}=-2.64) ([46–48]). Even if the precursors are partially metabolized, they can contribute to *N*-nitrosamine formation ([10]). For instance, typical biodegradation products of QACs are tertiary and secondary amines, which can lead to *N*-nitrosamine formation yields much higher than their parent compounds ([45,44]).
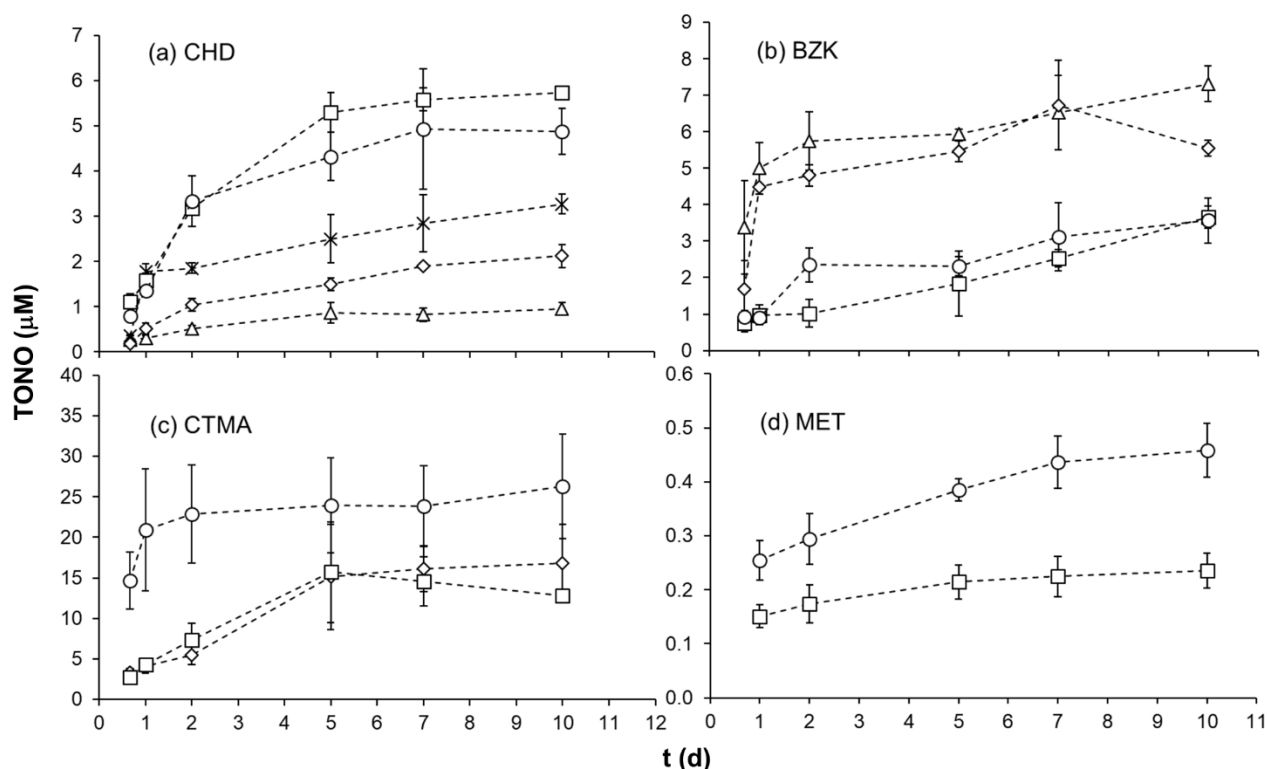
Figure 2 Kinetics of TONO formation at pH 7 for (a) CHD, (b) BZK, (c) CTMA and (d) MET as a function of initial molar NH₂Cl excess: 10- (triangles), 20- (diamonds), 40- (crosses), 100- (squares) and 200-fold (circles) NH₂Cl molar excess. Initial precursor concentration was set at 0.1 mM for CHD and 0.5 mM for the other compounds. Data represent the average ± standard deviation of three measurement repetitions on two experiment replicates.

Table 2 Molar yields of NDMA and TONO observed in chloramination formation potential (FP) experiments under experimental setups ES1 (reaction time: 7 days; initial precursor concentration: 0.1 mM for CHD, 0.5 mM for the other compounds; initial NH_2Cl molar excess: 10-fold for BZK, 200-fold for the other compounds) and ES2 (reaction time: 7 days; initial precursor concentration: 0.5 μM; initial NH_2Cl molar excess: 200-fold). Reported molar yields are the average values of multiple measurement repetitions (two for NDMA and three for TONO) on two experimental replicates.

Precursor	pH	Molar yield (%)		
		NDMA [a] average (range)	TONO [b] average ± st.dev.	
		ES1	ES1	ES2
Micropollutants				
Chlorhexidine hydrochloride (CHD)	6	<LOQ	2.64 ± 1.45	-
	7	<LOQ	4.93 ± 1.33	-
	8	<LOQ	11.92 ± 0.83	6.54 ± 0.39
Metformin dihydrochloride (MET)	6	<LOQ	0.04 ± 0.003	-
	7	<LOQ	0.09 ± 0.01	-
	8	<LOQ	0.21 ± 0.03	0.77 ± 0.32
Benzalkonium chloride (BZK)	6	<LOQ	0.68 ± 0.24	-
	7	<LOQ	1.31 ± 0.21	-
	8	0.56 (0.55-0.56)	2.12 ± 0.40	4.05 ± 0.38
Cetyl trimethyl ammonium chloride (CTMA)	6	<LOQ	1.15 ± 0.09	-
	7	<LOQ	4.77 ± 1.00	-
	8	<LOQ	4.93 ± 1.43	4.05 ± 0.01
Model compounds				
Tetramethyl ammonium chloride (TMA)	6	<LOQ	0.04 ± 0.002	-
	7	<LOQ	0.07 ± 0.004	-
	8	<LOQ	0.90 ± 0.08	-
Trimethyl amine (TrMA)	6	<LOQ	<LOQ	-
	7	<LOQ	0.03 ± 0.005	-
	8	0.10 [c]	0.29 ± 0.007	-
N,N-dimethylbutyl amine (DMBA)	6	<LOQ	<LOQ	-
	7	<LOQ	0.02 ± 0.004	-
	8	0.05 [c]	0.17 ± 0.03	-
N,N-dimethylbenzyl amine (DMBzA)	6	<LOQ	<LOQ	-
	7	1.22 (1.08-1.36)	0.72 ± 0.03	-
	8	5.05 (3.92-6.18)	3.27 ± 0.34	-

[a] LOQ for NDMA: 0.09±0.0001 μM.

[b] LOQ for TONO: 1.0±0.45 μM.

[c] NDMA concentration >LOQ only in one sample.

3.3 Total *N*-nitrosamine formation potential during chloramination of model tertiary and quaternary amines

N-nitrosamine formation potential by chloramination was also determined for various tertiary and one quaternary amine model compounds (Table 1): trimethyl amine (TrMA), *N,N*-dimethylbutyl amine (DMBA), *N,N*-dimethylbenzyl amine (DMBzA) and tetramethyl ammonium (TMA). Molar NDMA and TONO yields obtained in the pH range 6-8 are reported in Table 2. Similar to the selected micropollutants, for these model compounds, only NDMA was found at detectable concentrations from the US-EPA 8270 standard *N*-nitrosamines mix. Quantifiable NDMA and TONO concentrations were found for all the studied model tertiary amines (TrMA, DMBA and DMBzA). TrMA displayed TONO concentrations at pH 7 slightly higher than the LOQ, resulting in a molar conversion yield of 0.03%. A NDMA concentration higher than the LOQ was determined only at pH 8, with an average molar yield of 0.10%, while TONO concentrations corresponded to a molar yield of 0.29%. The TONO FP for TrMA at pH 8 was higher than the NDMA FP, which is probably due to the accuracy of the two analytical methods and related mainly to the different sample pre-treatment procedures. A formation of non-NDMA *N*-nitrosamines is not possible from TrMA. Furthermore, the TONO method applied in this study [28] tends to slightly overestimate NDMA concentrations (115%±5% recovery of NDMA from standard curve of US-EPA 8270 *N*-nitrosamines standard mix), which may be an additional explanation for the observed discrepancy.

NDMA was not detected in DMBA samples at pH 6 and 7, while TONO concentrations slightly above the LOQ (corresponding to 0.02% molar yield) were measured at pH 7. NDMA and TONO molar yields of 0.05% and 0.17%, respectively, were obtained at pH 8. Similar to TrMA, the NDMA FP observed for DMBA at pH 8 was lower than the TONO FP. In this case, a fraction of TONO concentration could be explained by the formation of *N*-nitrosodibutylamine, however, concentrations >LOQ could not be determined in any sample. The difference in NDMA and TONO concentrations can again be mainly attributed to the differences in the analytical methods.

Among the model tertiary amines, DMBzA displayed the highest *N*-nitrosamine formation potentials. Molar NDMA yields were, on average, 1.22% at pH 7 and 5.05% at pH 8, while molar TONO yields were 0.72% or 3.27% at pH 7 or 8, respectively. Again, the NDMA FPs resulted to be higher than TONO FPs in this case. However, considering the uncertainties associated to the two analytical methods, measured NDMA and TONO concentrations can be considered to be comparable, indicating that NDMA was the most prevalent *N*-nitrosamine present in the analysed samples. The relatively high formation of NDMA from DMBzA can be attributed to the low stability of the benzyl group, which is easily released from the N-atom ([6,15,49]). In fact, the benzyl group is a weaker base compared to alkyl groups and plays a stronger electron donating effect on the DMA moiety, resulting in higher NDMA formation rates ([10]).

Comparing the molar yields of NDMA and TONO for all the selected tertiary amines (MET, TrMA, DMBA and DMBzA), the role of the molecular structures of the precursors, in particular the type of the functional group bound to the DMA moiety, become evident. Even though it was not possible to evaluate the TONO composition, experimental results confirmed that the benzyl functional group is much more easily released than methyl, butyl or biguanide moieties, leading to significantly higher NDMA yields.

For TMA, the only tested quaternary amine model compound, NDMA concentrations higher than the LOQ were never detected, while quantifiable TONO FPs were found at all the pHs. TONO concentrations at pH 6 and 7 were slightly higher than LOQ, while relevant concentrations were measured at pH 8, corresponding to a 0.90% molar TONO yield. The significant difference between NDMA and TONO concentrations observed at pH 8 cannot be easily explained, because NDMA is expected to be the most prevalent *N*-nitrosamine formed from TMA. Even though the TONO composition observed for TMA is unclear, the obtained results show a link between the molecular

structures of QACs and *N*-nitrosamine formation. The TONO FP for TMA was much lower than for the QACs BZK and CTMA, with a significant difference in molar yields (difference >60% at pH 8). This indicates that the functional groups bound to the N-atom of QACs plays an important role for the *N*-nitrosamine conversion efficiency.

A previous study showed that formation of specific *N*-nitrosamines (i.e. NDMA and NDBA) from chloramination of QACs is mostly associated to QACs themselves rather than lower order amine impurities [6]. However, the negligible contribution of tertiary amine impurities has not been demonstrated for the TONO FP. The selected tertiary amine model compounds in the current study contain the same, or very similar, functional groups as potential impurities in the QACs. Although the aliphatic chain is shorter in DMBA compared to BZK and CTMA, previous studies have shown that the length of the alkyl group next to the nitrogen atom does not significantly affect the *N*-nitrosamine conversion yield [15]. Results of FP tests showed that molar *N*-nitrosamine yields of DMBA and TrMA were never high enough to explain *N*-nitrosamine formation from QACs by the presence of impurities (maximum estimated contribution to NDMA or TONO FPs of BZK and CTMA <1%). DMBzA, for which the highest NDMA FP was observed, could contribute up to the 45% of NDMA formation potential of BZK, if considering a maximum content of 5% as impurity (BZK purity >95%). In contrast, the maximum contribution of DMBzA impurities to the TONO FP of BZK would be ≤ 8%, indicating that most of the uncharacterized *N*-nitrosamine production is due to BZK itself. Hence, the results from this study indicate that the observed TONO FP could not be attributed to tertiary amine impurities and that QACs themselves are the dominant *N*-nitrosamine precursors.

3.4 Elucidation of the potential structures of unknown *N*-nitrosamines formed from quaternary ammonium compounds

TONO constituents formed from the selected consumer product ingredients were partially characterized only for BZK, for which it was possible to determine the NDMA FP. The molar NDMA:TONO ratio was on average 0.26. Even by taking the differences in the two analytical methods into account, the difference between NDMA and TONO concentrations can be considered significant. This indicates that a large fraction of the total *N*-nitrosamine pool consists of unknown compounds. So far, no known *N*-nitrosamine has been identified in the TONO pools formed from CHD, MET and CTMA. Because no compounds from the US-EPA 8270 standard *N*-nitrosamines mix were found, some other *N*-nitrosamines must be responsible for the measured TONO. Possible *N*-nitrosamine structures formed by CHD cannot be easily proposed from the molecular structure of the precursor. In contrast to most of the tertiary or quaternary amines studied in the literature, CHD does not contain a dialkylamino group which can be related to the formation of the corresponding *N*-nitrosamine, such as NDMA, NDEA or NDBA [6,7,10,15,49]. MET contains similar biguanide moieties as CHD (Table 1), however, it showed significantly lower *N*-nitrosamine FP. Comparing the molecular structures of the two precursors, the higher *N*-nitrosamine formation yield of CHD can be attributed to the aromatic moiety, which is bound to the end-membered N-atom of the biguanide group. In comparison, MET contains the same biguanide structure, however, with end membered DMA moiety. The low NDMA FP of MET has been explained by the electron-withdrawing effect of the biguanide group bound to DMA leading to a lower nucleophilicity of the N-atom [7,10,15]. In contrast, the chlorinated aromatic ring in the CHD structure could enhance the nucleophilic attack on the chloramine. Nevertheless, further studies are needed to verify these assumptions.

For QACs, the presence of only one N-atom limits the number of possible reactions with NH_2Cl leading to potential *N*-nitrosamine products. It has been demonstrated that *N*-nitrosamine formation from tertiary and quaternary amines involves the release of the functional groups bound to the nitrogen atom in the precursor molecule [15]. Various studies have shown that the structure of the leaving groups in precursors containing a DMA moiety strongly influences the formation of NDMA, resulting in

a large range of formation yields ([6,7,15,16]). However, most of these studies focused on NDMA formation and TONO measurements were rarely performed.

In the current study, the structures of other potential *N*-nitrosamines were hypothesized based on all possible leaving groups present in the precursor molecule. The potential *N*-nitrosamines resulting from chloramination of BZK and CTMA are shown in Table 3. For instance, the benzyl group and the aliphatic chain (C_nH_{2n+1}) bound to the N-atom in BZK are supposed to act as leaving groups during NDMA formation. Similarly, the release of one methyl group and the 16-C aliphatic chain ($C_{16}H_{33}$) may lead to the formation of NDMA from CTMA. The other *N*-nitrosamine structures were proposed by considering all the other potential leaving groups, including the methyl group, the benzyl group and the long-chain alkyl group for BZK, the methyl groups and the 16-C aliphatic chain for CTMA.

To test the formation of the proposed *N*-nitrosamines, the samples obtained by the TONO FP tests at pH 8 were analysed by high resolution LC-qTOF. The high accuracy and resolution of the obtained chromatograms allow proposing a compound based on its exact mass, in absence of analytical reference standards. The procedure described in section 2.3 was applied to screen the list of potential nitrosamines from the chromatograms, by extracting their exact masses (*m/z*) (calculated by the ChemCalc software and reported in Table 3, including the protonated molecules).

Among the hypothesized *N*-nitrosamines, a positive match was obtained for BZK. The full chromatogram of the BZK sample (treated with 10-fold molar excess of monochloramine at pH 8) is reported in S.I.4 (Figure S3). The extraction of the exact mass of $C_{13}H_{28}N_2O$ ($[M+H]^+=229.2279$) allowed to obtain a distinct peak (intensity of $8.56 \cdot 10^5$ arbitrary units) at a retention time of 7.34 min (Figure 3 a). The relative mass spectrum (Figure 3 b) showed a peak at *m/z*=229.2271, corresponding to a relative abundance of 93% and matching with high accuracy (error<0.1%) with two possible molecular formulas: (i) the hypothesized *N*-nitrosamine ($C_{13}H_{28}N_2O$, error=3.876 ppm, Table 3) and (ii) $C_{11}H_{27}N_5$ (error=1.981 ppm). The formation of the latter compound is highly improbable considering the investigated reaction system. The identified mass corresponded with a high level of confidence to *N*-nitroso-*N*-methyldodecylamine (Figure 3 a), a potential product of the reaction of chloramine with benzyldimethyldodecylamine, which is the most abundant constituent of the benzalkonium chloride mixture (about 70% abundance, according to the supplier (Sigma-Aldrich)).
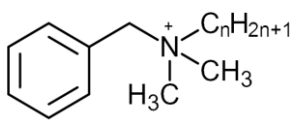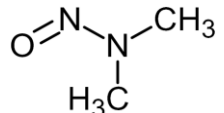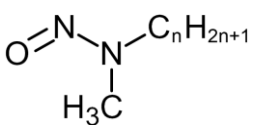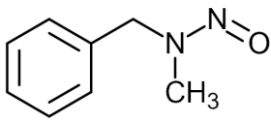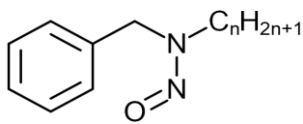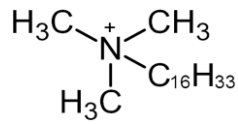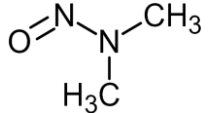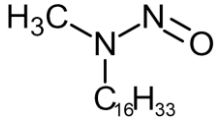
The detection of *N*-nitroso-*N*-methyldodecylamine was not unexpected and its formation at significant yield is consistent with previous results reported in the literature [6,15,49]. Because the benzyl group is an electron-donating group, which increases the electron density on the N-atom, a nucleophilic attack on the chloramine is favoured. In addition, benzyl-type functional groups are known to be better leaving groups than alkyl groups, both in tertiary and quaternary amine precursors ([6,15]). Hence, during chloramination of BZK homologues, *N*-nitroso-*N*-metylalkylamines are expected to have higher yields than benzyl-containing *N*-nitrosamines. Consistently, it was found previously that the molar yield of *N*-nitrosomethylbenzylamine from benzyldimethyltetradecylamine (the C-14 constituent of BZK) was only 0.016%, about 16-times lower than the molar NDMA yield ([6]).

High resolution LC-qTOF analysis of a CTMA sample did not lead to an identification of the hypothesized compound ($C_{17}H_{36}N_2O$) with enough confidence (results are reported in S.I.4, Figures S3 and S4). Moreover, the absence of reference standards did not allow determining an optimal sample extraction procedure and optimized analytical conditions for each proposed *N*-nitrosamine. Thus, the performed analyses must be considered as a first attempt to characterize the unknown fraction of TONO. Nevertheless, in the current study, in addition to NDMA, an additional *N*-nitrosamine from the TONO FP pool of BZK was potentially identified. This finding strongly supports the hypothesis that different leaving groups in the precursor molecule can lead to the formation of different *N*-nitrosamines.

N-nitroso-*N*-methyldodecylamine was found to be carcinogenic in experimental animals and its presence in personal care and household products has already been cause of concern in previous

studies ([50–54]). For instance, a T25 of 0.46 mg kg^{-1} d^{-1} (being the chronic dose rate giving tumours in the 25% of the tested animals ([55]) was determined on laboratory rats for *N*-nitroso-*N*-methyldodecylamine, which is comparable to the values obtained for other *N*-nitrosamines of the US-EPA 8270 standard mix (varying from 0.058 mg kg^{-1} d^{-1} of NDMA to 0.57 mg kg^{-1} d^{-1} of NPYR) ([54]). Hence, it may significantly contribute to the overall cancer potency of the total *N*-nitrosamine pool. Even though the high-resolution LC-qTOF results were not quantitative, they indicate that the uncharacterized fraction of TONO can be composed of species as hazardous as the compounds from the US-EPA 8270 standard *N*-nitrosamine mix. Even if a full characterization of the TONO pool is not always possible, coupling total and specific (i.e., US-EPA 8270 standard mix) *N*-nitrosamine analyses is an effective way to fully assess the potential hazardousness of *N*-nitrosamine precursors. Product identification in the TONO FP pool by LC-qTOF may lead to further insights into the formation of individual compounds, which might be of toxicological concern.

Table 3 Structure, formulas and exact masses of the hypothetical *N*-nitrosamines formed from BZK and CTMA.

Precursor	Hypothesized *N*-nitrosamines			
	Structure	Formula	Exact mass (*m/z*)	
			[M]$^+$	[M+H]$^+$
BZK n=8, 10, 12, 14, 16, 18		$C_2H_6N_2O$	74.0480	75.0558
	n=8, 10, 12, 14, 16, 18	$C_{n+1}H_{2n+4}N_2O$ n=8, 10, 12, 14, 16, 18	172.1576 200.1888 228.2202 256.2515 284.2828 312.3141	173.1654 201.1967 229.2279 257.2593 285.2906 313.3219
		$C_8H_{10}N_2O$	150.0793	151.0871
	n=8, 10, 12, 14, 16, 18	$C_{n+7}H_{2n+8}N_2O$ n=8, 10, 12, 14, 16, 18	248.1888 276.2202 304.2515 332.2828 360.3141 388.3454	249.1967 277.2280 305.2593 333.2906 361.3219 389.3532
CTMA		$C_2H_6N_2O$	74.0480	75.0558
		$C_{17}H_{36}N_2O$	284.2828	285.2906
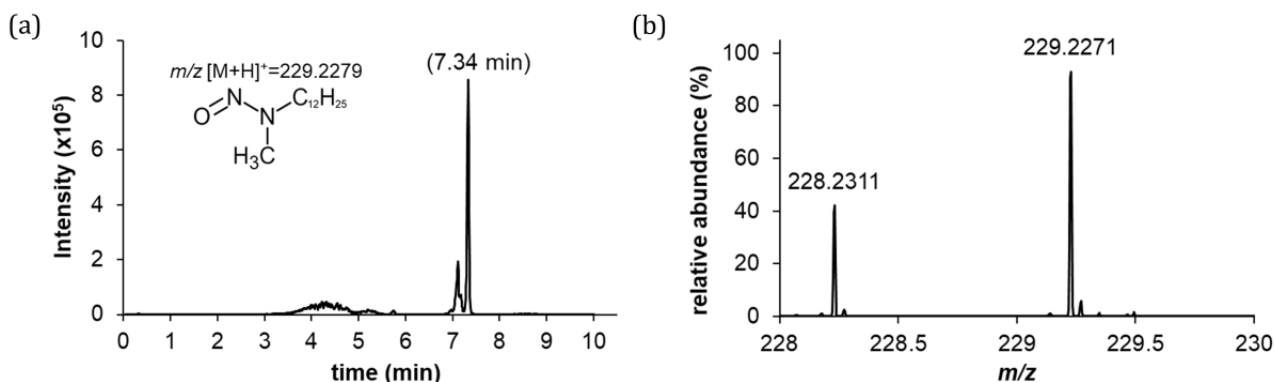
Figure 3 High resolution LC-qTOF results for a BZK sample (FP test at pH 8): (a) chromatogram obtained by extraction of the exact mass of $C_{13}H_{28}N_2O$ (*m/z* [M+H]+=229.2279); (b) mass spectrum at retention time=7.34 min.

3.5 Effect of precursors concentration on TONO formation potential

Experimental conditions adopted in ES1 were suitable for determination of the *N*-nitrosamine FP of the studied precursors and investigating the composition of the formed TONO compound pool. However, the precursor and the monochloramine concentrations were much higher compared to realistic systems, leading to the formation of extremely high *N*-nitrosamine concentrations. To validate the molar TONO yield values determined in ES1, FP tests were also conducted in ES2, with experimental conditions closer to real water matrices (pH 8, 0.5 µM precursor and 100 µM monochloramine, corresponding to 5.1 mg L^{-1} as NH$_2$Cl). Due to the lower *N*-nitrosamine concentrations produced under ES2, TONO concentrations were measured after sample pre-concentration by solid phase extraction (SPE).

As discussed above, the composition of the generated TONO compound pool is different for each precursor. Since the physico-chemical properties of the formed *N*-nitrosamines can strongly affect the efficiency of SPE ([9]), in this study, the recovery of TONO concentration by SPE was determined for the specific *N*-nitrosamine pools formed by each precursor, as reported in section 2.2. The TONO recovery efficiencies (values reported in S.I.5, Table S2) resulted to be quite low for all the precursors, with values of about 10%. Applying the obtained recovery efficiency values to the TONO concentrations measured in the FP tests (ES2), the molar TONO yields resulted, on average, equal to 6.54±0.39%, 4.05±0.38%, 4.05±0.02% and 0.77±0.32% for CHD, BZK, CTMA and MET, respectively. Despite the extremely different experimental conditions and the uncertainty associated to SPE, the molar TONO yields obtained under ES2 were comparable with those obtained in ES1 at pH 8 (Table 2). CHD and MET displayed, the highest and the lowest molar TONO yields, respectively, while intermediate values were obtained for QACs. Even though the molar TONO yields are slightly different, they are in the same order of magnitude for ES1 and ES2. This indicates that results obtained in ES1 can be considered representative for conditions more similar to those of real water matrices.

When dealing with TONO measurements in real water matrices, the recovery efficiency of SPE plays a key role and it can strongly vary with the TONO pool composition ([9]). In this study, the SPE extraction efficiency was also evaluated for a 0.16 µM US-EPA 8270 standard *N*-nitrosamine mix solution, both in terms of TONO and specific *N*-nitrosamine constituents. Some specific *N*-nitrosamines (such as NMOR, NDEA and NDBA) were not detected after SPE, denoting a very low recovery. Nevertheless, the average recovery efficiency of the TONO concentrations was 42%. The variability in the recovery efficiencies obtained for samples from FP tests demonstrates that the studied precursors lead to the formation of quite a large range of *N*-nitrosamines, having different affinities to the SPE material and probably yielding higher analytical uncertainty. The relatively low recovery of TONO concentration observed for the reacted samples could be due to the presence of unreacted precursor molecules,

having surface active properties and being present at high initial concentrations, which could form micellar aggregates with the *N*-nitrosamines present in solution and increase their hydrophilicity. Further studies are needed to elucidate the composition and the properties of the observed TONO pools and to optimize the SPE procedure.

4. Conclusions

Specific and total *N*-nitrosamine (TONO) formation potentials (FP) for different micropollutants (chlorhexidine, CHD, metformin, MET, benzalkonium chloride, BZK, and cetyltrimethylammonium chloride, CTMA) and model compounds (trimethylamine, TrMA, *N,N*-dimethylbutylamine, DMBA, *N,N*-dimethylbenzylamine, DMBzA, and tetramethylammonium, TMA) were determined at different pH values. All the micropollutants displayed relevant molar TONO yields, with maximum values at pH 8 varying between 0.21% (MET) and 11.92% (CHD). A quantifiable NDMA FP was determined only for BZK, with a molar yield of 0.56% (at pH 8) and corresponding to about 26% of the TONO FP. Generally, the formed TONO compounds consisted mostly from uncharacterized species, not included in the US-EPA 8270 *N*-nitrosamines standard mix.

The study of tertiary and quaternary model amines revealed a role of precursor molecular structures, in particular the nature of functional groups, in NDMA and TONO conversion yields: DMBzA displayed the highest molar NDMA yields, indicating that the presence of a benzyl functional group in tertiary amines containing a DMA moiety results in significantly higher NDMA formation. BZK and CTMA showed molar TONO yields much higher than TMA, suggesting that the formation of uncharacterized *N*-nitrosamines from QACs is favoured by the presence of benzyl and long-chain alkyl functional groups, instead of only methyl groups.

To identify the components of the TONO pools formed by BZK and CTMA, potential *N*-nitrosamine structures have been proposed. A screening procedure based on high resolution LC-qTOF analysis allowed to identify by high probability an uncharacterized *N*-nitrosamine (*N*-nitroso-*N*-methyldodecylamine) from the chloramination of BZK. The detection of a second *N*-nitrosamine species in addition to NDMA pointed out that different functional groups in QAC molecules can act as leaving group during chloramination and form different *N*-nitrosamine structures at significant yield. These results represent a first step in the understanding of *N*-nitrosamine formation during chloramination of QACs.

References

(1)   Richardson, S. D.; Ternes, T. A. Water analysis: emerging contaminants and current issues. *Anal. Chem.* **2014**, *86* (6), 2813–2848.

(2)   Krasner, S. W.; Mitch, W. A.; McCurry, D. L.; Hanigan, D.; Westerhoff, P. Formation, precursors, control, and occurrence of nitrosamines in drinking water: a review. *Water Res.* **2013**, *47* (13), 4433–4450.

(3)   Mitch, W. A.; Sedlak, D. L. Characterization and fate of N-nitrosodimethylamine precursors in municipal wastewater treatment plants. *Environ. Sci. Technol.* **2004**, *38* (5), 1445–1454.

(4)   Mitch, W. A.; Sharp, J. O.; Trussell, R. R.; Valentine, R. L.; Alvarez-Cohen, L.; Sedlak, D. L. N-nitrosodimethylamine (NDMA) as a drinking water contaminant: a review. *Environ. Eng. Sci.* **2003**, *20* (5), 389–404.

(5)   Zeng, T.; Mitch, W. A. Contribution of N-nitrosamines and their precursors to domestic sewage by greywaters and blackwaters. *Environ. Sci. Technol.* **2015**, *49* (22), 13158–13167.

(6)   Kemper, J. M.; Walse, S. S.; Mitch, W. A.; others. Quaternary amines as nitrosamine precursors: a role for consumer products? *Environ. Sci. Technol.* **2010**, *44* (4), 1224–1231.

(7)   Le Roux, J.; Gallard, H.; Croué, J.-P. Chloramination of nitrogenous contaminants (pharmaceuticals and pesticides): NDMA and halogenated DBPs formation. *Water Res.* **2011**, *45* (10), 3164–3174.

(8)   Schwarzenbach, R. P.; Escher, B. I.; Fenner, K.; Hofstetter, T. B.; Johnson, C. A.; Gunten, U. von; Wehrli, B. The Challenge of Micropollutants in Aquatic Systems. *Science* **2006**, *313* (5790), 1072–1077.

(9)   Dai, N.; Mitch, W. A. Relative importance of N-nitrosodimethylamine compared to total N-nitrosamines in drinking waters. *Environ. Sci. Technol.* **2013**, *47* (8), 3648–3656.

(10)   Shen, R.; Andrews, S. A. Demonstration of 20 pharmaceuticals and personal care products (PPCPs) as nitrosamine precursors during chloramine disinfection. *Water Res.* **2011**, *45* (2), 944–952.

(11)   Lee, C.; Schmidt, C.; Yoon, J.; Von Gunten, U. Oxidation of N-nitrosodimethylamine (NDMA) precursors with ozone and chlorine dioxide: kinetics and effect on NDMA formation potential. *Environ. Sci. Technol.* **2007**, *41* (6), 2056–2063.

(12)   Mitch, W. A.; Schreiber, I. M. Degradation of tertiary alkylamines during chlorination/chloramination: implications for formation of aldehydes, nitriles, halonitroalkanes, and nitrosamines. *Environ. Sci. Technol.* **2008**, *42* (13), 4811–4817.

(13)   Sacher, F.; von Gunten, U.; Lee, C.; Schmidt, C. *Strategies for minimizing nitrosamine formation during disinfection*; Water Environment Research Foundation, 2008.

(14)   Schmidt, C. K.; Sacher, F. Strategies for minimizing formation of NDMA and other nitrosamines during disinfection of drinking water. In *2006 Water Quality Technology Conference and Exposition Proceedings*; 2006.

(15)   Selbes, M.; Kim, D.; Ates, N.; Karanfil, T. The roles of tertiary amine structure, background organic matter and chloramine species on NDMA formation. *Water Res.* **2013**, *47* (2), 945–953.

(16)   Shen, R.; Andrews, S. A. NDMA formation kinetics from three pharmaceuticals in four water matrices. *Water Res.* **2011**, *45* (17), 5687–5694.

(17)   Choi, J.; Valentine, R. L. A kinetic model of N-nitrosodimethylamine (NDMA) formation during water chlorination/chloramination. *Water Sci. Technol.* **2002**, *46* (3), 65–71.

(18)   Choi, J.; Valentine, R. L. N-nitrosodimethylamine formation by free-chlorine-enhanced nitrosation of dimethylamine. *Environ. Sci. Technol.* **2003**, *37* (21), 4871–4876.

(19)   Shah, A. D.; Krasner, S. W.; Lee, C. F. T.; von Gunten, U.; Mitch, W. A. Trade-offs in disinfection byproduct formation associated with precursor preoxidation for control of N-nitrosodimethylamine formation. *Environ. Sci. Technol.* **2012**, *46* (9), 4809–4818.

(20)   Shah, A. D.; Mitch, W. A. Halonitroalkanes, halonitriles, haloamides, and N-nitrosamines: a critical review of nitrogenous disinfection byproduct formation pathways. *Environ. Sci. Technol.* **2011**, *46* (1), 119–131.

(21)   Zhang, A.; Li, Y.; Song, Y.; Lv, J.; Yang, J. Characterization of pharmaceuticals and personal care products as N-nitrosodimethylamine precursors during disinfection processes using free chlorine and chlorine dioxide. *J. Hazard. Mater.* **2014**, *276*, 499–509.

(22)   Chowdhury, Z. Nationwide assessment of nitrosamine occurrence and trends. **2012**.

(23)   Russell, C. G.; Blute, N. K.; Via, S.; Wu, X.; Chowdhury, Z.; others. Nationwide assessment of nitrosamine occurrence and trends. *J.-Am. Water Works Assoc.* **2012**, *104* (3), E205–E217.

(24)   Kulshrestha, P.; McKinstry, K. C.; Fernandez, B. O.; Feelisch, M.; Mitch, W. A. Application of an optimized total N-nitrosamine (TONO) assay to pools: placing N-nitrosodimethylamine (NDMA) determinations into perspective. *Environ. Sci. Technol.* **2010**, *44* (9), 3369–3375.

(25)   US EPA, O. of R. &. METHOD 521: DETERMINATION OF NITROSAMINES IN DRINKING WATER BY SOLID PHASE EXTRACTION AND CAPILLARY COLUMN GAS CHROMATOGRAPHY WITH LARGE VOLUME INJECTION AND CHEMICAL IONIZATION TANDEM MASS SPECTROMETRY (MS/MS) https://cfpub.epa.gov/si/si_public_record_report.cfm?dirEntryId=103912 (accessed Jul 18, 2017).

(26)   Schreiber, I. M.; Mitch, W. A. Influence of the order of reagent addition on NDMA formation during chloramination. *Environ. Sci. Technol.* **2005**, *39* (10), 3811–3818.

(27)   Bader, H.; Hoigné, J. Determination of ozone in water by the indigo method. *Water Res.* **1981**, *15* (4), 449–456.

(28)   Breider, F.; von Gunten, U. Quantification of Total N-Nitrosamine Concentrations in Aqueous Samples via UV-Photolysis and Chemiluminescence Detection of Nitric Oxide. *Anal. Chem.* **2017**, *89* (3), 1574–1582.

(29)   Chen, A.; Huebschmann, H. J.; Fangyan, L.; Foong, C. Y.; Harn, C. S. High Sensitivity Analysis of Nitrosamines Using GC-MS/MS, Alpha Analytical Pte. Ltd., Thermo Fisher Scientific. *Health Sci. Auth. HAS Singap.* **2012**.

(30)   Patiny, L.; Borel, A. ChemCalc: A Building Block for Tomorrow's Chemical Infrastructure. *J. Chem. Inf. Model.* **2013**, *53* (5), 1223–1228.

(31)   Agarwal, A.; Nelson, T. B.; Kierski, P. R.; Schurr, M. J.; Murphy, C. J.; Czuprynski, C. J.; McAnulty, J. F.; Abbott, N. L. Polymeric multilayers that localize the release of chlorhexidine from biologic wound dressings. *Biomaterials* **2012**, *33* (28), 6783–6792.

(32)   Devi, S. R. Studies on Stability and Configurational Changes of Nickel and Copper Ethambutol Dihydrochloride and Metformin Hydrochloride in both Cationic and Anionic Surfactants. *Int J Enginee Sci Inven* **2013**, *2* (4).

(33)   Park, S. H.; Padhye, L. P.; Wang, P.; Cho, M.; Kim, J.-H.; Huang, C.-H. N-nitrosodimethylamine (NDMA) formation potential of amine-based water treatment polymers: Effects of in situ chloramination, breakpoint chlorination, and pre-oxidation. *J. Hazard. Mater.* **2015**, *282*, 133–140.

(34)   Ding, W.-H.; Liao, Y.-H. Determination of alkylbenzyldimethylammonium chlorides in river water and sewage effluent by solid-phase extraction and gas chromatography/mass spectrometry. *Anal. Chem.* **2001**, *73* (1), 36–40.

(35)   Estévez, E.; del Carmen Cabrera, M.; Molina-Díaz, A.; Robles-Molina, J.; del Pino Palacios-Díaz, M. Screening of emerging contaminants and priority substances (2008/105/EC) in reclaimed water for irrigation and groundwater in a volcanic aquifer (Gran Canaria, Canary Islands, Spain). *Sci. Total Environ.* **2012**, *433*, 538–546.

(36)   Ferrer, I.; Furlong, E. T. Identification of alkyl dimethylbenzylammonium surfactants in water samples by solid-phase extraction followed by ion trap LC/MS and LC/MS/MS. *Environ. Sci. Technol.* **2001**, *35* (12), 2583–2588.

(37)   Martínez-Carballo, E.; Sitka, A.; González-Barreiro, C.; Kreuzinger, N.; Fürhacker, M.; Scharf, S.; Gans, O. Determination of selected quaternary ammonium compounds by liquid chromatography with mass spectrometry. Part I. Application to surface, waste and indirect discharge water samples in Austria. *Environ. Pollut.* **2007**, *145* (2), 489–496.

(38)   Ding, W.-H.; Tsai, P.-C. Determination of alkyltrimethylammonium chlorides in river water by gas chromatography/ion trap mass spectrometry with electron impact and chemical ionization. *Anal. Chem.* **2003**, *75* (8), 1792–1797.

(39)   Yavuz, M.; Oggioni, M.; Yetis, U.; Dilek, F. B. Biocides in drinking water system of Ankara, Turkey. *Desalination Water Treat.* **2015**, *53* (12), 3253–3262.

(40)   Boleda, M. R.; Galceran, M. T.; Ventura, F. Behavior of pharmaceuticals and drugs of abuse in a drinking water treatment plant (DWTP) using combined conventional and ultrafiltration and reverse osmosis (UF/RO) treatments. *Environ. Pollut.* **2011**, *159* (6), 1584–1591.

(41)   Scheurer, M.; Michel, A.; Brauch, H.-J.; Ruck, W.; Sacher, F. Occurrence and fate of the antidiabetic drug metformin and its metabolite guanylurea in the environment and during drinking water treatment. *Water Res.* **2012**, *46* (15), 4790–4802.

(42)   Garcia, M. T.; Campos, E.; Sanchez-Leal, J.; Ribosa, I. Effect of the alkyl chain length on the anaerobic biodegradability and toxicity of quaternary ammonium based surfactants. *Chemosphere* **1999**, *38* (15), 3473–3483.

(43)   Ikehata, K.; El-Din, M. G. Degradation of recalcitrant surfactants in wastewater by ozonation and advanced oxidation processes: a review. *Ozone Sci. Eng.* **2004**, *26* (4), 327–343.

(44)   Li, X.; Brownawell, B. J. Quaternary ammonium compounds in urban estuarine sediment environments-a class of contaminants in need of increased attention? *Environ. Sci. Technol.* **2010**, *44* (19), 7561–7568.

(45)   Ying, G.-G. Fate, behavior and effects of surfactants and their degradation products in the environment. *Environ. Int.* **2006**, *32* (3), 417–431.

(46)   Lindim, C.; van Gils, J.; Cousins, I. T.; Kühne, R.; Georgieva, D.; Kutsarova, S.; Mekenyan, O. Model-predicted occurrence of multiple pharmaceuticals in Swedish surface waters and their flushing to the Baltic Sea. *Environ. Pollut.* **2017**, *223*, 595–604.

(47)   Mansour, F.; Al-Hindi, M.; Saad, W.; Salam, D. Environmental risk analysis and prioritization of pharmaceuticals in a developing world context. *Sci. Total Environ.* **2016**, *557*, 31–43.

(48)   Trautwein, C.; Berset, J.-D.; Wolschke, H.; Kümmerer, K. Occurrence of the antidiabetic drug Metformin and its ultimate transformation product Guanylurea in several compartments of the aquatic cycle. *Environ. Int.* **2014**, *70*, 203–212.

(49)   Spahr, S.; Cirpka, O. A.; von Gunten, U.; Hofstetter, T. B. Formation of N-nitrosodimethylamine during chloramination of secondary and tertiary amines: Role of molecular oxygen and radical intermediates. *Environ. Sci. Technol.* **2016**, *51* (1), 280–290.

(50)   Hecht, S. S.; Morrison, J. B.; Wenninger, J. A. N-Nitroso-N-methyldodecylamine and N-nitroso-N-methyltetradecylamine in hair-care products. *Food Chem. Toxicol.* **1982**, *20* (2), 165–169.

(51)   Kamp, E.; Eisenbrand, G. Long-chain N-nitroso-N-methylalkylamines in commercial cosmetics, light-duty dishwashing liquids and household cleaning preparations. *Food Chem. Toxicol.* **1991**, *29* (3), 203–209.

(52)   Lijinsky, W.; Reuber, M. D.; Riggs, C. W. Carcinogenesis by combinations of N-nitroso compounds in rats. *Food Chem. Toxicol.* **1983**, *21* (5), 601–605.

(53)   Morrison, J. B.; Hecht, S. S. N-nitroso-N-methyldodecylamine and N-nitroso-N-methyltetradecylamine in household dishwashing liquids. *Food Chem. Toxicol.* **1982**, *20* (5), 583–586.

(54)   SCCS, S. C. on C. S.-E. C. Opinion on Nitrosamines and Secondary Amines in Cosmetic Products https://ec.europa.eu/health/sites/health/files/scientific_committees/consumer_safety/docs/sccs_o_090.pdf (accessed Aug 26, 2017).

(55)   Dybing, E.; Sanner, T.; Roelfzema, H.; Kroese, D.; Tennant, R. W. T25: a simplified carcinogenic potency index: description of the system and study of correlations between carcinogenic potency and species/site specificity and mutagenicity. *Basic Clin. Pharmacol. Toxicol.* **1997**, *80* (6), 272–279.

Supporting Information

S.I.1 Analyses of the USEPA 8270 *N*-nitrosamine mix by GC-MS/MS

The limits of detection (LOD) and quantification (LOQ) at the 95% confidence level of the analytical method were calculated based on the standard deviation (σ) of 12 measurement repetitions of 10 µg L^{-1} standard solutions (LOD=3.3×σ, LOQ=10×σ) performed during a period of about 8 months. LOD and LOQ values for each analyte are reported in Table S1.

Table S1 Limits of detection (LOD) and quantification (LOQ) at the 95% confidence level (average±standard deviation) for *N*-nitrosamine measurement by GC-MS (calibration range: 5-500 µg L^{-1}).

N-nitrosamine	LOD		LOQ	
	(µg L^{-1})	(µM)	(µg L^{-1})	(µM)
NDMA	2.00±0.03	0.03±0.00	6.80±0.08	0.09±0.00
NMEA	1.30±0.01	0.01±0.00	4.30±0.03	0.05±0.00
NDEA	1.00±0.01	0.01±0.00	3.40±0.03	0.03±0.00
NDPA	0.70±0.03	0.01±0.00	2.20±0.11	0.02±0.00
NDBA	0.20±0.08	0.00±0.00	0.80±0.01	0.01±0.00
NPIP	0.40±0.01	0.00±0.00	1.40±0.04	0.01±0.00
NPYR	1.30±0.01	0.01±0.00	4.30±0.02	0.04±0.00
NMOR	0.20±0.03	0.00±0.00	0.60±0.09	0.01±0.00
NDPhA	1.60±0.20	0.01±0.00	5.40±0.61	0.03±0.00

S.I.2 LC-qTOF analysis

5 mL samples were pre-treated by liquid/liquid extraction using 5 mL of dichloromethane (DCM). DCM was then replaced by 0.8 mL methanol and dried to 0.5 mL by a Rotavapor apparatus (40°C, 850 mbar).

LC-qTOF analyses were conducted on a Xevo G2-S qTOF mass spectrometer coupled to the Acquity UPLC Class Binary Solvent Manager and BTN Sample Manager (Waters, Corporation, Milford, MA). The separation was achieved using an ACQUITY UPLC® BEH C18 1.7 mm column, 2.1 mm x 50 mm (Waters) heated at 35° C. The mobile phase consisted of H$_2$O (0.1% formic acid) as eluent A and ACN (0.1%formic acid) as eluent B. The separation was carried out at 0.4 mL min^{-1} over a 10 min total run time using the following program: 0-2.5 min, isocratic 20% B; 2.5-7.5 min, 20-99% B; 7.5-8 min, isocratic 20% B; 8-10 min, isocratic 20% B for re-equilibration.

The sample manager system temperature was maintained at 15 °C and the injection volume was 5 µL. Mass spectrometer detection was operated in positive ionization using the ZSpray™ dual-orthogonal multimode ESI/APCI/ESCi® source. The TOF mass spectra were acquired in the sensitive mode over the range of *m/z* 50-1200 at an acquisition rate of 0.036 sec/spectra. The instrument was calibrated using a solution of sodium formate (0.01 mg L^{-1} in isopropanol/H$_2$O 90:10). A mass accuracy better than 5 ppm was achieved using a leucine encephalin solution as lock-mass (200 pg mL^{-1} in ACN/H$_2$O (50:50)) infused continuously using the LockSpray source. Source settings were as follows: cone, 25V; capillary, 3 kV, source temperature, 150° C; desolvation temperature, 500° C, cone gas, 10 L h^{-1}, desolvation gas, 500 L h^{-1}. Data were processed using MassLynx™ 4.1 software.

S.I.3 Kinetics of TONO formation

The kinetics of *N*-nitrosamine formation for CHD, MET, BZK and CTMA was investigated in ES1 by measuring: (1) TONO concentrations (results reported and discussed in section 3.1); (2) residual precursor concentrations (only for CHD and BZK) and (3) the decay of NH_2Cl over time in control solutions.

CHD and BZK concentrations were measured by HPLC equipped with a diode array detector (Dionex Ultimate 3000) using EC 125/3 nucleosil 100-5 C-18 column (Thermo Scientific). Where not specified, the used reagents were of HPLC purity grade. The CHD concentration was determined by modifying the method proposed by Below et al. (2004), using a mixture (70/30 v/v) of buffer solution (mixture of 0.25 M ammonia solution and 0.25 M acetic acid in the ratio 60/40, pH 8.7) and acetonitrile as eluent A and a mixture (20/80 v/v) of 0.25 M acetic acid and acetonitrile as eluent B. The gradient was modified as follows: 0–4 min 0% B, between 4 min and 11 min the concentration of eluent B was increased linearly up to 75%, then the concentration was maintained constant during 7 min. Finally, between 18 min and 20 min the concentration of eluent B was linearly decreased to 0% and then maintained at this level during 6 min. The flow rate was 0.8 mL min^{-1} and the sample injection was 75 µL. The BZK concentration was determined by modifying the isocratic method proposed by Labranche et al. (2006). A 20/80 mixture of methanol and phosphoric acid (pH 3.0; 7.5 mM) was used as mobile phase. The flow rate was 0.8 mL min^{-1}, the sample injection was 100 µL and column temperature was maintained at 25°C.

The results in Figure S1 show that the NH_2Cl concentration decreased significantly in the first 3 days, reaching an equilibrium residual value that is maintained over the rest of the tests. NH_2Cl decay was mainly due to disproportionation, occurring under the tested experimental conditions (*Jafvert and Valentine, 1992*; *Le Roux et al., 2011*; *Le Roux et al., 2012*).

The consumption of CHD and BZK during kinetic experiments was evaluated by measuring their residual concentration at different reaction times by HPLC methods (Figure S2). For BZK, concentrations <LOD (corresponding to consumption >95%) were obtained already at the shortest reaction time at all the NH_2Cl doses. For the lower NH_2Cl doses (10-, 20- and 40-fold molar excess), CHD consumption was >85% after 1 day and >97% after 7 days; at higher NH_2Cl doses (100- and 200-fold molar excess), CHD consumption was always >99% (residual concentrations <LOD).

Because of the large difference between NH_2Cl (Figure S1) and precursor (Figure S2) concentrations, NH_2Cl consumption by reaction with model compounds during kinetic experiments could be considered minimal.
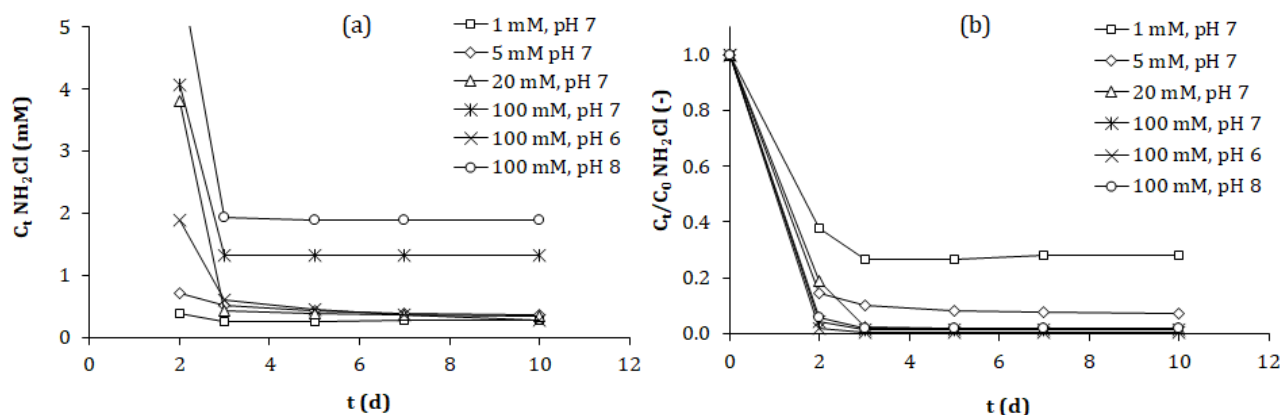
Figure S1 Monochloramine stability in the nitrosamine formation tests: (a) absolute and (b) normalized monochloramine concentrations over time as a function of initial NH_2Cl concentration and pH.
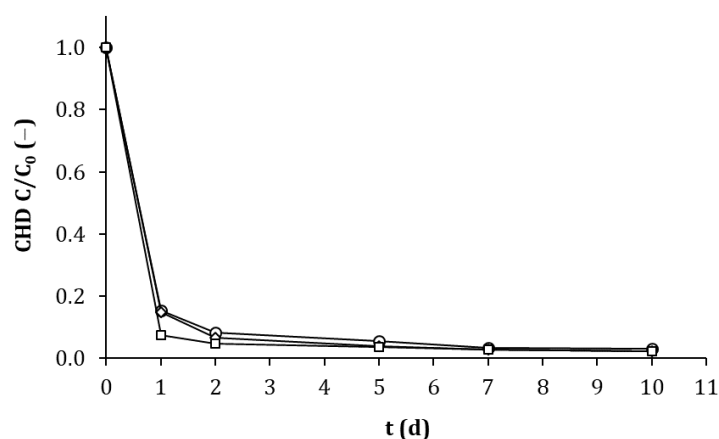
Figure S2 Evolution of the normalized chlorhexidine residual concentration as a function of the NH_2Cl dose (1 mM initial CHD concentration, pH 7): 10- (circles), 20- (diamonds) and 40-fold (squares) NH_2Cl molar excess (at 100- and 200-fold NH_2Cl molar excess, CHD concentrations were <LOD already after 1 d).

S.I.4 LC-qTOF data for BZK and CTMA samples

The full chromatograms (MS spectrum evaluated at m/z between 100 and 1200) of BZK and CTMA samples (ES1 FP tests at pH 8) are reported in Figure S3. The extraction of the exact mass of $C_{17}H_{36}N_2O$ ([M+H]$^+$=285.2906) from the CTMA chromatogram showed a peak (intensity of 8.43·10^3) at a retention time of 4.906 min, as shown in Figure S4a. The relative MS spectrum (Figure S4b) showed a small peak at *m/z*=285.295 that, however, does not match with enough accuracy with the investigated *N*-nitrosamine (error=15.462 ppm).

(a)

(b)
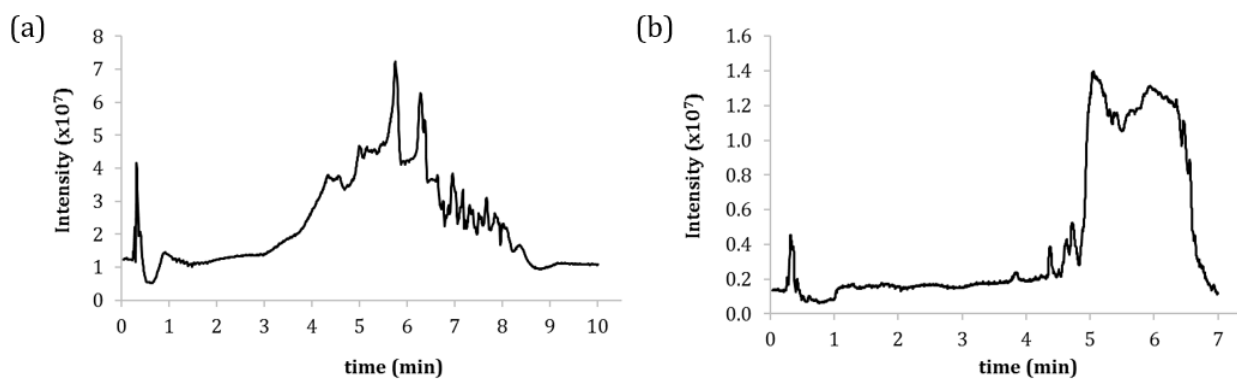
Figure S3 LC-qTOF results for (a) BZK and (b) CTMA samples treated with an excess of chloramine (ES1 FP test at pH 8).
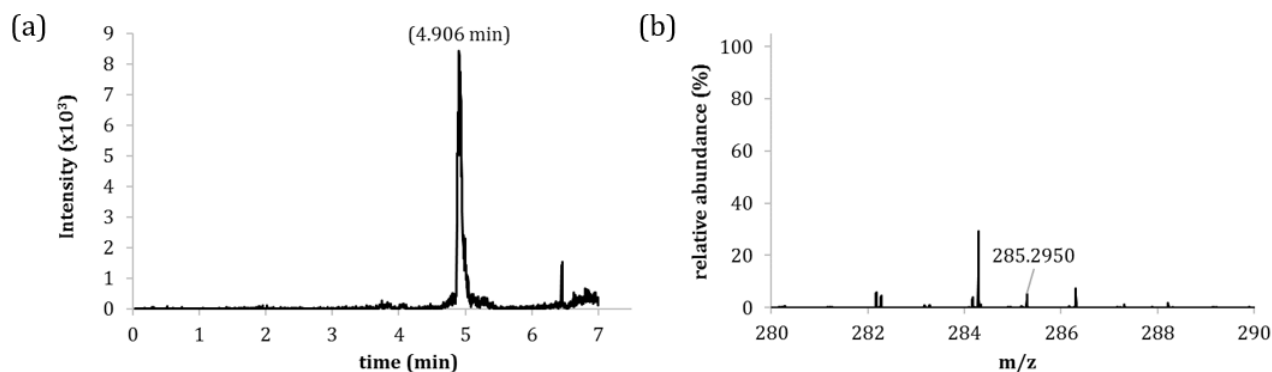
Figure S4 LC-qTOF results for CTMA sample treated with an excess of chloramine (FP test at pH 8): (a) chromatogram obtained by extraction of the exact mass of $C_{17}H_{36}N_2O$ (*m/z* [M+H]$^+$=285.2906); (b) mass spectrum at retention time=4.906 min.

S.I.5 Solid phase extraction efficiency

The recovery of TONO by SPE was specifically assessed for each selected compound, as described in section 2.3. TONO extraction efficiency was also evaluated for a solution containing 0.16 μM US-EPA 8270 standard *N*-nitrosamine mix, 1 mM phosphate buffer (pH 8) and 2 mM ascorbic acid.

TONO extraction efficiencies obtained for each precursor and the US-EPA 8270 standard *N*-nitrosamine mix are reported in Table S2 (average, minimum and maximum values of two repetitions).

Table S2 TONO extraction efficiency of SPE evaluated for different precursors and US-EPA 8270 standard *N*-nitrosamine mix (average, minimum and maximum values of two repetitions).

Precursor	average (%)	min (%)	max (%)
chlorhexidine (CHD)	9.8	5.8	13.7
benzalkonium chloride (BZK)	8.8	7.5	10.1
cetyltrimethylammonium chloride (CTMA)	8.1	7.7	8.5
metformin (MET)	11.4	10.5	12.3
US-EPA 8270-MIX	42.0	37.5	44.1

References

Below, H.; Lehan, N.; Kramer, A. HPLC determination of the antiseptic agent chlorhexidine and its degradation products 4-chloroaniline and 1-chloro-4-nitrobenzene in serum and urine. Microchimica Acta (2004), 146(2), 129-135.

Labranche, L. P.; Dumont, S. N.; Levesque, S.; Carrier, A. Rapid determination of total benzalkonium chloride content in ophthalmic formulation. Journal of pharmaceutical and biomedical analysis (2007), 43(3), 989-993.

Jafvert, C. T.; Valentine, R. L. Reaction scheme for the chlorination of ammoniacal water. *Environ. Sci. Technol.* **1992**, *26* (3), 577–586.

Le Roux, J.; Gallard, H.; Croué, J.-P. Chloramination of nitrogenous contaminants (pharmaceuticals and pesticides): NDMA and halogenated DBPs formation. *Water Res.* **2011**, *45* (10), 3164–3174.

Le Roux, J.; Gallard, H.; Croué, J.-P. Formation of NDMA and halogenated DBPs by chloramination of tertiary amines: the influence of bromide ion. *Environ. Sci. Technol.* **2012**, *46* (3), 1581–1589.

CHAPTER 5

Control of micropollutant precursors of *N*-nitrosamines by activated carbon adsorption

Abstract

Several nitrogenous micropollutants present in pharmaceutical and personal care products (PPCPs) are known to be potential precursors of *N*-nitrosamines, a class of potent human carcinogens formed during oxidative water treatments. The aim of this work was to study the effectiveness of activated carbon adsorption in reducing the *N*-nitrosamines formation potential (FP) of two PPCP precursors, benzalkonium chloride (BZK) and chlorhexidine (CHD), comparing two treatment options: the precursor removal before oxidation (pre-adsorption) and the *N*-nitrosamines removal after oxidation (post-adsorption). Relevant total *N*-nitrosamine FP (TONO) FP upon chloramination was observed for both the precursors, with maximum molar yields at pH 8 equal to 3.40% and 16.82% for BZK and CHD, respectively. The FP of a specific *N*-nitrosamine, NDMA, was determined only for BZK, showing a 0.56% molar yield. Preliminary pre- and post-adsorption equilibrium tests were conducted with two commercial GACs (GAC-V and GAC-M) and at two pH (6 and 8). The adsorption of both the precursors and TONO were found to be higher for GAC-V and to increase with the solution pH. Various doses of GAC-V (100-1000 mg L^{-1}) were then tested in pre- and post-adsorption equilibrium tests at pH 8. Both BZK and CHD were well removed by pre-adsorption (from 10% to 80-90% over the tested GAC doses), with equilibrium adsorption capacities up to 1.2 μmol mg^{-1}, for BZK, and 0.21 μmol mg^{-1}, for CHD; the TONO FP upon chloramination was reduced proportionally to the precursor removal during the pre-adsorption phase. The TONO pool formed by BZK was well removed by post-adsorption (equilibrium TONO adsorption capacities between 2 and 14 nmol mg^{-1}), with reduction of the TONO FP comparable to that of pre-adsorption, for a given GAC dose. On the other hand, a significant removal of the TONO pool formed by CHD (67%, 7.1 nmol mg^{-1}) was observed only at the highest GAC dose. Results indicated that pre-adsorption of *N*-nitrosamine precursors is the most effective option to reduce their *N*-nitrosamine FP, since post-adsorption efficiency can strongly vary with the TONO pool composition. Finally, pre-adsorption was tested under experimental conditions closer to real water matrices (initial precursor and monochloramine concentration of 0.5 μM and 100 μM, respectively). Dosing 10 and 40 mg L^{-1} of GAC-V, the TONO FP of the two precursors was reduced, respectively, of 58% and 75% for BZK, 39% and 45% for CHD (at equilibrium conditions). An adsorption phase before disinfection resulted to be an effective option to control *N*-nitrosamine formation also at low precursor concentrations.

Keywords: total *N*-nitrosamines (TONO), nitrogenous micropollutants, *N*-nitrosamines formation potential, activated carbon, adsorption.

1. Introduction

N-nitrosamines are a group of emerging disinfection by-products that can be formed during chloramination, chlorination and ozonation of drinking water and wastewater [1–3]. Toxicological studies have shown that various *N*-nitrosamines are particularly potent human carcinogens, with low nanogram-per-litre drinking water concentrations associated with a 10^{-6} lifetime excess cancer risk [4]. US-EPA listed 5 *N*-nitrosamines on the Contaminant Candidate List 3 and is considering regulation of *N*-nitrosamines as a group, while California has established a 10 ng L^{-1} notification level for *N*-nitrosodimethylamine (NDMA), *N*-nitrosodiethylamine (NDEA), and *N*-nitrosodipropylamine (NDPA) in drinking water [3,5,6].

Previous studies [2,6–8] showed that consumer products, such as pharmaceuticals, personal care and household products, typically discharged in municipal wastewater effluents but also present in drinking waters [9], can be important sources of *N*-nitrosamine precursors. Most of the works present in literature are focused on the formation of NDMA, being the most often detected species in tap water [10]. However, previous studies showed that NDMA is often a minor part of total *N*-nitrosamines (TONO) and that a relevant fraction of the TONO pool is constituted by uncharacterized species [5,6,11]. The measurement of both specific and total *N*-nitrosamines is not conventional, however it would allow to more properly assess the risk associated to the *N*-nitrosamine formation potential (FP) of specific precursors or real water matrices.

Chemical oxidants, such as chlorine, chloramine and ozone, are typically applied as disinfection treatment of drinking water and wastewater; in this case, the preliminary removal of *N*-nitrosamine precursors is the most adopted strategy for reducing *N*-nitrosamine formation potential [3]. In fact, disinfection is commonly the last step of water treatment train, so the addition of a further step for removing by-products is not always feasible. Moreover, *N*-nitrosamine formation could continue in distribution system, due to the slow formation kinetics and the presence of not completely removed precursors [3]. Methods for removing or deactivating *N*-nitrosamine precursors include coagulation, adsorption, pre-oxidation and filtration [3]. Despite few studies are available in literature, activated carbon adsorption is a promising solution for removing *N*-nitrosamine precursors and reducing their formation during subsequent disinfection. For instance, Hanigan et al. (2012) [12] showed that NDMA formation potential of a wastewater effluent (initial NDMA FP=544 ng L^{-1}) could be reduced by 91% with 75 mg L^{-1} of powdered activated carbon (PAC) and a contact time of 4 h. Similarly, Beita-Sandì et al. (2016) [13] showed that the application of PAC at doses up to 10 mg L^{-1} lead to about 20% removal of NDMA FP in a DWTP treating surface water (initial NDMA FP=32-75 ng L^{-1}). Lab- and pilot-scale column studies with granular activated carbon (GAC) showed that NDMA FP could be effectively decreased in wastewaters and surface waters, with breakthrough longer than those for dissolved organic carbon and UV absorbance at 254 nm [12]. The removal efficiency of activated carbon was also demonstrated towards specific *N*-nitrosamine precursors, such as secondary and tertiary amines present in pharmaceuticals, pesticides or deriving from degradation of N-containing compounds [12,14,15].

The same chemical oxidants used for water disinfection can be applied along the water treatment train as pre-oxidation phase [16]. In this case, another possibility to reduce the risk of *N*-nitrosamine presence in the effluent is their abatement after the oxidative treatment. UV radiation (at λ=175-275 nm) is the most effective way to destroy *N*-nitrosamines, even if the required doses (i.e. about 1000 mJ cm^2 for a log order reduction of NDMA [17]) are much higher than those adopted in UV disinfection [17,18]. Among sorption methods, zeolites are widely studied and were demonstrated to be effective towards different *N*-nitrosamines [20–22]. Dai et al. (2009) [19] studied the adsorption of NDMA by means of different activated carbons, obtaining adsorption capacities up to 25 mg g^{-1}. The same authors found that NDMA adsorption is strictly related to adsorbent porous structure and can be increased by surface modification.

Most of the studies regarding *N*-nitrosamine adsorption has focused on NDMA, that has relatively low affinity with nonpolar and hydrophobic adsorbents (as activated carbons), due to its high solubility in water, small molecular size and high polarity [20]. However, total *N*-nitrosamine pool can be composed by several species, having very different physical-chemical properties and affinity towards adsorbents [5]. de Ridder et al. (2012) [20] found that the adsorption capacity of some zeolites strongly varies towards different *N*-nitrosamines, being null for NDMA but significantly higher for more hydrophobic species such as *N*-nitrosodibutylamine (NDBA), *N*-nitrosodipropylamine (NDPA), *N*-nitrosopiperidine (NPIP), *N*-nitrosodiethylamine (NDEA) and *N*-nitrosomorpholine (NMOR). Similar behaviour was observed for granular activated carbon (GAC) in a pilot-scale study, with NDMA first appearing in the filter effluent, followed by NMOR and NDEA [21].

The few studies available in literature are limited to a small number of *N*-nitrosamines, namely those present in US-EPA 8270 *N*-nitrosamine standard mix [22]. No studies were found investigating the effectiveness of adsorption process in the removal of the total *N*-nitrosamines pool, which may contain a relevant fraction of uncharacterized species with different adsorptive properties.

The aim of this study was to investigate the possibility to reduce the *N*-nitrosamine formation potential of specific precursors by activated carbon adsorption. Two consumer products were selected as *N*-nitrosamine precursors: benzalkonium chloride (BZK), a quaternary ammonium compound used as disinfectant and surfactant agent, and chlorhexidine hydrochloride (CHD), an antiseptic agent used in disinfectants, pharmaceuticals and cosmetics. Being associated to consumer products, BZK and CHD can easily enter the aquatic system by wastewater discharge and arrive to natural water resources, potentially forming *N*-nitrosamines during drinking water oxidative treatments. For example, previous studies showed the presence of BZK homologues both in river waters and in wastewater effluents, at concentrations ranging from 10 ng L^{-1} [7,23] to 65 μg L^{-1} [24–26] , while CHD have been found in drinking water treatment plant influents at concentrations between 5 and 78 ng L^{-1} [27,28]. Two possible treatment solutions were considered: i) adsorption before oxidation (pre-adsorption), to reduce precursor concentration; ii) adsorption after oxidation (post-adsorption), to remove the formed *N*-nitrosamines and the residual precursors. With the aim of comparing these two treatment alternatives, a series of batch-scale experiments was conducted on model solutions, including: 1) *N*-nitrosamine formation potential tests [3], to evaluate the maximum production of *N*-nitrosamines during chloramination of the two precursors; 2) equilibrium adsorption tests with two commercial granular activated carbons, to determine the equilibrium adsorption capacities towards precursors and *N*-nitrosamines, also as a function of structural properties of the GACs.

2. Materials and methods

2.1 Chemicals and reagents

All the experiments were conducted in ultrapure water (Milli-Q, Millipore) buffered with sodium phosphate buffers at different pH values (6, 7 or 8), made from NaH_2PO_4 and Na_2HPO_4.

Benzalkonium chloride (>95%) and chlorhexidine dihydrochloride (>98%) were purchased by Sigma-Aldrich. Molecular structures and main properties of the studied compounds are reported in Table 1. Concentrated stock solutions of each precursor were prepared in ultrapure water.

US-EPA 8270 *N*-nitrosamine standard mix, containing *N*-nitrosodimethylamine (NDMA), *N*-nitrosodiethylamine (NDEA), *N*-nitrosomethylethylamine (NMEA), *N*-nitrosomorpholine (NMOR), *N*-nitrosodibutylamine (NDBA), *N*-nitrosopiperidine (NPIP), *N*-nitrosopyrrolidine (NPYR), *N*-nitrosodipropylamine (NDPA) and *N*-nitrosodiphenylamine (NDPhA), was purchased by Sigma-Aldrich.

Monochloramine stock solution was daily prepared as described by Le Roux et al. (2011) [8] using sodium hypochlorite (NaOCl, 15-20%, Sigma-Aldrich) and ammonium chloride (99.9%, VWR

Chemicals). The concentrations of monochloramine (NH_2Cl) and dichloramine ($NHCl_2$) (see section 2.3) in stock solution were measured after preparation; $NHCl_2$ concentration was always not quantifiable. Ascorbic acid, HPLC grade acetonitrile, dichloromethane and methanol were purchased by Sigma-Aldrich.

Two commercial granular activated carbons (Chemviron) were tested in adsorption experiments: Acticarbone NCL 1240 (GAC-V), of vegetal origin (coconut-based), and GAC-1240 (GAC-M), of mineral origin (coal-based). The main characteristics of the carbons are reported in S.I.1 (Table S1).

2.2 Experimental procedures

Experiments were conducted under two experimental setups (ES), denoted ES1 and ES2, differing for the initial concentration of precursors. The following experiments were carried out: a) preliminary chloramination FP tests under ES1 (section 2.2.1); b) pre-adsorption tests (equilibrium adsorption tests followed by chloramination FP tests) under ES1 (section 2.2.2); c) post-adsorption tests (chloramination FP tests followed by equilibrium adsorption tests) under ES1 (section 2.2.3); d) pre-adsorption tests under ES2 (section 2.2.4). Post-adsorption tests under ES2 were not performed because of the too high uncertainty in TONO quantification, due to the solid phase extraction procedure (as discussed in section 3.2.3). All the experiments were performed in duplicate, at room temperature (23°C) into amber borosilicate bottles.

Chloramination FP tests were conducted under dark and calm conditions. Reaction solutions were quenched at the end of the pre-determined reaction time by dosing an enough volume of ascorbic acid stock solution (280 mM) to get stoichiometric excess with respect to the initial NH_2Cl concentration. Quenched solutions were stored at 4°C in the dark till the analysis. The molar yield of *N*-nitrosamine formation was calculated as the ratio between the produced *N*-nitrosamine molar concentration and the initial precursor molar concentration.

Equilibrium adsorption tests were conducted on a magnetic stirrer (650 RPM) for a contact time of 48 h (according to preliminary tests, enough to reach equilibrium for all the investigated adsorbates). For each experimental trial, one test bottle was prepared without GAC addition (blank sample). The solid-phase equilibrium concentration of adsorbate, q_e ($\mu g\ mg^{-1}$), was calculated as follows:

e.1)
$$q_e = (C_0 - C_e)\frac{V}{M_{GAC}}$$

where V (L) is the volume of the liquid phase, M_{GAC} (mg) is the mass of the dosed GAC, C_0 and C_e are, respectively, the initial (blank sample) and residual equilibrium concentration of adsorbate at the end of contact time ($\mu g\ L^{-1}$).

2.2.1   *Preliminary chloramination FP tests in ES1*

Chloramination FP experiments at three different pH values (6, 7 and 8) were conducted under ES1 into vials containing 10 mL reaction solution, composed of variable volumes of precursor stock solution, sodium phosphate buffer, monochloramine stock solution and ultrapure water. Initial concentration of the precursors was set at 0.5 mM for BZK and 0.1 mM for CHD; the reaction time was 7 days and NH_2Cl initial concentration corresponded to a molar excess of 10- and 200-fold, for BZK and CHD, respectively. Experimental conditions adopted in FP tests were selected according to a series of preliminary kinetic tests (results reported in S.I.3). The concentrations of TONO and US-EPA 8270 standard mix *N*-nitrosamines (see section 2.3) were measured at the end of the FP tests.

2.2.2 Pre-adsorption tests in ES1

Equilibrium adsorption tests were conducted on 50 mL solutions composed of variable volumes of precursor stock solution and buffered ultrapure water (pH 6 and 8). Initial precursor concentration was set at 0.5 mM for BZK and 0.1 mM for CHD. At pH 6, a dose of 1000 mg L^{-1} was tested for both the GACs. At pH 8, five doses of GAC-V (100, 150, 200, 500 and 1000 mg L^{-1}) and one dose of GAC-M (1000 mg L^{-1}) were tested. After 48 h contact time, mixing was turned off to let GAC particles settling; 1 mL of solution was collected for measuring precursor residual concentration (see section 2.3), while 5 mL were transferred in amber borosilicate vials and tested in chloramination FP tests by adding 5 mL of monochloramine stock solution (leading to 10- and 200-fold NH$_2$Cl molar excess, for BZK and CHD, respectively). The produced TONO concentration (see section 2.3) was measured after a reaction time of 7 days.

2.2.3 Post-adsorption tests in ES1

Chloramination FP tests were performed on 250 mL solutions composed by buffered ultrapure water (pH 6 and 8), precursor (initial concentration of 0.25 mM and 0.05 mM for BZK and CHD, respectively) and monochloramine (10- and 200-fold NH$_2$Cl molar excess, for BZK and CHD, respectively). After 7 days, 1 mL was extracted for measuring TONO concentration (see section 2.3), while various aliquots of 50 mL each were obtained for equilibrium adsorption tests with GAC-V (for each pH, five tested doses: 100, 150, 200, 500 and 1000 mg L^{-1}) and GAC-M (1000 mg L^{-1} dose for each pH). After 48 h contact time, mixing was turned off to let GAC particles settling and 1 mL of solution was collected for measuring residual TONO concentration (see section 2.3).

2.2.4 Pre-adsorption tests in ES2

Pre-adsorption tests in ES2 were conducted on 0.5 L solution volume containing deionized water, 1 mM sodium phosphate buffer (pH 8) and 0.5 μM initial concentrations of precursor (BZK or CHD). Two doses of GAC-V (10 and 40 mg L^{-1}) were tested. At the end of contact time, solutions were filtered through a paper filter to remove GAC particles and pre-formed monochloramine stock solution was added to lead 100 μM NH$_2$Cl initial concentration and to start chloramination FP tests (7 days reaction time). At the end of 7 days reaction time, TONO concentration was measured after sample pre-concentration by solid phase extraction (see section 2.3).

2.3 Analytical methods

NH$_2$Cl and NHCl$_2$ concentrations were determined spectrophotometrically as described in Chapter 4 (section 2.3).

Total *N*-nitrosamine concentration was measured by a method based on UV photolysis and chemiluminescence measurement of nitric oxide. All the details about analytical method and instruments are reported in Breider and von Gunten (2017) ([29]). Chemiluminescence signal was related to TONO concentration by a standard curve, obtained with different concentrations of US-EPA 8270 *N*-nitrosamine standard mix (from 0.8 to 16.2 μM). The signal of test solutions in absence of monochloramine was compared with ultrapure water, to verify the absence of background signal. Calibration was daily repeated before each measurement trial. The limit of detection (LOD) and quantification (LOQ) at the 95% confidence level of the analytical method were calculated based on the standard error (SE) and the slope (m) of the calibration curve (LOD=3.3×SE/m, LOQ=10×SE/m). Average (±st. dev.) LOD and LOQ resulted equal to 0.3±0.15 μM and 1.0±0.45 μM, respectively. For each sample, TONO measurement was repeated three times.
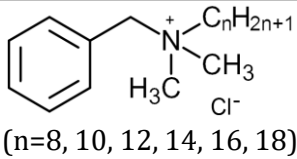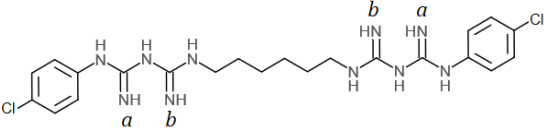
US-EPA 8270 standard mix *N*-nitrosamines were analyzed by GC-MS/MS (Trace 1310 Seies GC) according to the method described by Chen et al. (2012) ([30]). LOD and LOQ for the investigated

N-nitrosamines are reported in S.I.1 of Chapter 4 (Table S2). Measurement was repeated twice for each sample.

Samples obtained in FP tests under ES2 were pre-concentrated by solid phase extraction (SPE), as described in Chapter 4 (section 2.3).

BZK and CHD concentrations were measured by HPLC equipped with a diode array detector (Dionex Ultimate 3000) using EC 125/3 nucleosil 100-5 C-18 column (Thermo Scientific). Where not specified, the used reagents were of HPLC purity grade. BZK concentration was determined by modifying the isocratic method proposed by Labranche et al. (2006) ([31]). A 20/80 mixture of methanol and phosphoric acid (pH 3.0; 7.5 mM) was used as mobile phase. The flow rate was 0.8 mL min^{-1}, the sample injection was 100 μL and column temperature was maintained at 25°C. CHD concentration was determined by modifying the method proposed by Below et al. (2004) ([32]), using a mixture (70/30 v/v) of buffer solution (mixture of 0.25 M ammonia solution and 0.25 M acetic acid in the ratio 60/40, pH 8.7) and acetonitrile as eluent A and a mixture (20/80 v/v) of 0.25 M acetic acid and acetonitrile as eluent B. The gradient was modified as follows: 0–4 min 0% B, between 4 min and 11 min the concentration of eluent B was increased linearly up to 75%, then the concentration was maintained constant during 7 min. Finally, between 18 min and 20 min the concentration of eluent B was linearly decreased to 0% and then maintained at this level during 6 min. The flow rate was 0.8 mL min^{-1} and the sample injection was 75 μL. HPLC methods were calibrated by analysing standard solutions at different concentrations. Calibration curves, LOD and LOQ of the analytical methods are reported in S.I.2 (Table S3).

Table 1 Studied *N*-Nitrosamine precursors: molecular structure, molecular weight (MW) and pK_a values referred to the equilibrium C=NH$_2^+$ ⇆ C=NH + H$^+$ ([33]).

Precursor	Structure	MW (g mol^{-1})	pK_a
Benzalkonium chloride (BZK)	(n=8, 10, 12, 14, 16, 18)	283.4-423.4 (average 348.4)	-
Chlorhexidine hydrochloride (CHD)		578.4	2.20 [a] 10.30 [b]

3. Results and discussion

3.1 *N*-nitrosamine formation potential of the studied precursors

The *N*-nitrosamine formation potential of the studied precursors was evaluated by a series of preliminary chloramination tests under ES1 (section 2.2.1) at three pH values (6, 7 and 8). *N*-nitrosamine FP is the is the operationally defined maximum *N*-nitrosamine concentration that can be produced in excess of reagent, using NH$_2$Cl concentration and contact time much higher than applied during drinking water treatment ([3]). In this study, the experimental conditions to be adopted in the FP tests (i.e., reaction time, initial concentrations of precursors and monochloramine) under ES1 were selected according to a series of preliminary kinetic tests, whose results are reported in Chapter 4 (section 3.2). The results of FP tests are provided in Table 2, expressed as molar yield of TONO and NDMA formation, at different pH values. Molar yields in Table 2 are the average values obtained from all the FP tests performed in ES1 including blank samples of adsorption experiments (results discussed in the following sections). Both the precursors showed a relevant TONO FP, with molar

yields up to 3-4% for BZK and up to 17% for CHD, increasing with the pH of the solution. As already discussed in in Chapter 4 (section 3.2), the pH-dependence of *N*-nitrosamine formation can be explained by the NH_2Cl decay during FP experiments and, in the case of CHD, by the acid-base equilibrium of the compound.

NDMA concentration equal to 2.81 ± 0.134 μM (corresponding to a molar yield of 0.56%) was found in samples from FP tests with BZK at pH 8, while all the other samples displayed NDMA concentrations <LOQ (0.09 μM). None of the other *N*-nitrosamines of US-EPA 8270 standard mix was detected in any sample. Results indicated that the TONO pool formed by CHD was all composed by unknown species, not included in US-EPA 8270 standard mix; for BZK, NDMA contribution to TONO was only about 26% and the largest part of TONO pool resulted to be uncharacterized.

Results of FP tests indicated that the studied compounds can be important *N*-Nitrosamine precursors and can contribute to the TONO formation potential of chloraminated waters. Since most of the formed *N*-nitrosamines were not identified in the US-EPA 8270 standard mix species, TONO measurement resulted to be the most proper assay to evaluate the *N*-Nitrosamine FP of the two precursors.

Table 2 Molar yield of total *N*-nitrosamine (TONO) and NDMA formation observed in FP experiments (ES1) at pH 6, 7 and 8. For each experimental replicate, TONO and NDMA measurements were repeated three and two times, respectively. Average TONO molar yields at pH 6 and 8 consider all the FP tests performed under ES1, including blank samples of adsorption experiments (N: number of data).

Precursor	pH	TONO		NDMA	
		N	Molar yield (%) average ± st.dev.	N	Molar yield (%) average (range)
Benzalkonium chloride (BZK)	6	6	0.69 ± 0.153	2	<LOQ*
	7	2	1.31 ± 0.209	2	<LOQ*
	8	10	3.40 ± 0.213	2	0.56 (0.55-0.56)
Chlorhexidine hydrochloride (CHD)	6	6	2.15 ± 0.515	2	<LOQ*
	7	2	4.33 ± 1.342	2	<LOQ*
	8	10	16.82 ± 2.117	2	<LOQ*

* LOQ=0.09 μM

3.2 Control of *N*-Nitrosamine formation potential by activated carbon adsorption

The possibility to reduce the *N*-nitrosamine FP associated to the studied precursors by means of activated carbon was studied by adsorption and chloramination batch experiments. Two treatment solutions were compared: adsorption before (pre-adsorption) or after (post-adsorption) the oxidation treatment. In the first solution, precursors concentration can be reduced, limiting the potential formation of *N*-nitrosamines during chloramination. In the second solution, already formed *N*-nitrosamines can be reduced, depending on the compounds composing the TONO pool, together with residual precursors which could be responsible of the formation of additional *N*-nitrosamines along the distribution network due to slow reaction kinetics with NH_2Cl.

Adsorption and chloramination experiments were performed in ES1. Under these experimental conditions, the relatively high produced TONO concentrations can be determined without sample pre-concentration. Hence, obtained results are not affected by SPE recovery efficiency, that can be a relevant source of uncertainty when dealing with uncharacterized TONO pools [5]. Since adsorbate (precursors and by-products) concentrations were much higher than those detectable in water

treatment plants, indications for the design of full-scale systems (carbon dose, contact time) cannot be directly derived by these experiments; however, results can be used to compare the two treatment solutions and to highlight the parameters mainly influencing their performances.

3.2.1 Selection of GAC type and pH (ES1 setup)

The efficiency of the tested GACs on the analysed target contaminants, i.e. precursors in pre-adsorption tests and TONO in post-adsorption tests, was firstly evaluated. The equilibrium solid-phase concentrations (q_e) are shown in Figure 1 as a function of the type of GAC and the pH value. GAC-V showed adsorption capacities higher than GAC-M for all the adsorbates: in pre-adsorption tests, q_e values of BZK and CHD were, respectively, 16% and 17% higher for GAC-V than GAC-M; the difference between the two carbons was even higher in post-adsorption tests, with GAC-V showing q_e values 55% and 64% higher than GAC-M for the adsorption of the TONO pools formed by BZK and CHD, respectively. The higher adsorption capacities of GAC-V can be explained by the more developed pore structural properties (higher BET surface area, micropore volume and area) and higher iodine number (S.I.1, Table S1). Carbon surface and porous characteristics are so important factors influencing the adsorption of both the studied precursors and *N*-nitrosamines, although the properties of the TONO pool components are not fully known.

Having shown better performances for all the investigated cases, the influence of solution pH was tested only for GAC-V Pre-adsorption tests (Figure 1a) displayed a decrease of about 20% in BZK and CHD q_e values when passing from pH 8 to 6. The influence of the solution pH can be explained by looking at the chemical properties of both the carbons and the precursors: having a pH of point of zero charge (pH_{PZC}) of about 10 (S.I.1), GAC-V surface is supposed to be more protonated as the pH of the solution decreases. Being composed by positively charged quaternary ammonium compounds, BZK is expected to be less favourably adsorbed at lower pH values; similarly, the protonation of CHD molecule at lower pH values (due to different pK_a values, as discussed above) can enhance the electrostatic repulsion with the carbon surface, resulting in a lower uptake. Also the adsorption of TONO resulted to strongly depend on the solution pH, as displayed by the high difference between the q_e values observed at pH 6 and 8 in post-adsorption tests (Figure 1b). The acid-base equilibrium of *N*-nitrosamines may explain the decrease of adsorption capacity at lower pH. In fact, the fraction of positively charged *N*-nitrosamines, due to the protonation of O-atom in *N*-nitroso group, increases when decreasing the solution pH (depending on their dissociation constant). Hence, repulsive forces between carbon surface and *N*-nitrosamines are theoretically enhanced at lower pH. It must be pointed out that the initial TONO concentrations at pH 6 were 71% and 94% lower than those at pH 8, for BZK and CHD samples, respectively. Hence, the lower TONO adsorption capacity observed at pH 6 could have been also affected by the lower bulk concentration values and not only by the lower pH, since the bulk concentration affects the diffusion mass transfer both through the liquid film surrounding GAC particles and inside particle porosities. Further investigations are therefore needed to evaluate the relative role of pH and initial concentration in affecting adsorption capacity of GAC towards *N*-nitrosamines.
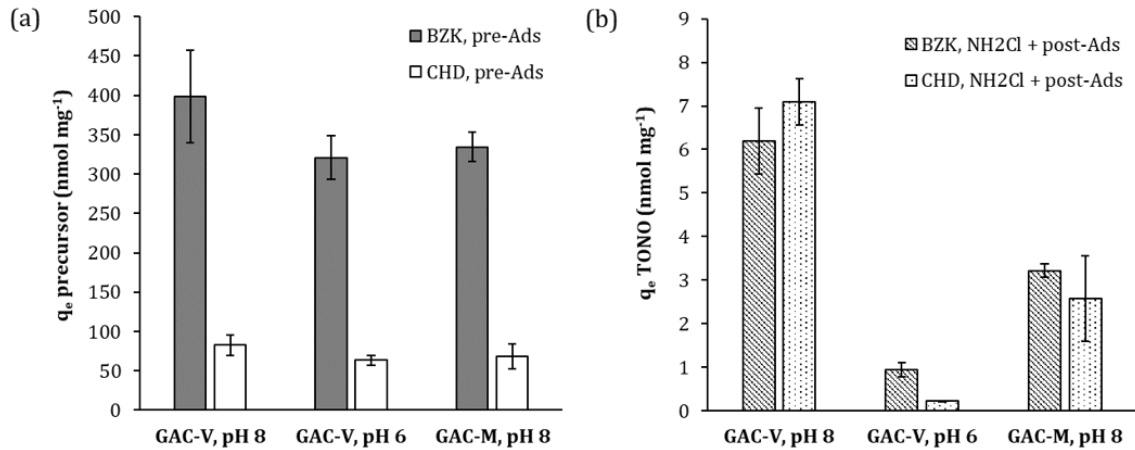
Figure 1 Equilibrium solid-phase concentrations (q_e) of the precursors in pre-adsorption experiments (a), and TONO in post-adsorption experiments (b), determined under ES1 (1000 mg L^{-1} GAC dose) for different pH and GAC types.

3.2.2   *Effect of GAC dose on precursor and N-nitrosamine removal (ES1)*

The two treatment solutions (pre- and post-adsorption) were then investigated by testing different activated carbon doses. According to the results reported above, the study was focused on GAC-V and the pH of the solutions was set at 8.

Pre-adsorption and post-adsorption experiments permitted to specifically assess the efficiency of GAC-V on the removal of precursors and N-nitrosamines, respectively.

Removal efficiencies (η ADS) observed for BZK and CHD at different GAC doses (M_{GAC}) in pre-adsorption experiments are reported in Figure 2a. Similar removal efficiencies were observed for the two compounds, passing from about 10% to 80-90% over the tested M_{GAC} range, proving the effectiveness of GAC-V in precursor reduction. Data were elaborated to determine the adsorption isotherms for BZK and CHD: Figure 2b shows experimental results reported as liquid- (C_e) vs. solid-phase (q_e) equilibrium concentrations. It can be observed that relatively high q_e values were obtained for both the precursors (up to 1.2 and 0.21 µmol mg^{-1} for BZK and CHD, respectively), displaying a high affinity with the selected activated carbon. Data series were interpolated by Freundlich and Langmuir isotherm models ([34]), whose equation are written, respectively, as:

e.2)
$$q_e = K_F C_e^{\frac{1}{n}}$$

e.3)
$$q_e = \frac{q_L K_L C_e}{1 + K_L C_e}$$

where K_F and $1/n$ are, respectively, the constant and the exponent of Freundlich equation; q_L and K_L are, respectively, the maximum adsorption capacity and equilibrium constant of Langmuir model. Parameters obtained by non-linear regression are reported in Table 3. Good agreement between observed and simulated data was obtained for BZK ($R^2 > 0.92$), while slightly lower determination coefficients were obtained for CHD ($R^2 = 0.70$). The adsorption equilibrium of both the adsorbates could be similarly described by the two models, but Freundlich model showed slightly higher determination coefficients and lower uncertainties in parameter estimates, as indicated by the narrower 95% confidence intervals. No references were found in literature about BZK and CHD adsorption, but results can be considered comparable with those reported for similar compounds. For instance, Krivova et al. (2013) ([35]) studied the adsorption of various cationic surfactants of quaternary ammonium bromide at high initial concentrations (0.5-5.0 mM), obtaining Freundlich constants between 0.25 and 0.78 (µmol mg^{-1})(L µmol^{-1})$^{1/n}$ and exponents between 0.2 and 0.5. Huang et al. (2016) ([36]) used a biochar adsorbent to remove metformin, a pharmaceutical known to be a NDMA

precursor and having a biguanide structure similar to CHD: the authors determined a K_F value of 0.006 $(\mu mol\ mg^{-1})(L\ \mu mol^{-1})^{1/n}$ and $1/n$ equal to 0.53, testing a high initial concentration range (0.05-3.6 mM) at 25°C.
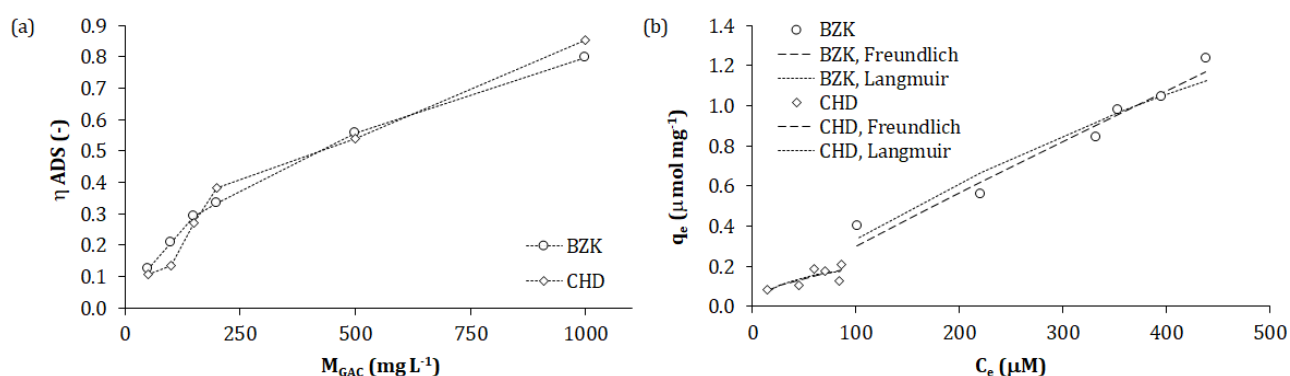
Figure 2 Results of pre-adsorption isotherm experiments for BZK and CHD: a) removal efficiency (η ADS) over GAC mass (M_{GAC}); b) solid-phase (q_e) vs. liquid-phase (C_e) concentrations (data observed and simulated by Freundlich and Langmuir models).

Table 3 Freundlich and Langmuir parameters (±95% confidence intervals) and determination coefficients (R^2) estimated by non-linear regression (6 data) for BZK and CHD.

Isotherm model	Precursor	BZK	CHD
Freundlich	$K_F\ [(\mu mol\ mg^{-1})(L\ \mu mol^{-1})^{1/n}]$	0.004±0.0094	0.023±0.0664
	$1/n\ [-]$	0.921±0.3721	0.460±0.6808
	$R^2\ [-]$	0.958	0.704
Langmuir	$q_L\ [\mu mol\ mg^{-1}]$	2.088±2.3753	0.249±0.2830
	$K_L\ [L\ \mu mol^{-1}]$	0.002±0.0056	0.028±0.0893
	$R^2\ [-]$	0.925	0.697

The efficiency of GAC-V in *N*-nitrosamines removal can be inferred based on data from post-adsorption experiments, reported in Figure 3. TONO removal efficiencies were very different for the two precursors: for CHD, a significant reduction of TONO concentration (67%) was observed only at the highest GAC dose (1000 mg L^{-1}), while no significant TONO removal was obtained at the other GAC masses. For BZK, on the contrary, a relevant abatement of TONO concentration was observed already at the lowest GAC doses, with removal efficiencies varying from 17% (150 mg L^{-1} GAC) to 81% (1000 mg L^{-1} GAC). The difference in efficiencies observed for the two precursors indicates a different composition of the formed N-nitrosamine pools. Except the NDMA fraction determined for BZK samples, the TONO concentrations observed in FP tests were not characterized, not corresponding to US EPA 8270 standard mix *N*-nitrosamines. However, the higher adsorbability of BZK TONO pool suggests a higher contribution of more hydrophobic compounds, resulting in a higher overall affinity with GAC-V. Despite further studies are needed to identify specific *N*-nitrosamines structures, results indicate that GAC adsorption efficiency strongly depends on the TONO pool composition, hence on the considered precursor. According to these results, the effectiveness of activated carbon adsorption in *N*-nitrosamine removal can be best evaluated by looking at the TONO concentration reduction, due to the high fraction of unknown N-nitrosamines expected during oxidative water treatment ([5,6]).

Experimental data did not allow to calibrate any adsorption isotherm model for *N*-nitrosamines. In fact, relevant CHD solid-phase concentrations have been observed only at the highest GAC dose, meaning an equilibrium adsorption capacity equal to 7 nmol mg^{-1}. Plotting q_e vs. C_e data for BZK (S.I.4, Figure S5) did not show any significant trend. The maximum equilibrium adsorption capacity

corresponded to 14 nmol mg^{-1}. No works were found in the literature studying activated carbon efficiency in TONO removal; however, TONO adsorption capacities determined in this study are in agreement with those obtained by previous works for specific *N*-nitrosamines: Dai et al. (2009) ([19]) determined NDMA adsorption capacities for three activated carbons (BET surface area: 1000-1700 m^2 g^{-1}, micropore volume: 0.25-0.42 cm^3 g^{-1}, average pore diameter: 2.11-2.35 nm) between 27 and 337 nmol mg^{-1}, even if obtained using NDMA standard solutions at higher concentrations (0.13-2.70 mM). Testing a commercial GAC (Norit, BET surface area: 807 m^2 g^{-1}), de Ridder et al. (2012) ([20]) determined quite lower adsorption capacities (varying between 0.05 and 0.32 nmol mg^{-1}) for NDBA and NDEA, in a range of residual liquid concentrations similar to this study (0.3-26.7 μM). As already pointed out, however, the affinity with activated carbon can strongly vary for different *N*-nitrosamines, which can have very different physical characteristics, for instance, ranging from polar *N*-nitrosodiethanolamine to apolar *N*-nitrosodipropylamine ([5]).

3.2.3 Comparison of pre-adsorption and post-adsorption treatment solutions for N-nitrosamine control

TONO concentrations obtained in both the pre-adsorption and post-adsorption experiments are shown in Figure 3.

Results show that, for both the precursors, a higher GAC mass dosed in the pre-adsorption phase corresponded to a lower TONO formation, which was reduced up to 81% and 73% at the highest GAC dose, for BZK and CHD, respectively. The reduction of TONO FP per mass unit of activated carbon (all the values provided in S.I.4, Figure S4) ranged between 1-9 nmol mg^{-1} for BZK and 6-22 nmol mg^{-1} for CHD, depending on the GAC dose. TONO molar yields calculated for the samples treated by GAC were almost constant, with average values of 4.6±0.68% and 17.3±2.04%, for BZK and CHD, respectively, and comparable to those calculated in blank samples (Table 2). The average molar yield for CHD was calculated without considering data obtained at 1000 mg L^{-1} GAC, for which resulted a higher value (33.3%). It must be pointed out that this value has been determined at the lowest CHD initial concentration, so molar yield calculation was more sensitive to CHD initial concentration value. Anyway, further investigation would be needed to evaluate TONO FP at lower precursor concentrations and to test the constancy of TONO formation molar yield. Except in the discussed case for CHD, TONO conversion yield resulted to be not dependent on the initial precursor concentration, indicating that TONO *N*-nitrosamine FP can be reduced proportionally to the removal of the precursor concentration in the pre-adsorption phase. Considering the high adsorption capacity of the studied activated carbon towards BZK and CHD, it can be concluded that the preliminary removal of precursor by a pre-adsorption phase is an effective strategy to reduce total *N*-nitrosamine formation upon chloramination.

As for post-adsorption tests, TONO molar yields in blank samples were equal to 3.05±0.373% and 20.98±1.578%, for BZK and CHD, respectively, directly comparable with the values obtained in pre-adsorption tests. For a given GAC dose, post-adsorption resulted to be always less effective than pre-adsorption in reducing TONO formation potential from CHD, with differences in removal efficiency from 17% to 73%, passing from 10 to 1000 mg L^{-1} GAC. On the contrary, for BZK, the abatement of TONO formation potential by post-adsorption resulted to be equal or even higher than that obtained by pre-adsorption, for a given GAC dose. The reduction of TONO FP per mass unit of activated carbon (all the values provided in S.I.4, Figure S5) by post-adsorption ranged between 2-14 nmol mg^{-1} for BZK and 0-7 nmol mg^{-1} for CHD, depending on the GAC dose.

Summarising (Figure 3b), the preliminary adsorption of precursors resulted to be most effective and reliable solution for reducing the *N*-nitrosamine FP associated to the studied precursors. In fact, both BZK and CHD showed high affinity with GAC and they can be easily removed by adsorption process, reducing the associated TONO FP upon disinfection. The abatement of TONO concentration by

post-adsorption resulted to be also effective, but the removal efficiency can be much different for each specific *N*-nitrosamine. Since TONO pool composition in real water matrices is expected to be much heterogeneous, due to the presence of several *N*-nitrosamine precursors, GAC performances must be carefully evaluated. Moreover, an adsorption phase is often already present (before disinfection) in the drinking water treatment trains, to control the concentration of NOM and many synthetic organic contaminants, while the addition of a GAC treatment step after disinfection would be less feasible, increasing the complexity of the treatment process and requiring another disinfection step before feeding drinking water into the distribution network.
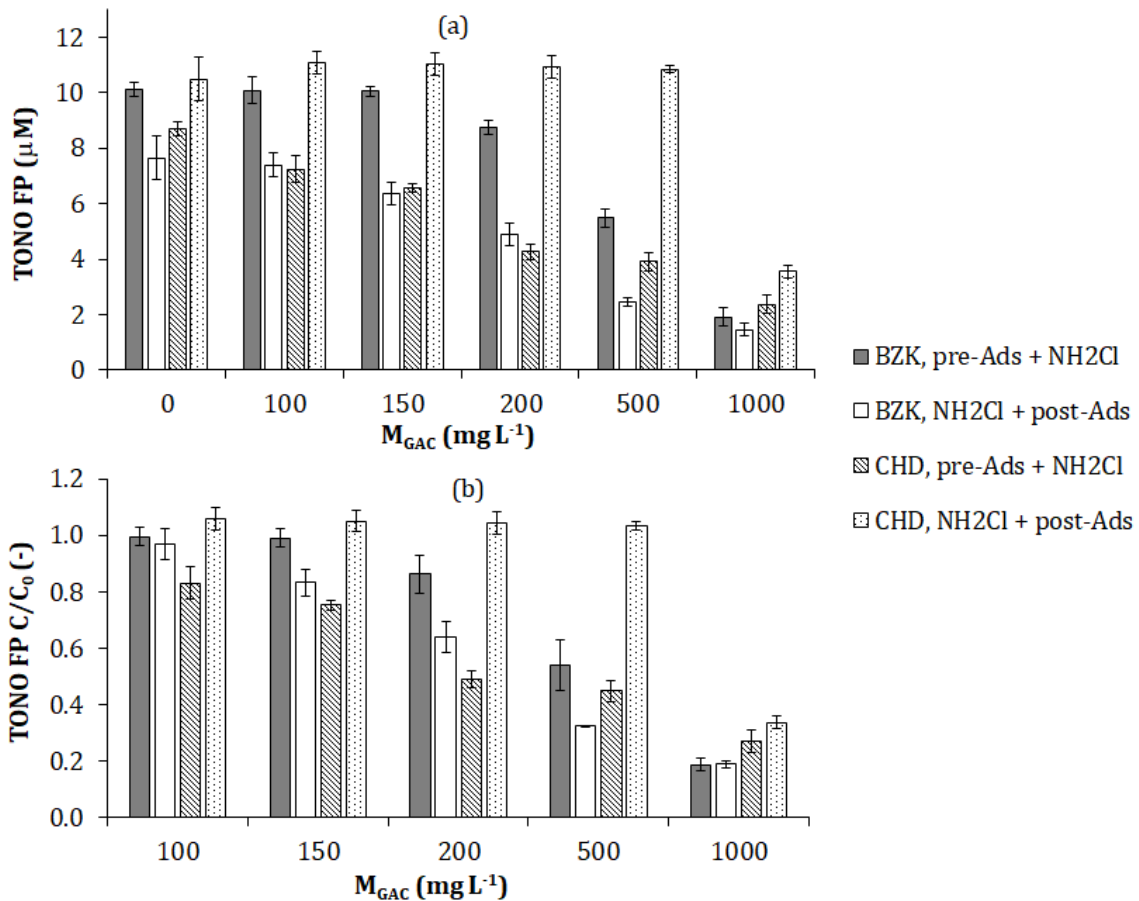
Figure 3 Total *N*-nitrosamine formation potential (TONO FP) obtained for BZK and CHD in pre-adsorption and post-adsorption experiments (ES1) at different GAC masses (M_{GAC}): a) TONO molar concentrations; b) TONO concentrations normalized respect to blank sample (M_{GAC}=0).

3.2.4   *Pre-adsorption effectiveness at low precursor concentrations*

The effectiveness of pre-adsorption in reducing TONO FP of BZK and CHD was finally investigated in ES2, having much lower initial concentrations of precursors and monochloramine, to test conditions more similar to those of real water matrices. The effect of activated carbon pre-adsorption was evaluated on the reduction of TONO FP after chloramination, while it was not possible to determine the precursor adsorption removal efficiency, due to the low initial concentration. TONO concentrations were calculated by considering the recovery efficiency of SPE, considering the low *N*-nitrosamine concentration produced under ES2. It is pointed out that TONO extraction efficiency resulted to be quite low for both the precursors, with average values of about 10% (7.5-10.2% for BZK and 5.8-13.7% for CHD). Such small values increase the uncertainty in the quantification of TONO concentrations and the molar yield determination.

Figure 4 shows TONO FP determined for BZK and CHD. Blank samples (M_{GAC}=0) displayed average TONO FP of 20.3 and 32.7 nM, corresponding to molar yields of 4.05±0.612% and 6.54±3.169% for BZK and CHD, respectively. Considering the uncertainty associated to SPE efficiency and the extremely different experimental conditions, these molar yield values can be considered quite well comparable with those obtained in ES1 (Table 2). Activated carbon pre-adsorption led to a relevant reduction of the TONO FP, between 54% and 73% for BZK, and between 39% and 45% for CHD, passing from 10 to 40 mg L^{-1} of GAC dose, respectively. Obtained results corresponded to TONO FP removal per mass unit of activated carbon of 1.09-0.37 nmol mg^{-1} and 1.27-0.37 nmol mg^{-1} for BZK and CHD, respectively. These quantities, being strictly related to the uptake of the precursors and representing the capability of the carbon to reduce TONO FP, revealed relevant adsorption capacities for both the precursors also at much lower initial concentrations. Considering the TONO molar yields determined in blank samples, the observed TONO FP removals would correspond to equilibrium solid-phase concentrations of the precursors equal to 225-666 nmol mg^{-1} (78-232 µg mg^{-1}) for BZK and 86-296 nmol mg^{-1} (50-171 µg mg^{-1}) for CHD, at residual liquid-phase concentrations of about 0.1-0.3 µM. A comparison between adsorption capacities determined under ES1 and ES2 is not easy, due to the wide range of covered liquid-phase concentration values and the uncertainty associated to SPE efficiency. However, the q_e values observed under the two ESs were comparable (a comparison is provided in S.I.4, Figure S4), indicating that GAC adsorption capacities are not dramatically affected by the precursor initial concentration.

Despite the many differences in the experimental conditions (i.e. adsorbent type and dose, contact time, water matrix, analysed *N*-nitrosamines), the results obtained in this study for TONO FP could be quite well compared with those observed by other authors for NDMA FP: Hanigan et al. (2012) observed a 74% reduction of the NDMA FP of wastewaters (initial NDMA FP=78-1390 ng L^{-1}) after 7 days contact time (assumable as equilibrium conditions), corresponding to adsorption capacities of 1-20 ng mg^{-1} [12]; Beita-Sandi et al. (2016) determined NDMA FP removal efficiencies of 30-40%, by testing 15 mg L^{-1} PAC in surface waters (70 ng L^{-1} initial NDMA FP), and 20-80% with 30 mg L^{-1} PAC dose in surface waters and wastewaters (20-569 ng L^{-1} initial NDMA FP), even if at shorter contact time (4 h) [13].

Although further studies are required to test the role of various factors on activated carbon performances (such as testing the competitive adsorption of different adsorbates and then real water matrices), results obtained under ES2 showed that activated carbon adsorption can be an effective strategy to reduce TONO FP also in presence of low precursor concentrations, leading to relevant removal efficiencies already at a carbon dose of 10 mg L^{-1}.
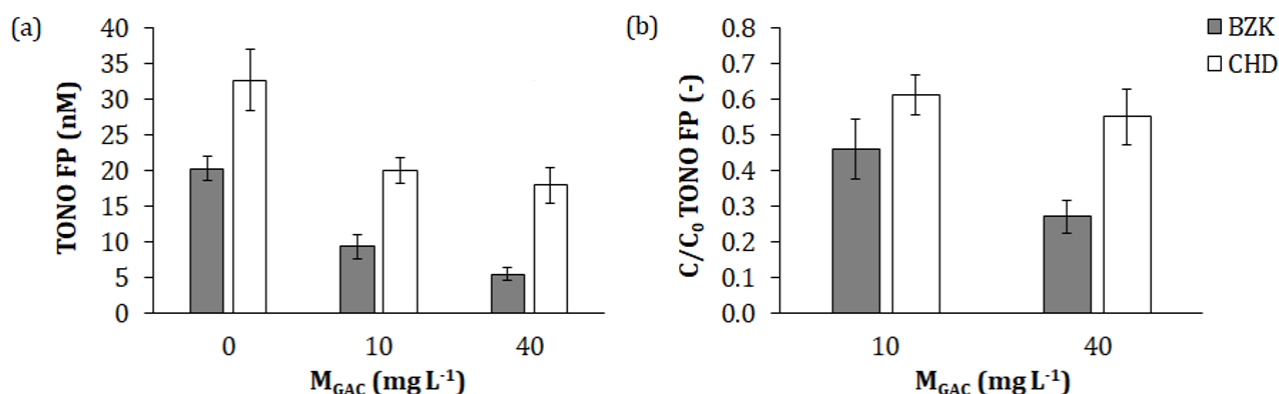
Figure 4 Effect of activated carbon pre-adsorption on TONO FP of BZK and CHD evaluated in ES2: (a) absolute TONO concentrations; (b) TONO concentrations normalized with respect to blank sample (M_{GAC}=0).

4. Conclusions

Two nitrogenous micropollutants associated to pharmaceutical and personal care products, benzalkonium chloride (BZK) and chlorhexidine (CHD), were studied as potential *N*-nitrosamine precursors. Both the compounds showed relevant total *N*-nitrosamine (TONO) formation potentials (FP) during chloramination, with maximum molar yields at pH 8 equal to 3.40% for BZK and 16.82% for CHD. The FP of a specific *N*-nitrosamine, NDMA, was determined only for BZK, showing a 0.56% molar yield. Activated carbon adsorption was tested as solution to reduce the TONO FP of the two precursors, by evaluating two treatment options: the precursor removal before chloramination (pre-adsorption), and the TONO removal after chloramination (post-adsorption). The adsorption of both the precursors and TONO were found to increase with the solution pH within the investigated range (6-8). Both BZK and CHD were well removed by pre-adsorption, with equilibrium adsorption capacities at pH 8 up to 1.2 and 0.21 μmol mg^{-1} for BZK and CHD, respectively (for 100-1000 mg L^{-1} GAC doses); the TONO FP upon chloramination was reduced up to 81% for BZK and 73% for CHD, almost proportionally to the precursor removal during the pre-adsorption phase. Post-adsorption tests at the various GAC doses (100-1000 mg L^{-1}) showed that GAC efficiency strongly depends on the TONO pool composition: for the TONO pool formed by BZK, equilibrium TONO adsorption capacities between 2 and 14 nmol mg^{-1} were observed, with TONO FP removal efficiency comparable to that of pre-adsorption, for a given GAC dose; for CHD, on the other hand, a significant reduction of TONO concentration (67%, 7.1 nmol mg^{-1}) was observed only at the highest GAC dose.

Based on the experimental results, the pre-adsorption of *N*-nitrosamine precursors is the most effective and reliable solution for reducing the *N*-nitrosamine FP. Pre-adsorption was found to be effective also under experimental conditions closer to real water matrices (initial precursor and monochloramine concentration of 0.5 μM and 100 μM, respectively), reducing the TONO FP of the two precursors of 58% and 75% for BZK, 39% and 45% for CHD, dosing 10 and 40 mg L^{-1} of GAC-V, respectively.

References

(1)   Richardson, S. D.; Ternes, T. A. Water analysis: emerging contaminants and current issues. *Anal. Chem.* **2014**, *86* (6), 2813–2848.

(2)   Mitch, W. A.; Sedlak, D. L. Characterization and fate of N-nitrosodimethylamine precursors in municipal wastewater treatment plants. *Environ. Sci. Technol.* **2004**, *38* (5), 1445–1454.

(3)   Krasner, S. W.; Mitch, W. A.; McCurry, D. L.; Hanigan, D.; Westerhoff, P. Formation, precursors, control, and occurrence of nitrosamines in drinking water: a review. *Water Res.* **2013**, *47* (13), 4433–4450.

(4)   Mitch, W. A.; Sharp, J. O.; Trussell, R. R.; Valentine, R. L.; Alvarez-Cohen, L.; Sedlak, D. L. N-nitrosodimethylamine (NDMA) as a drinking water contaminant: a review. *Environ. Eng. Sci.* **2003**, *20* (5), 389–404.

(5)   Dai, N.; Mitch, W. A. Relative importance of N-nitrosodimethylamine compared to total N-nitrosamines in drinking waters. *Environ. Sci. Technol.* **2013**, *47* (8), 3648–3656.

(6)   Zeng, T.; Mitch, W. A. Contribution of N-nitrosamines and their precursors to domestic sewage by greywaters and blackwaters. *Environ. Sci. Technol.* **2015**, *49* (22), 13158–13167.

(7)   Kemper, J. M.; Walse, S. S.; Mitch, W. A.; others. Quaternary amines as nitrosamine precursors: a role for consumer products? *Environ. Sci. Technol.* **2010**, *44* (4), 1224–1231.

(8)   Le Roux, J.; Gallard, H.; Croué, J.-P. Chloramination of nitrogenous contaminants (pharmaceuticals and pesticides): NDMA and halogenated DBPs formation. *Water Res.* **2011**, *45* (10), 3164–3174.

(9)   Schwarzenbach, R. P.; Escher, B. I.; Fenner, K.; Hofstetter, T. B.; Johnson, C. A.; Gunten, U. von; Wehrli, B. The Challenge of Micropollutants in Aquatic Systems. *Science* **2006**, *313* (5790), 1072–1077.

(10)   Chowdhury, Z. Nationwide assessment of nitrosamine occurrence and trends. **2012**.

(11)   Kulshrestha, P.; McKinstry, K. C.; Fernandez, B. O.; Feelisch, M.; Mitch, W. A. Application of an optimized total N-nitrosamine (TONO) assay to pools: placing N-nitrosodimethylamine (NDMA) determinations into perspective. *Environ. Sci. Technol.* **2010**, *44* (9), 3369–3375.

(12)   Hanigan, D.; Zhang, J.; Herckes, P.; Krasner, S. W.; Chen, C.; Westerhoff, P. Adsorption of N-nitrosodimethylamine precursors by powdered and granular activated carbon. *Environ. Sci. Technol.* **2012**, *46* (22), 12630–12639.

(13)   Beita-Sandí, W.; Ersan, M. S.; Uzun, H.; Karanfil, T. Removal of N-nitrosodimethylamine precursors with powdered activated carbon adsorption. *Water Res.* **2016**, *88*, 711–718.

(14)   Wu, Q.; Shi, H.; Ma, Y.; Adams, C.; Jiang, H.; Wang, J.; Eichholz, T.; Timmons, T. Removal of N-nitrosamine precursors in drinking water system using adsorption methods. *Sep. Purif. Technol.* **2015**, *156*, 972–979.

(15)   Chu, W.; Yao, D.; Gao, N.; Bond, T.; Templeton, M. R. The enhanced removal of carbonaceous and nitrogenous disinfection by-product precursors using integrated permanganate oxidation and powdered activated carbon adsorption pretreatment. *Chemosphere* **2015**, *141*, 1–6.

(16)   Crittenden, J. C.; Trussell, R. R.; Hand, D. W.; Howe, K. J.; Tchobanoglous, G. *MWH's water treatment: principles and design*; John Wiley & Sons, 2012.

(17)   Sharpless, C. M.; Linden, K. G. Experimental and model comparisons of low-and medium-pressure Hg lamps for the direct and H2O2 assisted UV photodegradation of N-nitrosodimethylamine in simulated drinking water. *Environ. Sci. Technol.* **2003**, *37* (9), 1933–1940.

(18)   Sedlak, D. L.; Kavanaugh, M. C. *Removal and destruction of NDMA and NDMA precursors during wastewater treatment*; WateReuse Foundation, 2006.

(19)   Dai, X.; Zou, L.; Yan, Z.; Millikan, M. Adsorption characteristics of N-nitrosodimethylamine from aqueous solution on surface-modified activated carbons. *J. Hazard. Mater.* **2009**, *168* (1), 51–56.

(20)   De Ridder, D. J.; Verberk, J.; Heijman, S. G.; Amy, G. L.; Van Dijk, J. C. Zeolites for nitrosamine and pharmaceutical removal from demineralised and surface water: mechanisms and efficacy. *Sep. Purif. Technol.* **2012**, *89*, 71–77.

(21)   Ho, L.; Grasset, C.; Hoefel, D.; Dixon, M. B.; Leusch, F. D.; Newcombe, G.; Saint, C. P.; Brookes, J. D. Assessing granular media filtration for the removal of chemical contaminants from wastewater. *Water Res.* **2011**, *45* (11), 3461–3472.

(22)   US EPA, O. of R. &. METHOD 521: DETERMINATION OF NITROSAMINES IN DRINKING WATER BY SOLID PHASE EXTRACTION AND CAPILLARY COLUMN GAS CHROMATOGRAPHY WITH LARGE VOLUME INJECTION AND CHEMICAL IONIZATION TANDEM MASS SPECTROMETRY (MS/MS) https://cfpub.epa.gov/si/si_public_record_report.cfm?dirEntryId=103912 (accessed Jul 18, 2017).

(23)   Clara, M.; Scharf, S.; Scheffknecht, C.; Gans, O. Occurrence of selected surfactants in untreated and treated sewage. *Water Res.* **2007**, *41* (19), 4339–4348.

(24)   Martínez-Carballo, E.; Sitka, A.; González-Barreiro, C.; Kreuzinger, N.; Fürhacker, M.; Scharf, S.; Gans, O. Determination of selected quaternary ammonium compounds by liquid chromatography with mass spectrometry. Part I. Application to surface, waste and indirect discharge water samples in Austria. *Environ. Pollut.* **2007**, *145* (2), 489–496.

(25)   Ferrer, I.; Furlong, E. T. Identification of alkyl dimethylbenzylammonium surfactants in water samples by solid-phase extraction followed by ion trap LC/MS and LC/MS/MS. *Environ. Sci. Technol.* **2001**, *35* (12), 2583–2588.

(26)   Ding, W.-H.; Liao, Y.-H. Determination of alkylbenzyldimethylammonium chlorides in river water and sewage effluent by solid-phase extraction and gas chromatography/mass spectrometry. *Anal. Chem.* **2001**, *73* (1), 36–40.

(27)   Yavuz, M.; Oggioni, M.; Yetis, U.; Dilek, F. B. Biocides in drinking water system of Ankara, Turkey. *Desalination Water Treat.* **2015**, *53* (12), 3253–3262.

(28)   Boleda, M. R.; Galceran, M. T.; Ventura, F. Behavior of pharmaceuticals and drugs of abuse in a drinking water treatment plant (DWTP) using combined conventional and ultrafiltration and reverse osmosis (UF/RO) treatments. *Environ. Pollut.* **2011**, *159* (6), 1584–1591.

(29)   Breider, F.; von Gunten, U. Quantification of Total N-Nitrosamine Concentrations in Aqueous Samples via UV-Photolysis and Chemiluminescence Detection of Nitric Oxide. *Anal. Chem.* **2017**, *89* (3), 1574–1582.

(30)   Chen, A.; Huebschmann, H. J.; Fangyan, L.; Foong, C. Y.; Harn, C. S. High Sensitivity Analysis of Nitrosamines Using GC-MS/MS, Alpha Analytical Pte. Ltd., Thermo Fisher Scientific. *Health Sci. Auth. HAS Singap.* **2012**.

(31)   Labranche, L.-P.; Dumont, S. N.; Levesque, S.; Carrier, A. Rapid determination of total benzalkonium chloride content in ophthalmic formulation. *J. Pharm. Biomed. Anal.* **2007**, *43* (3), 989–993.

(32)   Below, H.; Lehan, N.; Kramer, A. HPLC determination of the antiseptic agent chlorhexidine and its degradation products 4-chloroaniline and 1-chloro-4-nitrobenzene in serum and urine. *Microchim. Acta* **2004**, *146* (2), 129–135.

(33)   Agarwal, A.; Nelson, T. B.; Kierski, P. R.; Schurr, M. J.; Murphy, C. J.; Czuprynski, C. J.; McAnulty, J. F.; Abbott, N. L. Polymeric multilayers that localize the release of chlorhexidine from biologic wound dressings. *Biomaterials* **2012**, *33* (28), 6783–6792.

(34)   Foo, [5 5] KY; Hameed, B. H. Insights into the modeling of adsorption isotherm systems. *Chem. Eng. J.* **2010**, *156* (1), 2–10.

(35)   Krivova, M. G.; Grinshpan, D. D.; Hedin, N. Adsorption of C n TABr surfactants on activated carbons. *Colloids Surf. Physicochem. Eng. Asp.* **2013**, *436*, 62–70.

(36)   Huang, X.; Liu, Y.; Liu, S.; Li, Z.; Tan, X.; Ding, Y.; Zeng, G.; Xu, Y.; Zeng, W.; Zheng, B. Removal of metformin hydrochloride by Alternanthera philoxeroides biomass derived porous carbon materials treated with hydrogen peroxide. *Rsc Adv.* **2016**, *6* (83), 79275–79284.

Supporting Information

S.I.1 GAC characteristics

Surface characteristics of the carbons were determined by N_2 adsorption and desorption at T=77 K (Tristar II 3020 V1.03, Micrometrics Instruments Corporation), after pre-treatment of the samples for 4 h at T=150°C under nitrogen atmosphere. Carbon surface area was determined according to BET method, specific area and volume of micropores were determined by t-Plot method, pore size distribution was determined by BJH method ([1-3]).

The pH of point of zero charge (pH_{PZC}) of the carbons was determined by the pH drift method ([4]): 0.3 g of carbon were added in 100 mL of 0.01 N NaCl solution, after pH adjustment by means of 0.1 N HCl or NaOH solutions; for each GAC, 5 initial pH values were evaluated (in duplicate), measuring the final pH of the solution after 48 h of mixing on a magnetic stirrer; pH_{PZC} was determined plotting initial vs. final pH values.

Carbon-oxygen surface groups were determined by Boehm titration method ([5]): weighted carbon aliquots were dosed (at a concentration of about 500 mg L^{-1}) into 0.054 N NaOH, 0.051 N Na_2CO_3, 0.050 N $NaHCO_3$ and 0.072 N HCl solutions, respectively; after 24 h of agitation, solutions were filtered (0.22 μm PDVF filter) and titrated: basic solutions were retro-titrated with NaOH, while HCl solution was directly titrated. During titrations, nitrogen gas was continuously bubbled into the solutions.

Iodine number was determined according to ASTM4604.

All the results are reported in Table S1.

Table S1 Main properties of the tested GACs.

Adsorbent		**GAC-M**	**GAC-V**
Iodine number (mg g^{-1})		864	1135
BET surface area (m^2 g^{-1})		783	1151
t-plot micropore area (m^2 g^{-1})		241	933
t-plot micropore volume (cm^3 g^{-1})		0.105	0.364
BJH adsorption average pore diameter (nm)		3.227	3.439
pH_{PZC} (-)		9.7	10.0
Surface functional groups (meq g^{-1})	Total basic	1.813	1.966
	Carboxylic	0.062	0.039
	Lactonic	0.009	0.003
	Phenolic	0.360	0.116
	Total acid	0.431	0.158

S.I.2 LOD and LOQ of the analytical methods

The limit of detection (LOD) and quantification (LOQ) at the 95% confidence level of the HPLC methods for the analysis of BZK and CHD were calculated based on the standard error (SE) and the slope (m) of the calibration curves (LOD=3.3×SE/m, LOQ=10×SE/m). The parameters of the calibration curves and the LOD and LOQ values are reported in Table S2.

Table S2 Linear regression parameters of calibration curves, LOD and LOQ for HPLC analysis of BZK and CHD (calibration ranges: 10-500 μM for BZK, 0.5-100 μM for CHD).

analyte	slope	intercept	R^2	n. data	LOD (μM)	LOQ (μM)
BZK	0.0024	-0.0424	0.9984	13	47.7215	144.6107
CHD	2.4759	-3.3747	0.9998	22	2.2368	6.7781

S.I.3 TONO FP removal per mass unit of activated carbon
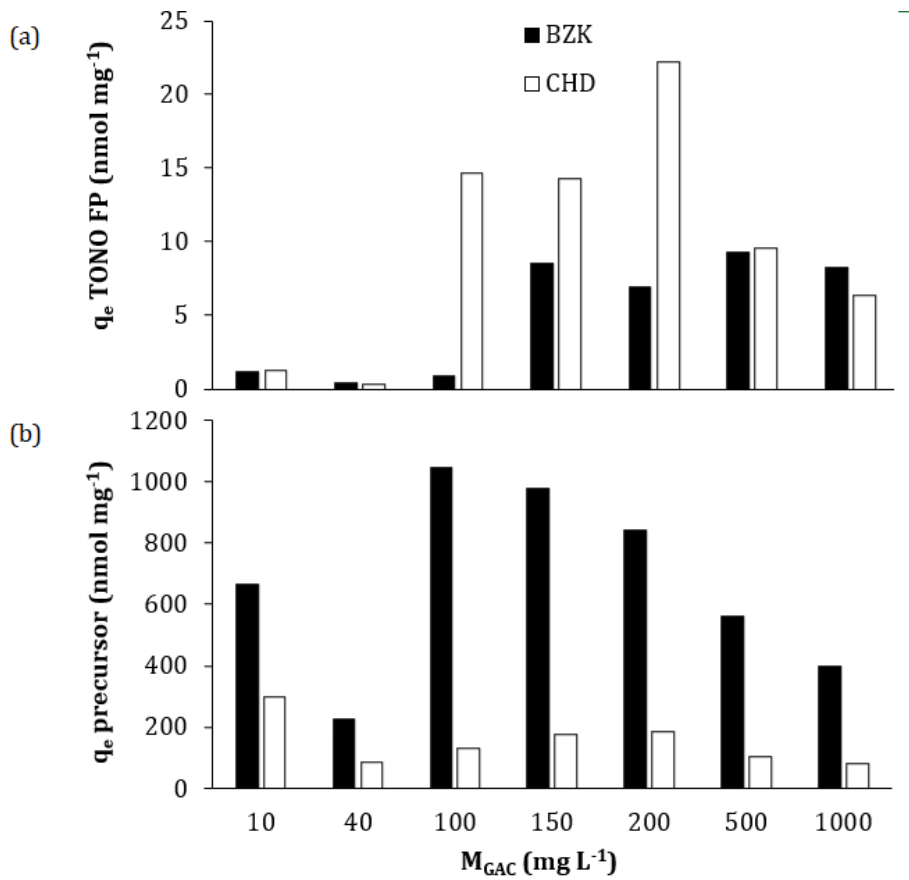
Figure S1 TONO FP (a) and precursor (b) reduction per mass unit of activated carbon (q_e) observed in pre-adsorption tests with BZK and CHD. Data at 10 and 40 mg L^{-1} GAC doses were obtained under ES2, data at 100-1000 mg L^{-1} GAC doses under ES1. Data at 10 and 40 mg L^{-1} GAC in (b) were estimated by considering TONO molar yields determined in blank samples.
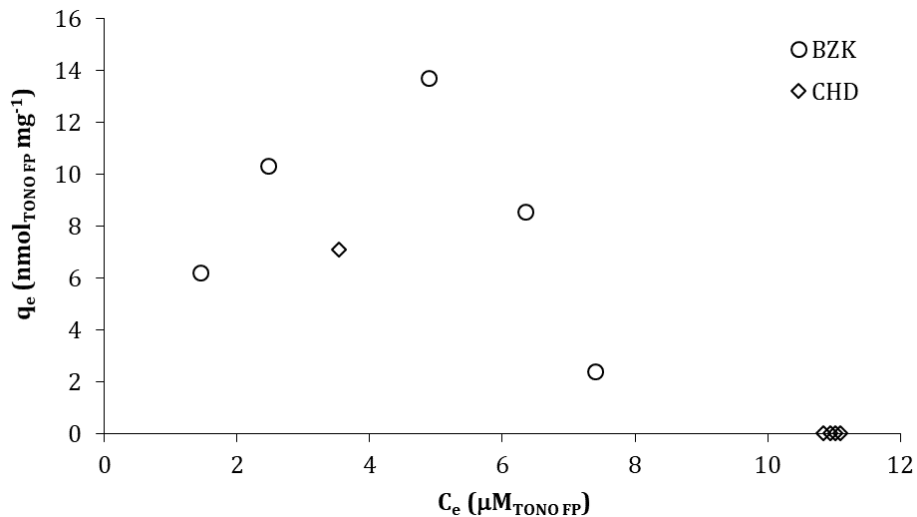
Figure S2 Liquid-phase (C_e) vs. solid-phase (q_e) TONO concentrations observed in post-adsorption tests (ES1) for BZK and CHD.

References

1) Brunauer, S.; Emmett, P. H.; Teller, E. Adsorption of gases in multimolecular layers. *J. Am. Chem. Soc.* **1938**, *60* (2), 309–319.

2) Barrett, E. P.; Joyner, L. G.; Halenda, P. P. The determination of pore volume and area distributions in porous substances. I. Computations from nitrogen isotherms. *J. Am. Chem. Soc.* **1951**, *73* (1), 373–380.

3) HORVÁTH, G.; Kawazoe, K. Method for the calculation of effective pore size distribution in molecular sieve carbon. *J. Chem. Eng. Jpn.* **1983**, *16* (6), 470–475.

4) Lopez-Ramon, M. V.; Stoeckli, F.; Moreno-Castilla, C.; Carrasco-Marin, F. On the characterization of acidic and basic surface sites on carbons by various techniques. *Carbon* **1999**, *37* (8), 1215–1221.

5) Boehm, H. P. Surface oxides on carbon and their analysis: a critical assessment. *Carbon* **2002**, *40* (2), 145–149.

6) Jafvert, C. T.; Valentine, R. L. Reaction scheme for the chlorination of ammoniacal water. *Environ. Sci. Technol.* **1992**, *26* (3), 577–586.

7) Le Roux, J.; Gallard, H.; Croué, J.-P. Chloramination of nitrogenous contaminants (pharmaceuticals and pesticides): NDMA and halogenated DBPs formation. *Water Res.* **2011**, *45* (10), 3164–3174.

8) Le Roux, J.; Gallard, H.; Croué, J.-P. Formation of NDMA and halogenated DBPs by chloramination of tertiary amines: the influence of bromide ion. *Environ. Sci. Technol.* **2012**, *46* (3), 1581–1589.

<div align="right">

CHAPTER 6

</div>

Prediction of VOC mixture breakthrough in real-scale GAC filters

Abstract

Homogeneous Surface Diffusion Model (HSDM) has been widely used to simulate the breakthrough of organic micropollutants in fixed-bed adsorbers, but its practical applicability in real-scale conditions is not fully established. In this study we have predicted the breakthrough of volatile organic compounds by the HSDM applied to full-scale granular activated carbon (GAC) adsorbers treating a complex groundwater matrix. Isotherm and short bed adsorber (SBA) tests were conducted to obtain equilibrium and mass-transfer coefficients for two contaminants (chloroform and tetrachloroethylene, PCE) and two GACs. Isotherm data were well described by Freundlich and Langmuir models, showing that single-component isotherms can be also used in complex water matrices, indirectly taking into account competition phenomena into the estimated parameters. The fitting of SBA data by HSDM was effective for chloroform, while PCE results were not well described, indicating that the combination of isotherm and SBA experiments to estimate HSDM parameters is not always effective, but it can depend on the characteristics of the adsorbate. Breakthrough data from the monitoring of two full-scale adsorbers were finally used to validate HSDM parameters for chloroform: its breakthrough was effectively simulated, without introducing any competition effect in HSDM equations. The model well reproduced also the release of the contaminant (resulting in chromatographic effect) by considering the variation of its influent concentration over time.

Keywords: Granular Activated Carbon (GAC), adsorption, Homogeneous Surface Diffusion Model (HSDM), fixed-bed breakthrough, Volatile Organic Compounds (VOCs).

This work has been submitted for publication to the journal 'Process Safety and Environmental Protection' and it is now under review.

1. Introduction

Contamination by organic micropollutants affects groundwater sources in many industrialized areas of the world ([1,2]). Many of these compounds, including volatile organic compounds (VOCs), trihalomethanes and pesticides, are proven to be hazardous for human health and are regulated by national drinking water regulations ([3]).

Adsorption onto granular activated carbon (GAC) was designated by the United States Environmental Protection Agency (US-EPA) as the best available technology for the treatment of many regulated organic pollutants ([4,5]); thanks to its removal effectiveness, relative low cost and management simplicity, it is the most widespread technology in drinking water treatment plants ([6]).

A fundamental step for the design and the management of a GAC system is the prediction of breakthrough profile, that is particularly important for estimating the operating costs ([7,8]). Different alternative methods to predict breakthrough profile were proposed in literature (*inter alia*,[9-11]), but a general procedure has not yet been established and the problem must be faced in each specific case ([12]).

Rapid Small Scale Column Tests (RSSCTs) are a suitable choice for testing GAC performances and many studies showed their accuracy in simulating full-scale data for several adsorbents and mixtures of contaminants (*inter alia*: [5,11,13-16]). However, RSSCTs display some limitations: first, experimental trials can be too much time consuming and expensive, especially when tests are planned for simulating large-scale GAC systems ([17]); in addition, scaled-up results often do not accurately fit real breakthrough profiles, due to an improper choice of the design approach (constant or proportional diffusivity) or to NOM interference on the adsorption of trace-organic contaminants ([16,18]).

An alternative approach involves the use of mathematical models ([17]). The most widely used models couple the description of the hydrodynamic transport through a fixed-bed filter with the description of the solute adsorption, considering a two-step diffusion mass transfer: through the external liquid-film and into the adsorbent grains. Depending on the description of diffusion mechanisms inside grains, different classes of models were developed (*inter alia*, Pore Diffusion Model and Pore Surface Diffusion Model) and, among these, the Homogeneous Surface Diffusion Model (HSDM) is one of the most widely referred to (*inter alia*, [19-25]). Despite being less time-consuming than pilot-scale tests or RSSCTs, the use of HSDM for breakthrough prediction in full-scale GAC systems is rather poor and mostly limited to specific research applications ([9,26]). So far, the main aspects to be faced regards the estimation of model parameters and the model adaptation to not-ideal working conditions (such as complex water mixture, time-varying flow rates and influent concentrations), typical of large-scale systems ([9,22,25,26]).

In the case of HSDM, the correct determination of site-specific equilibrium and mass-transfer coefficients is a key-point ([9]). Equilibrium parameters are commonly estimated by the determination of adsorption isotherms ([27]). Despite many isotherm models were proposed for describing single-solute adsorption ([28]), a proper description of competitive adsorption mechanisms in multi-component systems is an issue so far. In fact, the application of the main models proposed in literature (i.e. IAST model, Extended Langmuir model) is often not suitable for describing competitive adsorption in real water, requiring a high number of experiments and parameters to be determined ([29,30]), but anyway leading to not accurate and reliable results ([31,32]). Mass-transfer coefficients, being external and intraparticle mass-transfer coefficients, can be estimated by empirical correlations and relatively easy bench-scale experiments. As for external mass-transfer coefficient, many semi-empirical correlations were proposed with some dimensionless parameters, such as Reynolds (Re), Schmidt (Sc), and Sherwood (Sh) numbers (*inter alia*, [33-35]). However, these correlations are rarely accurate, strongly depending on the characteristics of the adsorbent grain and the case-specific hydrodynamic conditions ([25]). As for intraparticle mass transfer coefficient, different experimental procedures were proposed based on batch kinetic studies, such as Crank, Vermeulen and Reichenberg methods ([36,37]). However, the application of coefficients obtained in this way remains limited to the

study of adsorbent surface properties and there are only few works in literature in which they were used to simulate breakthrough of a fixed-bed adsorber [37].

Despite their relative higher complexity, Short Bed Adsorber tests (SBA) [22,38] are the most widely referred method for experimentally determining both mass transfer coefficients in GAC systems. Many papers showed the effectiveness of SBA tests in estimating model parameters and simulating breakthrough profiles for several contaminants (*inter alia*, [20–22,25]); however, practical applicability of SBA tests for full-scale adsorbers or real water media is not fully established, since most of the works dealt only with single-component adsorption and reported experimental results obtained under controlled conditions (synthetic solutions, stable experimental parameters).

Finally, the validation of the predictive model with large-scale data is a fundamental step for assessing its reliability. Simulation results are usually verified in pilot-scale columns, allowing to reproduce full-scale systems in a less time-consuming way. Model validation with full-scale data is rarely reported in literature; however, it represents the most effective way to verify model accuracy, since model sensitivity to the adopted parameters and the initial assumptions can vary with the scale of the GAC system [22]. Secondly, the variation of the operating parameters over time (i.e. flow rate, influent concentrations), usually occurring during full-scale operations, but not during short-lasting pilot-scale experiments, is an important aspect to be considered, since it can affect the adsorption process.

In this paper, the problem of the prediction of breakthrough profiles was faced for full-scale GAC adsorbers treating groundwater contaminated by a mixture of organic micropollutants (4 chlorinated solvents and 7 pesticides). HSDM was used to simulate the breakthrough profiles of the contaminants: equilibrium parameters were derived from isotherm determination, while mass-transfer coefficients were determined by SBA tests. All the experiments were performed on groundwater samples and the study was carried out for two kinds of commercial GAC, differing for the physical-chemical characteristics. First the ability of the tested methods to accurately estimate model parameters in a complex multi-component solution was assessed, validating results with data collected from the full-scale GAC adsorbers in 21 month monitoring. Then, the criteria for the application of HSDM to multi-component real water solution were defined, accounting also for variations of contaminant influent concentrations.

2. Materials and methods

2.1 Adsorbents

Two commercial granular activated carbons (Chemviron) were used: GAC-1240 (GAC-M) and Acticarbone NCL 1240 (GAC-V), being, respectively, of mineral (coal-based) and vegetal (coconut-based) origin. Apparent density (ρ_b) of the carbons in full-scale filters was measured according to ASTM D2854-89; apparent density of GAC bed during SBA tests was calculated as the ratio between the carbon mass and the bed volume; both in full-scale filters and SBA tests, the bed porosity (ε_b) was calculated assuming a GAC particle density (ρ_p) of 2100 kg m^{-3} [39]. Apparent density and bed porosity values are reported in Table 1. Grain size distribution of the GACs was determined by a mechanical sieve (Giuliani, I), using 7 different mesh sizes between 10 and 70. Results were used to determine average and median particle diameters (d_P). The granulometric curves are reported in Supporting Information (S.I.1), while calculated d_P median values are reported in Table 1.

Before batch adsorption tests and SBA tests, GAC samples were rinsed with deionized water into a magnetically stirred beaker for 15 min (1:1 volume ratio) and then dried at 105°C.

2.2 Full-scale adsorbers

Two real-scale operating adsorbers (3 m inner diameter, 1.85 m GAC bed height, 13 m^3 GAC volume), containing respectively GAC-M and GAC-V, located in a drinking water treatment plant (DWTP) in the

Milan urban area (Italy), were monitored during a period of 21 months (from 07 January 2015 to 29 September 2016). The DWTP, supplied by 22 capturing wells, includes 20 adsorbers operating in parallel and fed on about 500 L s^{-1}. Influent flowrate to the two adsorbers was measured by an ultrasonic flowmeter with a measurement time resolution of 10 s; influent and effluent flowrate from the two adsorbers was sampled every 2 weeks, determining the concentrations of VOCs and pesticides (see section 2.5). One of the 22 capturing wells, characterized by the highest contaminant concentrations, was selected to collect groundwater for the batch experiments and SBA tests.

2.3 Batch adsorption tests: kinetic and isotherm tests

Adsorption kinetics and isotherms were evaluated for the two GAC types in batch system, varying the contact time and the adsorbent dose.

For each set of experiments, weighted aliquots of GAC were added in 1 L Pyrex bottles; then the bottles were filled with groundwater and immediately sealed with a PTFE cap to minimize VOC volatilization; test bottles were mixed on a magnetic stirrer (550 RPM) for the selected contact times at the temperature of 23±2 °C. One test bottle in each set was prepared without GAC addition, in order to quantify contaminant losses due to volatilisation during the experimental procedure, as difference with contaminant concentration in raw groundwater.

Based on the results of preliminary tests (not reported), experiments for kinetics determination were carried out fixing the GAC dose (100 mg for both GAC types) and varying the contact time (1, 2, 3, 4, 5, 6, 7 and 72 h); tests for equilibrium isotherms were performed at a selected contact time (72 h) and varying the adsorbent mass (from 1 to 300 mg for GAC-M and from 1 to 100 mg for GAC-V). All the experiments were performed in duplicate.

At the end of each contact time, water samples were collected and analyzed for determining residual concentrations of VOCs, pesticides and Total Organic Carbon (TOC) (see section 2.5).

The amount of contaminant *i* adsorbed onto the solid phase, q_i (µg mg^{-1}), was calculated from experimental data as follows:

e.1)
$$q_i = \left(C_{0,i} - C_{res,i}\right)\frac{V}{M}$$

where V (L) is the volume of the liquid phase, M (mg) is the mass of the dosed adsorbent, $C_{0,i}$ and $C_{res,i}$ are respectively the initial and residual concentration of contaminant *i* (µg L^{-1}). $C_{0,i}$ was the concentration measured in raw groundwater reduced by the average volatilization loss observed during the experimental trials. On average, the volatilization loss observed during kinetic and isotherm experiments was, respectively, 18% and 13% for chloroform, 27% and 14% for tetrachloroethylene (PCE).

2.4 Short-Bed Adsorber tests

SBA tests ([22,38]) on GAC-V and GAC-M were performed into a glass column (inside diameter, d_C: 1 cm; GAC bed height, h_C: 4 cm). The weight of packed GAC aliquots (M_{GAC}) was preliminary determined. Average particle diameter of carbons (S.I.1) provided h_C/d_P over 20, allowing to neglect axial dispersion on the mass transfer ([25]). To limit contaminant volatilization during tests, groundwater captured by the well was continuously sent to a 10 L HDPE tank equipped with an overflow drain, so as to maintain zero-headspace conditions. The column operated down-flow and was fed on groundwater collected in the tank at constant flow rate, by a peristaltic pump (Watson-Marlow 120S). Before starting each test, deionized water was flushed through the preloaded column, in order to eliminate air bubbles and to ensure complete wetting of the carbon pores. Two flow rate values were tested with GAC-V: 7 and 19 mL min^{-1}, corresponding to axial velocities of about 5 and 15 m h^{-1}. Only 7 mL min^{-1} flow rate was tested with GAC-M. All the SBA tests were performed in duplicate, for a total of 6 trials, lasting 19.5 h each. Two tests (at 7 and 19 mL min^{-1} flow rate, respectively) were also

carried out in the same experimental setup but using glass beads instead of GAC (blank tests), in order to evaluate possible contaminant losses due to volatilization or the presence of dead zones. Influent and effluent water from the column was sampled at various contact times and analyzed for determining residual concentrations of VOCs and pesticides (see section 2.5). For each trial, 3 water samples at the column inlet (at 0, 7 and 16 h) and 17 at the outlet (with variable frequency) were collected. Difference of inlet and outlet concentration in blank tests was negligible for chloroform, equal to 5% and 7% for PCE at 7 and 19 mL min^{-1} flow rate, respectively, not showing significant trends over time. Water temperature was monitored over time and resulted almost constant over the SBA tests (on average, equal to 14.4±1.66 °C).

2.5 Analytical methods

All the samples were collected into 40 mL glass vials, stored at 4 °C and analyzed within 48 h. Samples coming from batch adsorption experiments were preliminary filtered through paper filter to separate activated carbons.

The concentration of 27 VOCs (listed in S.I.2) was determined by a gas-chromatographer (Agilent Technologies GC-6890N Series gas-chromatographer) coupled with a single quadrupole mass analyzer (Agilent Technologies MS 5793 Network mass analyzer) with a dynamic headspace system (Purge&Trap O-I-Analytical Eclipse 4660 with 4551-A auto-sampler), according to methods EPA 524.3-09 and EPA 5030C-03. Volatile fraction extraction was made by stripping with ultra-pure helium and concentration on multi-phasic filter at 20 °C, followed by filter heating at 200 °C.

The concentration of 26 pesticides (listed in S.I.2) was determined by a gas-chromatographer (Agilent Technologies GC-7890A gas-chromatographer) coupled with a triple quadrupole mass/mass detector (Agilent Technologies MSD-7000A mass detector) after solid phase extraction according to the APAT-IRSA 5060/03 method. Organic compounds were extracted (Autotrace SPE workstation Zymark) using methanol, water and acetone/isopropanol 9:1 for cartridge activation and elution (Chromabond HR-X SPE cartridges).

Details about the measurement of TOC are reported in S.I.2.

All the analyses have been performed by the laboratory of Metropolitana Milanese S.p.A. (MM), which manages the integrated water service in Milan (I).

2.6 Mathematical models

2.6.1   Isotherm models

Two adsorption isotherm models ([28]) were used to describe equilibrium data, being Freundlich and Langmuir models, whose equations are written as:

e.2)
$$q_e = K_F C_e^{\frac{1}{n}}$$

e.3)
$$q_e = \frac{q_L K_L C_e}{1 + K_L C_e}$$

where C_e (µg L^{-1}) is the equilibrium liquid concentration, K_F ((µg mg^{-1})(L µg^{-1})$^{1/n}$) and $1/n$ (-) are the constant and the exponent of Freundlich equation; q_L (µg mg^{-1}) and K_L (L µg^{-1}) are, respectively, the maximum adsorption capacity and the equilibrium constant of Langmuir model.

Isotherm models were calibrated fitting experimental data by least square method, estimating the parameters by non-linear regression analysis.

2.6.2   Fixed bed model

Adsorption onto GAC in lab and full scale fixed-bed columns was described by the HSDM, which is composed by two partial differential equations (PDE) describing, respectively, the mass transport

through the GAC bed (filter equation, e.4) and into the adsorbent grains (intraparticle equation, e.7) ([40]).

Filter equation is derived by the mass balance over an infinitesimal element of the filter in linear coordinates (z):

e.4)
$$\varepsilon \frac{\partial C_b}{\partial t} + v \frac{\partial C_b}{\partial z} + \frac{3(1 - \varepsilon_b)}{R_P} k_f (C_b - C_S) = 0$$

where t is time (s), ε_b is the bed porosity (dimensionless), v is the axial velocity (m s^{-1}), k_f is the external film mass transfer coefficient (m s^{-1}), R_p is the particle radius (m), C_b and C_S are adsorbate liquid concentrations in the bed and at the particle external surface (μg L^{-1}), respectively.

Intraparticle equation describes adsorbate transport through adsorbent grains (in radial coordinates, r), according to Fick's second law:

e.5)
$$\frac{\partial q}{\partial t} = \frac{1}{r^2} \frac{\partial}{\partial r} \left[D_S r^2 \frac{\partial q}{\partial r} \right]$$

where q is the solid phase concentration (μg mg^{-1}) and D_S is the surface diffusion coefficient (m^2 s^{-1}).

Initial and boundary conditions relative to equations e.4 and e.5 are provided in S.I.3.

An implicit finite difference method was applied to solve the set of PDEs: temporal derivatives in e.4 and e.5 were substituted by forward differences; backward and central differences were used for spatial derivatives in filter and intraparticle equations, respectively ([40]). The optimal grid width for the discretization of PDEs was determined in each simulation according to the values of model parameters, in order to guarantee the stability and the consistency of the numerical solution ([40]).

The values of k_f and D_S were estimated by minimizing the sum of square differences (SSE) between model output and the experimental data.

Model sensitivity to the parameters was assessed by a local sensitivity analysis method, varying one parameter at a time and keeping the others fixed ([41]). The Normalized Sensitivity Index (NSI) was calculated by normalizing the model output values using the following expression:

e.6)
$$NSI = \frac{[OUTPUT]_{max} - [OUTPUT]_{min}}{[OUTPUT]_{max}} \cdot \frac{[INPUT]_{max}}{[INPUT]_{max} - [INPUT]_{min}}$$

where [OUTPUT]$_{max}$ and [OUTPUT]$_{min}$ are the maximum and the minimum output values obtained when varying a model parameter in a range of values between [INPUT]$_{max}$ and [INPUT]$_{min}$. The simulated GAC bed effluent concentration values were considered as reference model output. In order to evaluate the influence of input parameter variations at different stages of the breakthrough profile, the NSI was calculated at different simulation time intervals, considering the relative values of C/C_0. More details about sensitivity analysis are reported in S.I.6.

2.7 Statistical analysis

Fitting of the models were performed by Matlab (Mathworks 2014).

Statistical elaborations were performed by IBM SPSS Statistics 21, statistical package.

Table 1 Parameters considered in simulations by HSDM.

adsorbent	simulation	M_{GAC} (g)	ρ_b (kg m^{-3})	ε_b (-)	median d_P (mm)
GAC-V	SBA tests	1.925	613	0.71	0.8
	Full-scale filters	5885·10^3	450	0.79	
GAC-M	SBA tests	1.496	476	0.77	1.1
	Full-scale filters	6146·10^3	470	0.78	

3. Results and discussion

The results presented in the following sections were aimed at predicting the breakthrough profiles of chloroform and PCE for two full-scale GAC adsorbers by the HSDM. The composition of the groundwater feeding the GAC adsorbers and used in the batch-scale experiments is shown in section 3.1. At first, isotherm tests were conducted to estimate the equilibrium parameters for the studied contaminants and adsorbents; the experimental results and their interpretation by isotherm models are presented in section 3.2. Secondly, SBA tests were conducted to estimate mass-transfer parameters, by fitting the experimental data by the HSDM (section 3.3). Finally, two full-scale GAC adsorbers were monitored to observe chloroform and PCE breakthroughs and to validate HSDM assumptions and parameters estimated in the previous batch-scale experiments (section 3.4).

3.1 Groundwater composition

Among the many VOCs detected in groundwater sampled for batch and SBA tests, PCE and chloroform were those present at the highest concentrations (on average, 34.0 ± 2.71 µg L^{-1} and 10.8 ± 0.50 µg L^{-1} for PCE and chloroform, respectively), while only two other VOCs were found at detectable levels, being trichloroethylene (TCE) and cis-1,2-dichloroethylene, displaying concentrations of 1.0 ± 0.50 µg L^{-1} and 0.6 ± 0.53 µg L^{-1}, respectively. Among pesticides, 3,6-dichloropiridazine and 2,6-dichlorobenzamide were present at the highest concentrations, on average 3.96 ± 1.216 µg L^{-1} and 0.10 ± 0.054 µg L^{-1}, respectively; the other compounds found at concentrations above the detection limit were atrazine (0.02 ± 0.014 µg L^{-1}), atrazine desisopropyl (0.01 ± 0.005 µg L^{-1}), atrazine desethyl (0.02 ± 0.011 µg L^{-1}), terbuthylazine (0.02 ± 0.008 µg L^{-1}) and terbuthylazine desethyl (0.02 ± 0.011 µg L^{-1}).

Therefore, batch studies for kinetics and isotherm determination, SBA tests and monitoring of full-scale adsorber breakthrough were focused on these compounds, but significant results were obtained only for PCE and chloroform, meaning that concentrations over the detection limit after contact with GAC were observed only for them.

The average concentration of TOC in the tested groundwater was 0.5 ± 0.01 mg L^{-1}. TOC removal up to 40% has been observed during batch experiments with both the GACs. However, the high dispersion of the data did not allow to determine any kinetic or isotherm model or to find relationships with the removal of the other organic micropollutants. Thus, TOC data are not further discussed in the following sections.

3.2 Batch adsorption tests: equilibrium isotherms

GAC masses and equilibrium contact time tested in isotherm experiments were selected according to the results of kinetic tests (S.I.4), showing that a contact time of 72 h was enough to reach the adsorption equilibrium for chloroform and PCE with all the tested GAC masses. Initial concentrations of PCE and chloroform in the groundwater sampled for isotherm experiments were, on average, 28.9 ± 6.01 µg L^{-1} and 9.3 ± 2.87 µg L^{-1} respectively.

Isotherm data, expressed as equilibrium solid phase concentration (q_e), calculated by e.1, as function of residual liquid phase concentration are plotted in Figure 1. PCE residual concentrations above the detection limit (DL) were obtained only for the lowest carbon doses, from 1 to 13 mg L^{-1} for GAC-V and from 1 to 34 mg L^{-1} for GAC-M; consequently, only these groups of data (shown in Figure 1) have been considered for isotherm calculations. Conversely, for the same adsorbent concentrations, removal of chloroform up to 43% and 30% was observed, for GAC-V and GAC-M, respectively, highlighting the higher affinity of PCE with respect to chloroform. However, plotting chloroform q_e vs. C_e data obtained at these carbon doses (empty symbols in Figure 1) resulted in randomly dispersed clouds of points. On the other hand, considering results obtained with the highest carbon doses (30-100 mg L^{-1} for GAC-V and 100-300 mg L^{-1} for GAC-M), for which PCE was completely removed ($C_e<DL$), chloroform q_e vs. C_e

data had a quite regular increasing trend, displaying the typical shape of isotherm curves (full symbols in Figure 1). Results confirmed the higher adsorption capacity of GAC-V towards both the contaminants and the higher adsorbability of PCE with respect to chloroform. Moreover, data suggested that chloroform adsorption is negatively affected by the presence of PCE, especially for low amounts of adsorbent, justifying the clouds of points. Chloroform and PCE compete for the same adsorption sites and, being PCE the compound preferentially adsorbed, the availability of adsorption sites for chloroform uptake could be limited at the lowest carbon doses, when PCE liquid concentration is not negligible.

The two most often used isotherm models, being Freundlich and Langmuir (e.2 and e.3), were adopted to describe experimental data. It must be pointed out that these models have been developed for describing the uptake of an adsorbate in a single component system; hence, the estimated equilibrium parameters are specifically referred to PCE and chloroform, but they permit to indirectly take into account competition phenomena, which reduce their removal extent, associated to the multi-component solution in which they are dissolved. Actually, equilibrium parameters estimated for a single compound in a multi-component solution represent a fundamental figure for defining the actual affinity between contaminant and carbon in real groundwater.

PCE isotherms were calibrated using all the data with a residual PCE concentration over DL, while only data obtained at the highest carbon doses were considered for chloroform. Results of non-linear regression are reported in Table 2: both the models well fit experimental data ($R^2>0.901$), with a slightly worse fitting only in the case of chloroform and GAC-M ($R^2=0.75$). Except for GAC-V and chloroform data, Langmuir model showed determination coefficients slightly higher than Freundlich model; however, estimated parameters of Freundlich model (fitting lines are shown in Figure 1) were affected by a lower uncertainty, as indicated by narrower 95% confidence intervals.

The estimated values of Freundlich constants well reflect the different adsorbability of the two compounds and the different adsorption capacities of the two carbons: for both the GACs, K_F values for PCE were at least 2 orders of magnitude higher than chloroform, while GAC-V showed K_F values more than 3 and 4 times higher than GAC-M, for chloroform and PCE, respectively. All the estimated Freundlich exponent values were comparable, indicating a similar adsorption intensity. The higher adsorbability of PCE was similarly reflected by the q_L values of Langmuir model, being about 30 and 100 times higher than those obtained for chloroform, for GAC-M and GAC-V, respectively. GAC-V showed a q_L value higher than GAC-M for PCE, while very similar values between the two carbons were obtained for chloroform. On the other hand, the different affinity of the two carbons towards chloroform was highlighted by the estimated K_L values of chloroform, being significantly lower for GAC-M. For the two carbons, comparable K_L values were obtained for PCE.

Both considering Freundlch and Langmuir model, the good data fitting suggested that single-component models could effectively describe adsorption also in a complex water mixture; however, they must be carefully used in the simulation of fixed bed adsorbers. In fact, parameters obtained for chloroform may be considered valid when the amount of GAC is enough to avoid PCE competition effects, corresponding to the lowest GAC doses in isotherm experiments. Considering the fixed-bed process, this condition corresponds to the first stages of breakthrough, when GAC is only partially saturated and its residual adsorption capacity is not limiting for chloroform uptake; as PCE adsorption increases, the availability of adsorption sites decreases, resulting in a change of equilibrium conditions at the solid/liquid interface, similarly to what observed in isotherm experiments for the lowest carbon doses.
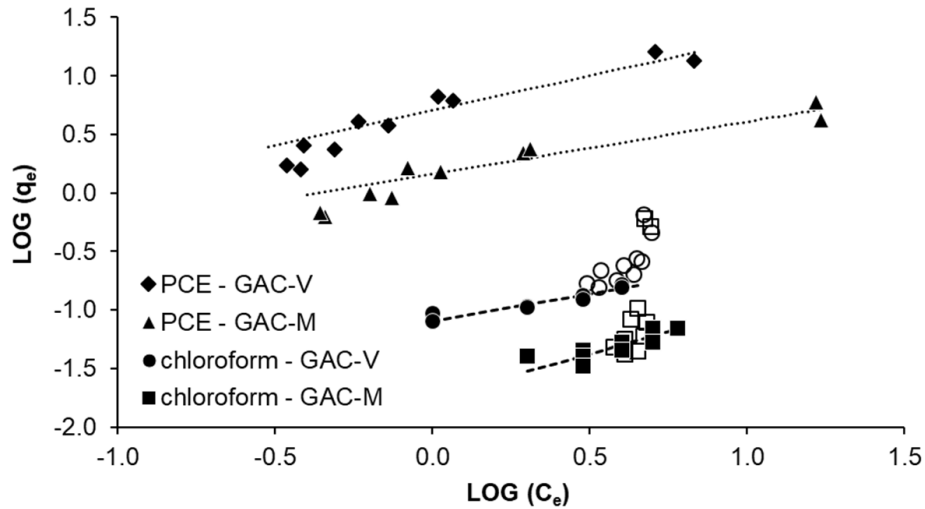
Figure 1 Solid phase vs. residual liquid phase concentration of PCE and chloroform for GAC-V and GAC-M: experimental data (symbols) and data simulated by Freundlich model (dashed lines). Empty symbols are chloroform data obtained at the lowest carbon doses (1-13 mg L^{-1} for GAC-V and 1-34 mg L^{-1} for GAC-M).

Table 2 Equilibrium parameters of isotherm models estimated by non-linear regression (estimate±95% confidence interval), number of fitted data and determination coefficients (R^2).

Isotherm model	parameters	chloroform		PCE	
		GAC-V	**GAC-M**	**GAC-V**	**GAC-M**
Freundlich	K_F [(μg mg^{-1})(L μg^{-1})$^{1/n}$]	$(80.4\pm9.90)\cdot10^{-3}$	$(17.7\pm9.40)\cdot10^{-3}$	5.1±1.40	1.4±0.47
	1/n [-]	0.47±0.115	0.76±0.364	0.59±0.171	0.45±0.131
	n. of data	9	10	10	10
	R^2	0.94	0.75	0.91	0.91
Langmuir	q_L [μg mg^{-1}]	0.2±0.06	0.2±0.39	21.9±6.41	6.0±1.29
	K_L [L μg^{-1}]	0.56±0.362	0.07±0.158	0.34±0.209	0.32±0.180
	n. of data	9	10	10	10
	R^2	0.90	0.76	0.95	0.93

3.3 Short-Bed Adsorber tests

During SBA tests, chloroform influent concentration was almost constant, ranging between 9 and 13 μg L^{-1} (on average 10.6±1.19 μg L^{-1}), while PCE influent concentration varied between 22 and 39 μg L^{-1} (on average 28.2±4.55 μg L^{-1}). During the same experimental trial, influent concentrations remained almost constant over time, not varying more than 10% and 13% for chloroform and PCE, respectively.

Chloroform and PCE breakthrough curves obtained by SBA tests for GAC-V and GAC-M are shown in Figure 3. All the curves showed that GAC bed depth was sufficiently shallow to obtain immediate breakthrough of both contaminants and an increasing trend over time, as recommended by Weber and Liu (1980) and Knappe et al. (1999) ([22,38]).

In order to evaluate the possible influence of axial velocity on adsorption kinetics, SBA tests with GAC-V were initially performed at two different velocities, being 5 and 15 m h^{-1}; breakthrough curves obtained for chloroform and PCE at the two velocities are both reported in Figure 2. ANOVA tests (results reported in S.I.5) showed that there was not significant difference between the data series, for neither chloroform (F=1.600, p-value=0.211) nor PCE (F=0.032, p-value=0.859). Besides the set velocity value, however, experimental results might have been also influenced by the concentration of

the contaminants in the influent water, which could not be controlled during the SBA tests. The influence of experimental parameters on SBA results was so tested by a series of ANCOVA tests, considering the normalized breakthrough concentration (C/C_0) as dependent variable. ANCOVA results, reported in S.I.5, confirmed that velocity did not significantly affect chloroform and PCE breakthrough; on the other hand, influent concentration of the contaminants was found to significantly influence the adsorption of both PCE and chloroform, indicating once again a possible competition for adsorption sites between the two contaminants, as observed in isotherm experiments.

Having verified the not significant role of axial velocity, SBA tests on GAC-M were then carried out fixing the velocity at 5 m h^{-1} (breakthrough curves for chloroform and PCE shown in Figure 2), to minimize the possible volatilization loss of contaminants during the experiments. The role of influent water characteristics was tested by ANCOVA (S.I.5), showing again the influence of PCE influent concentration in the adsorption of PCE itself and chloroform.

HSDM was then used to describe SBA results, in order to estimate external film mass transfer (k_f) and surface diffusion coefficient (D_S) for chloroform and PCE adsorption onto the two activated carbons. Freundlich parameters in Table 2, parameters in Table 1 and average influent concentrations observed during the experiments were used as model inputs. All the parameters were considered constant over simulation time. Being not significantly different, GAC-V data obtained at the two axial velocities were initially considered as a unique data series and simulations were run setting the axial velocity to the median value (10 m h^{-1}). According to Weber and Liu (1980) ([38]), k_f was determined from the initial intercept of the breakthrough curve (first 60 minutes), while D_S was then estimated fitting the rest of the breakthrough data. The estimated k_f and D_S values are reported in Table 3, together with the relative SSE and R^2 values; the corresponding simulated curves are reported in Figure 2.

3.3.1 Chloroform

As shown in Figure 2a, a good agreement between simulated and experimental data of chloroform was obtained for both the GACs, with SSE <2.7·10^{-2}, corresponding to R^2>0.91 (Table 3). Thus, HSDM can be considered effective in simulating chloroform data from SBA tests and it can be used for estimating the unknown mass-transfer coefficients also when working with a real groundwater influent.

Although experimental results for GAC-V were found to be not significantly dependent on the axial velocity, the influence of v in the estimation of the mass-transfer coefficients was tested: HSDM was separately calibrated on the data series obtained at the two velocities, obtaining k_f and D_S values about 2-times higher at 5 m h^{-1} with respect to values obtained at 15 m h^{-1} (Table 3). This finding indicated that HSDM was relatively sensitive to the parameter v, which influences the simulated breakthrough curve more than what observed in the SBA tests. To better interpret simulated data and estimated coefficients for chloroform adsorption, the model sensitivity to the parameters was evaluated as described in section 2.6.2. Average k_f and D_S values estimated at 5 m h^{-1} axial velocity (Table 3) were used as baseline for the following sensitivity analysis, varying one parameter at a time and calculating the NSI by e.6. Detailed results of sensitivity analysis are reported in S.I.6. Results showed that, when simulating chloroform adsorption in SBA tests, HSDM is strongly sensitive to the experimental parameters, namely R_P, ε, M_{GAC} and v. Small changes in these parameter values lead to significant variations in the simulated curves, especially in the first stages of chloroform breakthrough. Hence, the estimation of k_f, being evaluated in the first part of the curve, was strongly affected by these input parameters, which must be carefully evaluated; in fact, a not-accurate estimation of mass-transfer parameters can negatively influence the simulation of the full-scale breakthrough curve, as discussed in section 3.4. The effect of equilibrium parameters resulted to be lower than the experimental parameters: for instance, a 30% change in Freundlich constant or exponent values leads to a variation in C/C_0 values <15% for GAC-V and <5% for GAC-M.

3.3.2 PCE

Contrary to what observed for chloroform, PCE data were simulated less effectively by HSDM, as indicated by the higher SSE values (Table 3). Moreover, the immediate PCE breakthrough observed during SBA tests was never modelled by HSDM, since simulated curves (Figure 2b) displayed concentrations >0 after several minutes (about 24 min for GAC-M and 40 min for GAC-V).

The role of input parameters in the simulation of PCE breakthrough during SBA tests was so investigated by a sensitivity analysis, as reported in S.I.6. The time delay observed in the modeled curves could not be due to an improper assignment of the experimental input parameters, such as v, M_{GAC}, ε, R_P or C_0: in fact, a variation of these parameters within a quite wide range of reasonable values resulted in PCE breakthrough (C/C_0>0) not earlier than 24 min for GAC-M and 40 min for GAC-V. Finally, it was found that a more adequate simulation of the observed SBA data, reproducing the immediate breakthrough of PCE, could be obtained only by reducing the Freundlich constant values of, at least, one order of magnitude (simulation results not reported). In other words, the delay in the simulated breakthrough curve was due to the high solute distribution coefficient (Dg) of PCE adopted in HSDM simulation, being related to the equilibrium solid-phase concentration ([40]). In fact, the Dg estimated for PCE ($1.1·10^6$) was much higher than that calculated for chloroform ($2.0·10^4$) and those found in previous studies applying HSDM to SBA tests (S.I.7). An overestimation of equilibrium adsorption capacity, represented by Freundlich parameters, could so explain the mismatch between experimental and modeled PCE data. According to HSDM assumptions, the adsorption process is described as a sequential two-step diffusion mechanism: i) diffusion through the external liquid film (film diffusion); ii) diffusion into the adsorbent surface (surface diffusion), with the first step dependent on the hydrodynamic conditions, affecting the thickness of the liquid film ([25,42]). The adsorption capacity observed for chloroform and PCE during batch isotherm experiments were not limited by film diffusion, which was promoted by mixing conditions; consequently, PCE displayed much higher adsorptivity than chloroform, due to the higher affinity with carbon surface active sites, related to PCE apolarity and higher hydrophobicity (S.I.10, Table S7). During fixed-bed process (i.e. SBA tests), on the other hand, the less favorable hydrodynamic conditions (laminar flow, Reynolds number between 1 and 6) enhance the resistance to the film diffusion. Diffusive transfer through the external liquid film may become limiting for PCE, resulting in a slower adsorption rate; PCE uptake may be so reduced, resulting in much lower adsorption capacities. The different dependence of PCE and chloroform on film diffusion resistance can be explained, at first, by their different liquid diffusivity (diffusion coefficients in water equal to $8.20·10^{-10}$ m s^{-1} and $1.00·10^{-9}$ m s^{-1} for PCE and chloroform, respectively ([43])); secondly, the diffusion inside the liquid filling carbon porosities (pore diffusion), not directly considered in HSDM, can also represent a limiting step for PCE adsorption, due to the slightly higher molecular dimensions (S.I.10). According to these hypothesis, the equilibrium adsorption capacity estimated for PCE by isotherm experiments can be considered not fully representative of the conditions hold in fixed-bed adsorbers, at lab-, pilot- or full-scale. The importance of diffusive transport during fixed-bed process cannot be easily evaluated by batch experiments and further efforts are needed to better investigate the reasons of the difference observed for PCE and chloroform. Results showed that the correspondence between equilibrium conditions in batch and fixed-bed experiments may be not guaranteed, but it may depend on the characteristics of the adsorbate. Thus, combining isotherm and SBA tests is not always an effective way to estimate accurate HSDM parameters. Moreover, it was found that, contrary to what observed for chloroform, the simulation of PCE breakthrough was much more sensitive to isotherm parameters, which reflected the higher equilibrium adsorption capacity.

In this study, because of the low correspondence between HSDM and SBA test data, D_S and k_f values obtained for PCE must be carefully considered for full-scale process simulation. In fact, an

overestimation of adsorption capacity could have determined a wrong estimation of the full-sale breakthrough curve and consequently of the GAC lifetime.
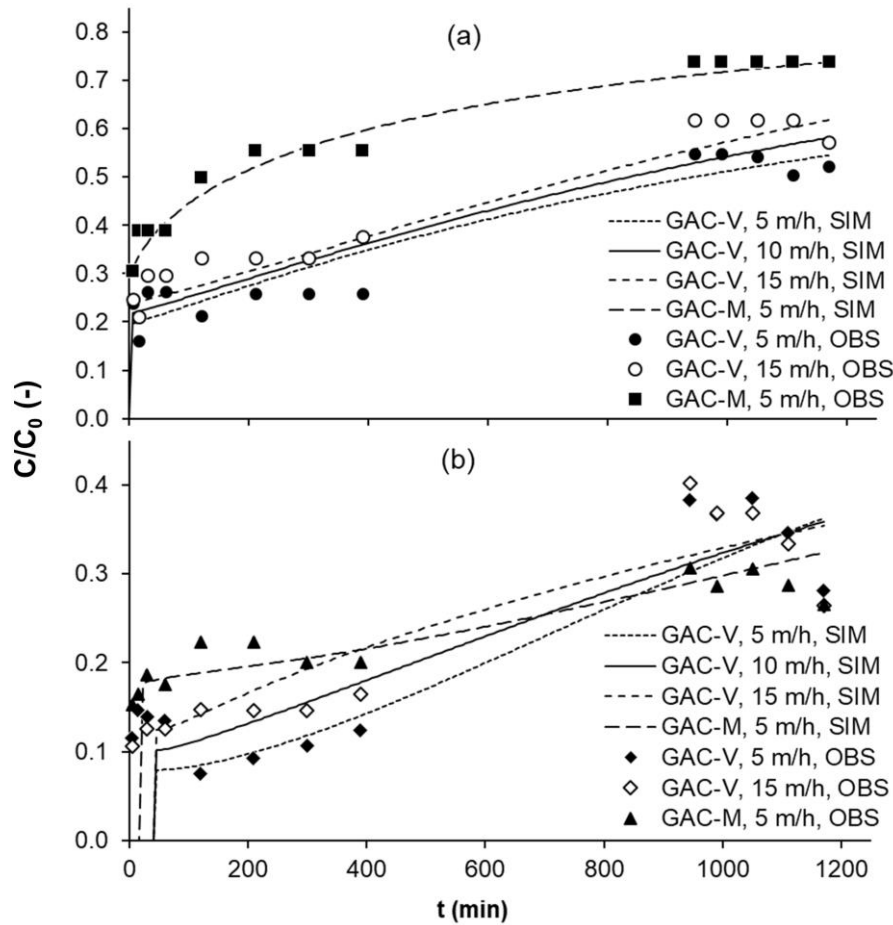
Figure 2 Normalized effluent concentration of chloroform (a) and PCE (b) over time in SBA tests: average observed data (average values of two experiment repetitions) and data simulated by HSDM.

Table 3 Values of film mass transfer coefficient (k_F), surface diffusion coefficient (D_S), sum of square differences (SSE) and determination coefficients (R^2) estimated fitting SBA data by HSDM.

adsorbent	adsorbate	v (m h^{-1})	k_f (m s^{-1})	D_S (m^2 s^{-1})	SSE (-)	R^2 (-)
GAC-V	chloroform	5	$2.8 \cdot 10^{-5}$	$7.9 \cdot 10^{-15}$	$2.7 \cdot 10^{-2}$	0.91
		10	$4.1 \cdot 10^{-5}$	$2.5 \cdot 10^{-14}$	$4.4 \cdot 10^{-2}$	0.93
		15	$6.7 \cdot 10^{-5}$	$4.5 \cdot 10^{-14}$	$1.4 \cdot 10^{-2}$	0.96
	PCE	5	$4.1 \cdot 10^{-5}$	$5.0 \cdot 10^{-18}$	$7.6 \cdot 10^{-2}$	0.70
		10	$7.3 \cdot 10^{-5}$	$2.6 \cdot 10^{-17}$	$1.3 \cdot 10^{-1}$	0.75
		15	$1.0 \cdot 10^{-4}$	$4.6 \cdot 10^{-17}$	$3.6 \cdot 10^{-1}$	0.76
GAC-M	chloroform	5	$3.8 \cdot 10^{-5}$	$4.4 \cdot 10^{-14}$	$1.5 \cdot 10^{-2}$	0.96
	PCE	5	$5.3 \cdot 10^{-5}$	$7.2 \cdot 10^{-16}$	$5.7 \cdot 10^{-2}$	0.39

3.4 Full-scale column monitoring and simulation

Water flow rate was different for the two monitored adsorbers and it was not constant over time, varying between 14 and 34 L s^{-1}. Average influent concentrations of chloroform and PCE during the monitoring period were 4.0±0.88 and 17.9±5.00 µg L^{-1}, respectively. All the measured flowrate and C_{IN} values are reported in S.I.8 (Figures S.4 and S.5).

Figure 3 shows chloroform and PCE breakthrough observed for the two adsorbers, expressed as C/C_{IN} over the treated bed volumes (BV). Obtained breakthrough profiles showed a big difference in the mass transfer zone (MTZ) length of the two compounds, reflecting their different affinity towards activated carbons. In fact, chloroform breakthrough was early and very fast for both the GACs, appearing in the effluent after about $7 \cdot 10^3$ and $16 \cdot 10^3$ treated BV, for GAC-M and GAC-V, respectively. On the other hand, PCE appeared much later in the effluent (after about $41 \cdot 10^3$ and $49 \cdot 10^3$ BV for GAC-M and GAC-V, respectively) and displayed a very slow breakthrough profile. Moreover, chloroform effluent concentrations exceeded influent concentration, showing that chloroform adsorption is highly reversible and that the contaminant can be easily released by the activated carbon. In fact, mass balance calculations (S.I.8, Figure S.6) showed that chloroform previously adsorbed was completely released by the two carbons after about $80 \cdot 10^3$ treated BV.

The concentration of PCE and chloroform adsorbed onto the solid-phase over time (q_t) in full-scale filters was calculated from the observed data (S.I.8, Figure S.7). Chloroform reached maximum q_t values of $0.133\ \mu g\ mg^{-1}$ and $0.055\ \mu g\ mg^{-1}$, for GAC-V and GAC-M, respectively; these values are quite well comparable to the theoretical values estimated by Freundlich isotherm assuming the equilibrium concentration equal to the average influent concentration ($4.0\ \mu g\ L^{-1}$), corresponding to $0.150\ \mu g\ mg^{-1}$ for GAC-V and $0.049\ \mu g\ mg^{-1}$ for GAC-M. On the other hand, PCE reached equilibrium q_t values of $3.657\ \mu g\ mg^{-1}$ and $3.031\ \mu g\ mg^{-1}$, for GAC-V and GAC-M, respectively, while the theoretical adsorption capacities estimated by Freundlich isotherm were much higher, corresponding to $27.751\ \mu g\ mg^{-1}$ for GAC-V and $5.096\ \mu g\ mg^{-1}$ for GAC-M. The mismatch observed for PCE supports the hypothesis discussed in section 3.4 about an overestimation of the equilibrium constants, confirming that, conversely to chloroform, PCE adsorption is strongly limited during the fixed-bed process with respect to batch-test conditions.

HSDM was used to simulate the observed breakthrough curves for the two GACs, adopting the parameters previously estimated: in detail, Freundlich equilibrium parameters in Table 2 and parameters in Table 1. Axial velocity (derived from the measured flow rate) and influent concentration values over simulation time were calculated by stepwise linear functions built with the values observed during filter monitoring (S.I.8). The values of k_F and D_S estimated by SBA tests (Table 3) were used; for GAC-V, all the sets of mass-transfer parameters estimated at different axial velocities were tested in simulations.

As discussed in section 3.3.2, SBA tests did not allow to estimate reliable diffusion coefficients for PCE. As expected, in fact, the simulation of PCE breakthrough (S.I.9, Figure S8), did not lead to an accurate fitting of the experimental data.

Chloroform breakthrough curves simulated by HSDM are reported in Figure 3, showing a good correspondence between simulated and observed data both for GAC-V and GAC-M. Prediction performances of HSDM could be considered satisfactory, especially considering the large spatial and temporal scale of the simulated process. For both the carbons, chloroform breakthrough occurrence and slope were quite accurately modeled, reproducing the MTZ advancement observed in full-scale filters. Moreover, the model accurately reproduced the fluctuation of chloroform breakthrough curves as well as the contaminant release, resulting in C/C_{IN} values over 1. Looking at the results of isotherm experiments, this behavior could be initially attributed to the competition phenomena between chloroform and PCE. However, HSDM equations were not modified to consider possible interactions between the contaminants, that were simulated independently of each other, as in the case of a mono-component system. According to model assumptions, the release of chloroform could be mainly attributed to the variation of the inlet concentration over time, determining a gradient inversion at the external surface of adsorbent grains. These results suggested, at first, that strong variations in C_{IN} values over time must be carefully considered in real GAC systems, since chloroform release could

result in effluent concentrations exceeding regulation limits. Secondly, including competition phenomena in HSDM equations was not necessary for an accurate simulation of chloroform breakthrough, but it was enough to determine equilibrium and mass-transfer coefficients on representative real water matrices.

For GAC-V, a slight difference in the breakthrough profiles was obtained by considering the sets of k_f and D_S values estimated at different velocities. Considering the 5%, 50% and 95% breakthrough stages, the difference between the curves simulated at the minimum and maximum velocities (5 and 15 m h^{-1}) was only of 4300 BV (28 d), 1400 BV (6 d) and 1600 BV (10 d), respectively. It can be concluded that, for the prediction of chloroform breakthrough in a large GAC system, the water velocity set during SBA tests did not have a fundamental role, due to the relatively low sensitivity of the model to the mass-transfer coefficients. Water velocity through full-scale filters strongly varied over time (S.I.8, Figure S.4), so none of the sets of mass-transfer coefficients could be considered fully representative. Results suggest that the adoption of a relatively low water velocity during SBA tests (i.e. 5 m h^{-1}) was the most preferable choice, reducing the risk of contaminant volatilization during SBA trials and giving slightly more conservative predictions (earlier breakthrough time).

Model sensitivity to the parameters was evaluated also for full-scale conditions (results reported in S.I.6). Considering the simulation of chloroform adsorption, HSDM resulted to be much more sensitive to all the parameters in the very first stages of the breakthrough profile. Hence, a good estimation of input parameters was fundamental for accurately predicting the breakthrough time. The knowledge of the moment in which effluent concentration reaches values >0 is important for an efficient design of a GAC system, especially considering the high slope of the breakthrough profile, rapidly leading to the complete exhaustion. For both the GACs, the effect of the parameters representing operating conditions or GAC geometry resulted to be relevant: high NSI values were obtained for the particle radius R_P, confirming the importance of an accurate evaluation of grain size distribution. In this sense, the choice of the most proper R_P value and the eventual introduction of a shape factor play an important role in modeling results. In this work, R_P was calculated from the median diameter, having been estimated from the grain size distribution with more precision than the average diameter. However, due to the high spatial and temporal variability of GAC grain size and shape in large-scale adsorbers ([25]), the high sensitivity to R_P represents an important limitation in HSDM application. Moreover, v and C_{IN} (with different relative importance, depending on the GAC) had a strong effect on modeling results. The combination of these two parameters represents the mass of contaminant fed into the filter over time. Obtained results showed that, for a full-scale system having highly variable influent water characteristics, it is important to evaluate the time variation of these parameters with an enough high time resolution. Isotherm coefficients showed NSI values higher than the ones for mass-transfer coefficients and comparable to the experimental parameters (v, M_{GAC}, R_P and C_{IN}). Hence, an accurate estimation of equilibrium parameters by batch-scale experiments is important for an accurate simulation of the breakthrough curve. The effect of mass-transfer coefficients resulted to be lower than the other parameters, except for the high NSI values obtained for D_S for the first part of the curve, thus more affecting the prediction of the breakthrough time.
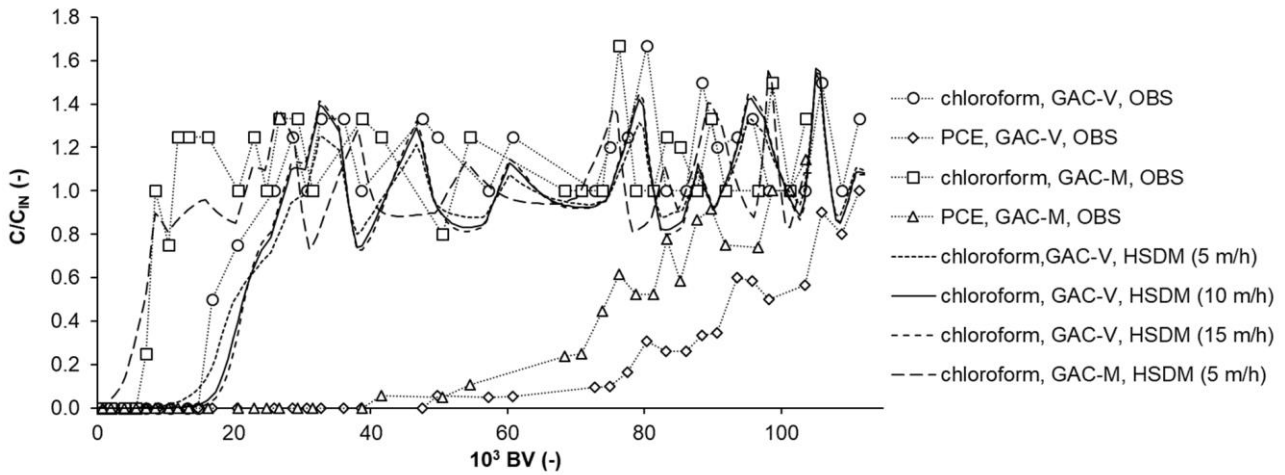
Figure 3 Chloroform and PCE breakthrough for GAC-M and GAC-V full-scale filters: observed and simulated (HSDM) data. GAC-V simulated curves were obtained considering mass-transfer coefficients estimated by SBA tests at different axial velocities.

4. Conclusions

The problem of breakthrough profile prediction was faced for full-scale GAC adsorbers treating groundwater contaminated by a mixture of organic micropollutants. The HSDM was used to simulate the adsorption of chloroform and PCE onto two different activated carbons (GAC-V and GAC-M), estimating the model parameters by laboratory experiments (isotherm and SBA tests).

Isotherm experiments showed that chloroform adsorption can be limited by PCE, competing for the same adsorption sites and having higher affinity with the GACs. However, Freundlich and Langmuir single-component models resulted effective in describing equilibrium adsorption also in a complex water mixture. Chloroform SBA data were well described by HSDM, allowing to estimate mass-transfer coefficients for both the GACs. On the other hand, HSDM did not enable to accurately simulate PCE SBA data. Sensitivity analysis of the model indicated that the not satisfactory results could be due to an overestimation of equilibrium adsorption capacity derived by isotherm experiments. These findings suggested that, contrary to chloroform, PCE adsorption can be limited by diffusive resistances during the fixed-bed process, which are not properly described in HSDM assumptions.

Chloroform breakthrough profiles for two full-scale adsorbers were finally simulated to validate the parameters estimated by isotherm and SBA tests. HSDM resulted to effectively predict chloroform breakthrough curves, including the release of the contaminant resulting in fluctuating breakthrough curves with C/C_{IN} values >1.

Various key aspects regarding the use of the HSDM for predicting the breakthrough profiles in full-scale GAC adsorbers were highlighted, focusing on the different phases of the simulation process (experimental parameter estimation, model implementation, full-scale validation) and on the role of the contaminant characteristics. The main results pointed-out by this study are:

- single-component isotherm models can be used to describe multi-component equilibrium adsorption, indirectly taking into account competition phenomena;
- the water velocity adopted in SBA tests has not a significant role in the estimation of mass-transfer parameters and in the accuracy of full-scale predictions;
- the combination of isotherm and SBA tests to estimate HSDM parameters is not always effective, but it may depend on the adsorbate characteristics, as observed for PCE;
- considering time-variable axial velocity and influent concentration in the HSDM allows to accurately simulate the release of a contaminant, without introducing competitive effects into the model equations;

- the HSDM sensitivity to the parameters varies with the adsorbability of the contaminant (i.e. chloroform vs. PCE) and the scale of the simulated process (i.e. SBA tests vs. full-scale column).

References

(1)   Williams, P.; Benton, L.; Warmerdam, J.; Sheehan, P. *Comparative risk analysis of six volatile organic compounds in California drinking water*; ACS Publications, 2002.

(2)   Luo, Y.; Guo, W.; Ngo, H. H.; Nghiem, L. D.; Hai, F. I.; Zhang, J.; Liang, S.; Wang, X. C. A review on the occurrence of micropollutants in the aquatic environment and their fate and removal during wastewater treatment. *Sci. Total Environ.* **2014**, *473*, 619–641.

(3)   Register, F. National primary and secondary drinking water regulations. *Fed Reg* **1989**, *54*, 22062–22160.

(4)   Sotelo, J. L.; Rodríguez, A.; Álvarez, S.; García, J. Removal of caffeine and diclofenac on activated carbon in fixed bed column. *Chem. Eng. Res. Des.* **2012**, *90* (7), 967–974.

(5)   Westerhoff, P.; Yoon, Y.; Snyder, S.; Wert, E. Fate of endocrine-disruptor, pharmaceutical, and personal care product chemicals during simulated drinking water treatment processes. *Environ. Sci. Technol.* **2005**, *39* (17), 6649–6663.

(6)   Oxenford, J. L.; Lykins, B. W. Conference summary: practical aspects of the design and use of GAC. *J.-Am. Water Works Assoc.* **1991**, *83* (1), 58–64.

(7)   Yu, Z.; Peldszus, S.; Huck, P. M. Adsorption of selected pharmaceuticals and an endocrine disrupting compound by granular activated carbon. 2. Model prediction. *Environ. Sci. Technol.* **2009**, *43* (5), 1474–1479.

(8)   Kennedy, A. M.; Reinert, A. M.; Knappe, D. R.; Ferrer, I.; Summers, R. S. Full-and pilot-scale GAC adsorption of organic micropollutants. *Water Res.* **2015**, *68*, 238–248.

(9)   Worch, E. Fixed-bed adsorption in drinking water treatment: a critical review on models and parameter estimation. *J. Water Supply Res. Technol.-Aqua* **2008**, *57* (3), 171–183.

(10)   Crittenden, J. C.; Reddy, P. S.; Arora, H.; Trynoski, J.; Hand, D. W.; Perram, D. L.; Summers, R. S. Predicting GAC performance with rapid small-scale column tests. *J. Am. Water Works Assoc.* **1991**, 77–87.

(11)   Anumol, T.; Sgroi, M.; Park, M.; Roccaro, P.; Snyder, S. A. Predicting trace organic compound breakthrough in granular activated carbon using fluorescence and UV absorbance as surrogates. *Water Res.* **2015**, *76*, 76–87.

(12)   Pe\lech, R.; Milchert, E.; Bartkowiak, M. Fixed-bed adsorption of chlorinated hydrocarbons from multicomponent aqueous solution onto activated carbon: Equilibrium column model. *J. Colloid Interface Sci.* **2006**, *296* (2), 458–464.

(13)   Corwin, C. J.; Summers, R. S. Adsorption and desorption of trace organic contaminants from granular activated carbon adsorbers after intermittent loading and throughout backwash cycles. *Water Res.* **2011**, *45* (2), 417–426.

(14)   Morley, M. C.; Henke, J. L.; Speitel Jr, G. E. Adsorption of RDX and HMX in rapid small-scale column tests: Implications for full-scale adsorbers. *J. Environ. Eng.* **2005**, *131* (1), 29–37.

(15)   Summers, R. S.; Kim, S. M.; Shimabuku, K.; Chae, S.-H.; Corwin, C. J. Granular activated carbon adsorption of MIB in the presence of dissolved organic matter. *Water Res.* **2013**, *47* (10), 3507–3513.

(16)   Knappe, D. R.; Snoeyink, V. L.; Roche, P.; Prados, M. J.; Bourbigot, M.-M. The effect of preloading on rapid small-scale column test predictions of atrazine removal by GAC adsorbers. *Water Res.* **1997**, *31* (11), 2899–2909.

(17)   Jarvie, M. E.; Hand, D. W.; Bhuvendralingam, S.; Crittenden, J. C.; Hokanson, D. R. Simulating the performance of fixed-bed granular activated carbon adsorbers: Removal of synthetic organic chemicals in the presence of background organic matter. *Water Res.* **2005**, *39* (11), 2407–2421.

(18)   Corwin, C. J.; Summers, R. S. Scaling trace organic contaminant adsorption capacity by granular activated carbon. *Environ. Sci. Technol.* **2010**, *44* (14), 5403–5408.

(19)   Pérez-Foguet, A.; Casoni, E.; Huerta, A. Dimensionless analysis of HSDM and application to simulation of breakthrough curves of highly adsorbent porous media. *J. Environ. Eng.* **2012**, *139* (5), 667–676.

(20)   Rossner, A.; Knappe, D. R. MTBE adsorption on alternative adsorbents and packed bed adsorber performance. *Water Res.* **2008**, *42* (8), 2287–2299.

(21)   Ho, L.; Newcombe, G. Granular activated carbon adsorption of 2-methylisoborneol (MIB): pilot- and laboratory-scale evaluations. *J. Environ. Eng.* **2010**, *136* (9), 965–974.

(22)   Knappe, D. R.; Snoeyink, V. L.; Roche, P.; Prados, M. J.; Bourbigot, M.-M. Atrazine removal by preloaded GAC. *Am. Water Works Assoc. J.* **1999**, *91* (10), 97.

(23)   Schideman, L. C.; Mariñas, B. J.; Snoeyink, V. L.; Campos, C. Three-component competitive adsorption model for fixed-bed and moving-bed granular activated carbon adsorbers. Part I. Model development. *Environ. Sci. Technol.* **2006**, *40* (21), 6805–6811.

(24)   Zhang, Q.; Crittenden, J.; Hristovski, K.; Hand, D.; Westerhoff, P. User-oriented batch reactor solutions to the homogeneous surface diffusion model for different activated carbon dosages. *Water Res.* **2009**, *43* (7), 1859–1866.

(25)   Richard, D.; Núñez, M. de L. D.; Schweich, D. Adsorption of complex phenolic compounds on active charcoal: breakthrough curves. *Chem. Eng. J.* **2010**, *158* (2), 213–219.

(26)   Heijman, S. G. J.; Hopman, R. Activated carbon filtration in drinking water production: model prediction and new concepts. *Colloids Surf. Physicochem. Eng. Asp.* **1999**, *151* (1), 303–310.

(27)   Moreno-Castilla, C. Adsorption of organic molecules from aqueous solutions on carbon materials. *Carbon* **2004**, *42* (1), 83–94.

(28)   Foo, [5 5] KY; Hameed, B. H. Insights into the modeling of adsorption isotherm systems. *Chem. Eng. J.* **2010**, *156* (1), 2–10.

(29)   Erto, A.; Lancia, A.; Musmarra, D. A modelling analysis of PCE/TCE mixture adsorption based on Ideal Adsorbed Solution Theory. *Sep. Purif. Technol.* **2011**, *80* (1), 140–147.

(30)   Najm, I. N.; Snoeyink, V. L.; Lykins Jr, B. W.; Adams, J. Q. Using powdered activated carbon: a critical review. *J. Am. Water Works Assoc.* **1991**, 65–76.

(31)   Newcombe, G.; Morrison, J.; Hepplewhite, C.; Knappe, D. R. U. Simultaneous adsorption of MIB and NOM onto activated carbon: II. Competitive effects. *Carbon* **2002**, *40* (12), 2147–2156.

(32)   Ebie, K.; Li, F.; Azuma, Y.; Yuasa, A.; Hagishita, T. Pore distribution effect of activated carbon in adsorbing organic micropollutants from natural water. *Water Res.* **2001**, *35* (1), 167–179.

(33)   Williamson, J. E.; Bazaire, K. E.; Geankoplis, C. J. Liquid-phase mass transfer at low Reynolds numbers. *Ind. Eng. Chem. Fundam.* **1963**, *2* (2), 126–129.

(34)   Wilson, E. J.; Geankoplis, C. J. Liquid mass transfer at very low Reynolds numbers in packed beds. *Ind. Eng. Chem. Fundam.* **1966**, *5* (1), 9–14.

(35)   Yoshida, F.; Ramaswami, D.; Hougen, O. A. Temperatures and partial pressures at the surfaces of catalyst particles. *AIChE J.* **1962**, *8* (1), 5–11.

(36)   Cotoruelo, L. M.; Marqués, M. D.; Rodríguez-Mirasol, J.; Rodríguez, J. J.; Cordero, T. Lignin-based activated carbons for adsorption of sodium dodecylbenzene sulfonate: Equilibrium and kinetic studies. *J. Colloid Interface Sci.* **2009**, *332* (1), 39–45.

(37)   García-Mateos, F. J.; Ruiz-Rosas, R.; Marqués, M. D.; Cotoruelo, L. M.; Rodríguez-Mirasol, J.; Cordero, T. Removal of paracetamol on biomass-derived activated carbon: modeling the fixed bed breakthrough curves using batch adsorption experiments. *Chem. Eng. J.* **2015**, *279*, 18–30.

(38)   Weber Jr, W. J.; Liu, K. T. Determination of mass transport parameters for fixed-bed adsorbers. *Chem. Eng. Commun.* **1980**, *6* (1–3), 49–60.

(39)   Crittenden, J. C.; Trussell, R. R.; Hand, D. W.; Howe, K. J.; Tchobanoglous, G. *MWH's water treatment: principles and design*; John Wiley & Sons, 2012.

(40)   Sperlich, A.; Schimmelpfennig, S.; Baumgarten, B.; Genz, A.; Amy, G.; Worch, E.; Jekel, M. Predicting anion breakthrough in granular ferric hydroxide (GFH) adsorption filters. *Water Res.* **2008**, *42* (8), 2073–2082.

(41)   Hamby, D. M. A review of techniques for parameter sensitivity analysis of environmental models. *Environ. Monit. Assess.* **1994**, *32* (2), 135–154.

(42)   Baup, S.; Jaffre, C.; Wolbert, D.; Laplanche, A. Adsorption of pesticides onto granular activated carbon: determination of surface diffusivities using simple batch experiments. *Adsorption* **2000**, *6* (3), 219–228.

(43)   US EPA, O. Superfund Soil Screening Guidance https://www.epa.gov/superfund/superfund-soil-screening-guidance (accessed Aug 28, 2017).

Supporting Information

S.I.1 GAC grain size distributions

Table S1 Grain size distribution, mean and median particle diameters (d_P) determined for GAC-V and GAC-M.

Mean sieve opening (mm)	Retained fraction (-)	
	GAC-V	GAC-M
2.000	0.000	0.011
1.500	0.056	0.141
1.000	0.319	0.512
0.600	0.425	0.262
0.400	0.195	0.068
0.355	0.003	0.001
0.212	0.001	0.003
Mean d_P (mm)	0.936	1.159
Median d_P (mm)	0.804	1.146
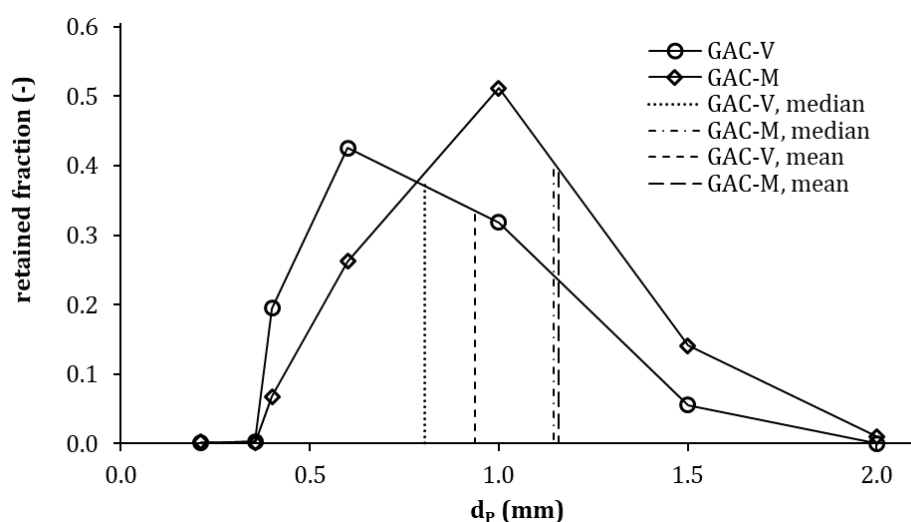
Figure S1 Grain size distribution of GAC-V and GAC-M.

S.I.2 Analytical methods

The 27 analyzed VOCs were: 1,1,2,2-tetrachloroethane, 1,1,2-trichloroethane, 1,1-dichloroethane, 1,2-dichloroethane, 1,2-dichloropropane, benzene, bromodichloromethane, bromoform, carbon tetrachloride, chloroform, cis-1,2-dichloroethene, dibromochloromethane, ethylbenzene, Freon-11, Freon-113, Freon-141b, hexachlorobutadiene, methyl chloroform, methyl tert-butyl ether, m+p-xylene, o-xylene, styrene, tetrachloroethene, toluene, trans-1,2-dichloroethene, trichloroethene, vinyl chloride.

The 26 analyzed pesticides were: 1,5-pentamethylenetetrazole, 2,4,6-trimethoxy-1,3,5-triazine, 2,6-dichlorobenzamide, 3,6-dichloropyridazine, alachlor, ametryn, atrazine, atrazine-desethyl, atrazine-desisopropyl, bromacil, cyanazine, hexazinone, lindane, metolachlor, molinate, oxadiazon, pendimethalin, prometryn, Propanil, propazine, sebuthylazin, simazine, terbuthylazine, terbuthylazin-desethyl, tris(2-chloroethyl)phosphate, β-BHC.

TOC analysis was performed using a Total Organic Carbon analyzer (Shimadzu Corporation TOC-VCPN analyzer) according to Non-Purgeable Organic Carbon (NPOC) method: sample was pre-treated by correcting the pH to 2-3 and bubbling an inert gas (N_2). Sample was then introduced into a combustion

tube filled with an oxidation catalyst (Pt) and heated to 680 °C (converting the carbon component to CO_2). Carrier gas (N_2, 150 mL min^{-1}) carried the combustion products to an electronic dehumidifier and through a halogen scrubber. Finally, the CO_2 in the carried gas was measured in a non-dispersive infrared (NDIR) gas analyzer. TOC concentration corresponded to CO_2 concentration.

S.I.3 Fixed-bed model: initial and boundary conditions

Initial (e.S.1) and boundary conditions (e.S.2) relative to filter equation (e.4, section 2.6.2) are expressed as follows:

e.S.1) $$C_b \, (t=0, z) = 0$$

e.S.2) $$C_b \, (t>0, z=0) = C_{IN}$$

where C_{IN} is the influent concentration (μg L^{-1}).

Initially, solid phase concentration in the intraparticle equation (e.4, section 2.6.2) is considered null:

e.S.3) $$q \, (t=0, z, r) = 0$$

Boundary conditions at the center (r=0) and at the external surface of the adsorbent grain (r=R_P) are respectively:

e.S.4) $$\frac{\partial q}{\partial r} = 0, \text{ r=0}$$

e.S.5) $$\rho_b D_S \frac{\partial q}{\partial r} = k_f (C_b - C_S), \text{ r=}R_P$$

where ρ_b is the bulk density of the adsorbent in the fixed-bed (mg m^{-3}). In equation e.10, the relationship between q(r=R_P) and C_S was given by Freundlich equation (e.2, section 2.6.1).

S.I.4 Adsorption kinetics

Concentration of PCE and chloroform in sampled groundwater was on average 34.0±2.71 μg L^{-1} and 10.8±0.50 μ L^{-1}. Figure S2 shows the effect of contact time on the removal of PCE and chloroform by GAC-M and GAC-V, in terms of q_t, calculated by e.1. A series of tests performed at a mixing intensity of 900 RPM (not reported) confirmed that the rotation speed kept during the experiments (550 RPM) was not limiting for the adsorption kinetics; thus, obtained results can be considered not affected by limitations in mass transfer through the stationary liquid layer around the adsorbent grains. PCE had a higher affinity towards both the carbons with respect to chloroform, approaching higher q_t values. GAC-V showed higher adsorption capacity for chloroform and especially for PCE, with respect to GAC-M.

Experimental data from kinetic studies were interpolated with three models, being pseudo-first order, pseudo-second order and hyperbolic kinetics ([1,2]), whose equations are expressed as follows, respectively:

e.S.6) $$\frac{dq_t}{dt} = k'(q_e - q_t)$$

e.S.7) $$\frac{dq_t}{dt} = k''(q_e - q_t)^2$$

e.S.8) $$\frac{dq_t}{dt} = \frac{k_H q_e}{(1 + k_H t)^2}$$

where q_e and q_t are the amounts of adsorbate (μg mg^{-1}) at equilibrium and at time t, respectively; k' (h^{-1}), k'' (mg μg^{-1} h^{-1}) and k_H (h^{-1}) are the rate constants. Equations e.S.6, e.S.7 and e.S.8 were integrated and calibrated fitting experimental data by least square method, estimating the parameters by non-linear regression analysis.

All the models were effective in simulating observed data ($R^2 > 0.89$), but the highest determination coefficients and the lowest uncertainties of parameters' estimates (evaluated by 95% confidence interval) were obtained by pseudo-first order kinetic (fitting curves shown in Figure S2). The parameters estimated for the kinetic models are reported in Table S2.

According to the results of kinetic experiments, a relatively long contact time of 72 h was adopted in isotherm experiments, to assure equilibrium conditions for all the tested GAC doses.
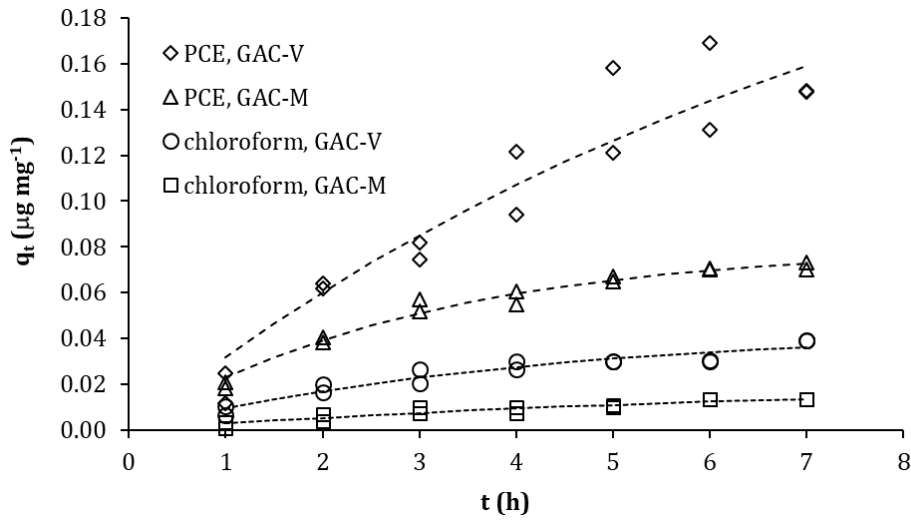
Figure S2 Adsorption kinetics of PCE and chloroform onto GAC-V (100 mg L^{-1}) and GAC-M (300 mg L^{-1}): experimental data (dots) and fitting curves (dotted lines) simulated by pseudo-first order model.

Table S2 Parameters of kinetic models (estimate ± 95% confidence interval), number of fitted data and determination coefficients (R^2).

kinetic model	parameter	GAC-V		GAC-M	
		PCE	**chloroform**	**PCE**	**chloroform**
Pseudo-first order	k' (h^{-1})	0.12 ± 0.136	0.24 ± 0.119	0.34 ± 0.066	0.14 ± 0.140
	q$_e$ (µg mg^{-1})	0.27 ± 0.216	0.04 ± 0.011	0.08 ± 0.007	0.02 ± 0.014
	n. of data	14	14	14	14
	R^2 (-)	0.89	0.92	0.98	0.89
Pseudo-second order	k'' (mg µg^{-1} h^{-1})	0.15 ± 0.351	2.70 ± 2.693	2.32 ± 1.907	2.45 ± 5.008
	q$_e$ (µg mg^{-1})	0.48 ± 0.479	0.07 ± 0.023	0.11 ± 0.017	0.04 ± 0.030
	n. of data	14	14	14	14
	R^2 (-)	0.89	0.92	0.97	0.89
hyperbolic	k$_H$ (h^{-1})	0.07 ± 0.097	0.18 ± 0.115	0.26 ± 0.086	0.09 ± 0.106
	q$_e$ (µg mg^{-1})	0.48 ± 0.479	0.07 ± 0.023	0.11 ± 0.017	0.04 ± 0.030
	n. of data	14	14	14	14
	R^2 (-)	0.89	0.92	0.97	0.89

S.I.5 Statistical analysis on SBA results

Chloroform and PCE data obtained by SBA tests with GAC-V at 5 and 15 m h^{-1} velocities were compared by an analysis of variance (ANOVA), considering C/C$_0$ values as dependent variable and testing the effect of the factor v. Results are reported in Table S3.

Chloroform and PCE data obtained by SBA tests with GAC-V and GAC-M were further analyzed by an analysis of covariance (ANCOVA), considering C/C$_0$ values as dependent variable and testing the effect of the covariates time (t), influent concentrations of the contaminants (C$_0$) and v (only for GAC-V data). Results are reported in Table S4.

Table S3 Results of ANOVA performed on results of SBA tests for GAC-V: effect of water velocity (v) (DF: degrees of freedom, SS$_{adj}$: adjusted sum of squares, MS$_{adj}$: adjusted mean square, F: Fisher statistic value).

dependent variable	Test	SS$_{adj}$	DF	MS$_{adj}$	F	p-value
C/C$_0$ chloroform	Between groups	0.042	1	0.042	1.600	0.211
	Within groups	1.633	62	0.026	-	-
	Total	1.675	63	-	-	-
C/C$_0$ PCE	Between groups	0.001	1	0.001	0.032	0.859
	Within groups	1.042	62	0.017	-	-
	Total	1.043	63	-	-	-

Table S4 Results of ANCOVA performed on SBA tests results (DF: degrees of freedom, SS$_{adj}$: adjusted sum of squares, MS$_{adj}$: adjusted mean square, F: Fisher statistic value, S: standard error of the estimates, R^2: determination coefficient, R$^2_{adj}$: adjusted determination coefficient, R$^2_{pred}$: predicted determination coefficient).

Source	DF	SS$_{adj}$	MS$_{adj}$	F	p-value	S	R^2	R$^2_{adj}$	R$^2_{pred}$
chloroform, GAC-V									
C$_0$ chloroform	1	0.037	0.037	12.71	0.001	0.054	0.899	0.892	0.882
C$_0$ PCE	1	0.164	0.164	56.76	<0.001				
v	1	0.000	0.000	0.00	0.967				
time	1	1.35340	1.353	469.03	<0.001				
Error	58	0.167	0.003	-	-				
Total	62	1.662	-	-	-				
PCE, GAC-V									
C$_0$ chloroform	1	0.034	0.034	10.84	0.002	0.056	0.794	0.780	0.758
C$_0$ PCE	1	0.025	0.025	7.93	0.007				
v	1	0.004	0.004	1.39	0.243				
time	1	0.650	0.6450	209.89	<0.001				
Error	58	0.180	0.003	-	-				
Total	62	0.872	-	-	-				
chloroform, GAC-M									
C$_0$ chloroform	1	0.002	0.002	0.53	0.474	0.054	0.910	0.900	0.899
C$_0$ PCE	1	0.037	0.037	12.84	0.001				
time	1	0.622	0.622	215.83	<0.001				
Error	30	0.087	0.003	-	-				
Total	33	0.945	-	-	-				
PCE, GAC-M									
C$_0$ chloroform	1	0.002	0.002	0.86	0.360	0.044	0.670	0.640	0.593
C$_0$ PCE	1	0.034	0.034	17.29	<0.001				
time	1	0.098	0.098	50.52	<0.001				
Error	30	0.058	0.002	-	-				
Total	33	0.177	-	-	-				

S.I.6 Sensitivity Analysis

Model sensitivity to the parameters was assessed at two spatial and temporal scales, relative to SBA tests and full-scale filters.

The Normalized Sensitivity Index (NSI) was calculated by normalizing the model output values using the following expression:

e.S.9)
$$NSI = \frac{[OUTPUT]_{max} - [OUTPUT]_{min}}{[OUTPUT]_{max}} \cdot \frac{[INPUT]_{max}}{[INPUT]_{max} - [INPUT]_{min}}$$

where [OUTPUT]$_{max}$ and [OUTPUT]$_{min}$ are the maximum and the minimum output values obtained when varying a model parameter in a range of values between [INPUT]$_{max}$ and [INPUT]$_{min}$. The simulated C/C_{IN} values at different stages of the breakthrough profile were considered as reference model output. In order to evaluate the influence of input parameter variations at different stages of breakthrough curves, the NSI was calculated at various simulation time intervals, considering the relative values of C/C_{IN}. During simulations, all the parameters were considered constant over time. The obtained NSI values are summarized in Tables S5.

Table S5 Normalized Sensitivity Index (NSI) values calculated for HSDM when simulating PCE and chloroform breakthrough for GAC-M during SBA test and full-scale operations. For PCE, the minimum breakthrough time (time at which $C/C_{IN}>0$) obtained for each simulation is also reported.

SBA, GAC-M, PCE				Simulation time (min)			
				48	400	800	1200
parameter	[INPUT]$_{min}$	[INPUT]$_{max}$	Minimum breakthrough time (min)	NSI (-)			
M_{GAC} (g)	1.122	1.87	36	0.833	0.804	0.762	0.717
ε (-)	0.58	0.97	30	1.421	0.756	0.430	0.266
R_P (mm)	0.42	0.72	30	1.412	1.268	1.108	0.964
C_0 (μg L^{-1})	23	33	36	0.013	0.182	0.267	0.296
v (m h^{-1})	5	15	36	0.714	0.590	0.479	0.400
$1/n$ (-)	0.32	0.58	24	0.006	0.161	0.301	0.359
K_F (μg mg^{-1})(L μg^{-1})$^{1/n}$	0.97	1.91	24	0.026	0.255	0.327	0.343
k_f (m s^{-1})	4.9E-05	5.7E-05	36	1.198	0.742	0.459	0.296
D_S (m^2 s^{-1})	6.10E-16	8.70E-16	36	0.002	0.146	0.213	0.235

SBA, GAC-M, chloroform			Simulation time (min)				
			6	30	400	800	1200
parameter	[INPUT]$_{min}$	[INPUT]$_{max}$	NSI (-)				
M_{GAC} (g)	1.122	1.87	0.577	0.395	0.127	0.088	0.071
ε (-)	0.58	0.97	0.556	0.158	0.005	0.001	0.001
R_P (mm)	0.42	0.72	0.835	0.564	0.146	0.097	0.075
C_0 (μg L^{-1})	9	13	0.074	0.085	0.034	0.024	0.019
v (m h^{-1})	5	15	0.474	0.255	0.065	0.044	0.035
$1/n$ (-)	0.39	1.12	0.153	0.196	0.127	0.100	0.085
K_F (μg mg^{-1})(L μg^{-1})$^{1/n}$	0.008	0.027	0.161	0.159	0.073	0.052	0.043
k_f (m s^{-1})	3.80E-05	4.00E-05	0.584	0.192	0.006	0.002	0.001
D_S (m^2 s^{-1})	3.40E-15	5.60E-15	0.077	0.144	0.063	0.044	0.035

(continues in the following page)

(continues from the previous page)

SBA, GAC-V, PCE				Simulation time (min)			
				200	400	800	1200
parameter	$[INPUT]_{min}$	$[INPUT]_{max}$	Minimum breakthrough time (min)	NSI (-)			
M_{GAC} (g)	1.44	2.41	48	1.014	0.983	0.900	0.800
ε (-)	0.58	0.97	42	2.867	1.834	0.808	0.368
R_P (mm)	0.30	0.50	48	2.959	2.216	1.616	1.357
C_0 (μg L^{-1})	23	33	48	0.078	0.217	0.370	0.404
v (m h^{-1})	5	15	48	1.789	1.486	0.996	0.686
1/n (-)	0.2	0.92	48	0.026	0.184	0.218	0.209
K_F (μg mg^{-1})(L μg^{-1})$^{1/n}$	4.2	6.0	48	0.196	0.501	0.754	0.772
k_f (m s^{-1})	3.1E-05	5.1E-05	48	0.968	0.801	0.480	0.244
D_S (m^2 s^{-1})	3.7E-18	6.2E-18	48	0.011	0.067	0.191	0.265

SBA, GAC-V, chloroform			Simulation time (min)				
			6	30	400	800	1200
parameter	$[INPUT]_{min}$	$[INPUT]_{max}$	NSI (-)				
M_{GAC} (g)	1.44	2.41	0.821	0.800	0.465	0.316	0.245
ε (-)	0.58	0.97	1.868	1.291	0.069	0.014	0.004
R_P (mm)	0.30	0.50	1.965	1.865	0.724	0.411	0.290
C_0 (μg L^{-1})	9	13	0.020	0.122	0.304	0.215	0.165
v (m h^{-1})	5	15	1.002	0.895	0.284	0.172	0.128
1/n (-)	0.35	0.58	0.003	0.130	0.534	0.438	0.368
K_F (μg mg^{-1})(L μg^{-1})$^{1/n}$	0.070	0.090	0.057	0.294	0.527	0.376	0.295
k_f (m s^{-1})	2.1E-05	3.5E-05	0.801	0.674	0.071	0.016	0.004
D_S (m^2 s^{-1})	5.9E-15	9.9E-15	0.018	0.123	0.218	0.152	0.117

Full-scale filter, GAC-V, chloroform			Simulation time (d)			
			70	100	150	200
parameter	$[INPUT]_{min}$	$[INPUT]_{max}$	NSI (-)			
M_{GAC} (kg)	4609	7356	1.646	1.029	0.279	0.075
ε (-)	0.58	0.97	0.197	0.020	0.013	0.005
R_P (mm)	0.30	0.50	10.303	0.053	0.157	0.077
C_{IN} (μg L^{-1})	3	5	8.938	0.992	0.176	0.044
v (m h^{-1})	7.2	16.4	1.633	0.976	0.359	0.119
1/n (-)	0.35	0.58	1.112	0.665	0.244	0.081
K_F (μg mg^{-1})(L μg^{-1})$^{1/n}$	0.070	0.090	2.913	1.231	0.311	0.083
k_f (m s^{-1})	2.1E-05	3.5E-05	0.177	0.021	0.014	0.005
D_S (m^2 s^{-1})	5.9E-15	9.9E-15	0.782	0.036	0.083	0.043

(continues in the following page)

(continues from the previous page)

Full-scale filter, GAC-M, chloroform			Simulation time (d)			
			20	40	60	100
parameter	[INPUT]$_{min}$	[INPUT]$_{max}$	NSI (-)			
M_{GAC} (kg)	4609	7356	1.331	0.579	0.219	0.023
ε (-)	0.58	0.97	0.259	0.014	0.016	0.003
R_P (mm)	0.42	0.72	3.211	0.034	0.131	0.034
C_{IN} (μg L^{-1})	3	5	0.801	0.206	0.069	0.007
v (m h^{-1})	7.2	16.4	7.506	1.084	0.318	0.031
1/n (-)	0.39	1.12	0.427	0.336	0.224	0.071
K_F (μg mg^{-1})(L μg^{-1})$^{1/n}$	0.008	0.027	0.428	0.296	0.146	0.022
k_f (m s^{-1})	3.80E-05	4.00E-05	0.210	0.019	0.019	0.003
D_S (m^2 s^{-1})	3.40E-15	5.60E-15	0.549	0.005	0.066	0.018

S.I.7 Evaluation of solute distribution parameters

The solute distribution parameter relative to PCE and chloroform during SBA tests was calculated as follows [3]:

e.S.10)
$$Dg = \frac{\rho_b \cdot q_0}{\varepsilon_b \cdot C_0}$$

where the maximum adsorption capacity (q_0) was estimated by Freundlich isotherm equation considering the parameters determined in batch experiments and the average influent chloroform and PCE concentrations (C_0) observed during SBA tests. The calculated values are shown in Figure S3, compared to those found in the literature for other compounds, in studies using HSDM to interpret SBA data: atrazine [4], MTBE [5], 2-Methylisoborneol (MIB) [6], catechol [7], trichloroethylene (TCE) and p-dichlorobenzene (p-DCB) [8]. Dg values from the literature were calculated based on the information provided in the manuscripts (isotherm parameters, influent concentrations, fixed-bed parameters).
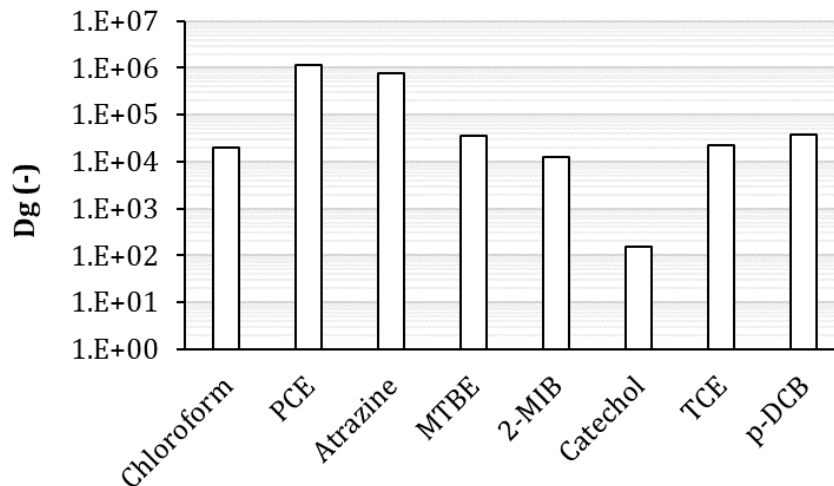
Figure S3 Solute distribution parameter (Dg) determined for chloroform and PCE during SBA tests in this study and for other compounds studied in the literature.

S.I.8 Full-scale filters monitoring

Figure S4 shows the values of water flow rate (Q) measured at the filter inlet and axial velocity (v) through GAC filter, calculated as the ratio between Q and the area of filter section (S=7.07 m^2). Figure S5 reports inlet concentrations of chloroform and PCE measured during the monitoring period. During

simulations by HSDM, v and C_{IN} values for a given time step were determined interpolating two consecutive observed data by linear regression.

Figure S5 shows mass balances of chloroform and PCE in influent and effluent waters. The cumulated mass of a contaminant at a time instant t ($M_{CUM,t}$) was calculated as:

e.S.11) $$M_{CUM,t} = C_t \cdot V_f \cdot (BV_t - BV_{t-1}) + M_{CUM,t-1}$$

where C_t is the influent or effluent contaminant concentration measured at time t, V_f is the filter volume (13 m³), BV_t and BV_{t-1} are the bed volumes treated at time t and t-1, respectively.

Chloroform and PCE concentrations adsorbed onto the solid-phase over time, q_t (µg mg⁻¹), are reported in Figure S7 and were calculated as:

e.S.12) $$q_t = (C_{IN,t} - C_{EF,t}) \cdot V_f \cdot (BV_t - BV_{t-1}) \cdot \frac{1}{M_{GAC}} + q_{t-1}$$

where $C_{IN,t}$ and $C_{EF,t}$ are the influent and effluent contaminant concentrations measured at time t and M_{GAC} is the mass of carbon in the filter. Figure S6 also reports the maximum adsorption capacities (q_0) estimated by Freundlich isotherm equation, considering the parameters determined in batch experiments and the average chloroform and PCE concentrations observed during filter monitoring.
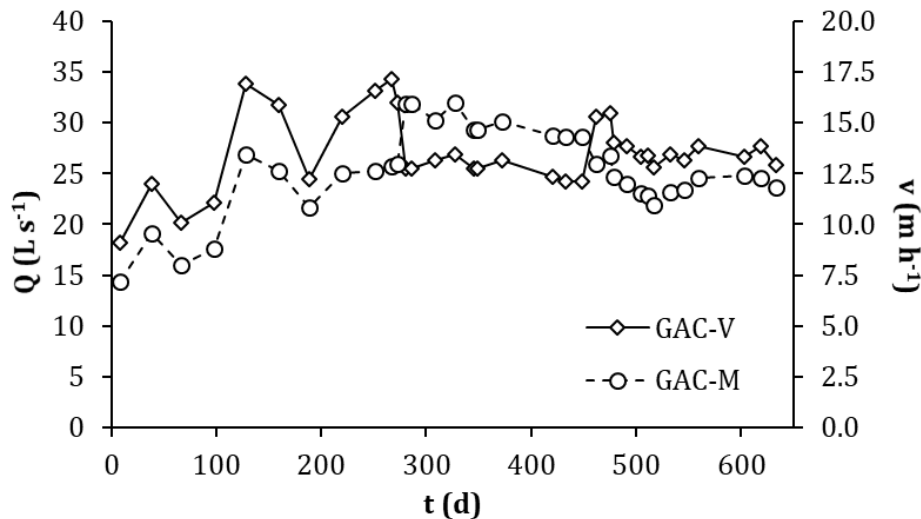
Figure S4 Water flow rate (Q) and velocity (v) over time observed for GAC-V and GAC-M full scale filters.
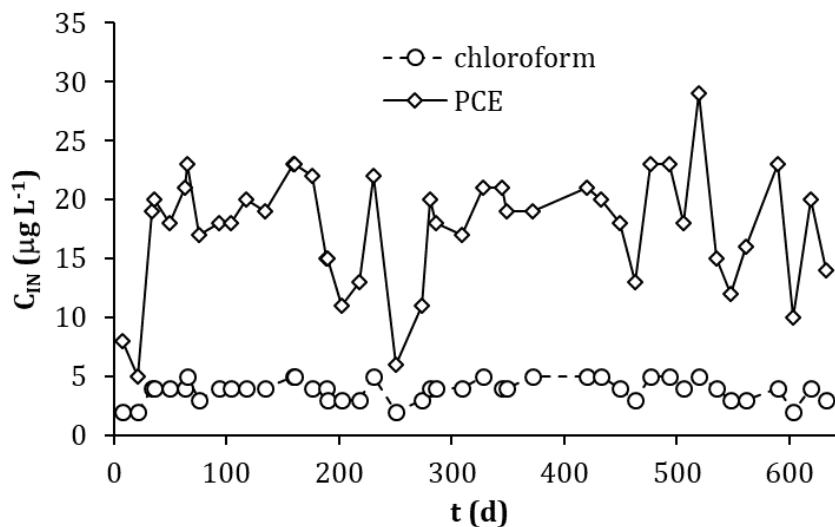
Figure S5 Influent PCE and chloroform concentrations measured during monitoring of full scale filters.
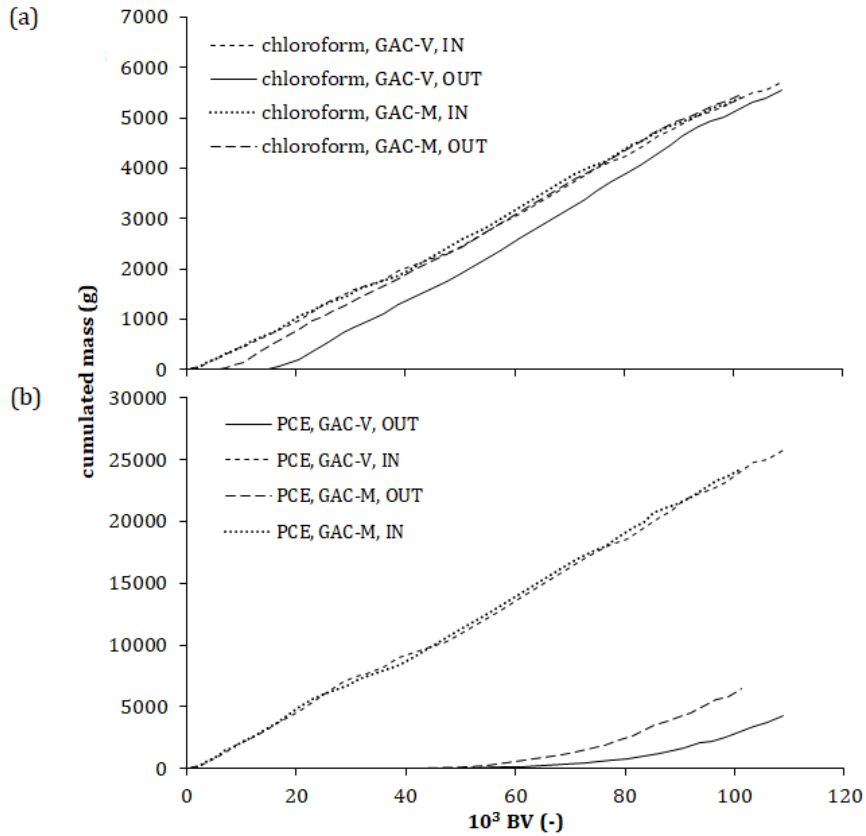
Figure S6 Chloroform (a) and PCE (b) influent and effluent cumulated masses calculated during monitoring of full scale filters.
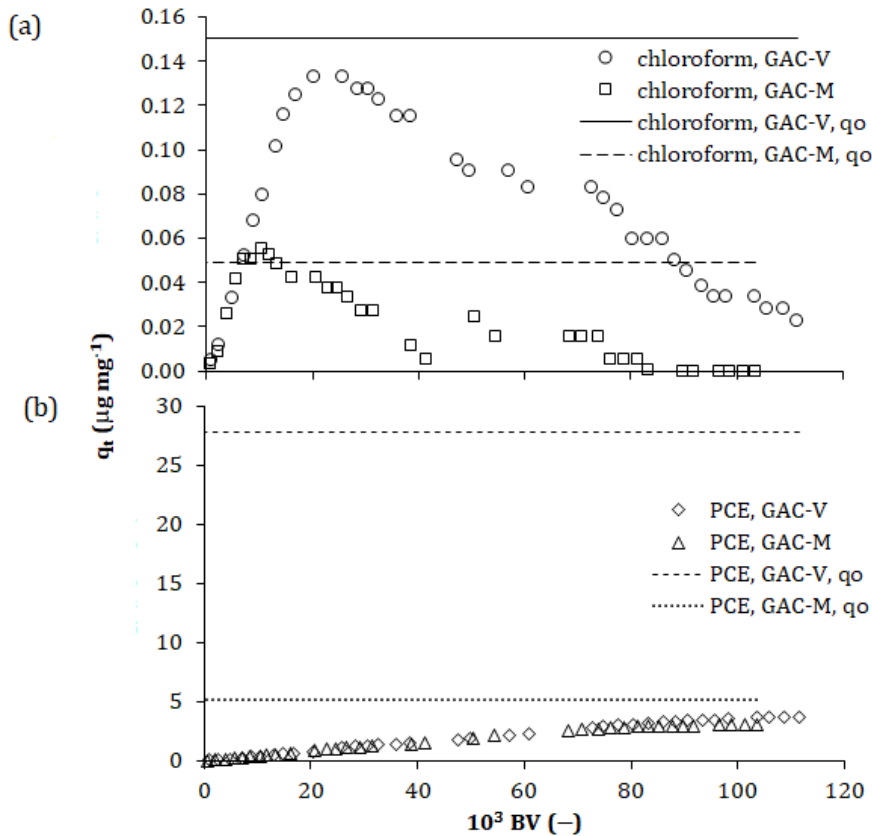
Figure S7 Chloroform (a) and PCE (b) solid-phase concentrations over time calculated for GAC-V and GAC-M in full-scale filters. Dashed lines represent the maximum adsorption capacity (q_0) calculated by Freundlich isotherms.

S.I.9 PCE breakthrough simulation in full-scale filters
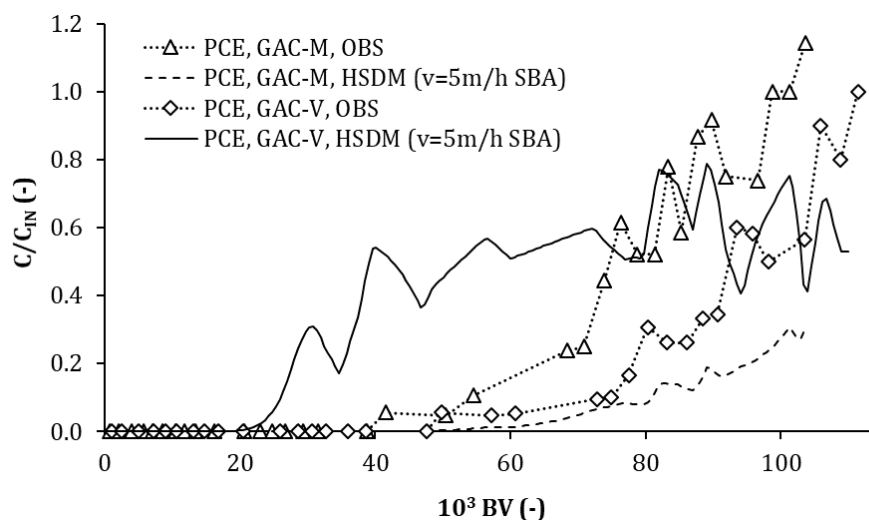
Figure S8 PCE breakthrough for GAC-M and GAC-V full-scale filters: observed and simulated data.

S.I.10 Adsorbate physical-chemical properties

Table S7 Physical-chemical properties of the investigated adsorbates.

| Parameter	Reference	chloroform	PCE
Van der Waals volume ($Å^3$)	9	70.37	93.42
Van der Waals surface area ($Å^2$)		102.21	122.96
Solvent accessible surface area ($Å^2$)		240.29	253.16
Topological polar surface area ($Å^2$)		0.00	0.00
Minimum projection area ($Å^2$)		20.36	19.13
Maximum projection area ($Å^2$)		26.61	36.54
Minimum projection radius ($Å$)		3.09	3.18
Maximum projection radius ($Å$)		3.18	3.86
Octanol-water partition coefficient $logP_{oct/wat}$ (-)		1.83	2.62
Solubility logS (-)		-1.67	-2.64
Molar mass (g mol^{-1})		119.37	165.82
Molar refractivity (cm^3 mol^{-1})		21.37	50.77
Polarizability ($Å^3$)		8.37	11.91
Vapor pressure at 20°C (Pa)	10	26263	1867
Molecular density (g cm^{-3})		1.50	1.62
Diffusion coefficient in water (m^2 s^{-1})		$1.0 \cdot 10^{-9}$	$8.2 \cdot 10^{-10}$

[9] predicted by Chemaxon (https://chemicalize.com/).

[10] US EPA, O. Superfund Soil Screening Guidance https://www.epa.gov/superfund/superfund-soil-screening-guidance (accessed Aug 28, 2017).

References

(1) García-Mateos, F. J.; Ruiz-Rosas, R.; Marqués, M. D.; Cotoruelo, L. M.; Rodríguez-Mirasol, J.; Cordero, T. Removal of paracetamol on biomass-derived activated carbon: modeling the fixed bed breakthrough curves using batch adsorption experiments. *Chem. Eng. J.* **2015**, *279*, 18–30.

(2) Azizian, S. Kinetic models of sorption: a theoretical analysis. *J. Colloid Interface Sci.* **2004**, *276* (1), 47–52.

(3) Sperlich, A.; Schimmelpfennig, S.; Baumgarten, B.; Genz, A.; Amy, G.; Worch, E.; Jekel, M. Predicting anion breakthrough in granular ferric hydroxide (GFH) adsorption filters. *Water Res.* **2008**, *42* (8), 2073–2082.

(4) Knappe, D. R.; Snoeyink, V. L.; Roche, P.; Prados, M. J.; Bourbigot, M.-M. Atrazine removal by preloaded GAC. *Am. Water Works Assoc. J.* **1999**, *91* (10), 97.

(5) Rossner, A.; Knappe, D. R. MTBE adsorption on alternative adsorbents and packed bed adsorber performance. *Water Res.* **2008**, *42* (8), 2287–2299.

(6) Ho, L.; Newcombe, G. Granular activated carbon adsorption of 2-methylisoborneol (MIB): pilot- and laboratory-scale evaluations. *J. Environ. Eng.* **2010**, *136* (9), 965–974.

(7) Richard, D.; Núñez, M. de L. D.; Schweich, D. Adsorption of complex phenolic compounds on active charcoal: breakthrough curves. *Chem. Eng. J.* **2010**, *158* (2), 213–219.

(8) Smith, E. H., & Weber Jr, W. J. (1989). Evaluation of mass-transfer parameters for adsorption of organic compounds from complex organic matrixes. *Environ. Sci. Technol.*, *23*(6), 713-722.

<div align="right">

CHAPTER 7

</div>

Modelling and optimization of a full-scale GAC adsorption system for chlorinated solvent removal in a multi-component real drinking water

Abstract

Several design and operating aspects can affect the costs of granular activated carbon (GAC) adsorption process, including filter configuration (parallel or lead-lag), filter number and size, and replacement strategy. The aim of this study is to define the optimal design and management criteria for a full-scale GAC system treating groundwater contaminated by a mixture of organic micropollutants. Five full-scale operating GAC filters, containing different types of GAC and treating different groundwater influents, were monitored, observing the breakthrough of tetrachloroethylene (PCE), chloroform and trichloroethylene (TCE). A strong correlation between GAC iodine number and the contaminant throughputs was observed, indicating that iodine number can be effectively used to predict filter life-time. Thomas model was then calibrated on the observed data and used to simulate a full-scale GAC system under different configurations (parallel and lead-lag), design (filter number and size) and managing parameters (exhausted GAC replacement strategies) as a function of the target contaminants and treatment objective (5%, 50% or 95% breakthrough). The simulation of a parallel configuration showed that the GAC specific throughput (V_{SP}) increases with the filter number (lower axial velocity) and size (higher EBCT) when considering a restrictive treatment objective, but it decreases for slack treatment objectives, independently from the selected target contaminant. Staggering the filter replacement in parallel configuration was found to increase the V_{SP} over the long period, but determining a higher frequency of replacement operations. For all the target contaminants, the advantages of staggered operations are maximized when considering high treatment objectives (95% breakthrough). Finally, various configurations (parallel and lead-lag) having representative EBCTs and axial velocities were simulated and compared considering three parameters affecting the management of the GAC adsorption phase: the V_{SP}, the number of replaced filters and the number of replacement operations over a 10-year period. The best configuration was found to depend on the target contaminant and the treatment objective and to be a compromise between the three conflicting objectives.

Keywords: granular activated carbon; adsorption; full-scale process simulation; optimization.

1. Introduction

Water sources in many industrialized areas of the world are contaminated by organic micropollutants, most of which are regulated by national drinking water regulations ([1-3]). Adsorption onto granular activated carbon (GAC) was designated by the United States Environmental Protection Agency (US-EPA) as the best available technology for the treatment of many regulated organic micropollutants, including volatile organic compounds (VOCs), trihalomethanes and pesticides ([4-6]). Despite the high GAC adsorption capacity towards many contaminants, GAC treatment stage can have high operating and maintenance costs. Adsorbent costs typically contribute to a large portion of total operating costs ([7,8]); hence, determining the optimal design parameters and operating strategies to minimize adsorbent usage rate (AUR) is fundamental to improve the overall efficiency of the treatment system. Several design and operating aspects can affect adsorbent usage rate, including empty-bed contact time (EBCT), the number of in-parallel filters, their configuration (parallel or lead-lag) and replacement strategy ([7,9]). Previous studies ([7-12]) compared the performances of different filter configurations by simulating the operation of ideal GAC treatment systems under selected sets of conditions; most of these studies based the comparisons on two parameters: the shape of the breakthrough profile of the target contaminant, expressed as mass transfer zone (MTZ) length, and the treatment objective, expressed as the ratio between the effluent and the influent concentration (C/C_{IN}). Crittenden et al. (1987) ([11]) stated that bed-in series configuration (also known as lead-lag) is the most efficient option for short MTZ length (<1 bed) and restrictive treatment objective ($C/C_{IN}<0.05$), while parallel configuration is more suitable for longer MTZ and less restrictive treatment objective ($C/C_{IN}>0.30$). Dvorak et al. (2008) ([7]) obtained similar results simulating the adsorption of VOCs: parallel filters with blended effluent resulted the best configuration for $C/C_{IN}>0.3$, while lead-lag configuration resulted in the lowest AUR when $C/C_{IN}<0.1$; MTZ length of the contaminant resulted important only for treatment objectives between 0.1 and 0.3. Dvorak and Maher (1999) ([9]) simulated a parallel configuration with effluent blending and staggered filter replacement; considering the removal of TOC up to $C/C_{IN}=0.35$, the authors found that AUR can be strongly reduced by increasing the EBCT and the number of parallel filters, but implying a more frequent replacement of GAC filters. Other authors ([8,10]) developed a framework to compare the AUR of different filter configurations, including single filters, lead-lag and parallel filters, both with and without by-pass, as a function of breakthrough curve shape and treatment objective. It should be stressed that most of the studies available in the literature deals with ideal small-size GAC systems composed by few adsorbers ([8-11]). On the other hand, for a given filter configuration, AUR estimation can strongly depend on the size of the treatment plant, involving the total flow rate to be treated and the hydraulic limitations on filter number and size. To the best authors' knowledge, no studies in the literature evaluated large GAC system efficiency during long-term operations, considering several operating cycles, associated to carbon reactivation, and evaluating all the involved engineering aspects, such as filter replacement frequency, design and hydraulic complexity of the system. Hence, despite general indications can be derived from the literature, GAC system simulation is always required to properly select the best adsorption configuration in specific full-scale situations ([8]).

A fundamental step for accurately simulating a GAC treatment system is the prediction of the concentration-time profile from breakthrough curve for a single filter ([13]). Different alternative methods to predict breakthrough profile were proposed in literature (*inter alia* [14-16]), but a general procedure has not yet been established ([17]). The predictive methods mostly referred to, including Rapid Small Scale Column Tests (RSSCT), Homogeneous Surface Diffusion Model (HSDM), Linear Driving Force (LDF) model ([5,16,18-25]), are relatively simple and rapid; however, the accuracy of the results is not always guaranteed, since model parameters, determined by lab-scale tests, are often not representative of full-scale conditions ([14,21,24,26,27]); moreover, model sensitivity to the parameters and the initial assumptions can vary with the scale of the GAC system, but simulation results are rarely

verified at full-scale ([28]). Often, an accurate and reliable evaluation of breakthrough profile in full-scale GAC systems can be obtained only by pilot- or full-scale data, requiring, however, relatively time- and cost-consuming monitoring campaigns. When pilot- or full-scale data are available, breakthrough curves can be well interpreted by a group of widely used mathematical models, such as Adams-Bohart, Bed Depth Service Time (BDST), Thomas, Clark and Yoon–Nelson models ([29,30]). These models are composed by a single equation describing the concentration-time profile in a continuous flowing system and they allow to describe the adsorption kinetic into an ideal GAC filter as a function of few and easily known operating parameters (i.e. water flow rate, GAC mass, influent concentration). On the other hand, the validity of this class of models is limited to the range of conditions used for calibration and their predictive performances has been rarely validated under different operating conditions. Considering the limitations of the main models proposed in the literature, further efforts are still needed to develop new methods to predict GAC filter breakthrough, combining model accuracy, wide-range validity and simplicity in obtaining case-specific parameters.

The main goal of this work was to determine the optimal design parameters and managing strategy for a full-scale GAC system (about 500 L s^{-1} total flow rate) treating groundwater contaminated by several organic micropollutants (VOCs and pesticides). Firstly, five full-scale filters containing different GAC types (of different origins and reactivation stages) and fed on two different groundwater matrices were monitored for about 15 to 21 months to observe the breakthrough profiles of the present contaminants and their dependence on the GAC type and water composition. The observed data were then used: i) to find a correlation between contaminant breakthrough and GAC physical-chemical properties, to develop a simple and fast tool to predict GAC life-time; ii) to calibrate a kinetic model (Thomas model) then used to simulate different GAC system configurations (filter size and connection) and to evaluate their performances as a function of the considered target contaminant and the treatment objective. The optimal configurations and strategies for exhausted GAC replacement were also assessed considering the GAC specific throughput and the frequency of GAC replacement operations during a long-term time frame (10 years).

2. Materials and methods

2.1 Studied adsorbents

Two commercial granular activated carbons (Chemviron) were studied: GAC-1240 (GAC-M) and Acticarbone® NCL 1240 (GAC-V), being, respectively, of mineral (coal-based) and vegetal (coconut-based) origin. GAC-V belonged to a virgin stock (GAC-V-v), while both virgin (GAC-M-v) and reactivated (GAC-M-r) stocks of GAC-M were used in this study. Reactivated carbon had been previously used until partial exhaustion and subjected to thermal treatment to restore its adsorption capacity. Various physical-chemical and textural properties of the studied carbons have been determined (results reported in Table 1): iodine number was determined according to ASTM4604. Surface and textural characteristics were determined by N$_2$ adsorption and desorption at T=77 K (Tristar II 3020 V1.03, Micrometrics Instruments Corporation), after pre-treatment of the samples for 4 h at T=150°C under nitrogen atmosphere. Carbon surface area was determined according to BET method ([31]), specific area and volume of micropores were determined by t-Plot method ([32]), pore size distribution was determined by BJH method ([33]). GAC apparent density (ρ_b) was measured according to ASTM D2854-89.

2.2 Monitoring of full-scale filters

The monitored full-scale GAC filters belonged to two drinking water treatment plants (DWTPs), named DWTP-1 and DWTP-2, located in the Milan urban area (Italy) and each fed on about 500 L s^{-1} of groundwater. DWTP-1 and DWTP-2 included 20 and 18 filters, respectively, operating in parallel. All

the filters had 3 m inner diameter (D_i), 1.85 m GAC bed height (H_i) and contained 13 m^3 GAC volume (V_i).

Two filters were selected from DWTP-1, containing respectively GAC-M-r and GAC-V-v, while three filters containing, respectively, GAC-M-r, GAC-M-v and GAC-V-v were selected from DWTP-2. It is pointed out that the monitoring of DWTP-1 filters corresponded to that discussed in the study presented in Chapter 6. Filters in DWTP-1 and DWTP-2 were monitored during a period of 21 months and 15 months, respectively. Influent flowrate to each filter was measured by an ultrasonic flowmeter, with a measurement time resolution of 10 s. The bed volumes, BV_j (-), treated by a filter at a given time t_j (s) were calculated as:

e.1)
$$BV_j = \frac{(t_j - t_{j-1}) \cdot Q_{avg,j}}{V_i} + \sum_{j=1}^{j-1} BV_j$$

where $Q_{avg,j}$ (L s^{-1}) is the average flow rate measured between t_j and t_{j-1}.

Influent and effluent flowrate from the filters was sampled about every 2 weeks, determining the concentrations of VOCs and pesticides (see section 2.4).

Table 1 Physical-chemical and textural properties of the carbons into the monitored filters (before starting operations).

DWTP	DWTP-1		DWTP-2		
GAC type	GAC-V-v	GAC-M-r	GAC-V-v	GAC-M-v	GAC-M-r
Iodine number (mg g^{-1})	1135	864	1135	993	804
BET surface area (m^2 g^{-1})	1151	767	1203	1011	764
t-plot micropore area (m^2 g^{-1})	933	241	946	697	346
t-plot micropore volume (cm^3 g^{-1})	0.364	0.104	0.383	0.283	0.330
BJH average pore diameter (nm)	3.439	3.227	3.329	2.845	3.321
ρ_b (kg m^{-3})	450	470	585	752	720

2.3 Analytical methods for water samples

All the water samples were collected into 40 mL glass vials, stored at 4 °C and analyzed within 48 h.

The concentrations of 27 VOCs (listed in S.I.2 of Chapter 6) were determined by gas-chromatographer (Agilent Technologies GC-6890N Series gas-chromatographer) coupled with a single quadrupole mass analyzer (Agilent Technologies MS 5793 Network mass analyzer) with a dynamic headspace system (Purge&Trap O-I-Analytical Eclipse 4660 with 4551-A auto-sampler), according to methods EPA 524.3-09 and EPA 5030C-03. Volatile fraction extraction was made by stripping with ultra-pure helium and concentration on multi-phasic filter at 20 °C, followed by filter heating at 200 °C.

The concentrations of 26 pesticides (listed in S.I.2 of Chapter 6) were determined by a gas-chromatographer (Agilent Technologies GC-7890A gas-chromatographer) coupled with a triple quadrupole mass/mass detector (Agilent Technologies MSD-7000A mass detector) after solid phase extraction according to the APAT-IRSA 5060/03 method. Organic compounds were extracted (Autotrace SPE workstation Zymark) using methanol, water and acetone/isopropanol 9:1 for cartridge activation and elution (Chromabond HR-X SPE cartridges).

All the analyses have been performed by the laboratory of Metropolitana Milanese S.p.A. (MM), which manages the integrated water service in Milan (I).

2.4 Modelling

Experimental data obtained from full-scale filter monitoring have been interpreted by Thomas model, as described in section 2.4.1. The parameters estimated for a single filter were then used to simulate a

GAC system composed by various identical GAC filters operating under different configurations, as described in section 2.4.2.

2.4.1 Single filter breakthrough modelling

For a given contaminant, the breakthrough of a fixed-bed filter '*i*' was described by the Thomas model, whose equation is written as:

e.2)
$$\left[\frac{C_t}{C_{IN}}\right]_i = \left[1 + exp\left(k_{Th} \cdot q_e \cdot M_i \cdot Q_i^{-1} - k_{Th} \cdot C_{IN} \cdot t\right)\right]^{-1}$$

where C_{IN} ($\mu g\ L^{-1}$) is the influent contaminant concentration measured during filter monitoring, C_t ($\mu g\ L^{-1}$) is the effluent concentration at time t (s), k_{Th} ($L\ \mu g^{-1}\ s^{-1}$) is the Thomas rate constant, q_e ($\mu g\ g^{-1}$) is the equilibrium adsorbate solid-phase concentration, M_i (g) is the GAC mass in the filter and Q_i ($L\ s^{-1}$) is water flow rate fed on the filter (S.I.1). M_i was calculated as:

e.3)
$$M_i = V_i \cdot \rho_b$$

where V_i is the filter volume and ρ_b ($g\ m^{-3}$) is the apparent density of the GAC bed (Table 1). K_{Th} and q_e were estimated fitting experimental data by non-linear regression analysis using the least square method (Matlab, Mathworks 2014).

2.4.2 GAC system modelling

A Matlab code (Matlab, Mathworks 2014) was created to simulate the theoretical behaviour of a GAC system composed by various GAC filters. The GAC system was represented as a matrix containing n_f columns, where n_f corresponds to the number of filters, while the rows contained the filter effluent concentration ($[C_t/C_{IN}]_i$) at sequentially time intervals, calculated by the Thomas model.

Two configurations were modelled (Figure 1): A) n_f single filters in parallel with effluent blending; B) n_p pairs of lead-lag filters with effluent blending.

In both configurations, each filter (configuration A) or each pair of lead-lag filters (configuration B) was assumed to receive the same influent concentration (C_{IN}) and the same fraction of the total flow rate ($Q_i=Q_{tot}/n_f= Q_{tot}/n_p$). In configuration B, influent concentration of lead filters was equal to C_{IN}, while lag filters were assumed to receive lead filters effluent. At each time step, the normalized concentration of contaminant in the effluent to the GAC system ($[C_t/C_{IN}]_{tot}$) was calculated as:

e.4)
$$\left[\frac{C_t}{C_{IN}}\right]_{tot} = \frac{1}{N} \cdot \sum_{i=1}^{N} \left[\frac{C_t}{C_{IN}}\right]_i$$

where N corresponds to the number of parallel (n_f) or lag (n_p) filters.

At the beginning of each simulation, all the filters were assumed to contain fresh GAC, so $[C_t/C_{IN}]_i$ values in each matrix column were calculated starting from t=0. When $[C_t/C_{IN}]_{tot}$ reached a given treatment objective, a group of n_R columns in the matrix was replaced giving a new effluent profile, calculated starting again from t=0; this operation represented the replacement of a group of n_R GAC filters by fresh GAC, having a restored adsorption capacity. In configuration A, groups of n_R filters were replaced sequentially; in configuration B, once the lag filters effluent reaches the treatment objective, all the lead filters were replaced and switched to the lag position.

For each configuration, different scenarios were simulated by varying the filter number (from 16 to 40), volume (from 13 to 18 m³) and the replacement strategy (substitution of 100%, 50% or 25% of the filters at treatment objective attainment). Each scenario was evaluated considering two target contaminants (hence two sets of Thomas model parameters, corresponding to different breakthrough profiles) and three treatment objectives (5%, 50% and 95% breakthrough). The specific throughput, V_{SP} ($L\ g^{-1}$), representing the volume of water treated per unit mass of adsorbent, was considered to compare the performances of the GAC system under different scenarios. For a fixed treatment objective, namely for a fixed $[C_t/C_{IN}]_{tot}$ value, V_{SP} has been calculated as:

e.5)
$$V_{SP} = \frac{t_{BT} \cdot Q_{tot}}{M_i \cdot n_R}$$

where t_{BT} (s) is the time to breakthrough at the treatment objective.

When working with staggered operations (i.e. configuration A with $n_r < n_f$ and configuration B), the time interval for GAC replacement (the time at which the blended effluent $[C_t/C_{IN}]_{tot}$ reaches the treatment objective, corresponding to t_{BT}) changes after system start-up until a steady-state time interval [9]. Before steady-state, the specific throughput is different at each GAC replacement, being dependent on t_{BT} (equation e.5). Since many replacements can occur before steady-state conditions, in this scenario, the specific throughput ($V_{SP,T}$) was evaluated for a time frame (T) of 10 years, considering the contributions of all replacement operations occurring during T:

e.6)
$$V_{SP,T} = \frac{T \cdot Q_{tot}}{M_i \cdot N_R} = \frac{T \cdot Q_{tot}}{M_i \cdot n_R \cdot N_O}$$

where N_R corresponds to the total number of filters replaced in 10 years and N_O is the number of replacement operations (replacement of a group of n_R filters when treatment objective is reached in the blended effluent).
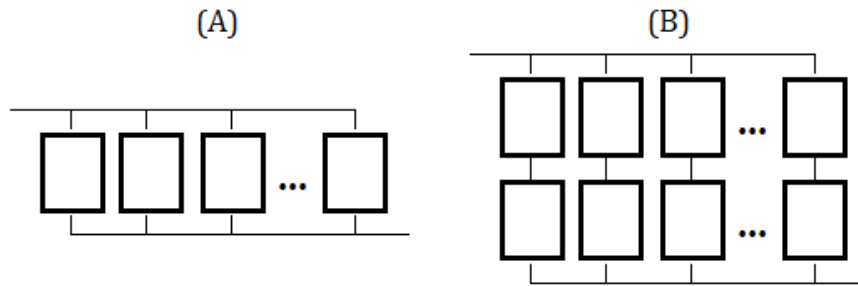

Figure 1 Scheme of the simulated configurations: A) single filters in parallel with effluent blending; B) pairs of lead-lag filters with effluent blending.

3. Results and discussion

3.1 Full-scale filter monitoring

Both the groundwaters fed on DWTP-1 and DWTP-2 contained various VOCs and pesticides at detectable levels, with influent concentrations varying over time. Among VOCs, tetrachloroethylene (PCE), chloroform, trichloroethylene (TCE) and cis-1,2-dichloroethylene were found at detectable levels in DWTP-1 influent water, displaying concentrations (average±st.dev.) of $17.7\pm4.98\ \mu g\ L^{-1}$, $3.9\pm0.90\ \mu g\ L^{-1}$, $1.0\pm0.50\ \mu g\ L^{-1}$ and $0.6\pm0.53\ \mu g\ L^{-1}$, respectively. Pesticides found at concentrations above the detection limit were 3,6-dichloropiridazine ($3.96\pm1.216\ \mu g\ L^{-1}$), 2,6-dichlorobenzamide ($0.10\pm0.054\ \mu g\ L^{-1}$), atrazine ($0.02\pm0.014\ \mu g\ L^{-1}$), atrazine desisopropyl ($0.01\pm0.005\ \mu g\ L^{-1}$), atrazine desethyl ($0.02\pm0.011\ \mu g\ L^{-1}$), terbuthylazine ($0.02\pm0.008\ \mu g\ L^{-1}$) and terbuthylazine desethyl ($0.02\pm0.011\ \mu g\ L^{-1}$). PCE ($25.9\pm5.88\ \mu g\ L^{-1}$), chloroform ($12.0\pm1.87\ \mu g\ L^{-1}$) and TCE ($4.5\pm0.84\ \mu g\ L^{-1}$) were the VOCs detected in DWTP-2 influent water, while 3,6-dichloropiridazine ($2.19\pm0.545\ \mu g\ L^{-1}$), 2,6-dichlorobenzamide ($0.38\pm0.081\ \mu g\ L^{-1}$), tris(2-chloroethyl)phosphate ($0.09\pm0.021\ \mu g\ L^{-1}$) and atrazine ($0.06\pm0.040\ \mu g\ L^{-1}$) were found among pesticides. The monitored filters also differed for the water flow rate, varying over time and ranging between 7 and 48 L s^{-1} (all measured values in S.I.1).

Thanks to the higher influent concentration, complete breakthrough profile could have been monitored only for PCE and chloroform in DWTP-1, for PCE, chloroform and TCE in DWTP-2. Figure 2 shows PCE and chloroform breakthrough data observed for all the monitored filters, expressed as C_t/C_{IN} over the treated BV (observed data reported in Figure 2-a correspond to those reported in Figure 3 of Chapter 6). TCE breakthrough profiles observed in DWTP-2 filters are reported in S.I.2 (Figure S2). The observed data were synthetized by determining the throughputs, expressed in bed

volumes, to 5%, 50% and 95% breakthrough ($BV_{5\%}$, $BV_{50\%}$ and $BV_{95\%}$, respectively) for each contaminant. Based on the available data resolution, $BV_{5\%}$, $BV_{50\%}$ and $BV_{95\%}$ (Table 2) were determined interpolating two consecutive observed data by linear regression. Due to an irregular peak observed in the effluent concentration data (Figure 2b), the $BV_{5\%}$ of PCE for GAC-M-v in DWTP-2 could have not been accurately determined. The length (L_{MTZ}) of the mass transfer zone (MTZ) was estimated by the following expression ([34]):

$$e.7) \qquad L_{MTZ} = \frac{(t_{95\%} - t_{5\%}) \cdot H_i}{\dfrac{(t_{95\%} + t_{5\%})}{2}}$$

where $t_{95\%}$ and $t_{5\%}$ are the observed times to 95% and 5% breakthrough, respectively. L_{MTZ} estimates are reported in Table 2.

Looking at data in Figure 2 and Table 2, it could be observed a strong difference in the MTZ length of the contaminants, reflecting their different affinity towards GAC. For all the monitored filters, chloroform was the first contaminant to appear in the effluent, with an early and very fast breakthrough, passing from 5% to 95% in less than 10^4 BV. On the other hand, PCE was always the last compound to appear in the effluent and displayed a very slow breakthrough profile. TCE, detected only in the three filters in DWTP-2, showed intermediate characteristics in terms of throughput values and slope of breakthrough profile. For all the monitored filters, chloroform effluent concentrations exceeded the influent one immediately after the complete exhaustion of the breakthrough profile; the same behavior was observed for TCE in GAC-M-r of DWTP-2. C_t/C_{IN} values higher than 1 are due to the release of the two contaminants previously adsorbed onto activated carbon, indicating highly reversible adsorption bounds.

As shown by throughput values in Table 2, in DWTP-1, GAC-V-v showed higher adsorption capacities than GAC-M-r towards both chloroform (throughputs to 5%, 50% and 95% breakthrough at least 1.3 times higher) and PCE ($BV_{5\%}$, $BV_{50\%}$ and $BV_{95\%}$ 14-25% higher); in DWTP-2, adsorption capacities towards all the contaminants followed the order GAC-V-v>GAC-M-v>GAC-M-r: GAC-V-v showed throughput values 30-40% and 25% higher than GAC-M-v for chloroform and TCE, respectively, while the difference in the throughputs calculated for GAC-M-v and GAC-M-r was 40-70% for chloroform and about 20% for TCE. In general, it could be concluded that vegetal-based carbon has higher adsorption capacity than mineral-based carbon and that virgin GAC-M-v has better performances than reactivated GAC-M-r, guaranteeing the treatment of much more bed volumes and significantly longer filter life-times (for instance, about 40-50 days and 50-60 days longer considering the 5% breakthrough of chloroform and TCE, respectively).

Comparing GAC-V-v data obtained in DWTP-1 and DWTP-2, it was possible to observe the effect of water matrix on chloroform and PCE adsorption: the breakthrough of both the contaminants was faster in DWTP-2 (5%, 50% and 95% chloroform breakthroughs, respectively, 23%, 12% and 26% earlier than in DWTP-1), probably due to the higher influent concentrations, determining a faster exhaustion of carbon adsorption capacity. It is pointed out that GAC-M-r in the two DWTPs did not belong to the same carbon stock, as evidenced by data in Table 1, since they have been previously used under different conditions and subjected to different exhaustion-reactivation cycles. Hence, comparing the data of the GAC-M-r filters in the two DWTPs is not possible to evaluate only the effect of water matrix separating the one due to the carbon's characteristics.
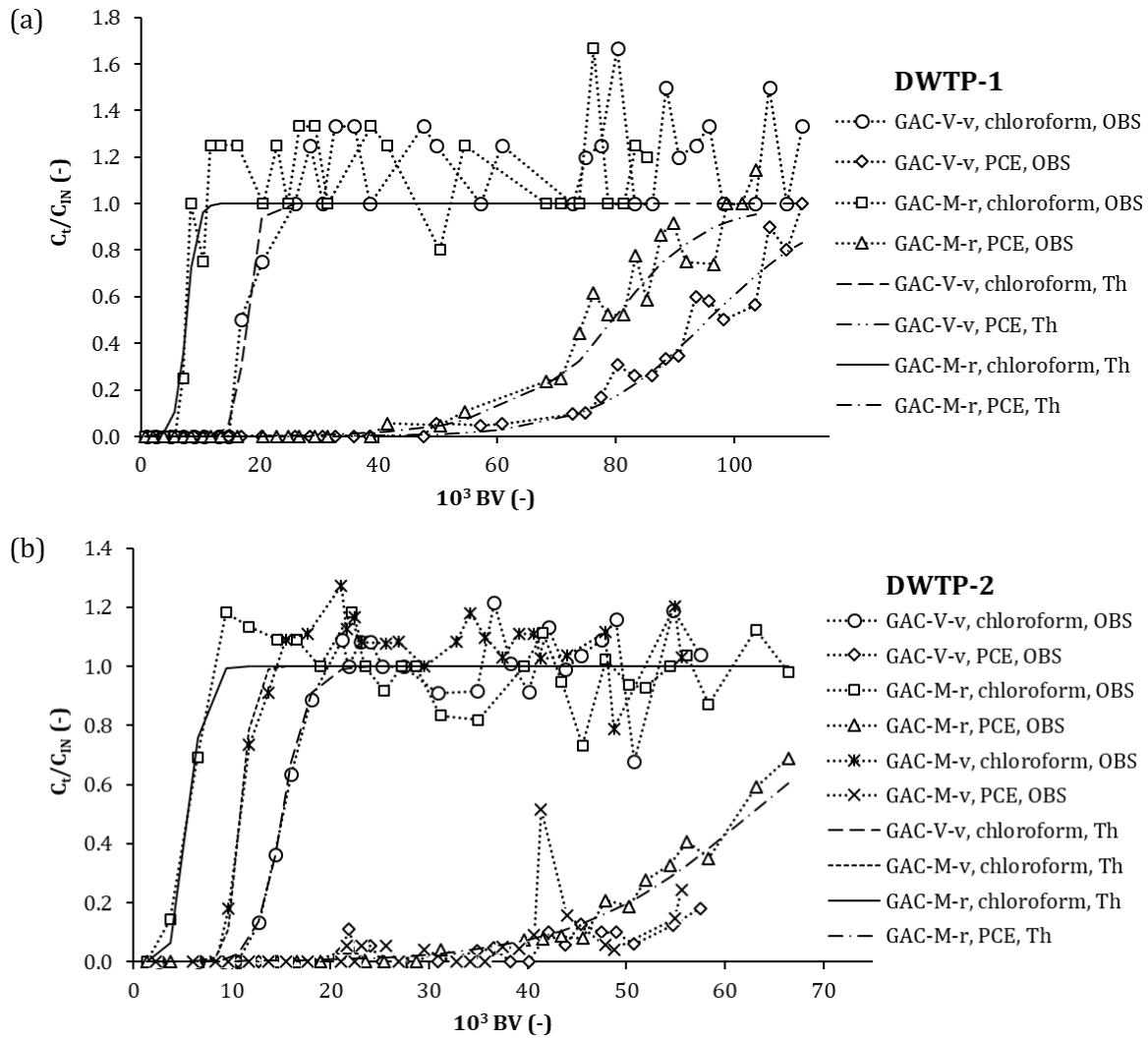
Figure 2 Chloroform and PCE breakthrough for filters containing GAC-V-v, GAC-M-r and GAC-M-v in DWTP-1 (a) and DWTP-2 (b): observed data and fitting curves (Thomas model).

Table 2 Observed throughputs to 5%, 50% and 95% breakthrough and estimated MTZ length (L_{MTZ}) for chloroform, PCE and TCE in the monitored filters.

DWTP		DWTP-1		DWTP-2		
GAC type		GAC-V-v	GAC-M-r	GAC-V-v	GAC-M-v	GAC-M-r
chloroform	10^3 $BV_{5\%}$	15.0	6.0	11.5	8.7	2.2
	10^3 $BV_{50\%}$	17.0	7.5	15.0	10.5	5.5
	10^3 $BV_{95\%}$	25.0	8.2	18.5	13.5	8.0
	L_{MTZ} (m)	0.69	0.74	1.12	1.10	1.59
PCE	10^3 $BV_{5\%}$	50.0	40.0	41.0	-	35.5
	10^3 $BV_{50\%}$	92.0	75.0	-	-	61.5
	10^3 $BV_{95\%}$	111.0	97.0	-	-	-
	L_{MTZ} (m)	1.37	1.35	-	-	-
TCE	10^3 $BV_{5\%}$	-	-	40.5	40.0	32.0
	10^3 $BV_{50\%}$	-	-	53.0	46.5	37.0
	10^3 $BV_{95\%}$	-	-	-	57.0	46.0
	L_{MTZ} (m)	-	-	-	0.68	0.81

GAC adsorption capacity is known to be related to its physical-chemical and textural properties, such as iodine number, BET surface area and micropore size characteristics ([35]). Data obtained by filter monitoring were analysed to find a correlation between GAC properties (parameters in Table 1) and the observed throughputs for chloroform, PCE and TCE breakthroughs (Table 2). Calculating pairwise linear correlation coefficients among the data of all the monitored filters (S.I.3, Table S1), iodine number resulted to be the parameter most correlated to the observed throughput values, for all the considered contaminants and breakthrough values. The most robust dataset was available for chloroform (data from all the 5 filters). Observed $BV_{5\%}$, $BV_{50\%}$ and $BV_{95\%}$ values for chloroform as a function of GAC iodine number are shown in Figure 3, together with linear regression curves and the relative determination coefficients (R^2): a strong correlation was observed, as indicated by the good data fitting by linear regressions ($R^2>0.87$, p-value<0.02). GAC iodine number (I_2N) can be so considered an effective indicator of adsorption capacity towards chloroform and can be well correlated to the velocity of MTZ shift through the filter. The estimated regression curves (parameter estimates±95% confidence intervals, determination coefficient, adjusted determination coefficient, p-value and number of data) are shown in equations e.8-e.10:

e.8)
$$BV_{5\%} = (-2.2 \pm 1.71) \cdot 10^4 + (31.0 \pm 17.18) \cdot I_2N$$
(R^2=0.92, R^2_{adj}=0.89, p-value=0.01, n=5)

e.9)
$$BV_{50\%} = (-2.0 \pm 1.01) \cdot 10^4 + (31.5 \pm 10.17) \cdot I_2N$$
(R^2=0.97, R^2_{adj}=0.96, p-value<0.01, n=5)

e.10)
$$BV_{95\%} = (-2.9 \pm 3.12) \cdot 10^4 + (44.4 \pm 31.31) \cdot I_2N$$
(R^2=0.87, R^2_{adj}=0.83, p-value=0.02, n=5)

A similar correlation was observed for PCE and TCE (data shown in S.I.3, Figure S3), although a lower number of data was available for these contaminants, since complete breakthrough profiles were not observed in all the filters.

Despite the relatively low number of data, results indicate that GAC iodine number could be effectively used to predict the breakthrough of different contaminants and to estimate filter life-time. A wider monitoring campaign including more GAC filters could provide an enough large dataset to calibrate a more robust correlation model. Such tool could be potentially used for two main applications: 1) establishing the minimum iodine number to be required to the GAC supplier, in order to guarantee a minimum GAC bed life-time; 2) predicting contaminant breakthrough only based on the determination of iodine number of fresh GAC (at the beginning of the operations). Regarding the second application, this kind of model would represent a relatively simple, fast and cost-saving predictive tool. In fact, physical-chemical and textural properties of GAC (such as iodine number, BET surface area and micropore size characteristics) are often provided by adsorbent suppliers and are commonly determined in full-scale filters. On the other hand, most of the predictive models used in the literature are cost- and time-consuming, requiring the monitoring of pilot- or full-scale filters or the conduction of laboratory experiments for the calibration of model parameters.
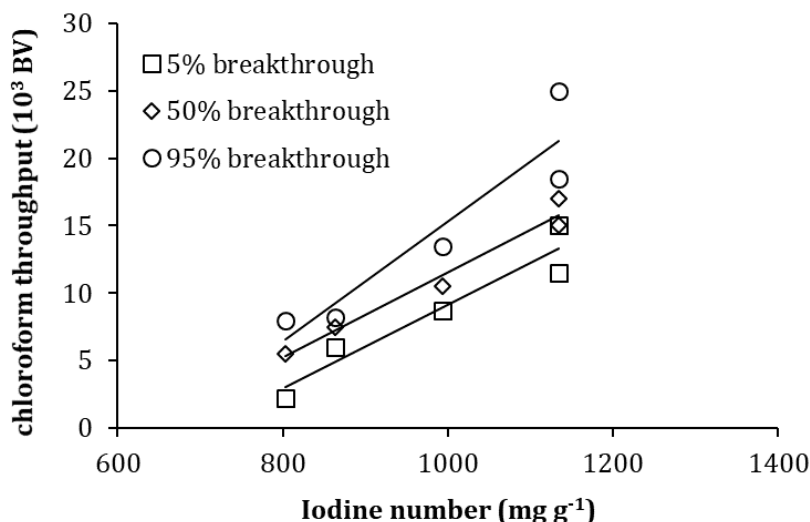
Figure 3 Observed chloroform throughput (to 5%, 50% and 95% breakthrough) vs. GAC iodine number. Linear regression curves are reported.

3.2 Breakthrough data fitting by Thomas model

Breakthrough data observed for the monitored filters were fitted by the Thomas model to determine the Thomas rate constant (k_{Th}) and equilibrium solid-phase concentration (q_e). The rate constant reflects the slope of breakthrough profile (a higher k_{Th} corresponds to a sharper curve), while q_e corresponds to the fixed-bed maximum adsorption capacity of the contaminant ([29]). Parameters and determination coefficients estimated for different filters and contaminants are listed in Table 3. Simulated breakthrough curves for PCE and chloroform in DWTP-1 and DWTP-2 filters are shown in Figure 2, while TCE data for DWTP-2 are shown in S.I.1 (Figure S1). The monitored PCE breakthroughs for GAC-V-v and GAC-M-v in DWTP-2 were too short for accurately estimating model parameters.

Observed data were well fitted by Thomas model, as indicated by the high determination coefficients of non-linear regression (R^2=0.80-0.99). Parameters' estimates reflected quite well the different adsorption capacities observed for the carbons, with q_e values following the order GAC-V-v>GAC-M-r in DWTP-1 and GAC-V-v>GAC-M-v>GAC-M-r in DWTP-2. Consistently with observed data, for the same GAC, adsorption capacities of the contaminants followed the order PCE>TCE>chloroform, while an opposite trend was observed for rate constant values, reflecting the different slope of breakthrough profiles. Thomas model can be so considered effective to simulate PCE, TCE and chloroform breakthroughs from the monitored GAC filters, and it was used to simulate full-scale GAC systems composed by various filters (see following sections).

Thomas model parameters for chloroform and GAC-V-v have been estimated both in DWTP-1 and DWTP-2. Despite being the same carbon, parameter values for the two DWTP were quite different, with GAC-V-v in DWTP-2 showing an almost double q_e, indicating a higher adsorption capacity, and about 5-times lower k_{Th}, due to the more extended MTZ. Results suggest that Thomas model parameters were case-specific and strictly dependent on filter operating conditions and water matrix composition. Thomas model parameters calibrated on a single filter cannot be considered generally valid and used to predict the breakthrough of other filters; accurate model parameters can be determined only by fitting pilot- or full-scale data obtained under specific conditions which, however, can be time-consuming and expensive.

Table3 Thomas model parameters and determination coefficients (R^2) estimated by fitting experimental breakthrough curves by non-linear regression.

DWTP		DWTP-1		DWTP-2		
GAC type		GAC-V-v	GAC-M-r	GAC-V-v	GAC-M-v	GAC-M-r
chloroform	k_{Th} (L μg^{-1} s^{-1})	$5.0 \cdot 10^{-7}$	$4.0 \cdot 10^{-7}$	$1.0 \cdot 10^{-7}$	$2.0 \cdot 10^{-7}$	$2.0 \cdot 10^{-7}$
	q_e (μg g^{-1})	$1.5 \cdot 10^2$	$8.0 \cdot 10^1$	$3.1 \cdot 10^2$	$1.7 \cdot 10^2$	$9.5 \cdot 10^1$
	R^2 (-)	0.99	0.89	0.99	0.95	0.92
PCE	k_{Th} (L μg^{-1} s^{-1})	$1.1 \cdot 10^{-8}$	$1.1 \cdot 10^{-8}$	-	-	$8.0 \cdot 10^{-9}$
	q_e (μg g^{-1})	$3.8 \cdot 10^3$	$3.2 \cdot 10^3$	-	-	$2.5 \cdot 10^3$
	R^2 (-)	0.97	0.96	-	-	0.95
TCE	k_{Th} (L μg^{-1} s^{-1})	-	-	$6.6 \cdot 10^{-8}$	$8.2 \cdot 10^{-8}$	$1.8 \cdot 10^{-7}$
	q_e (μg g^{-1})	-	-	$3.4 \cdot 10^2$	$2.1 \cdot 10^2$	$2.1 \cdot 10^2$
	R^2 (-)	-	-	0.89	0.94	0.80

3.3 GAC system optimization

A full-scale GAC system composed by various parallel GAC filters was simulated with the aim of optimizing some of the most important design and operating parameters (filter configuration, number, volume and replacement strategy). An ideal set of identical filters containing GAC-V-v and treating groundwater of DWTP-1 was selected as case study; chloroform and PCE were considered as target contaminants, to test GAC performances for two extremely different breakthrough profiles. Chloroform and PCE simulated breakthrough profiles were used for simulations. In all the simulated scenarios, the GAC system was assumed to treat a constant water flow rate (Q_{tot}) equal to 476 L s^{-1}, having constant chloroform and PCE influent concentrations (3.9 μg L^{-1} and 17.7 μg L^{-1}, respectively), corresponding to the average values observed during DWTP-1 monitoring. The V_{SP} values to 5%, 50% and 95% breakthrough of both the contaminants were calculated during each simulation and considered to assess the overall performance of the GAC system.

3.3.1   *Effect of EBCT and axial velocity on parallel filters*

The influence of EBCT of single filters in configuration A (Figure 1) was evaluated running simulations varying the number of parallel filters (n_f) and the filter volume (V_i). In fact, EBCT results from the combination of water axial velocity (v_i), dependent on n_f in parallel configuration, and single filter volume:

$$e.11) \quad EBCT_i = \frac{V_i \cdot n_f}{Q_{tot}} = \frac{V_i}{Q_i} = \frac{V_i}{v_i \cdot S_i}$$

where S_i is the surface of single filters (7.1 m^2). For n_f values from 16 to 40, filter volumes ranging between 13 and 18 m^3 were evaluated, to guarantee axial velocity and EBCT values typical of full-scale operations (about 5-15 m h^{-1} and 5-30 min, respectively ([36])). All the n_f filters were assumed to be simultaneously replaced by fresh GAC at breakthrough attainment ($n_R = n_f$).

According to equation e.5, EBCT may have a double opposite effect on the specific throughput of the GAC system: a higher EBCT (both obtained by increasing n_f or V_i) determines a delay of the breakthrough (longer t_{BT}), favouring V_{SP}; on the other hand, the overall GAC mass to be replaced at breakthrough increases, with a detrimental effect on V_{SP}. Hence, it is worth to evaluate the most efficient combinations of n_f and V_i as a function of the target contaminant and the treatment objective.

The values of specific throughput and breakthrough time calculated for PCE are shown in Figure 5, as a function of v_i and $EBCT_i$ resulting from the investigated n_f and V_i ranges, being quantities independent from the GAC system size (Q_{tot}, V_i, S_i and n_f) and so having a general validity. Since the results for PCE and chloroform showed very similar trends, data relative to chloroform are reported in S.I.4 (Figure S4). Simulations showed that, for a fixed v_i, the breakthrough time (Figure 5b) linearly increases from

30% (5% breakthrough) to 40% (95% breakthrough) over the investigated EBCT range, while, for a fixed $EBCT_i$, passing from 15 to 5 m h^{-1} velocity determines t_{BT} from 2- (5% breakthrough) to 3-times (95% breakthrough) higher. On the other hand, the influence of both filter EBCT and water velocity on V_{SP} was dependent on the treatment objective (Figure 5a): for a restrictive treatment objective (i.e. 5% breakthrough), V_{SP} increases when increasing $EBCT_i$ or decreasing v_i (namely when increasing the filter volume or number), while the behaviour becomes opposite when exploiting more filter capacity (i.e. 95% breakthrough). GAC system efficiency resulted to be almost independent on $EBCT_i$ and v_i when considering the 50% breakthrough. The variation of V_{SP} is linear with v_i, but not linear with $EBCT_i$, showing a saturation trend. Hence, the influence of EBCT variation (by modifying the filter volume or number) on the specific throughput is much more important for lower V_i and n_f values, namely for relatively small GAC systems composed by a lower total mass of carbon. For the GAC system sizes simulated in this study, an $EBCT_i$ increase of 1.5-times at constant v_i (corresponding to a V_i increase from 13 m^3 to 18 m^3, keeping n_f fixed) leads to a 20-30% increase (5% breakthrough) or 13-16% decrease (95% breakthrough) of V_{SP}; for a fixed $EBCT_i$ (fixed V_i), an axial velocity reduction from 16 to 5 m h^{-1} (i.e. passing from 16 to 40 parallel filters) determines V_{SP} 4-14% higher (5% breakthrough) or 3-6% lower (95% breakthrough).

In full-scale applications, the treatment objective is usually set to low breakthrough values, such as 5%; in these cases, results showed that a higher EBCT is the most suitable solution to: i) reduce GAC usage rate (meanwhile increasing the specific throughput), with relevant reduction of operating costs; ii) increase the breakthrough time, corresponding to less frequent GAC replacement operations. On the other hand, for high treatment objectives, the increase of V_{SP} obtained by lower EBCT must be weighted with the increase of replacement operation frequency, due to shorter breakthrough times. In general, the choice of the best configuration (combination of n_f and V_i) must be chosen balancing all the costs associated to a higher filter number or size (higher capital costs, space demand and complexity of the system) and considering the complexity of maintenance operations (frequency of replacement operations).
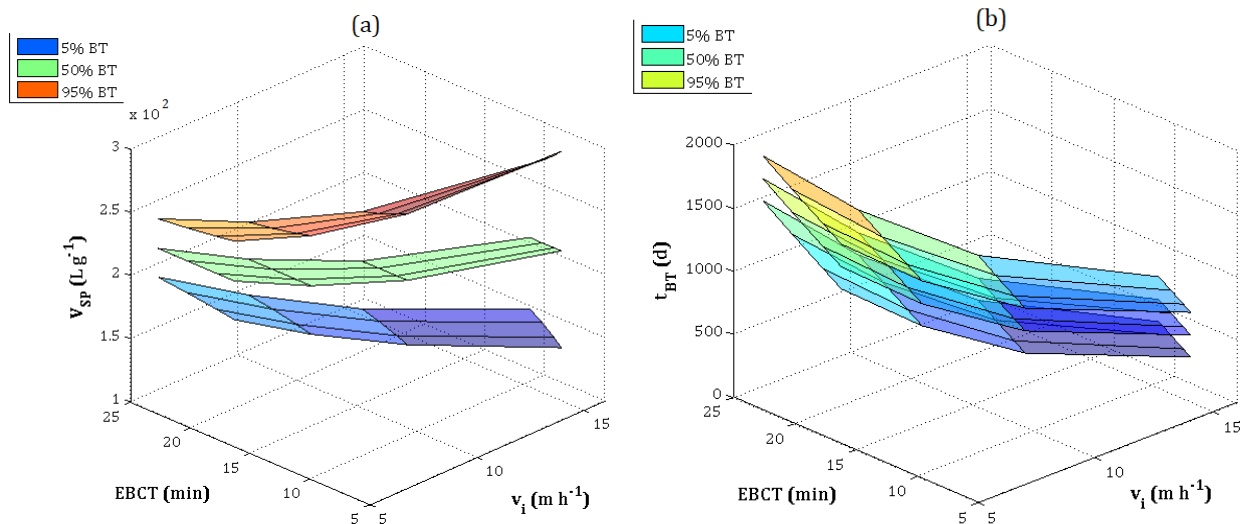

Figure 5 (a) Specific throughput (V_{SP}) and (b) breakthrough time (t_{BT}) calculated for PCE in configuration A as a function of EBCT, axial velocity (v_i) and treatment objective (5%, 50% or 95% breakthrough).

3.3.2   *Effect of GAC replacement strategy in parallel configuration*

A possible solution to reduce the adsorbent usage rate in configuration A is to stagger the filter operations, by replacing with fresh GAC only a sub-group of filters when the treatment objective is reached. Staggering filter operation allows to increase the effluent concentration from single filters above the target limit, but never surpassing the treatment objective in the blended effluent. GAC is so exploited for a longer time, reducing the AUR and increasing the V_{SP} ([7]).

A GAC system having a fixed number of parallel filters (n_f=20) with equal volume (13 m^3) was simulated considering the replacement of 100% (A1: n_R=n_f=20, not-staggered operations), 50% (A2: n_R=10) or 25% (A3: n_R=5) of the filters at treatment objective attainment. GAC into the filters was assumed to be replaced by fresh GAC having constant performances, hence assuming that the breakthrough profiles were identical at each cycle. The possible decrease of GAC adsorption capacity after reactivation, as observed in full-scale filter monitoring, was not considered in the present study.

$V_{SP,T}$ (equation e.6), N_R and N_O values calculated for 10-years simulations are shown in Table 4 (configurations A1, A2 and A3); for each simulation, minimum, maximum and steady-state time intervals for GAC replacement (t_{BT}) are provided in S.I.4 (Table S2). The configuration with 25% of filter substitutions (A3) does not always lead to feasible solutions: considering 5% and 50% breakthrough of PCE and chloroform, in fact, some breakthrough times before the steady state resulted to be too much short, down to 41 and 4-5 days for PCE and chloroform, respectively (at least 93% lower than t_{BT} of configuration A1). The same applies to the case of 5% chloroform breakthrough when replacing 50% of the filters (15 days minimum t_{BT}). Despite being not practically applicable, the results of these scenarios are anyway reported in Table 4.

Results in Table 4 showed that staggered operations allow to increase the specific throughput strongly depending on the treatment objective: considering 5% breakthrough, the simultaneous replacement of 50% or 25% of the filters determine an increase of $V_{SP,T}$ up to 9% and 19% for chloroform and PCE, respectively, compared to not-staggered operations; on the other hand, considering 50% and 95% breakthrough, $V_{SP,T}$ values up to 3-times higher can be obtained by replacing filter sub-groups. Staggering the reactivation operations of some filter groups is so an effective way to reduce GAC usage rate, even if the advantage is slight when the treatment objective is set at restrictive values (i.e. 5% breakthrough). The advantage of staggering filter operations is evident also looking at the number of filters replaced (N_R) during the whole time frame, that can be significantly reduced when replacing simultaneously 50% or 25% of the filters. As for $V_{SP,T}$, the reduction of N_R obtained by staggering filter replacement is dependent on the treatment objective, being more important when considering 95% with respect to 5% breakthrough.

As already pointed out, the main drawback of staggered operations is the reduction of replacement time intervals, resulting in more frequent filter replacement operations. Since replacement time interval is shorter than single bed life time, N_O increases when passing to 25% and 50% replacements of filter groups, as shown in Table 4. The increase of N_O is even more important when considering restrictive treatment objective, i.e. 5% breakthrough: in fact, staggered operations determine a relatively small increase of $V_{SP,T}$ against a detrimental increase of N_O, being almost doubled by halving the fraction of filters simultaneously substituted. Despite the different number of filters (n_R) replaced at each operation, the frequency of replacement operations must be also considered when selecting the best management strategy for the GAC system. The benefits obtained by the increase of specific throughput due to staggering filter operations must be so weighted with the higher complexity of system managing. Depending on the operating costs involved in GAC replacement operations (i.e. use of virgin or reactivated GAC, transport costs, GAC volumes), the best compromise between the savings associated to lower N_R and the costs associated to higher N_O values must be found.

3.3.3 Comparison between lead-lag and parallel configuration

Configuration B consisted in n_P pairs of lead-lag filters placed in series, with all the pairs operating in parallel with effluent blending. Since MTZ in each lead-lag pair is let move through both the filters until the lag column effluent reaches the treatment objective, GAC in lead filters can be more exploited, improving the AUR. Moreover, staggering the replacement of lead and lag filters in each pair allows to further increase bed life time.

A GAC system composed by 20 pairs of lead-lag filters (n_P=20, n_f=40) having an equal volume of 13 m^3 was simulated. The resulting water velocity was 12 m h^{-1} while the EBCT of single filters corresponded to 9 min; however, each lead-lag pair can be considered as a single filter having an EBCT of 18 min (treating the same flow rate but in a double GAC volume with respect to a single filter). As for parallel configuration with staggered operations, specific throughput was evaluated for a time frame (T) of 10 years by equation e.6. The calculated t_{BT} values were always long enough to consider the solution as feasible (minimum t_{BT} of 460 and 115 days, considering 5% PCE and chloroform breakthrough, respectively). $V_{SP,T}$, N_R and N_O values calculated for PCE and chloroform breakthroughs are reported in Table 4 (configuration B).

The performances of configuration B were firstly compared with those of configurations A1, A2 and A3, having the same water velocity (v_i=12 m h^{-1}) but half the EBCT (9 min). It is pointed out that system performances under the two configurations were assessed by considering only a limited set of factors contributing to the overall treatment costs. For example, lead-lag filters typically imply hydraulic heads higher than parallel configuration, resulting in higher energy demand for water pumping. On the other hand, lead-lag configuration can be potentially more exploited and the effluent quality can be monitored less frequently, since lag filters can be considered as a barrier of lead filters towards, for instance, pollution episodes and strong variation of influent concentrations. Being strictly case specific, these aspects were not taken into account in this study, although they can significantly affect operating and capital costs.

Results reported in Table 4 show that, for treatment objective at 5% breakthrough, configuration B gives higher $V_{SP,T}$ values (14% and 19% higher, considering PCE and chloroform, respectively) and a lower number of replaced filters and replacement operations (12-16% lower) with respect to configuration A1 (not staggered operations). The higher V_{SP} provided by configuration B are due to: i) the double EBCT of lead-lag pairs in configuration B with respect to parallel filters in configuration A1 (consistently with the results discussed in section 3.3.1); ii) the effect of staggering the operations of lead and lag filters, increasing the life-time of single filters. Staggering filter replacements in parallel configuration (A2) allows to obtain $V_{SP,T}$ and N_R values similar to those of configuration B, but with even more frequent replacement operations (N_O values at least 2 times higher). Overall, for a stringent treatment objective, configuration B gives more advantages than configuration A1 and A2, both in terms of GAC usage rate and complexity of replacement operations. Considering higher treatment objectives (i.e. 50% PCE and 95% PCE and chloroform breakthroughs), parallel configuration becomes the most efficient solution only when staggered replacement operations are adopted (A2 and A3), giving, for both the target contaminants, higher V_{SP} and lower N_R, even if higher N_O values.

Secondly, results of configuration B were compared with those obtained simulating a parallel configuration (not-staggered operations), denoted A4, having the same number of filters (n_f=40) of equal volume (V_i=13 m^3), resulting in EBCT of single filters of 18 min and axial velocity of 6 m h^{-1}. Data reported in Table 4 (A4 and B) show that, considering the 5% breakthrough as treatment objective, the comparison between system performances depends on the target contaminant: considering PCE, the specific throughput is more favourable for configuration A4 (V_{SP} 17% higher), with N_R 14% lower with respect to configuration B. Considering chloroform, higher $V_{SP,T}$ can be obtained by lead-lag configuration (10% higher with respect to configuration A4), together with a lower number of replaced filters (about 10% difference, corresponding to 60 filters in 10 years). Similar results were

obtained considering higher treatment objectives (50% and 95% breakthrough), with configuration B giving V_{SP} and N_R higher than configuration A4 for chloroform, vice versa for PCE. Therefore, for the same total volume of GAC, the reduction of water velocity (i.e. configuration A4) is the most favourable solution to increase V_{SP} in the case of slow breakthrough profiles (i.e. PCE); on the contrary, increasing EBCT by a lead-lag configuration is more suitable for early and sharp breakthroughs (i.e. chloroform). Independently from the target contaminant and the treatment objective, configuration A4 always gives lower N_O values, meaning less frequent and simpler GAC replacement operations. The choice between lead-lag and parallel configurations must so result from the balance of the involved operating aspects, considering the specific throughput and the management of filter replacements.

Finally, configuration B was compared with a system composed by 29 parallel filters of 18 m³ volume (configuration A5), hence constituted by the same total GAC volume, but distributed in a lower number of filters of larger volume (with EBCT=18 min and v_i=8 m h⁻¹). The selected n_f and V_i values of configuration A5 were, respectively, the lowest and the largest value allowing to respect the constrains in filter EBCT and velocity (see section 3.3.1). As shown in Table 4, both for PCE and chloroform and for all the considered treatment objectives, configuration A5 gives lower N_O values. Hence, a more compact distribution of the whole GAC volume in few and larger parallel filters allows to obtain a simpler system management, optimizing GAC replacement operations. The number of filters substituted in 10 years is also lower for configuration A5; however, the resulting V_{SP} is not always more favourable with respect to configuration B, due to the higher mass of GAC replaced at each operation. Regarding PCE adsorption, a trend with the treatment objective have not been observed: configuration A5 gives V_{SP} more favourable than configuration B when considering 5% and 95% breakthrough, while, for 50% breakthrough, configuration B gives higher V_{SP}. Considering chloroform, V_{SP} obtained by lead-lag configuration are slightly better than those of parallel configuration, for all the treatment objectives. It is pointed out that the difference in V_{SP} values calculated for the two configurations was never relevant, varying between 2% and 17%.

3.3.4 Selection of the optimal configuration

Finally, the six configurations evaluated in section 3.3.3 were compared to find the most efficient option for the studied GAC system. It is pointed out that these are only a subset of possible configurations, having been selected because of the representativeness of the design parameters (EBCT and v_i). More combinations of design and operating parameters could be selected and investigated, depending on the case-specific requirements and constrains.

The choice of the best configuration is a multi-objective optimization problem, where the best solution is a compromise between multiple conflicting objectives ([37]), namely the maximization of V_{SP} and minimization of N_R and N_O. A graphical comparison between V_{SP}, N_R and N_O values of the various configurations for each scenario is shown in S.I.4 (Figure S5). A unique optimal solution (nondominated or Pareto optimal solution ([37])), allowing to optimize both the GAC usage rate and the management of GAC replacement operations, could have been found in two scenarios: configuration A5, when considering PCE 5% breakthrough, and configuration A4, when considering PCE 50% breakthrough (excluding configuration A3, giving not feasible t_{BT}, as discussed in section 3.3.2). For the other treatment objectives, both in case of PCE and chloroform, nondominated solution to the multi-objective optimization problem have not been found, since individual optimal solution to each objective corresponded to different configurations. To find a unique solution which minimizes the objective conflict, the 3 objectives were scalarized in a single one by a distance function method ([37]): for a given scenario (target contaminant and treatment objective) the single objective function (D) was calculated as:

e.12)

$$D = \sum_{i}^{N} \omega_i \cdot d_i = \sum_{i}^{N} \omega_i \cdot \left| \frac{y_i(x) - \bar{y}_i}{\bar{y}_i} \right|,$$

$$\bar{y}_i = \min(y_i(x)),$$

where d_i is the normalized distance function for a i-th objective, $y_i(x)$ is the i-th objective value (-V_{SP}, N_R or N_O) for a given configuration x (A1, A2, A3, A4, A5, B) and N (3) is the number of objectives; the minimum objective value calculated among the tested configurations was considered as demand-level $\bar{y}_i$, representing the individual optimum for a i-th objective; ω_i is a dimensionless weight coefficient, initially considered equal for each objective (ω_i=1/N). The calculated d_i values are reported in Table 4 together with the respective V_{SP}, N_R or N_O values, while D values for each scenario are shown in Figure 6. According to the initial assumptions, configurations A5 and A4 resulted to be the best compromise for restrictive treatment objectives (5% and 50% PCE and chloroform breakthroughs), while configurations A3 and A2 (staggered filter replacement) were the most favourable options for 95% breakthroughs; configurations A1 and B showed intermediate D values considering 5% and 50% breakthroughs, getting dramatically worse for 95% breakthrough treatment objective.

Such kind of objective scalarization provides a simple way to solve objective conflicts and to visualize the best compromise solutions. However, in full-scale cases, the choice of the best configuration results from decision maker priorities and on the relative importance given to each objective, according to the case-specific conditions and all the involved costs. Looking at d_i values in Table 4, for instance, it can be observed that configuration A4 is always the best solution for the objective N_O (d=0), hence giving the simplest management of replacement operations; on the other hand, the d_i values for the objectives V_{SP} and N_R can have a relatively high contribution on the single objective function D, as in the case of high treatment objectives (95% breakthrough). The most suitable option must be so determined setting the proper values of demand-level ($\bar{y}_i$) and weight coefficient (ω_i) for each objective.

4. Conclusions

The breakthrough of chloroform, TCE and PCE was monitored in five full-scale filters containing different GAC types and fed on two different groundwater matrices. Data displayed: 1) the different affinity of the contaminants with the GACs, following the order PCE>TCE>chloroform; 2) the higher adsorption capacities of vegetal-based GAC with respect to mineral-based GAC, and that of virgin GAC with respect to reactivated GAC; 3) the faster breakthrough of PCE and chloroform in presence of higher influent concentrations, for the same GAC. The contaminant throughputs were found to be well correlated with the GAC iodine number, which can be used to predict GAC life-time.

The observed breakthrough profiles were well described by the Thomas model, which was calibrated and used to simulate a full-scale GAC system under different configurations and scenarios. Increasing the number and the volume of filters in a parallel configuration (leading to lower water axial velocities and higher EBCTs) was found to improve the GAC specific throughput when considering restrictive treatment objective (5% breakthrough), while the trend becomes opposite for high treatment objective (95% breakthrough). In parallel configuration, replacing only a subgroup of filters (50% or 25%) at breakthrough allows to increase the specific throughput over the long period, but determining a higher frequency of replacement operations (resulting in not feasible cycle-time when considering restrictive treatment objectives).

The performances of various configurations, including parallel configurations with different filter number and volume and a lead-lag configuration, were compared over a 10 years period. Considering three conflicting objectives, the maximization of specific throughput and the minimization of the number of replaced filters and replacement operations, a unique optimal solution was found only when considering 5% and 50% PCE breakthrough as treatment objective. In the other scenarios, the

best configuration was a compromise between savings and costs associated to GAC replacement operations. The relative benefits and drawbacks of different configurations vary with the target contaminant (thus with the breakthrough profile) and the treatment objective.

Table 4 Specific throughput ($V_{SP,T}$), number of replaced filters (N_R) and number of replacement operations (N_O) calculated for 10-years operations simulating PCE and chloroform ($CHCl_3$) breakthroughs under different configurations. Values between brackets are the normalized objective distances with respect to the minimum value observed for a given scenario (d_i in equation e.12).

Configuration	Treatment objective	5% BT		50% BT		95% BT	
	Contaminant	PCE	CHCl$_3$	PCE	CHCl$_3$	PCE	CHCl$_3$
A) n_f=20, V_i=13 m^3, EBCT=9 min, not-staggered operations	$V_{SP,T}$ (L g^{-1})	159.5 (0.27)	34.5 (0.16)	255.2 (0.20)	41.2 (0.24)	319.0 (0.69)	47.3 (0.73)
	N_R (-)	160 (0.84)	740 (0.50)	100 (0.25)	620 (0.34)	80 (2.20)	540 (2.72)
	N_O (-)	8 (1.67)	37 (1.18)	5 (1.50)	31 (1.07)	4 (1.00)	27 (0.93)
A) n_f=20, V_i=13 m^3, EBCT=9 min, 50% of filters replaced	$V_{SP,T}$ (L g^{-1})	182.3 (0.16)	36.5 (0.16)	319.0 (0.00)	54.3* (-)	638.1 (0.37)	91.2 (0.48)
	N_R (-)	140 (0.61)	700 (0.50)	80 (0.00)	470* (-)	40 (0.60)	280 (0.93)
	N_O (-)	14 (3.67)	70 (1.18)	8 (3.00)	47* (-)	4 (1.00)	28 (1.00)
A) n_f=20, V_i=13 m^3, EBCT=9 min, 25% of filters replaced	$V_{SP,T}$ (L g^{-1})	189.1* (-)	37.5* (-)	392.6* (-)	65.4* (-)	1020.9 (0.00)	176.0 (0.00)
	N_R (-)	135* (-)	680* (-)	65* (-)	390* (-)	25 (0.00)	145 (0.00)
	N_O (-)	27* (-)	136* (-)	13* (-)	78* (-)	5 (1.50)	29 (1.07)
A) n_f=40, V_i=13 m^3, EBCT=18 min, not-staggered operations	$V_{SP,T}$ (L g^{-1})	212.7 (0.02)	37.5 (0.09)	319.0 (0.00)	42.5 (0.22)	319.0 (0.69)	45.6 (0.74)
	N_R (-)	120 (0.38)	680 (0.38)	80 (0.00)	600 (0.29)	80 (2.20)	560 (2.86)
	N_O (-)	3 (0.00)	17 (0.00)	2 (0.00)	15 (0.00)	2 (0.00)	14 (0.00)
A) n_f=29, V_i=18 m^3, EBCT=18 min, not-staggered operations	$V_{SP,T}$ (L g^{-1})	217.1 (0.00)	38.3 (0.07)	217.1 (0.32)	40.7 (0.25)	325.6 (0.68)	46.5 (0.74)
	N_R (-)	87 (0.00)	493 (0.00)	87 (0.09)	464 (0.00)	58 (1.32)	406 (1.80)
	N_O (-)	3 (0.00)	17 (0.00)	3 (0.50)	16 (0.07)	2 (0.00)	14 (0.00)
B) n_f=40, n_P=20, V_i=13 m^3, EBCT=18 min**, lead-lag	$V_{SP,T}$ (L g^{-1})	182.3 (0.16)	41.2 (0.00)	255.2 (0.20)	45.6 (0.16)	319.0 (0.69)	53.2 (0.70)
	N_R (-)	140 (0.61)	620 (0.26)	100 (0.25)	560 (0.21)	80 (2.20)	480 (1.31)
	N_O (-)	7 (1.33)	31 (0.82)	5 (1.50)	28 (0.87)	4 (1.00)	24 (0.71)

* not-feasible solution because of too much short breakthrough times during transitory period.
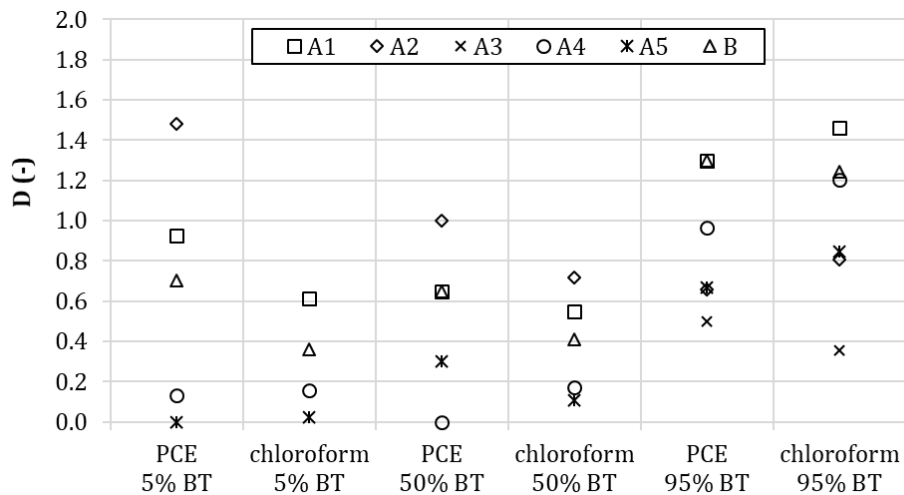** EBCT=18 min for each lead-lag pair, 9 min for single filters.

Figure 6 Single objective function (D) calculated for each configuration under different scenarios.

References

(1)   Williams, P.; Benton, L.; Warmerdam, J.; Sheehan, P. *Comparative risk analysis of six volatile organic compounds in California drinking water*; ACS Publications, 2002.

(2)   Luo, Y.; Guo, W.; Ngo, H. H.; Nghiem, L. D.; Hai, F. I.; Zhang, J.; Liang, S.; Wang, X. C. A review on the occurrence of micropollutants in the aquatic environment and their fate and removal during wastewater treatment. *Sci. Total Environ.* **2014**, *473*, 619–641.

(3)   Register, F. National primary and secondary drinking water regulations. *Fed Reg* **1989**, *54*, 22062–22160.

(4)   Sotelo, J. L.; Rodríguez, A.; Álvarez, S.; García, J. Removal of caffeine and diclofenac on activated carbon in fixed bed column. *Chem. Eng. Res. Des.* **2012**, *90* (7), 967–974.

(5)   Westerhoff, P.; Yoon, Y.; Snyder, S.; Wert, E. Fate of endocrine-disruptor, pharmaceutical, and personal care product chemicals during simulated drinking water treatment processes. *Environ. Sci. Technol.* **2005**, *39* (17), 6649–6663.

(6)   Oxenford, J. L.; Lykins, B. W. Conference summary: practical aspects of the design and use of GAC. *J.-Am. Water Works Assoc.* **1991**, *83* (1), 58–64.

(7)   Dvorak, B. I.; Morley, M.; Denning, P. Relative Impact on GAC Usage Rates of Operating Strategies for Treatment of Contaminated Groundwater. *Pract. Period. Hazard. Toxic Radioact. Waste Manag.* **2008**, *12* (2), 60–69.

(8)   Stewart, B. A.; New, C. W.; Hosni, A. A.; Dvorak, B. I. Framework for Evaluating Sorbent Usage Rate of Various Sorption Column Configurations with and without Bypass Blending. *J. Environ. Eng.* **2012**, *139* (4), 554–563.

(9)   Dvorak, B. I.; Maher, M. K. GAC contactor design for NOM removal: implications of EBCT and blending. *J. Environ. Eng.* **1999**, *125* (2), 161–165.

(10)   Denning, P. C.; Dvorak, B. I. Maximizing sorbent life: Comparison of columns in parallel, lead-lag series, and with bypass blending. *Water Environ. Res.* **2009**, *81* (2), 206–216.

(11)   Crittenden, J. C.; Hand, D. W.; Arora, H.; Lykins Jr, B. W. Design considerations for GAC treatment of organic chemicals. *J. Am. Water Works Assoc.* **1987**, 74–82.

(12)   Hutchins, R. A. Designing granular activated carbon systems for maximum performance. In *Proceedings of the Annual WWEMA Industrial Pollution Conference*; 1977; pp 491–512.

(13)   Kennedy, A. M.; Reinert, A. M.; Knappe, D. R.; Ferrer, I.; Summers, R. S. Full-and pilot-scale GAC adsorption of organic micropollutants. *Water Res.* **2015**, *68*, 238–248.

(14)   Worch, E. Fixed-bed adsorption in drinking water treatment: a critical review on models and parameter estimation. *J. Water Supply Res. Technol.-Aqua* **2008**, *57* (3), 171–183.

(15)   Crittenden, J. C.; Reddy, P. S.; Arora, H.; Trynoski, J.; Hand, D. W.; Perram, D. L.; Summers, R. S. Predicting GAC performance with rapid small-scale column tests. *J. Am. Water Works Assoc.* **1991**, 77–87.

(16)   Anumol, T.; Sgroi, M.; Park, M.; Roccaro, P.; Snyder, S. A. Predicting trace organic compound breakthrough in granular activated carbon using fluorescence and UV absorbance as surrogates. *Water Res.* **2015**, *76*, 76–87.

(17)   Pelech, R.; Milchert, E.; Bartkowiak, M. Fixed-bed adsorption of chlorinated hydrocarbons from multicomponent aqueous solution onto activated carbon: Equilibrium column model. *J. Colloid Interface Sci.* **2006**, *296* (2), 458–464.

(18)   Corwin, C. J.; Summers, R. S. Adsorption and desorption of trace organic contaminants from granular activated carbon adsorbers after intermittent loading and throughout backwash cycles. *Water Res.* **2011**, *45* (2), 417–426.

(19)   Morley, M. C.; Henke, J. L.; Speitel Jr, G. E. Adsorption of RDX and HMX in rapid small-scale column tests: Implications for full-scale adsorbers. *J. Environ. Eng.* **2005**, *131* (1), 29–37.

(20)   Summers, R. S.; Kim, S. M.; Shimabuku, K.; Chae, S.-H.; Corwin, C. J. Granular activated carbon adsorption of MIB in the presence of dissolved organic matter. *Water Res.* **2013**, *47* (10), 3507–3513.

(21)   Knappe, D. R.; Snoeyink, V. L.; Roche, P.; Prados, M. J.; Bourbigot, M.-M. The effect of preloading on rapid small-scale column test predictions of atrazine removal by GAC adsorbers. *Water Res.* **1997**, *31* (11), 2899–2909.

(22)   Ho, L.; Newcombe, G. Granular activated carbon adsorption of 2-methylisoborneol (MIB): pilot- and laboratory-scale evaluations. *J. Environ. Eng.* **2010**, *136* (9), 965–974.

(23)   Rossner, A.; Knappe, D. R. MTBE adsorption on alternative adsorbents and packed bed adsorber performance. *Water Res.* **2008**, *42* (8), 2287–2299.

(24)   Richard, D.; Núñez, M. de L. D.; Schweich, D. Adsorption of complex phenolic compounds on active charcoal: breakthrough curves. *Chem. Eng. J.* **2010**, *158* (2), 213–219.

(25)   García-Mateos, F. J.; Ruiz-Rosas, R.; Marqués, M. D.; Cotoruelo, L. M.; Rodríguez-Mirasol, J.; Cordero, T. Removal of paracetamol on biomass-derived activated carbon: modeling the fixed bed breakthrough curves using batch adsorption experiments. *Chem. Eng. J.* **2015**, *279*, 18–30.

(26)   Jarvie, M. E.; Hand, D. W.; Bhuvendralingam, S.; Crittenden, J. C.; Hokanson, D. R. Simulating the performance of fixed-bed granular activated carbon adsorbers: Removal of synthetic organic chemicals in the presence of background organic matter. *Water Res.* **2005**, *39* (11), 2407–2421.

(27)   Corwin, C. J.; Summers, R. S. Scaling trace organic contaminant adsorption capacity by granular activated carbon. *Environ. Sci. Technol.* **2010**, *44* (14), 5403–5408.

(28)   Knappe, D. R.; Snoeyink, V. L.; Roche, P.; Prados, M. J.; Bourbigot, M.-M. Atrazine removal by preloaded GAC. *Am. Water Works Assoc. J.* **1999**, *91* (10), 97.

(29)   Han, R.; Wang, Y.; Zhao, X.; Wang, Y.; Xie, F.; Cheng, J.; Tang, M. Adsorption of methylene blue by phoenix tree leaf powder in a fixed-bed column: experiments and prediction of breakthrough curves. *Desalination* **2009**, *245* (1–3), 284–297.

(30)   Baral, S. S.; Das, N.; Ramulu, T. S.; Sahoo, S. K.; Das, S. N.; Chaudhury, G. R. Removal of Cr (VI) by thermally activated weed Salvinia cucullata in a fixed-bed column. *J. Hazard. Mater.* **2009**, *161* (2), 1427–1435.

(31)   Brunauer, S.; Emmett, P. H.; Teller, E. Adsorption of gases in multimolecular layers. *J. Am. Chem. Soc.* **1938**, *60* (2), 309–319.

(32)   Barrett, E. P.; Joyner, L. G.; Halenda, P. P. The determination of pore volume and area distributions in porous substances. I. Computations from nitrogen isotherms. *J. Am. Chem. Soc.* **1951**, *73* (1), 373–380.

(33)   HORVÁTH, G.; Kawazoe, K. Method for the calculation of effective pore size distribution in molecular sieve carbon. *J. Chem. Eng. Jpn.* **1983**, *16* (6), 470–475.

(34)   Guo, J.; Lua, A. C. Textural and chemical characterizations of adsorbent prepared from palm shell by potassium hydroxide impregnation at different stages. *J. Colloid Interface Sci.* **2002**, *254* (2), 227–233.

(35)   Zietzschmann, F.; Altmann, J.; Ruhl, A. S.; Dünnbier, U.; Dommisch, I.; Sperlich, A.; Meinel, F.; Jekel, M. Estimating organic micro-pollutant removal potential of activated carbons using UV absorption and carbon characteristics. *Water Res.* **2014**, *56*, 48–55.

(36)   Crittenden, J. C.; Trussell, R. R.; Hand, D. W.; Howe, K. J.; Tchobanoglous, G. *MWH's water treatment: principles and design*; John Wiley & Sons, 2012.

(37)   Miettinen, K. *Nonlinear Multiobjective Optimization, volume 12 of International Series in Operations Research and Management Science*; Kluwer Academic Publishers, Dordrecht, 1999.

Supporting Information

S.I.1 Flow rate of monitored filters

Water flow rate (Q_i) measured during filter monitoring are shown in Figure S2. Average Q_i values were equal to 27.0±3.77 L s^{-1} for GAC-V-v and 25.3±4.46 L s^{-1} for GAC-M-r in DWTP-1 filters, equal to 20.2±7.50 L s^{-1}, 23.3±5.27 L s^{-1} and 19.4±10.56 L s^{-1}, for GAC-V-v, GAC-M-v and GAC-M-r, respectively, in DWTP-2 filters.
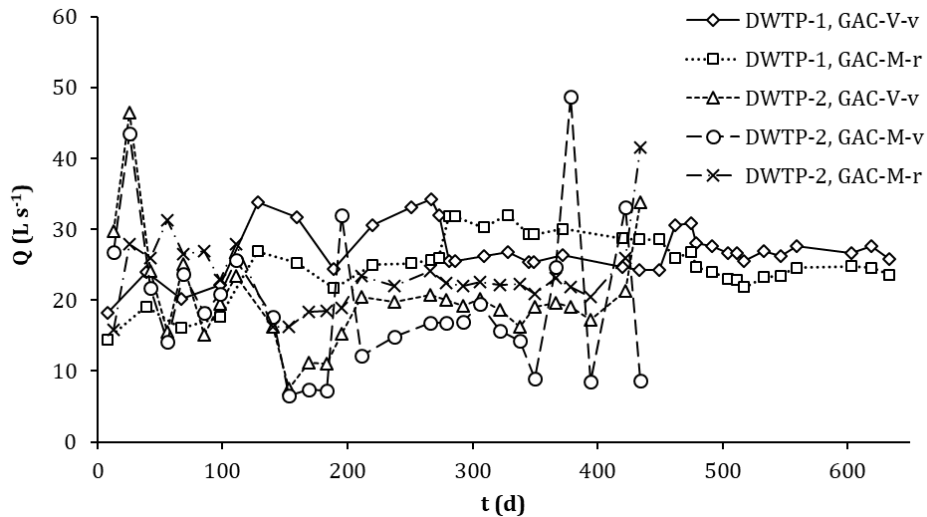

Figure S1 Water flow rate (Q_i) over time observed for monitored filters.
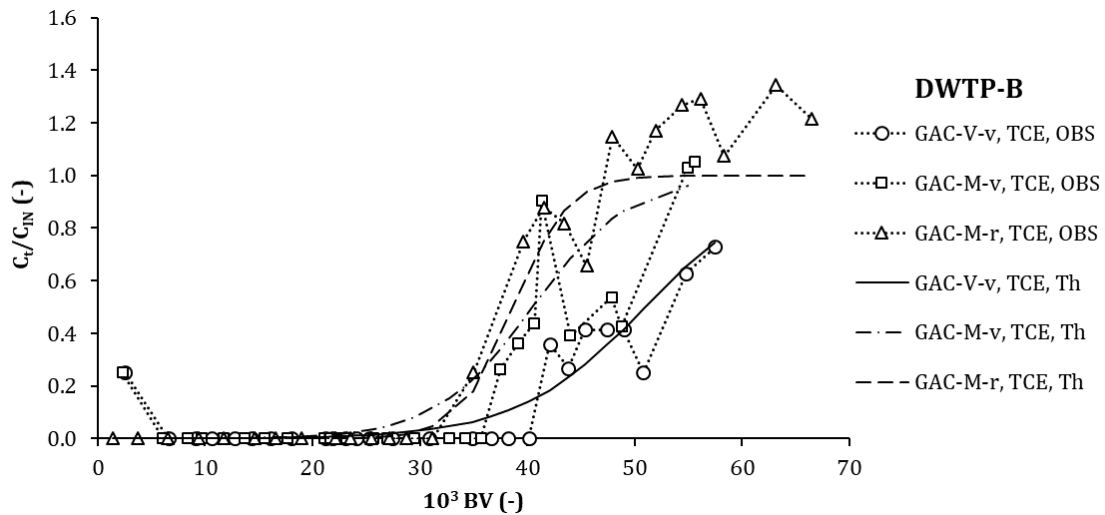
S.I.2 TCE breakthrough for DWTP-2

Figure S2 TCE breakthrough for filters containing GAC-V-v, GAC-M-r and GAC-M-v in DWTP-2: observed data and fitting curves (Thomas model).

S.I.3 Correlations with characterization parameters

Table S1 Pearson coefficients and p-values of linear correlation between carbon properties and observed throughputs (BV to 5%, 50% and 95% breakthrough). Pearson coefficient values corresponding to a p-value<0.05 are in bold. The number of data (N) is also reported.

|	N	Iodine number	BET surface area	t-plot micropore volume	t-plot micropore area	BJH average pore diameter
		Pearson coefficient				
chloroform $BV_{5\%}$	5	**0.96**	0.86	0.44	**0.88**	0.22
chloroform $BV_{50\%}$	5	**0.98**	**0.93**	0.57	0.94	0.30
chloroform $BV_{95\%}$	5	**0.93**	**0.89**	0.64	0.92	0.36
PCE $BV_{5\%}$	4	0.77	0.63	0.26	0.69	0.72
PCE $BV_{50\%}$	3	0.96	0.81	0.19	0.83	0.61
PCE $BV_{95\%}$	2	-	-	-	-	-
TCE $BV_{5\%}$	3	0.93	0.88	0.09	0.93	-0.44
TCE $BV_{50\%}$	3	**>0.99**	>0.99	0.44	**>0.99**	-0.09
TCE $BV_{95\%}$	2	-	-	-	-	-
		p-value				
chloroform $BV_{5\%}$	5	1.0E-02	6.3E-02	4.6E-01	4.7E-02	7.2E-01
chloroform $BV_{50\%}$	5	2.2E-03	2.4E-02	3.1E-01	1.8E-02	6.2E-01
chloroform $BV_{95\%}$	5	2.0E-02	4.1E-02	2.5E-01	2.8E-02	5.5E-01
PCE $BV_{5\%}$	4	2.3E-01	3.7E-01	7.4E-01	3.1E-01	2.8E-01
PCE $BV_{50\%}$	3	1.8E-01	4.0E-01	8.8E-01	3.8E-01	5.8E-01
PCE $BV_{95\%}$	2	-	-	-	-	-
TCE $BV_{5\%}$	3	2.5E-01	3.2E-01	9.4E-01	2.4E-01	7.1E-01
TCE $BV_{50\%}$	3	1.7E-02	8.5E-02	7.1E-01	6.4E-03	9.4E-01
TCE $BV_{95\%}$	2	-	-	-	-	-
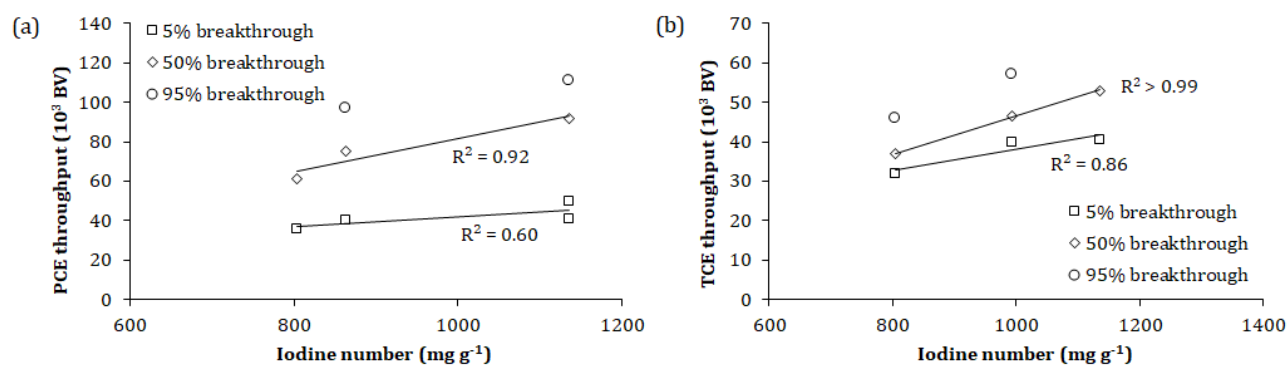
Figure S3 Observed PCE (a) and TCE (b) throughput (to 5%, 50% and 95% breakthrough) vs. GAC iodine number. Linear regression curves and relative determination coefficients (R^2) are reported.
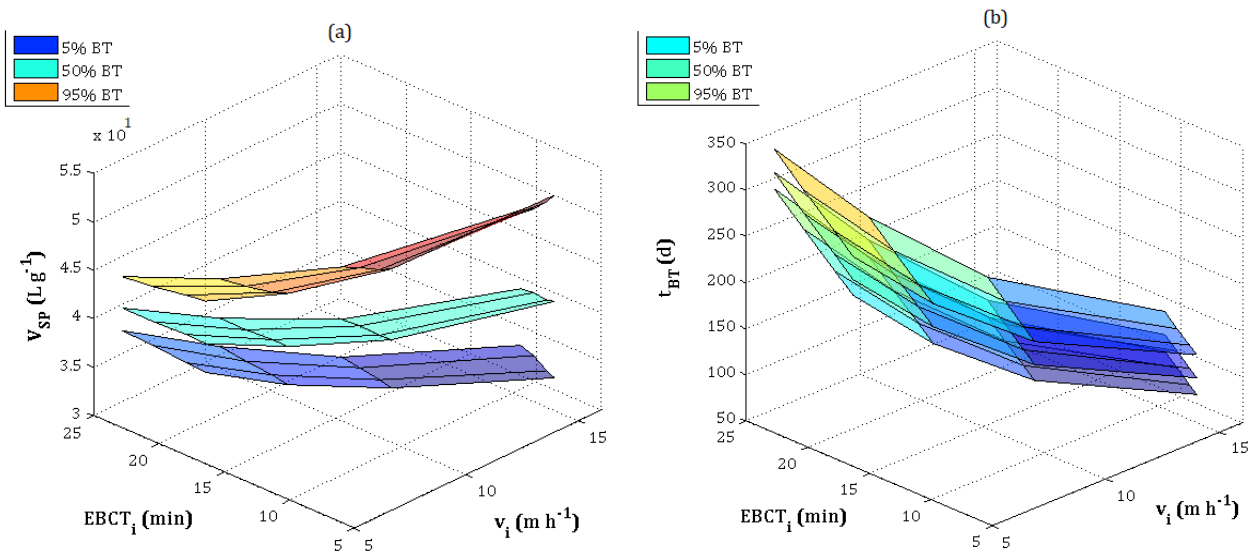
S.I.4 GAC system optimization

Figure S4 (a) Specific throughput (V_{SP}) and (b) breakthrough time (t_{BT}) calculated for chloroform in configuration A as a function of EBCT, axial velocity (v_i) and treatment objective (5%, 50% or 95% breakthrough).

Table S2 Results of simulations of configuration A1, A2 and A3 in a time frame of 10 years: minimum, maximum and steady-state breakthrough time (t_{BT}), number of replacement operations before steady-state.

A1: 100% of filters simultaneously substituted ($n_r = n_f = 20$)					n° of replacements before steady-state
Treatment objective	Target contaminant	t_{BT} (d)			
		Steady-state	min	max	
5% BT	PCE		441		1
	chloroform		98		1
50% BT	PCE		616		1
	chloroform		115		1
95% BT	PCE		791		1
	chloroform		133		1

A2: 50% of filters simultaneously substituted ($n_r = 10$, $n_f = 20$)					n° of replacements before steady-state
Treatment objective	Target contaminant	t_{BT} (d)			
		Steady-state	min	max*	
5% BT	PCE	-	152	333	>20
	chloroform	-	15	87	>20
50% BT	PCE	411	308	460	6
	chloroform	77	58	92	4
95% BT	PCE	746	746	746	1
	chloroform	128	128	128	1

(*continues in the next page*)

(continues from the previous page)

A3: 25% of filters simultaneously substituted (n_r=5, n_f=20)					
Treatment objective	Target contaminant	t_{BT} (d)			n° of replacements before steady-state
		Steady-state	min	max*	
5% BT	PCE	-	18	320	>20
	chloroform	-	5	89	>20
50% BT	PCE	243	41	275	8
	chloroform	46	4	55	8
95% BT	PCE	698	698	698	4
	chloroform	123	123	133	5

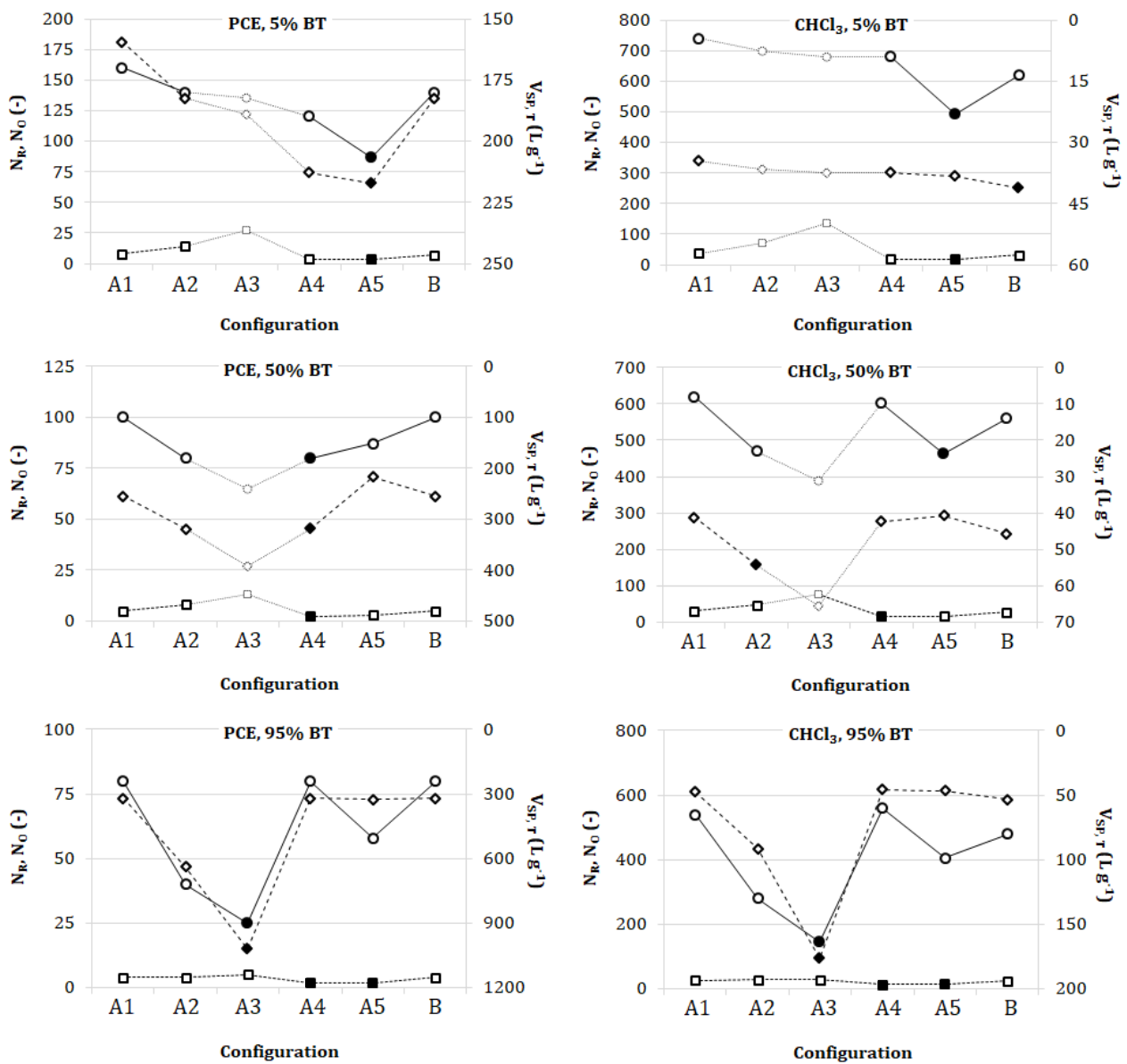* t_{BT} of the first cycle excluded (equal to that observed in configuration A1)

Figure S5 Values of V_{SP} (diamonds), N_R (circles) and N_O (squares) calculated for each configuration under different scenarios (target contaminants and treatment objectives). Full symbols represent the best objective value among the various configurations. Light symbols represent not feasible solutions due to too much short breakthrough times.